

# **Dynamic Effect of Variation of River Water Level on Riverbank Erosion**

Thesis submitted by

**Debasish Biswas**

**Doctor of Philosophy (Engineering)**

**SCHOOL OF WATER RESOURCES ENGINEERING**

**FACULTY OF INTERDISCIPLINARY STUDIES, LAW &  
MANAGEMENT**

**JADAVPUR UNIVERSITY**

**KOLKATA, INDIA**

**2024**

**JADAVPUR UNIVERSITY**  
**KOLKATA 700032, INDIA**

INDEX NO: D-7/ISLM/84/18

**1. Title of the thesis:**

**Dynamic Effect of Variation of River Water Level on Riverbank Erosion**

**2. Name, Designation & Institution of the Supervisors:**

**a. Prof. (Dr.) Asis Mazumdar**

Professor & Director,  
School of Water Resources Engineering,  
Jadavpur University, Kolkata –700032,  
West Bengal, India

**b. Dr. Sanchayan Mukherjee**

Associate Professor,  
Mechanical Engineering Department,  
Kalyani Government Engineering College,  
Kalyani–741235, West Bengal, India

**c. Dr. Arijit Dutta**

Assistant Professor,  
Mechanical Engineering Department,  
Alipurduar Government Engineering and  
Management College, Alipurduar–  
736206, West Bengal, India

**3. List of publications:**

*Journal Publications*

1. Biswas, D., Dutta, A., Mukherjee, S. and Mazumdar, A., (2020) “Effect of Cohesive and Seepage Force on A Bank Sediment Particle.” Indian Science Cruiser, Volume 34, No 1, Pages- 21-26. ISSN: 0970-4256. DOI:[10.24906/isc/2020/v34/i1/195949](https://doi.org/10.24906/isc/2020/v34/i1/195949)



2. Biswas, D., Dutta, A., Mukherjee, S. and Mazumdar, A., (2024). “A New Approach to Transformation of Micro Analysis into Macro Analysis of Forces to Study the Dynamic Behaviour of Riverbank Morphology.” *ISH Journal of Hydraulic Engineering* (Print ISSN 0971-5010 Online ISSN 2164-3040), Taylor and Francis, (Available online) (DOI: <https://doi.org/10.1080/09715010.2024.2317884>)

*International Conference Publications*

1. Biswas, D., Dutta, A., Mukherjee, S. and Mazumdar, A., (March, 2020) “A Dynamic Analysis of Riverbank Erosion.” In: Dawn S., Balas V., Esposito A., Gope S. (eds) *Intelligent Techniques and Applications in Science and Technology. ICIMSAT 2019. Learning and Analytics in Intelligent Systems*, vol 12. Springer, Cham. pp 337-345. Print ISBN: 978-3-030-42362-9. Online ISBN: 978-3-030-42363-6. Print ISSN: 2662-3447. Online ISSN: 2662-3455. DOI:[10.1007/978-3-030-42363-6\\_40](https://doi.org/10.1007/978-3-030-42363-6_40).
2. Biswas, D., Dutta, A., Mukherjee, S. and Mazumdar, A., (January, 2020) “Computational Analysis of Effect of Water Impurity on a Riverbank Particle.” *Contemporary Issues in Computing*. DOI: [10.26480/cic.01.2020.64.66](https://doi.org/10.26480/cic.01.2020.64.66).
3. Biswas, D., Dutta, A., Mukherjee, S. and Mazumdar, A., (February 2021) “Micro Analysis of Riverbank Sediment Stability under Different Wetted Surface Conditions.” *IOP Conference Series Materials Science and Engineering* 1080(1):012042. DOI: [10.1088/1757-899X/1080/1/012042](https://doi.org/10.1088/1757-899X/1080/1/012042).
4. Biswas, D., Dutta, A., Mukherjee, S. and Mazumdar, A., (April, 2021) “Stability Analysis of a Riverbank for Different Microstructural Arrangements of the Particles.” In: Roy P.K., Roy M.B., Pal S. (eds) *Advances in Water Resources Management for Sustainable Use. Lecture Notes in Civil Engineering*, vol 131. ISBN 978-981-33-6411-0, ISSN 2366-2557, ISSN 2366-2565 (electronic), Springer, Singapore. DOI:[10.1007/978-981-33-6412-7\\_2](https://doi.org/10.1007/978-981-33-6412-7_2).
5. Biswas, D., Dutta, A., Mukherjee, S. and Mazumdar, A., (July, 2021) “Effect of Liquid Bridge Volume on Cohesive Sediment Motion.” In: Ghosh S.K., Ghosh K., Das S., Dan P.K., Kundu A. (eds) *Advances in Thermal Engineering, Manufacturing, and Production Management. ICTEMA 2020. Lecture Notes in Mechanical Engineering*. ISBN 978-981-16-2346-2, ISSN 2195-4356, ISSN 2195-4364 (electronic), Springer, Singapore. DOI:[10.1007/978-981-16-2347-9\\_2](https://doi.org/10.1007/978-981-16-2347-9_2).
6. Biswas, D., Dutta, A., Mukherjee, S. and Mazumdar, A., (January 2022) “Riverbank Erosion for Different Levels of Impurity of Water—A Micro-analysis.” *Advanced Modelling and Innovations in Water Resources Engineering* (pp.719-728). *Select Proceedings of AMIWRE 2021. Lecture*

Notes in Civil Engineering (LNCE, volume 176). ISBN: 978-981-16-4629-4.  
ISSN:2366-2557. E-ISSN: 2366-2565. Springer, Singapore.  
DOI:[10.1007/978-981-16-4629-4\\_50](https://doi.org/10.1007/978-981-16-4629-4_50).

#### **4. List of Patents: NIL**

#### **5. List of Presentations in National / International Conferences/Workshops:**

1. Biswas, D., Dutta, A., Mukherjee, S. and Mazumdar, A., “Determination of Escape Velocity of a Particle on Riverbank under Cohesive and Seepage Force.” National Conference on Trends and Advances in Mechanical Engineering (TAME-2019), February 15-16, 2019.
2. Biswas, D., Dutta, A., Mukherjee, S. and Mazumdar, A., “A dynamic Analysis of Riverbank Erosion.” 1<sup>st</sup> International Conference on Innovation in Modern Science and Technology (ICIMSAT-2019), September 20-21, 2019.
3. Biswas, D., Dutta, A., Mukherjee, S. and Mazumdar, A., “Stability Analysis of a Riverbank for Different Microstructural Arrangements of the Particles.” International Conference on Sustainable Water Resources Management under Changed Climate, March 13-15, 2020.
4. Biswas, D., Dutta, A., Mukherjee, S. and Mazumdar, A., “Comparative Study of Effect of Water Impurity on a Sediment Particle in Riverbank Stability Computation.” 1st International Conference on Contemporary Issues in Computing, ICCIC 2020, 25th - 26th July 2020. (Received Best Paper Award).
5. Biswas, D., Dutta, A., Mukherjee, S. and Mazumdar, A., “Effect of Liquid Bridge Volume on Cohesive Sediment Motion.” International Conference on Thermal Engineering and Management Advances, ICTEMA-2020, December 19-20, 2020.
6. Biswas, D., Dutta, A., Mukherjee, S. and Mazumdar, A., “Micro Analysis of Riverbank Sediment Stability under Different Wetted Surface Conditions.” 3rd International Conference on Advances in Mechanical Engineering and its Interdisciplinary Areas (ICAMEI-2021), January 6, 2021.
7. Biswas, D., Dutta, A., Mukherjee, S. and Mazumdar, A., “Riverbank Erosion for Different Levels of Impurity of Water – A Micro Analysis.” National Conference on Advanced Modelling and Innovations in Water Resources Engineering (AMIWRE-2020), NIT Jamshedpur, February 20-21, 2021.

**JADAVPUR UNIVERSITY**  
**FACULTY OF INTERDISCIPLINARY STUDIES, LAW &  
MANAGEMENT**

**“Statement of Originality”**

I **Debasish Biswas** registered on **14.01.2019** do hereby declare that this thesis entitled **“Dynamic effect of variation of river water level on riverbank erosion”** contains literature survey and original research work done by the undersigned candidate as part of Doctoral studies.

All information in this thesis have been obtained and presented in accordance with existing academic rules and ethical conduct. I declare that, as required by these rules and conduct, I have fully cited and referred all materials and results that are not original to this work.

I also declare that I have checked this thesis as per the “Policy on Anti Plagiarism, Jadavpur University, 2019”, and the level of similarity as checked by iThenticate software is 8 %.

*Debasish Biswas.*  
Signature of Candidate:

Date: *28/05/2024.*

Certified by Supervisor(s):  
(Signature with date, seal)

1. 

**Dr Asis Mazumdar**  
*Professor & Director*  
School of Water Resources Engineering  
Jadavpur University, Kolkata-700 032

2. *Sanchayalini*

**Associate Professor**  
Department of Mechanical Engineering  
Kalyani Govt. Engg. College, Kalyani, Nadia

3. *Arijit Dutta*

**Assistant Professor**  
Mechanical Engineering  
Alipurdur Government  
Engineering & Management College  
Alipurdur

**JADAVPUR UNIVERSITY**  
**FACULTY OF INTERDISCIPLINARY STUDIES, LAW &**  
**MANAGEMENT**

**CERTIFICATE FROM THE SUPERVISORS**


This is to certify that the thesis entitled “**Dynamic effect of variation of river water level on riverbank erosion**” submitted by **Debasish Biswas** who got his name registered on D-7/ISLM/84/18 dated 14<sup>th</sup> January, 2019 under the Faculty of Interdisciplinary Studies, Law & Management for the award of Ph. D. (Engineering) degree of Jadavpur University, is absolutely based upon his own work under the supervision of Prof. (Dr.) Asis Mazumdar, Dr. Sanchayan Mukherjee and Dr. Arijit Dutta and that neither his thesis nor any part of the thesis has been submitted for any degree/diploma or any other academic award anywhere before.

1.  28/05/2024

Signature of the Supervisor

with date and Office Seal


**Dr Asis Mazumdar**  
Professor & Director  
School of Water Resources Engineering  
Jadavpur University, Kolkata-700 032

2.  28/5/2024

Signature of the Supervisor

with date and Office Seal

**Associate Professor**  
Department of Mechanical Engineering  
Kalyani Govt. Engg. College, Kalyani, Nadia

3.  28/05/2024

Signature of the Supervisor

with date and Office Seal

**Assistant Professor**  
Mechanical Engineering  
Jadavpur Government  
Engineering & Management College  
Kolkata

*Dedicated to my Father, Mother, Wife, Brother and to  
my immediate family*

# ACKNOWLEDGEMENT

---

First and foremost, I would like to express my sincere gratitude to my supervisors, Prof. (Dr.) Asis Mazumdar, Dr. Sanchayan Mukherjee and Dr. Arijit Dutta, for their extensive support, encouragement and unparalleled guidance throughout the entire journey. Their invaluable insights and expertise have significantly contributed to the completion of this dissertation.

I am deeply grateful to my family for their unwavering support and understanding. To my parents, Shri. Kartick Chandra Biswas and Smt. Archana Biswas, your love and belief in me have been a constant source of strength. I am grateful to my brother, Dr. Ashis Biswas, for his unwavering belief in me and his words of support.

I would especially like to thank my lovely wife, Smt. Rupa Ghosh. Your endless patience, unwavering support, and boundless love have been my anchor throughout this challenging journey. Your understanding and sacrifices have made it possible for me to dedicate the necessary time and effort to this research. Thank you for being my rock and my inspiration.

I would also like to extend my heartfelt gratitude to Dr. Sourabh Kumar Das, the Principal of Kalyani Government Engineering College. Special thanks are due to my colleagues of Mechanical Engineering Department, Kalyani Government Engineering College. Your support, encouragement, and understanding have been instrumental in balancing my professional responsibilities and academic pursuits.

I would also like to thank the members of my thesis committee, for their time, effort, and constructive feedback, which have greatly improved the quality of this work.

Finally, I extend my heartfelt thanks to everyone who contributed, in one way or another, to the successful completion of this thesis. Your support and encouragement have been invaluable, and I am deeply grateful to each one of you.

**Debasish Biswas**

**May 2024**

# SYNOPSIS

---

Riverbank erosion has long had a significant impact on civilization, particularly with regard to agriculture, human settlement, and flood defence. Man-made facilities are also destroyed by land loss resulting from local riverbank collapse. The researchers are therefore very keen to learn more about the riverbank's stability. The result of bank erosion is riverbank failure. Alluvial terraces and productive floodplains were created over time as a result of riverbank erosion, a natural process. In actuality, some of the banks of even stable river systems are eroding. However, compared to unstable systems, erosion often happens at a considerably slower rate and smaller scale in stable systems. Rivers and streams can undergo abrupt, dramatic alterations due to natural disasters like flooding. Moreover, stream management and land usage might set off erosion reactions. The reactions can be complicated, sometimes impairing stability for decades and frequently leading to faster rates of disintegration. Bank erosion is hastened by management practices such as improper catchment use and deforestation, ill-managed extraction of sand and gravel, and projects affecting the natural course of flow of the stream.

Bank scour and mass failure are the two broad categories into which the different mechanisms of stream bank erosion can be divided. Both will frequently be present in cases of bank instability, with either scour or mass failure predominating. The erosive strength of flowing water rises with flow speed, and scour may occur. A clear indication of scour processes is undercutting of the bank toe. The main goals of effective scour management techniques are to reduce flow velocity through strategically placed vegetation and, in certain situations, bank stabilisation engineering.

The term “mass failure” refers to the several bank erosion mechanisms that cause portions of the bank to slide or topple into the stream. Collapse or slumping are common terms used to describe mass failure. The most visible indications of these processes are sections of slumping bank materials or bare, nearly vertical banks. Although the causes of these kinds of failures are frequently unclear, human and/or natural factors may be involved.

The majority of studies conducted in the subject of riverbank stability are based on experimental findings, which are essentially various case studies connected to a specific river system. For the other river systems, the conclusions pertaining to a particular river have very little physical significance. Also, these kinds of experiments require large investments and consume time. So, it is quite obvious to find out general expressions for riverbank stability with less time and less investigation cost which are applicable for any kind of river system. So, the necessity of the analytical approach is very important. Many researchers have tried to find out an analytical solution in microscopic level. But macroscopic approach to find out the riverbank stability is yet to be investigated. The volumetric rate of erosion has been determined through microscopic study in relation to escape velocity, which is thought to be the most important parameter for determining the stability of bank surfaces. The rate of bank material deterioration is measured by particle escape velocity. Reduced escape velocity translates into a larger volumetric erosion rate, which denotes reduced riverbank stability.

Studying the stability analysis of the riverbank in a dynamic flow scenario with fluctuating water levels is the primary goal of this work. The two categories into which this study has been divided are micro-analysis of the riverbank system and macro-analysis of the riverbank system. Firstly, taking into account the



microscopic forces, a micro-analysis of the particle has been conducted considering well established “Truncated-Pyramid Model” developed by Mukherjee and Mazumdar (2010) meant for microscopic arrangement of particles. Particle escape velocity has been calculated to assess how various microscopic forces affect the stability of the riverbank system. In order to provide visual representations of the stability under various circumstances, the escape velocity change with various parameters, including the water-bridge volume, grain (particle) diameter, and inter-grain distance, has been plotted. To investigate the dynamic behaviour under various water level circumstances both the situations of water level rising and falling have been investigated.

Secondly, a right-angled trapezoidal tension crack failure block has been investigated in order to examine macro-analysis. The common bank angle considered here is of  $60^\circ$  which is in line with Darby and Thorne (1996). Here, in this section transformation of well-established microscopic force analysis into macroscopic force analysis has been implemented which are more practical and comparable with the field data analysis. Using a newly developed method, the microscopic forces in this instance have been converted into a macroscopic force system as a function of number of particles for tends to infinite number of particles using Newton’s forward interpolation series calculation, and the various macroscopic forces have also been taken into consideration while analysing the stability in terms of escape velocity, as the escape velocity is considered to be the most significant parameter to measure the stability of the bank surfaces. Lower escape velocity implies higher the value of volumetric erosion rate which indicates less stability of the riverbank. It has been studied how the escape velocity changes as the number of particles in the tension fracture varies. To evaluate the dynamic behaviour of the riverbank system, here,

changing water level situations were investigated as well for both the circumstance of increasing and dropping water level.

In the microscopic analysis, two different studies have been made. Firstly, varying particle sizes with a fixed value of liquid-bridge volume and secondly, varying liquid-bridge volume with a fixed value of particle size. The escape velocity variations have been plotted against the inter-particle distance for both conditions pertaining to water level rising and falling, for three different degrees of exposure ( $e$ ) of the particle, Fully exposed [ $e = 1.0$ ], Half exposed [ $e = 0.5$ ] and Fully submerged [ $e = 0.0$ ]. The results of adverse effect of inter-particle distances, particle size and the positive influence of liquid-bridge volume on escape velocity have been observed and discussed. From the analyses, it can also be concluded that increasing degrees of exposure reduce the particle escape velocity. Again, this velocity is less in case of water level falling compared to that of water level rising when the other parameters remain constant.

In the macroscopic analysis, a right-angled trapezoidal failure block with infinite number of particles has been investigated while it is subjected to different varying conditions. Three different analyses have been made by varying one parameter, keeping other two parameters fixed. These are liquid-bridge volume, inter-particle distance and number of particle. The results have been plotted with both number of base particles and number of total particles in the failure block, for rise and fall of water level. All three cases show a positive influence on the escape velocity of the block. This is because though the microscopic forces reduce the effect of macroscopic forces (hydrostatic force and pore water pressure force), the macroscopic forces increase at a higher rate. So, by and large, the system escape velocity rises

giving the bank greater stability. It can also be observed that the increasing number of particles increases the escape velocity. This is a testimony of the fact that a bigger size chunk requires more forces to dislodge from the bank surface. Lastly, the graphs of escape velocity are plotted for different free surface heights for different number of total particles in the block to study the dynamic behaviour and its effect on the stability of the riverbank. With an increase in the free surface height from 0 to riverbank height ( $H$ ), the escape velocity and, hence the stability increases steadily.

Therefore, the newly devised macroscopic analysis has enough potential to play a significant role in the present scenario in terms of suggesting more generalised expressions for escape velocity to predict the stability of the riverbanks. This approach has the capability to incorporate variabilities associated with different riverbank systems of different nature. It can successfully complement the field studies and experimental investigations, being a reasonably robust theoretical approach. In a nut-shell, the present work analyzes the behaviour of a particle or a block subjected to changing circumstances. This may estimate the future scenario based on the present.

# TABLE OF CONTENTS

---

<b>Acknowledgement</b>	i
<b>Synopsis</b>	ii
<b>Table of Contents</b>	vii
<b>List of Figures</b>	ix
<b>List of Tables</b>	xx
<b>Nomenclature</b>	xxii
<b>Chapter 1: Introduction</b>	
1.1 Introduction	1.1
1.2 Literature Review	1.2
1.3 Purpose of Study	1.10
1.4 Objectives	1.11
<b>Chapter 2: Microscopic Analysis</b>	
2.1 Introduction	2.1
2.2 Force Calculation	2.3
2.2.1 Particle Cohesive Force	2.3
2.2.2 Particle Pore Pressure Force	2.5
2.3 Structure of the Model with Free-Body Diagram	2.6
2.4 Escape Velocity Calculation	2.8
2.5 Results	2.11
2.5.1 Escape Velocity Variation for Particles of Different Sizes	2.11
2.5.1.1 <i>Escape Velocity Variation for Water Level Rising</i>	2.11
2.5.1.2 <i>Escape Velocity Variation for Water Level Falling</i>	2.21
2.5.2 Escape Velocity Variation for Different Liquid-Bridge Volumes	2.31
2.5.2.1 <i>Escape Velocity Variation for Water Level Rising</i>	2.32
2.5.2.2 <i>Escape Velocity Variation for Water Level Falling</i>	2.42
2.6 Discussions	2.52
<b>Chapter 3: Macroscopic Analysis</b>	
3.1 Introduction	3.1
3.2 Force Calculation	3.3
3.2.1 Particle Cohesive Force	3.5
3.2.2 Particle Pore Pressure Force	3.7

3.2.3	Hydrostatic Confining Pressure Force	3.8
3.2.4	Weight of the failure block	3.9
3.3	Transformation of Microscopic Force System into Macroscopic Force System	3.9
3.3.1	For Water Level Rising	3.10
3.3.1.1	$F_x$ Calculation	3.11
3.3.1.2	$F_y$ Calculation:	3.16
3.3.2	For Water Level Falling	3.19
3.3.2.1	$F_x$ Calculation	3.21
3.3.2.2	$F_y$ Calculation:	3.24
3.4	Results	3.28
3.4.1	Escape Velocity Variation for Different Inter-Particle Distances	3.28
3.4.1.1	<i>Escape Velocity Variation with Number of Base Particles</i>	3.29
3.4.1.2	<i>Escape Velocity Variation with Number of Total Particles</i>	3.37
3.4.2	Escape Velocity Variation for Different Liquid-Bridge Volumes	3.45
3.4.2.1	<i>Escape Velocity Variation with Number of Base Particles</i>	3.45
3.4.2.2	<i>Escape Velocity Variation with Number of Total Particles</i>	3.53
3.4.3	Escape Velocity Variation for Different Size of Particles	3.61
3.4.3.1	<i>Escape Velocity Variation with Number of Base Particles</i>	3.61
3.4.3.2	<i>Escape Velocity Variation with Number of Total Particles</i>	3.69
3.4.4	Escape Velocity Variation with Free Surface Height	3.77
3.5	Discussions	3.81
<b>Chapter 4: Conclusion</b>		
4.1	Concluding Remarks	4.1
4.2	Future Scope	4.4
<b>References</b>		5.1

# LIST OF FIGURES

---

Figure No.	Caption	Page No.
<b>Chapter 2</b>		
<b>Fig. 2.1</b>	Dissimilar soil grains with toroid shaped entrapped inter-granular liquid-bridge	2.4
<b>Fig. 2.2</b>	Inter-particle water lens geometry for pore-pressure force measurement	2.5
<b>Fig. 2.3</b>	Groups of particles organised according to the “Truncated Pyramid Model” (showing a broader picture of the two adjoining particles)	2.6
<b>Fig. 2.4</b>	Particle 11’s Free-body diagram under different force conditions with moments about Instantaneous Centre <i>I</i> .	2.8
<b>Fig. 2.5</b>	Changes in escape velocity with inter-particle spacing for 0.390 mm particle radius in a fully exposed [ $e = 1.0$ ] scenario for rising river-water level	2.14
<b>Fig. 2.6</b>	Changes in escape velocity with inter-particle spacing for 0.395 mm particle radius in a fully exposed [ $e = 1.0$ ] scenario for rising river-water level	2.14
<b>Fig. 2.7</b>	Changes in escape velocity with inter-particle spacing for 0.400 mm particle radius in a fully exposed [ $e = 1.0$ ] scenario for rising river-water level	2.15
<b>Fig. 2.8</b>	Changes in escape velocity with inter-particle spacing for 0.405 mm particle radius in a fully exposed [ $e = 1.0$ ] scenario for rising river-water level	2.15
<b>Fig. 2.9</b>	Changes in escape velocity with inter-particle spacing for 0.410 mm particle radius in a fully exposed [ $e = 1.0$ ] scenario for rising river-water level	2.16
<b>Fig. 2.10</b>	Changes in escape velocity with inter-particle spacing for 0.390 mm particle radius in a half submerged [ $e = 0.5$ ] scenario for rising river-water level	2.16
<b>Fig. 2.11</b>	Changes in escape velocity with inter-particle spacing for 0.395 mm particle radius in a half submerged [ $e = 0.5$ ] scenario for rising river-water level	2.17

<b>Figure No.</b>	<b>Caption</b>	<b>Page No.</b>
<b>Fig. 2.12</b>	Changes in escape velocity with inter-particle spacing for 0.400 mm particle radius in a half submerged [ $e = 0.5$ ] scenario for rising river-water level	2.17
<b>Fig. 2.13</b>	Changes in escape velocity with inter-particle spacing for 0.405 mm particle radius in a half submerged [ $e = 0.5$ ] scenario for rising river-water level	2.18
<b>Fig. 2.14</b>	Changes in escape velocity with inter-particle spacing for 0.410 mm particle radius in a half submerged [ $e = 0.5$ ] scenario for rising river-water level	2.18
<b>Fig. 2.15</b>	Changes in escape velocity with inter-particle spacing for 0.390 mm particle radius in a fully submerged [ $e = 0.0$ ] scenario for rising river-water level	2.19
<b>Fig. 2.16</b>	Changes in escape velocity with inter-particle spacing for 0.395 mm particle radius in a fully submerged [ $e = 0.0$ ] scenario for rising river-water level	2.19
<b>Fig. 2.17</b>	Changes in escape velocity with inter-particle spacing for 0.400 mm particle radius in a fully submerged [ $e = 0.0$ ] scenario for rising river-water level	2.20
<b>Fig. 2.18</b>	Changes in escape velocity with inter-particle spacing for 0.405 mm particle radius in a fully submerged [ $e = 0.0$ ] scenario for rising river-water level	2.20
<b>Fig. 2.19</b>	Changes in escape velocity with inter-particle spacing for 0.410 mm particle radius in a fully submerged [ $e = 0.0$ ] scenario for rising river-water level	2.21
<b>Fig. 2.20</b>	Changes in escape velocity with inter-particle spacing for 0.390 mm particle radius in a fully exposed [ $e = 1.0$ ] scenario for falling river-water level	2.24
<b>Fig. 2.21</b>	Changes in escape velocity with inter-particle spacing for 0.395 mm particle radius in a fully exposed [ $e = 1.0$ ] scenario for falling river-water level	2.24
<b>Fig. 2.22</b>	Changes in escape velocity with inter-particle spacing for 0.400 mm particle radius in a fully exposed [ $e = 1.0$ ] scenario for falling river-water level	2.25

<b>Figure No.</b>	<b>Caption</b>	<b>Page No.</b>
<b>Fig. 2.23</b>	Changes in escape velocity with inter-particle spacing for 0.405 mm particle radius in a fully exposed [ $e = 1.0$ ] scenario for falling river-water level	2.25
<b>Fig. 2.24</b>	Changes in escape velocity with inter-particle spacing for 0.410 mm particle radius in a fully exposed [ $e = 1.0$ ] scenario for falling river-water level	2.26
<b>Fig. 2.25</b>	Changes in escape velocity with inter-particle spacing for 0.390 mm particle radius in a half submerged [ $e = 0.5$ ] scenario for falling river-water level	2.26
<b>Fig. 2.26</b>	Changes in escape velocity with inter-particle spacing for 0.395 mm particle radius in a half submerged [ $e = 0.5$ ] scenario for falling river-water level	2.27
<b>Fig. 2.27</b>	Changes in escape velocity with inter-particle spacing for 0.400 mm particle radius in a half submerged [ $e = 0.5$ ] scenario for falling river-water level	2.27
<b>Fig. 2.28</b>	Changes in escape velocity with inter-particle spacing for 0.405 mm particle radius in a half submerged [ $e = 0.5$ ] scenario for falling river-water level	2.28
<b>Fig. 2.29</b>	Changes in escape velocity with inter-particle spacing for 0.410 mm particle radius in a half submerged [ $e = 0.5$ ] scenario for falling river-water level	2.28
<b>Fig. 2.30</b>	Changes in escape velocity with inter-particle spacing for 0.390 mm particle radius in a fully submerged [ $e = 0.0$ ] scenario for falling river-water level	2.29
<b>Fig. 2.31</b>	Changes in escape velocity with inter-particle spacing for 0.395 mm particle radius in a fully submerged [ $e = 0.0$ ] scenario for falling river-water level	2.29
<b>Fig. 2.32</b>	Changes in escape velocity with inter-particle spacing for 0.400 mm particle radius in a fully submerged [ $e = 0.0$ ] scenario for falling river-water level	2.30
<b>Fig. 2.33</b>	Changes in escape velocity with inter-particle spacing for 0.405 mm particle radius in a fully submerged [ $e = 0.0$ ] scenario for falling river-water level	2.30



<b>Figure No.</b>	<b>Caption</b>	<b>Page No.</b>
<b>Fig. 2.34</b>	Changes in escape velocity with inter-particle spacing for 0.410 mm particle radius in a fully submerged [ $e = 0.0$ ] scenario for falling river-water level	2.31
<b>Fig. 2.35</b>	Changes in escape velocity with inter-particle spacing for 10 nl liquid-bridge volume in a fully exposed [ $e = 1.0$ ] scenario for rising river-water level	2.34
<b>Fig. 2.36</b>	Changes in escape velocity with inter-particle spacing for 15 nl liquid-bridge volume in a fully exposed [ $e = 1.0$ ] scenario for rising river-water level	2.35
<b>Fig. 2.37</b>	Changes in escape velocity with inter-particle spacing for 20 nl liquid-bridge volume in a fully exposed [ $e = 1.0$ ] scenario for rising river-water level	2.35
<b>Fig. 2.38</b>	Changes in escape velocity with inter-particle spacing for 25 nl liquid-bridge volume in a fully exposed [ $e = 1.0$ ] scenario for rising river-water level	2.36
<b>Fig. 2.39</b>	Changes in escape velocity with inter-particle spacing for 30 nl liquid-bridge volume in a fully exposed [ $e = 1.0$ ] scenario for rising river-water level	2.36
<b>Fig. 2.40</b>	Changes in escape velocity with inter-particle spacing for 10 nl liquid-bridge volume in a half submerged [ $e = 0.5$ ] scenario for rising river-water level	2.37
<b>Fig. 2.41</b>	Changes in escape velocity with inter-particle spacing for 15 nl liquid-bridge volume in a half submerged [ $e = 0.5$ ] scenario for rising river-water level	2.37
<b>Fig. 2.42</b>	Changes in escape velocity with inter-particle spacing for 20 nl liquid-bridge volume in a half submerged [ $e = 0.5$ ] scenario for rising river-water level	2.38
<b>Fig. 2.43</b>	Changes in escape velocity with inter-particle spacing for 25 nl liquid-bridge volume in a half submerged [ $e = 0.5$ ] scenario for rising river-water level	2.38
<b>Fig. 2.44</b>	Changes in escape velocity with inter-particle spacing for 30 nl liquid-bridge volume in a half submerged [ $e = 0.5$ ] scenario for rising river-water level	2.39

<b>Figure No.</b>	<b>Caption</b>	<b>Page No.</b>
<b>Fig. 2.45</b>	Changes in escape velocity with inter-particle spacing for 10 nl liquid-bridge volume in a fully submerged [ $e = 0.0$ ] scenario for rising river-water level	2.39
<b>Fig. 2.46</b>	Changes in escape velocity with inter-particle spacing for 15 nl liquid-bridge volume in a fully submerged [ $e = 0.0$ ] scenario for rising river-water level	2.40
<b>Fig. 2.47</b>	Changes in escape velocity with inter-particle spacing for 20 nl liquid-bridge volume in a fully submerged [ $e = 0.0$ ] scenario for rising river-water level	2.40
<b>Fig. 2.48</b>	Changes in escape velocity with inter-particle spacing for 25 nl liquid-bridge volume in a fully submerged [ $e = 0.0$ ] scenario for rising river-water level	2.41
<b>Fig. 2.49</b>	Changes in escape velocity with inter-particle spacing for 30 nl liquid-bridge volume in a fully submerged [ $e = 0.0$ ] scenario for rising river-water level	2.41
<b>Fig. 2.50</b>	Changes in escape velocity with inter-particle spacing for 10 nl liquid-bridge volume in a fully exposed [ $e = 1.0$ ] scenario for falling river-water level	2.44
<b>Fig. 2.51</b>	Changes in escape velocity with inter-particle spacing for 15 nl liquid-bridge volume in a fully exposed [ $e = 1.0$ ] scenario for falling river-water level	2.45
<b>Fig. 2.52</b>	Changes in escape velocity with inter-particle spacing for 20 nl liquid-bridge volume in a fully exposed [ $e = 1.0$ ] scenario for falling river-water level	2.45
<b>Fig. 2.53</b>	Changes in escape velocity with inter-particle spacing for 25 nl liquid-bridge volume in a fully exposed [ $e = 1.0$ ] scenario for falling river-water level	2.46
<b>Fig. 2.54</b>	Changes in escape velocity with inter-particle spacing for 30 nl liquid-bridge volume in a fully exposed [ $e = 1.0$ ] scenario for falling river-water level	2.46
<b>Fig. 2.55</b>	Changes in escape velocity with inter-particle spacing for 10 nl liquid-bridge volume in a half submerged [ $e = 0.5$ ] scenario for falling river-water level	2.47

<b>Figure No.</b>	<b>Caption</b>	<b>Page No.</b>
<b>Fig. 2.56</b>	Changes in escape velocity with inter-particle spacing for 15 nl liquid-bridge volume in a half submerged [ $e = 0.5$ ] scenario for falling river-water level	2.47
<b>Fig. 2.57</b>	Changes in escape velocity with inter-particle spacing for 20 nl liquid-bridge volume in a half submerged [ $e = 0.5$ ] scenario for falling river-water level	2.48
<b>Fig. 2.58</b>	Changes in escape velocity with inter-particle spacing for 25 nl liquid-bridge volume in a half submerged [ $e = 0.5$ ] scenario for falling river-water level	2.48
<b>Fig. 2.59</b>	Changes in escape velocity with inter-particle spacing for 30 nl liquid-bridge volume in a half submerged [ $e = 0.5$ ] scenario for falling river-water level	2.49
<b>Fig. 2.60</b>	Changes in escape velocity with inter-particle spacing for 10 nl liquid-bridge volume in a fully submerged [ $e = 0.0$ ] scenario for falling river-water level	2.49
<b>Fig. 2.61</b>	Changes in escape velocity with inter-particle spacing for 15 nl liquid-bridge volume in a fully submerged [ $e = 0.0$ ] scenario for falling river-water level	2.50
<b>Fig. 2.62</b>	Changes in escape velocity with inter-particle spacing for 20 nl liquid-bridge volume in a fully submerged [ $e = 0.0$ ] scenario for falling river-water level	2.50
<b>Fig. 2.63</b>	Changes in escape velocity with inter-particle spacing for 25 nl liquid-bridge volume in a fully submerged [ $e = 0.0$ ] scenario for falling river-water level	2.51
<b>Fig. 2.64</b>	Changes in escape velocity with inter-particle spacing for 30 nl liquid-bridge volume in a fully submerged [ $e = 0.0$ ] scenario for falling river-water level	2.51
<b>Chapter 3</b>		
<b>Fig. 3.1</b>	Free-body diagram of trapezoidal failure block alongside river water	3.4
<b>Fig. 3.2</b>	Dissimilar soil grains with toroid shaped entrapped inter-granular liquid-bridge	3.6

<b>Figure No.</b>	<b>Caption</b>	<b>Page No.</b>
<b>Fig. 3.3</b>	Particle arrangement with the different micro-level forces direction in trapezoidal failure block with $n$ number of base particles for water level rising	3.10
<b>Fig. 3.4</b>	Various micro-level forces with directions for water level rising for $n = 3$	3.11
<b>Fig. 3.5</b>	Particle arrangement with the different micro-level forces direction in trapezoidal failure block with $n$ number of base particles for water level falling	3.20
<b>Fig. 3.6</b>	Various micro-level forces with directions for water level falling for $n = 3$	3.21
<b>Fig. 3.7</b>	Escape velocity variation with number of base particles for inter-particle distance of 0.145 mm for water level falling	3.32
<b>Fig. 3.8</b>	Escape velocity variation with number of base particles for inter-particle distance of 0.150 mm for water level falling	3.32
<b>Fig. 3.9</b>	Escape velocity variation with number of base particles for inter-particle distance of 0.155 mm for water level falling	3.33
<b>Fig. 3.10</b>	Escape velocity variation with number of base particles for inter-particle distance of 0.160 mm for water level falling	3.33
<b>Fig. 3.11</b>	Escape velocity variation with number of base particles for inter-particle distance of 0.165 mm for water level falling	3.34
<b>Fig. 3.12</b>	Escape velocity variation with number of base particles for inter-particle distance of 0.145 mm for water level rising	3.34
<b>Fig. 3.13</b>	Escape velocity variation with number of base particles for inter-particle distance of 0.150 mm for water level rising	3.35
<b>Fig. 3.14</b>	Escape velocity variation with number of base particles for inter-particle distance of 0.155 mm for water level rising	3.35
<b>Fig. 3.15</b>	Escape velocity variation with number of base particles for inter-particle distance of 0.160 mm for water level rising	3.36
<b>Fig. 3.16</b>	Escape velocity variation with number of base particles for inter-particle distance of 0.165 mm for water level rising	3.36

<b>Figure No.</b>	<b>Caption</b>	<b>Page No.</b>
<b>Fig. 3.17</b>	Escape velocity variation with number of total particles for inter-particle distance of 0.145 mm for water level falling	3.40
<b>Fig. 3.18</b>	Escape velocity variation with number of total particles for inter-particle distance of 0.150 mm for water level falling	3.40
<b>Fig. 3.19</b>	Escape velocity variation with number of total particles for inter-particle distance of 0.155 mm for water level falling	3.41
<b>Fig. 3.20</b>	Escape velocity variation with number of total particles for inter-particle distance of 0.160 mm for water level falling	3.41
<b>Fig. 3.21</b>	Escape velocity variation with number of total particles for inter-particle distance of 0.165 mm for water level falling	3.42
<b>Fig. 3.22</b>	Escape velocity variation with number of total particles for inter-particle distance of 0.145 mm for water level rising	3.42
<b>Fig. 3.23</b>	Escape velocity variation with number of total particles for inter-particle distance of 0.150 mm for water level rising	3.43
<b>Fig. 3.24</b>	Escape velocity variation with number of total particles for inter-particle distance of 0.155 mm for water level rising	3.43
<b>Fig. 3.25</b>	Escape velocity variation with number of total particles for inter-particle distance of 0.160 mm for water level rising	3.44
<b>Fig. 3.26</b>	Escape velocity variation with number of total particles for inter-particle distance of 0.165 mm for water level rising	3.44
<b>Fig. 3.27</b>	Escape velocity variation with number of base particles for liquid-bridge volume of 10 nl for water level falling	3.48
<b>Fig. 3.28</b>	Escape velocity variation with number of base particles for liquid-bridge volume of 15 nl for water level falling	3.48
<b>Fig. 3.29</b>	Escape velocity variation with number of base particles for liquid-bridge volume of 20 nl for water level falling	3.49
<b>Fig. 3.30</b>	Escape velocity variation with number of base particles for liquid-bridge volume of 25 nl for water level falling	3.49
<b>Fig. 3.31</b>	Escape velocity variation with number of base particles for liquid-bridge volume of 30 nl for water level falling	3.50

<b>Figure No.</b>	<b>Caption</b>	<b>Page No.</b>
<b>Fig. 3.32</b>	Escape velocity variation with number of base particles for liquid-bridge volume of 10 nl for water level rising	3.50
<b>Fig. 3.33</b>	Escape velocity variation with number of base particles for liquid-bridge volume of 15 nl for water level rising	3.51
<b>Fig. 3.34</b>	Escape velocity variation with number of base particles for liquid-bridge volume of 20 nl for water level rising	3.51
<b>Fig. 3.35</b>	Escape velocity variation with number of base particles for liquid-bridge volume of 25 nl for water level rising	3.52
<b>Fig. 3.36</b>	Escape velocity variation with number of base particles for liquid-bridge volume of 30 nl for water level rising	3.52
<b>Fig. 3.37</b>	Escape velocity variation with number of total particles for liquid-bridge volume of 10 nl for water level falling	3.56
<b>Fig. 3.38</b>	Escape velocity variation with number of total particles for liquid-bridge volume of 15 nl for water level falling	3.56
<b>Fig. 3.39</b>	Escape velocity variation with number of total particles for liquid-bridge volume of 20 nl for water level falling	3.57
<b>Fig. 3.40</b>	Escape velocity variation with number of total particles for liquid-bridge volume of 25 nl for water level falling	3.57
<b>Fig. 3.41</b>	Escape velocity variation with number of total particles for liquid-bridge volume of 30 nl for water level falling	3.58
<b>Fig. 3.42</b>	Escape velocity variation with number of total particles for liquid-bridge volume of 10 nl for water level rising	3.58
<b>Fig. 3.43</b>	Escape velocity variation with number of total particles for liquid-bridge volume of 15 nl for water level rising	3.59
<b>Fig. 3.44</b>	Escape velocity variation with number of total particles for liquid-bridge volume of 20 nl for water level rising	3.59
<b>Fig. 3.45</b>	Escape velocity variation with number of total particles for liquid-bridge volume of 25 nl for water level rising	3.60
<b>Fig. 3.46</b>	Escape velocity variation with number of total particles for liquid-bridge volume of 30 nl for water level rising	3.60

<b>Figure No.</b>	<b>Caption</b>	<b>Page No.</b>
<b>Fig. 3.47</b>	Escape velocity variation with number of base particles for radius of particle of 0.390 mm for water level falling	3.64
<b>Fig. 3.48</b>	Escape velocity variation with number of base particles for radius of particle of 0.395 mm for water level falling	3.64
<b>Fig. 3.49</b>	Escape velocity variation with number of base particles for radius of particle of 0.400 mm for water level falling	3.65
<b>Fig. 3.50</b>	Escape velocity variation with number of base particles for radius of particle of 0.405 mm for water level falling	3.65
<b>Fig. 3.51</b>	Escape velocity variation with number of base particles for radius of particle of 0.410 mm for water level falling	3.66
<b>Fig. 3.52</b>	Escape velocity variation with number of base particles for radius of particle of 0.390 mm for water level rising	3.66
<b>Fig. 3.53</b>	Escape velocity variation with number of base particles for radius of particle of 0.395 mm for water level rising	3.67
<b>Fig. 3.54</b>	Escape velocity variation with number of base particles for radius of particle of 0.400 mm for water level rising	3.67
<b>Fig. 3.55</b>	Escape velocity variation with number of base particles for radius of particle of 0.405 mm for water level rising	3.68
<b>Fig. 3.56</b>	Escape velocity variation with number of base particles for radius of particle of 0.410 mm for water level rising	3.68
<b>Fig. 3.57</b>	Escape velocity variation with number of total particles for radius of particle of 0.390 mm for water level falling	3.72
<b>Fig. 3.58</b>	Escape velocity variation with number of total particles for radius of particle of 0.395 mm for water level falling	3.72
<b>Fig. 3.59</b>	Escape velocity variation with number of total particles for radius of particle of 0.400 mm for water level falling	3.73
<b>Fig. 3.60</b>	Escape velocity variation with number of total particles for radius of particle of 0.405 mm for water level falling	3.73
<b>Fig. 3.61</b>	Escape velocity variation with number of total particles for radius of particle of 0.410 mm for water level falling	3.74

<b>Figure No.</b>	<b>Caption</b>	<b>Page No.</b>
<b>Fig. 3.62</b>	Escape velocity variation with number of total particles for radius of particle of 0.390 mm for water level rising	3.74
<b>Fig. 3.63</b>	Escape velocity variation with number of total particles for radius of particle of 0.395 mm for water level rising	3.75
<b>Fig. 3.64</b>	Escape velocity variation with number of total particles for radius of particle of 0.400 mm for water level rising	3.75
<b>Fig. 3.65</b>	Escape velocity variation with number of total particles for radius of particle of 0.405 mm for water level rising	3.76
<b>Fig. 3.66</b>	Escape velocity variation with number of total particles for radius of particle of 0.410 mm for water level rising	3.76
<b>Fig. 3.67</b>	Escape velocity variation with free surface height for number of total particles of 20000	3.79
<b>Fig. 3.68</b>	Escape velocity variation with free surface height for number of total particles of 40000	3.79
<b>Fig. 3.69</b>	Escape velocity variation with free surface height for number of total particles of 60000	3.80
<b>Fig. 3.70</b>	Escape velocity variation with free surface height for number of total particles of 80000	3.80
<b>Fig. 3.71</b>	Escape velocity variation with free surface height for number of total particles of 100000	3.81



# LIST OF TABLES

---

Table No.	Caption	Page No.
<b>Chapter 2</b>		
<b>Table 2.1:</b>	Escape velocity variation for different particle sizes with inter-particle distance for water level rising	2.12
<b>Table 2.2:</b>	Escape velocity variation for different particle sizes with inter-particle distance for water level falling	2.22
<b>Table 2.3:</b>	Escape velocity variation for different liquid-bridge volumes with inter-particle distance for water level rising	2.32
<b>Table 2.4:</b>	Escape velocity variation with inter-particle distance for different liquid-bridge volumes for water level falling	2.42
<b>Chapter 3</b>		
<b>Table 3.1:</b>	$x$ -directional series values for first series	3.13
<b>Table 3.2:</b>	Newton's Forward Interpolation Chart for first series of $x$ -direction	3.13
<b>Table 3.3:</b>	$x$ -directional series values for second series	3.15
<b>Table 3.4:</b>	Newton's Forward Interpolation Chart second series of $x$ -direction	3.15
<b>Table 3.5:</b>	$y$ -directional series values	3.18
<b>Table 3.6:</b>	Newton's Forward Interpolation Chart of $y$ -direction	3.18
<b>Table 3.7:</b>	$x$ -directional series values	3.22
<b>Table 3.8:</b>	Newton's Forward Interpolation Chart of $x$ -direction	3.23
<b>Table 3.9:</b>	$y$ -directional series values	3.25
<b>Table 3.10:</b>	Newton's Forward Interpolation Chart of $y$ -direction	3.25
<b>Table 3.11:</b>	Escape velocity variation with number of base particles for different inter-particle distances	3.29
<b>Table 3.12:</b>	Escape velocity variation with number of total particles for different inter-particle distances	3.37
<b>Table 3.13:</b>	Escape velocity variation with number of base particles for different liquid-bridge volumes	3.45
<b>Table 3.14:</b>	Escape velocity variation with number of total particles for different liquid-bridge volumes	3.53

<b>Table No.</b>	<b>Caption</b>	<b>Page No.</b>
<b>Table 3.15:</b>	Escape velocity variation with number of base particles for different sizes particle	3.61
<b>Table 3.16:</b>	Escape velocity variation with number of total particles for different sizes particle	3.69
<b>Table 3.17:</b>	Escape velocity variation with free surface height	3.77

## Nomenclature

---

$d_p$	Inter-particle distance between two adjacent spherical particles (mm)
$R$	Radius of a spherical particle (mm)
$\sigma$	Surface tension coefficient (N / m)
$F_c$	Capillary cohesive force between two adjacent particles (N)
$\forall_l$	Inter-particle liquid bridge volume (nl)
$\emptyset$	Angle of contact ( $^\circ$ )
$F_p$	Pore pressure force (N)
$P_p$	Pore water pressure (N / m <sup>2</sup> )
$\beta$	Water content index angle ( $^\circ$ )
$\rho$	Water density (kg / m <sup>3</sup> )
$\rho_s$	Soil grain material density (kg / m <sup>3</sup> )
$g$	Gravitational acceleration (m / s <sup>2</sup> )
$\theta$	Angle of contact between solid and liquid interface ( $^\circ$ )
$\gamma_w$	Specific weight of water (N / m <sup>3</sup> )
$I$	Instantaneous Centre
$F_x$	Hydrostatic force per unit length in a horizontal plane (N / m)
$F_y$	Hydrostatic force per unit length in a vertical plane (N / m)
$W$	The fluid block's weight per unit length (N / m)
$F_R$	Resultant hydrostatic force per unit length (N / m)
$\alpha$	Angular acceleration (rad / s <sup>2</sup> )
$e$	Degree of exposure

$H$	Height of the tension crack (m)
$b$	Base width of the failure block (m)
$w$	Top width of the failure block (m)
$H_w$	Free surface water column height of the river (m)
$F_{cp}$	Hydrostatic confining pressure force (N)
$F_{cpx}$	$x$ -directional hydrostatic confining pressure force (N)
$F_{cpy}$	$y$ -directional hydrostatic confining pressure force (N)
$F_g$	Net weight of the failure block (N)
$n$	Number of base particles in the failure block
$N$	Total number of particles in the failure block
$x_o$	$x$ -coordinate of centre of gravity (mm)
$y_o$	$y$ -coordinate of centre of gravity (mm)
$A_w$	Volume of water entrapped per unit length in $z$ -direction (mm <sup>2</sup> )
$A_s$	Total particles surface area (mm <sup>2</sup> )
$a_s$	Surface area of a particle (mm <sup>2</sup> )
$d_t$	Average diameter of the tube (mm)
$F_x$	$x$ -directional macroscopic force (N)
$F_y$	$y$ -directional macroscopic force (N)
$f$	Resultant impending acceleration (m / s <sup>2</sup> )
$V_{esc}$	Escape velocity (m / s)

**CHAPTER 1**  
**INTRODUCTION**

# Chapter 1

## Introduction

### 1.1 Introduction

Riverbank erosion has long had a significant impact on civilization, particularly with regard to agriculture, human settlement, and flood defence. Man-made facilities are also destroyed by land loss resulting from local riverbank collapse. The researchers are therefore very keen to learn more about the riverbank's stability. The result of bank erosion is riverbank failure. Alluvial terraces and productive floodplains were created over time as a result of riverbank erosion, a natural process. In actuality, some of the banks of even stable river systems are eroding. However, compared to unstable systems, erosion often happens at a considerably slower rate and smaller scale in stable systems. Rivers and streams can undergo abrupt, dramatic alterations due to natural disasters like flooding. Moreover, stream management and land usage might set off erosion reactions. The reactions can be complicated, sometimes impairing stability for decades and frequently leading to faster rates of disintegration. Bank erosion is hastened by management practices such as improper catchment use and deforestation, ill-managed extraction of sand and gravel, and projects affecting the natural course of flow of the stream.

Bank scour and mass failure are the two broad categories into which the different mechanisms of stream bank erosion can be divided. Both will frequently be present in cases of bank instability, with either scour or mass failure predominating. The erosive strength of flowing water rises with flow speed, and scour may occur. A clear indication of scour processes is undercutting of the bank toe. The main goals of

effective scour management techniques are to reduce flow velocity through strategically placed vegetation and, in certain situations, bank stabilisation engineering.

The term “mass failure” refers to the several bank erosion mechanisms that cause portions of the bank to slide or topple into the stream. Collapse or slumping are common terms used to describe mass failure. The most visible indications of these processes are sections of slumping bank materials or bare, nearly vertical banks. Although the causes of these kinds of failures are frequently unclear, human and/or natural factors may be involved.

## **1.2 Literature Review**

The riverbed does not deteriorate or worsen while it is in dynamic equilibrium, although erosion can occur on the riverbanks for a variety of reasons that lead to bank instability. Odgaard and Mosconi (1987)<sup>1</sup> dealt with erosion control with submerged vanes for an Iowan stream bend. Odgaard (1987)<sup>2</sup> linked the rate of riverbank erosion with the stream flow depth near the bank. The main aim was to lessen or eliminate the flow's helical motion, which was the primary source of bank undermining. The summer of 1985 saw the installation of the system. Data gathered from surveys conducted in the spring of 1986 was used to assess its performance. Planar bank stability was hypothesised by Osman and Thorne (1988)<sup>3</sup>, Beeson and Doyle (1995)<sup>4</sup> through a field study evaluated the bends in the four stream reaches affected due to floods causing extensive riverbank erosion. It was discovered that the likelihood of measurable erosion occurring during flood events was almost five times higher in bends devoid of riparian vegetation compared to those with vegetation. By incorporating hydrostatic pressure and pore-water pressure, Darby and Thorne (1996)<sup>5</sup>

created a new model that can be used to estimate the failure surface of steep, cohesive, non-layered riverbanks. The ability of their method to forecast the riverbanks' stability in the event of a mass failure has been successfully demonstrated. Darby and Thorne (1996)<sup>6</sup> devised a probabilistic approach to predict the longitudinal extent of mass failures by employing mixed layer theory. Darby and Thorne (1996)<sup>7</sup> expanded the scheme given by Osman and Thorne by taking into account hydrostatic confining pressure and pore-water pressure terms. The basic transport modes are identified as bed and suspended load by Coufal (1997)<sup>8</sup>. Wash load can be considered part of the suspended load or can be treated separately. For river engineering; both suspended and bed loads provoke morphology changes of the bottom. Nevertheless the contribution of bed load can be more significant, above all if the uppermost soil layer of the river bed behaves as an active layer. Total bed load is the part of the sediment movement forming a continuous contact with the channel bottom. Suspended loads are generally the dominant transport mode in lower river reaches or in tidal rivers where fine sediment beds prevail. According to Abernethy and Rutherford (1998)<sup>9</sup>, wind-thrown trees in the upper reaches are mostly to blame for the transfer of bank silt to the flow. The importance of vegetation-induced flow resistance increases in situations when the primary erosion mechanism is the direct entrainment of bank material by rivers. Vegetation plays a vital role in stabilising banks in reaches where bank slumping is the predominant erosion process because it increases bank shear strength due to root reinforcement. The slumping process was shown to be mostly unaffected by other factors, such as tree surcharge and changed bank hydrology. Fripp et al. (1998)<sup>10</sup> classified the bed and bank stability as well as the possibility for bank erosion qualitatively using a visual hydraulic assessment. Rinaldi M. & Casagli N. (1999)<sup>11</sup> worked on partially saturated soils formed bank



stability and adverse pore water pressure impacts on Italy's Sieve River. An analytical model dealing with sediments suspended and carried with the stream was combined with inter-decadal aerial photography, inter-seasonal field observations of riverbank stability, river water flow, impacts on clarity of water by Green et al. (1999)<sup>12</sup>. They validated their field study data with a source term in their transport model. A computational stability investigation of steep cohesive riverbanks was carried out by Darby et al. (2000)<sup>13</sup>. Pitois et al. (2001)<sup>14</sup> proposed a function that takes capillary and viscous forces into account when calculating the energy of rupture of a liquid-bridge between two spheres. Likos and Lu (2002)<sup>15</sup> have developed some successive series of equations for the purpose of describing the inter-granular forces due to negative pore-water pressure for spherical particles. Rim and Gay (2002)<sup>16</sup> calculated the soil moisture content on daily basis for two watersheds applying energy balance and analysis of water budget. Their findings proved that basic measures of the energy and water balance can provide reliable estimates of soil moisture in small watersheds. Darby and Delbono (2002)<sup>17</sup>, in their study, devised a model for analysis of flow characteristics, sediment transport and topography of the river bed. Their model evolved through a comparative analysis of the observed and anticipated bed topography in two study reaches. It was discovered that, at least in the vicinity of bend apices, model predictions of bed topography were satisfactory. A new stream flow and sediment transport simulation model related to water quality was proposed by Zeng and Beck (2003)<sup>18</sup>. Pyle et al. (2003)<sup>19</sup> showed digital photogrammetry use for the extraction of high resolution digital elevation models (DEMs) of rapidly deteriorating riverbanks from terrestrial oblique stereo-pairs in context with Erdas Imagine-a simulation tool. Johanson et al. (2003)<sup>20</sup> proposed a theory related to bulk material cohesive nature. One of the river systems in North America most heavily

contaminated with mercury is the Carson River in west-central Nevada, where Carroll et al. (2004)<sup>21</sup> conducted research. Sediment transport mechanisms, especially during overbank flows, were primarily responsible for the mercury's passage through that system. Floodplain deposits and channel bank debris are linked to the majority of that mercury. They added the "divided channel approach" to an existing hydrodynamic model for simulation of extreme scenarios and prediction of floodplain depths and velocities. Jang and Shimizu (2005)<sup>22</sup> created a two-dimensional numerical model to mimic the processes of channel evolution for a straight river having higher width-to-depth ratio and non-cohesive riverbanks. They described a naturally shaped boundary using a movable boundary-based reference frame, presuming that bank erosion and sediment deposition take place in the lateral direction. A high-order Godunov scheme was used to determine the flow field. Duan (2005)<sup>23</sup> asserted and demonstrated in her analytical model that the suspended weight of the particle, the force of cohesion, and the lift force acting on a grain - all are significant while maintaining dynamic equilibrium. A force analysis may be used to calculate the speed of the sediment particle tending to separate. She proved that the cohesive force depends on many parameters related to bank having a significant impact on the phenomenon of bank erosion. A study was conducted by Kotoky et al. (2005)<sup>24</sup> on a specific section of the Brahmaputra river channel. They discovered that high slope, effect of weathering on the water content in the soil, sediment flow and heterogeneity of bank materials are the key factors involved and responsible for riverbank erosion. They opined that the primary causes of bank erosion processes were variations in the scale and kind of shear failure. Soulie et al. (2006)<sup>25</sup> suggested a relation between the acting forces and the irregular radii of the particles' geometric characteristics. Larsen et al. (2006)<sup>26</sup> correlated the stream power with the riverbank erosion. They established relationships

between the daily flow rates of a river and the rates of bank erosion. Lenzi et al. (2006)<sup>27</sup> proposed a method to find the discharge in effect with relation to the sediment transport for a mountainous river. To get more insight into the conditions that lead to channel formation in streams with boulder beds and steep gradients, they made a rigorous field study in the Italian Alps. Meunier et al. (2006)<sup>28</sup> studied a proglacial river and measured the sediment load. A significant landslide caused a braided plain to form, creating a condensed and easy-to-understand study area. The braided plain's exit was found to have a mass balance. They found that suspension was the predominant route of conveyance throughout the domain of measurement. Julian and Torres (2006)<sup>29</sup> conducted a study to identify and evaluate the controls on erodibility of a cohesive riverbank. The context of bank erosion was established at three transects using the values of some independent factors. According to their findings, flow peak intensities determine how much hydraulic erosion occurs on cohesive riverbanks. Ultimately, this led to development of a model for calculation of erosion rates of riverbanks having mixed constituents of silt and clay. Osman and Thorne's (1988)<sup>7</sup> work was expanded further by Darby and Thorne (2006)<sup>30</sup>, who highlighted the fallout of the development of a tension crack on bank stability. They illustrated a numerical process needed to apply the model with a case study. Amiri-Tokaldany, E., and Darby, S. E. (2006)<sup>31</sup> created their models for analysing the stability for layered riverbanks. The impacts of a positive pore water pressure on the saturated portion of the bank and a negative pore water pressure on the unsaturated one are taken into account in the new model. Furthermore, taken into consideration are the impacts of water in tension cracks and the confining pressure, hydrostatic by nature, brought on by the stream water level on the stability analysis. They evaluated their model using field data sets from two locations. The findings indicate that there was some

consistency between the observed and projected values of bank stability. Richefeu et al. (2007)<sup>32</sup> came out with a three-dimensional method applicable to numerical analysis of a wet-particle medium. The fundamental laws and principles of friction, enhanced by an inter-particle capillary force, served as the foundation of their method. They demonstrated how the latter may be stated as a distinct, fundamental function of the volume of the liquid-bridge and the gap between two spherical grains. The Laplace-Young equation's direct integration was used to compare and analyse the scales of length pertaining to the developed expression. They applied that method to straightforward compression loadings and direct shear loadings to demonstrate and validate it. The sediment load of an Algerian river was measured by Achite and Ouillon (2007)<sup>33</sup> over a span of twenty-two hydrological years (1973–1995). 1432 paired data were used to build regression associations between the concentration of suspended particles and water discharge. They discovered a strong correlation between the mean annual suspended sediment production and the annual mean daily discharge standard deviation. Because of this extremely considerable inter-annual variability, they had trouble determining an appropriate timeframe for the purpose of calculating a reference value for sediment budgets. In order to examine fluctuations in the context of climate changes, they decided it was necessary to carry out a series of measurements over an extended period of time. A 3-D finite-volume morpho-dynamic model for simulation of stream flow and sediment transport in a curved open channel with non-flexible walls was devised by Khosronejad et al. (2007)<sup>34</sup>. Riverbed material and corresponding load fractions were distinguished using a mixed-size grain transport function by Amiri-Tokaldany et al. (2007)<sup>35</sup>, who linked deformation of a river bed with bank erosion. To demonstrate the procedure, they integrated the bank stability analysis with Bridge's (1992) model for equilibrium bed topography. In order

to estimate the critical strength for erosion and the other parameters related to fluvial erosion, Papanicolaou et al. (2007)<sup>36</sup> came out with an approach that enables an acceptable description of the shear stress distribution near the riverbank in presence of secondary currents. It was demonstrated in their investigation that the depth-averaged measure of the side-wall shear stress was quadrupled in presence of secondary currents. The ratio of the maximum to the depth-averaged measure of the side-wall shear stress was shown to be more than five. The results of their study indicated that, while natural channels with complicated geometries may not benefit from using the depth-averaged measure of the side-wall shear stress as a reliable estimate of the fluid shear stress value, simpler geometries might. Mu and Su (2007)<sup>37</sup> analysed liquid bridge between spherical particles with Newtonian fluid. Assuming perfect wet condition they have analysed the effects of separation distance and liquid volume on liquid-bridge of static type. They also studied the relation between liquid-bridge volume and rupture energy. In order to replicate the migration processes of a meandering river, Chen and Duan (2008)<sup>38</sup> applied a two-dimensional depth-averaged numerical model. The model was combined with a newly created bank erosion model. Bank collapse, lateral erosion, and bed degradation all affect the rate of erosion of a riverbank. Unlike other models, this one linked the rate of erosion to both stream and sediment flows near the bank. The calculation of the rate of bank erosion also took into account the height of the bank, the slope, and the thickness of a pair of layers in the surface of a riverbank. Singh and Kundu (2008)<sup>39</sup> measured the erosion index for surface and subsurface layers of twenty six soil subgroups of eastern India. They found highest value of erosion index in 0-15 cm layers. According to the results found by them erosion index had decreased with soil depth. They calculated the correlation coefficient of the erosion index with different properties of soil. They suggested, on

the basis of their findings, that all soil subgroups of eastern India require some soil and water conservation measures. Zhang et al. (2008)<sup>40</sup>, in their design, a compliant MEMS device actuates two flat, smooth parallel plates that house a liquid inside a capillary bridge. The plates were actuated sinusoidally. To analyse the data, approximate closed-form equations that account for both capillary forces and viscoelastic flow are created. Also it contained a water quality component incorporated into it that was not there at that time in the other models. Using the updated Revised Morgan, Morgan, and Finney (RMMF) model, Velmurugan et al. (2008)<sup>41</sup> conducted a study to evaluate the risk of spatial soil erosion in the Andaman Islands. Using observations from field plots, they calibrated the model, and it projected soil loss that was relatively close to the observed value. Additionally, during agriculture, particularly under plantation crops on the upper slopes, the model predicted comparatively increased soil erosion. They recommended taking certain conservation steps to minimise soil loss and stop erosion as much as feasible. Greimann et al. (2008)<sup>42</sup> developed an unsteady total load equation to apply in depth-averaged models used to analyse sediment transport. “Truncated Pyramid Model” for the orientation of particles was proposed by Mukherjee and Mazumdar (2010)<sup>43</sup>. They have studied the impact of the inter-grain separation length on the erosion along a bank of river under the action of cohesive force. They have shown that the escape velocity is a function of separation distance between sediment particles for cohesive soil. Mukherjee (2011)<sup>44</sup> applied “Truncated Pyramid Model” to find particle escape velocity for different sizes of the particle under different volume of liquid-bridge entrapped between the particles. K. El KadiAbderrezzak et al. (2014)<sup>45</sup> introduced and discussed the impacts of a specific scaling approach in case of heterogeneous grain size. This method looked into the starting movement for every grain size class and the

bank stability coefficient between the model and the prototype while loosening the strong similarity requirements for the Shields number as well as the grain Reynolds number. The linear viscoelastic characteristic of small quantities of a fluid was measured by Bravo et al. (2014)<sup>46</sup> have presented a numerical technique for the early movement of sediment beyond bed forms. They used the discrete element method (DEM) as the foundation for their approach, modelling the landform's micromechanics as a collection of inflexible spheres reacting through friction and contact. In order to forecast the boundary shear stress field caused by the fluid flow, which results in drag and lift forces acting over the particles, they have used the continuous finite element approximation. They have compared the numerical outcomes with Shields' replicating results. In the laboratory settings, critical conditions have been evaluated for incipient motions of cohesive sediment by Zhang and Yu (2017)<sup>47</sup>. By adjusting various water level circumstances, Thi and Minh (2019)<sup>48</sup> evaluated river stability and calculated the hydraulic erosion rate numerically. From 1979 through 2019, the annual bank erosion on the underwater erosion map was monitored at several cross sections along the western United States' free-flowing, meandering Powder River by Moody (2022)<sup>49</sup>.

### **1.3 Purpose of Study**

Studying the stability analysis of the riverbank in a dynamic flow scenario with fluctuating water levels is the primary goal of this work. The two categories into which this study has been divided are micro-analysis of the riverbank system and macro-analysis of the riverbank system. Firstly, taking into account the microscopic forces, a micro-analysis of the particle has been conducted considering well established “Truncated-Pyramid Model” meant for microscopic arrangement of

particles. Particle escape velocity has been calculated to assess how various microscopic forces affect the stability of the riverbank system. In order to provide visual representations of the stability under various circumstances, the escape velocity change with various parameters, including the water-bridge volume, grain (particle) diameter, and inter-grain distance, has been plotted. To investigate the dynamic behaviour under various water level circumstances both the situations of water level rising and falling have been investigated.

Secondly, a right-angled trapezoidal tension crack failure block has been investigated in order to examine macro-analysis. Using a newly invented method, the microscopic forces in this instance have been converted into a macroscopic force system as a function of number of particles for tends to infinite number of particles using Newton's forward interpolation series calculation, and the various macroscopic forces have also been taken into consideration while analysing the stability in terms of escape velocity. It has been studied how the escape velocity changes as the number of particles in the tension fracture varies. To evaluate the dynamic behaviour of the riverbank system, here, changing water level situations were investigated as well for both the circumstance of increasing and dropping water level.

## **1.4 Objectives**

The principal goals of this research are

- Determination of the escape velocity of the particles for microscopic particle arrangement using conservation of angular-momentum principle with different particle radii keeping liquid-bridge volume at a fixed value for three different degrees of exposure for both the situations of water level rising and falling.



- Determination of the escape velocity of the particles for microscopic particle arrangement using conservation of angular-momentum principle with different liquid-bridge volumes keeping particle radius at a fixed value for three different degrees of exposure for both the situations of water level rising and falling.
- Determination of the escape velocity of the particles for macroscopic particle arrangement using newly invented method of transformation of microscopic forces into macroscopic force system for different inter-particle distances keeping particle diameter and water-bridge volume at fixed value for both the situations of water level rising and falling.
- Determination of the escape velocity of the particles for macroscopic particle arrangement using newly invented method of transformation of microscopic forces into macroscopic force system for different liquid-bridge volumes keeping distance between a pair of particles and particle diameter at a fixed value for both the situations of water level rising and falling.
- Determination of the escape velocity of the particles for macroscopic particle arrangement using newly invented method of transformation of microscopic forces into macroscopic force system for different particle sizes keeping inter-particle distance and water-bridge volume at fixed value for both the situations of water level rising and falling.
- Determination of the escape velocity of the particles for macroscopic particle arrangement using newly invented method of transformation of microscopic forces into macroscopic force system for different free surface heights for different number of total particles in the block to study the dynamic behaviour

and its effect on the stability of the riverbank for both the situations of water level rising and falling.

**CHAPTER 2**  
**MICROSCOPIC ANALYSIS**

## **Chapter 2**

### **Microscopic Analysis**

#### **2.1 Introduction**

The river system and flood protection have taken its toll on human habitat and civilisation as a whole from ancient times to the present. The majority of civilizations grew up around river streams in order to support human existence and economic development. Because of the concomitant loss of land, riverbank failure damages man-made infrastructure. It is evident from historical accounts that the majority of civilisations collapsed as a result of either flooding or erosion of riverbanks. Thus, experts have grown interest in analysing riverbank stability since the dawn of civilisation.

The majority of studies conducted in the subject of riverbank stability are based on experimental findings, which are essentially various case studies connected to a specific river system. For the other river systems, the conclusions pertaining to a particular river have very little physical significance. Also, these kinds of experiments require large investments and consume time. Therefore, it is necessary to determine universal expressions for riverbank stability that can apply to every type of river system and require less time and money for research. Thus, an analytical method may prove to be a more universally viable option. The volumetric rate of erosion has been determined through microscopic study in relation to escape velocity, which is thought to be the most important parameter for determining the stability of bank surfaces. The rate of bank material deterioration is measured by particle escape velocity. Reduced

escape velocity translates into a larger volumetric erosion rate, which denotes reduced riverbank stability.

The intricate process of riverbank erosion involves multiple forces acting on the bank particles. Erosion causes land loss and jeopardises flood protection. In comparison to unstable systems, stable systems erode on a much smaller scale. Over time, a river's flow direction changes. The intricate nature of bank failure is the outcome. These are mostly topics for experimentation, maybe for an extended period of time with certain constraints. Conversely, a theoretical method focuses mostly on force analysis. It is guided by the dynamics of river flow. Here, a study of the particle arrangement using the already published “Truncated pyramid model (TPM)” has been studied. The inter-granular cohesive force, hydrostatic force, pore water pressure force, and submerged particle weight are the forces that are taken into account.

Plans have been made to conduct analysis on half-exposed, fully immersed, and fully exposed particles vis-a-vis instances of rising and falling water levels with various particle sizes and different liquid-bridge volumes. Rather than using linear momentum as previously considered, the concept of conservation of angular momentum is used to find the particle escape velocity and how it varies for different particle sizes depending on the water concentration and inter-particle spacing.

This study examines how the dynamic behaviour of confined water affects bank soil particle erosion as a function of rising and falling water levels. Water level fluctuations have a direct impact on the rate of bank erosion in terms of escape velocity at the macro and micro-levels, which is ultimately a major contributing factor to mass failure. Consequently, the hydraulic natures of the river and bank erosion are directly correlated in this study.

## 2.2 Force Calculation

This section considers the forces at the microscopic level: the submerged particle weight, the hydrostatic force, the pore water pressure force, and the inter-granular cohesive force.

### 2.2.1 Particle Cohesive Force

Considering toroidal or parabolic structured liquid-bridge between the two adjacent grains, an expression for the calculation of cohesive force was developed by Soulie et al. (2006)<sup>25</sup> for two dissimilar grains. Two different sized particles with radii  $R_1$  and  $R_2$  and the inter-particle gap of  $d_p$  have been shown in Fig. 2.1 and the expression developed by them is as follows

For two different grains, Soulie et al. (2006)<sup>25</sup> produced a formula to calculate cohesive force, taking into consideration a toroidal or parabolic constructed liquid-bridge between the two adjacent grains. Fig. 2.1 depicts two distinct particle sizes with radii of  $R_1$  and  $R_2$ , as well as the inter-particle gap of  $d_p$ . The expression of the cohesive force is as follows:

$$F_c = \sigma \times \pi \times \sqrt{R_1 \times R_2} \times \left[ \exp \left\{ A \times \left( \frac{d_p}{R_{max}} \right) + B \right\} + C \right] \quad (2.1)$$

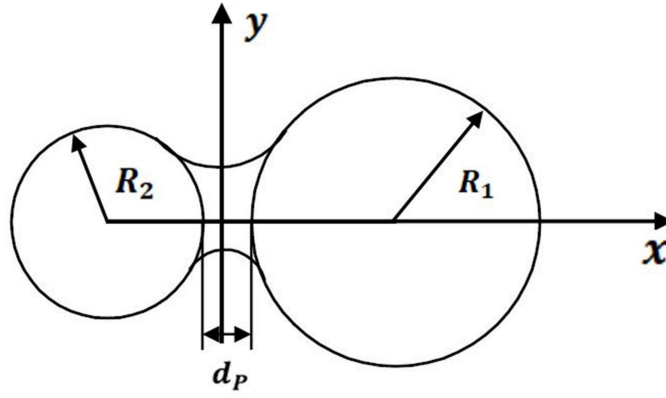


**Fig. 2.1** Dissimilar soil grains with toroid shaped entrapped inter-granular liquid-bridge [Soulie et al. (2006)<sup>25</sup>]

$F_c$  has been used to represent the capillary cohesive force between two different grains in this instance. Additionally,  $\sigma=0.073$  N/m (pure water) has been used to denote the surface tension coefficient. This expression can be simplified, by taking equal particle sizes into account, as

$$F_c = \sigma \times \pi \times R \times \left[ \exp \left\{ A \times \left( \frac{d_p}{R} \right) + B \right\} + C \right] \quad (2.2)$$

The parameters A, B, and C are dependent on the inter-granular liquid-bridge volume ( $\forall_l$ ) and grain radius ( $R$ ). The following expressions can be used to assess A, B, and C:

$$A = -1.1 \times (\forall_l / R^3)^{(-0.53)} \quad (2.3a)$$

$$B = \left[ 0.48 - 0.0082 \times \ln \left( \frac{\forall_l}{R^3} \right) - \left\{ 0.96 + 0.148 \times \ln \left( \frac{\forall_l}{R^3} \right) \right\} \times \emptyset^2 \right] \quad (2.3b)$$

$$C = \left[ 0.078 + 0.0018 \times \ln \left( \frac{\forall_l}{R^3} \right) \right] \quad (2.3c)$$

Here,  $\emptyset$  represents the angle of contact. It has been considered to be  $0^\circ$  for pure water.

### 2.2.2 Particle Pore Pressure Force

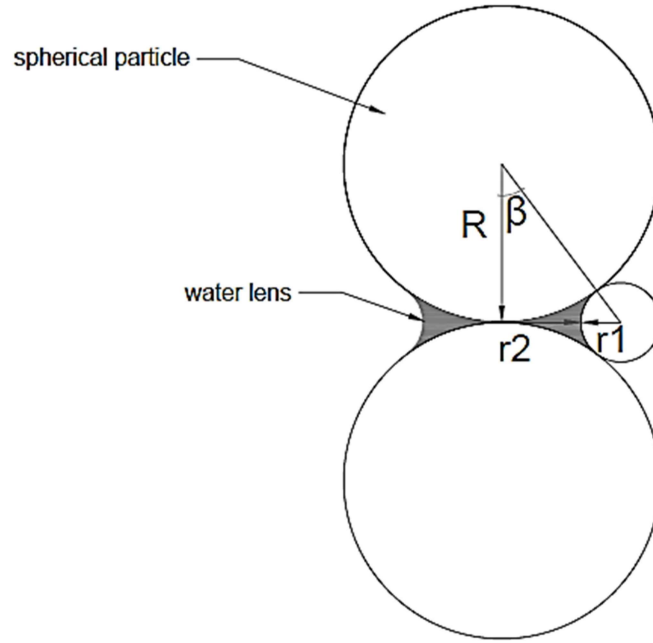


**Fig. 2.2** Inter-particle water lens geometry for pore pressure force measurement

The following equations, which were developed by Likos and Lu (2002)<sup>15</sup>, can be used to determine the induced pore pressure force for fully saturated soil grains:

$$F_p = \pi \times P_w \times r_2^2 + 2 \times \pi \times \sigma \times r_2 \quad (2.4)$$

Here, the pore water pressure  $P_w$  has been considered as 10 kPa [Likos and Lu (2002)<sup>15</sup>] and

$$r_2 = R \times [\tan \beta - \sec \beta + 1] \quad (2.5)$$

Here,  $\beta$  = Water content index angle =  $45^\circ$  for fully saturated particles [Likos and Lu (2002)<sup>15</sup>].



## 2.3 Structure of the Model with Free-Body Diagram

The forces acting on the particle in this instance, such as the hydrostatic force, pore pressure force, capillary cohesive force, and the particle's submerged weight, have all been analysed using the “Truncated Pyramid Model (TPM)”. Three distinct levels of particle exposure scenarios, such as fully submerged ( $e=0$ ) scenario, half submerged ( $e=0.5$ ) scenario, and fully exposed ( $e=1.0$ ) scenario, have been evaluated for both rising and falling water levels. Utilising the conservation of angular momentum theorem, the particle's escape velocity has been measured. Fig. 2.3 illustrates the configuration of particles in the “Truncated Pyramid Model (TPM).”

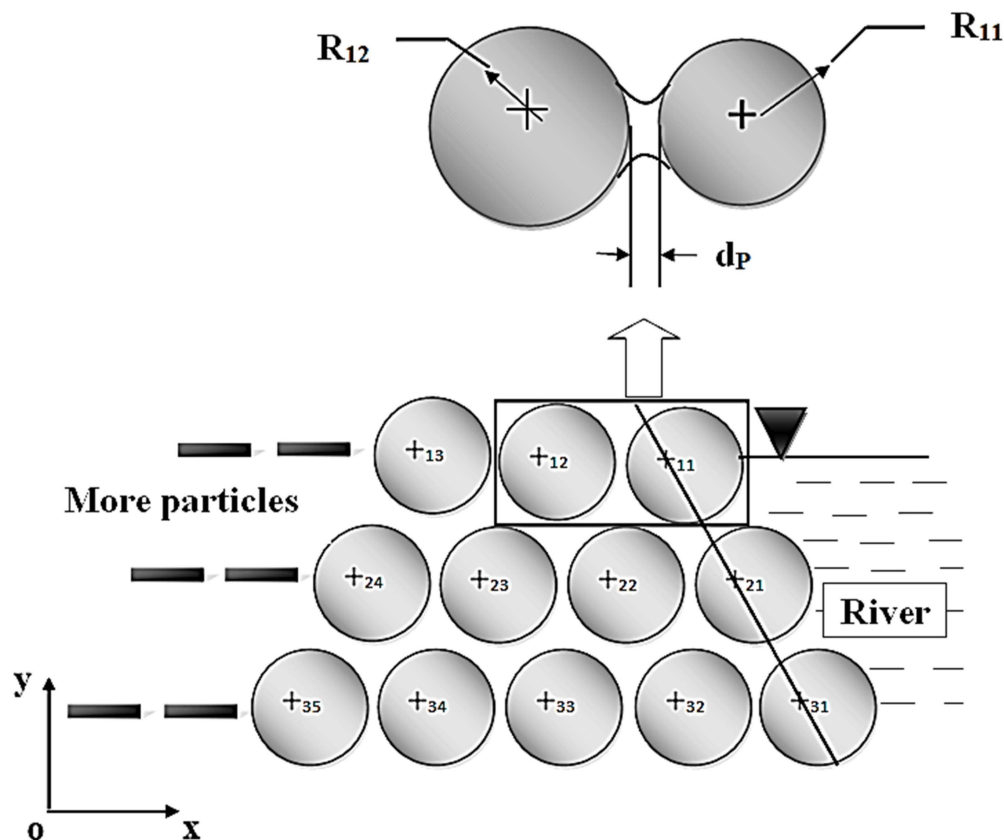


**Fig. 2.3** Groups of particles organised according to the “Truncated Pyramid Model”

(showing a broader picture of the two adjoining particles)

In this model, when a small amount of water settles on top of two neighbours, it is anticipated to get stuck between the inter-grain gaps between each spherically formed particle, creating a pyramidal bank structure. Grain size enhancement is generally considered to occur in both the negative x- and negative y-direction (Fig. 2.3). This implies the fact that river side particle is most vulnerable with respect to detachment from the bank surface. The average particle size has served as the foundation for the current investigation. For the force study, the uppermost and rightmost particle (Particle 11) has been considered since it is the most fragile. There has been no consideration of the force of friction between the spherical particle and the water, and it has been assumed that the material is isotropic. Fig. 2.4 displays the particle 11's free body diagram. The particle 11 tilts towards the point  $I$ , its instantaneous centre of rotation. Thus, in order to compute the expression of angular acceleration using the conservation of angular momentum theorem, the moment has been taken for all of the forces with respect to that particular location (point  $I$ ) has been taken into consideration. After that, linear acceleration has been calculated, and lastly, the escape velocity has been calculated because it depends on the particle's radius and linear velocity.

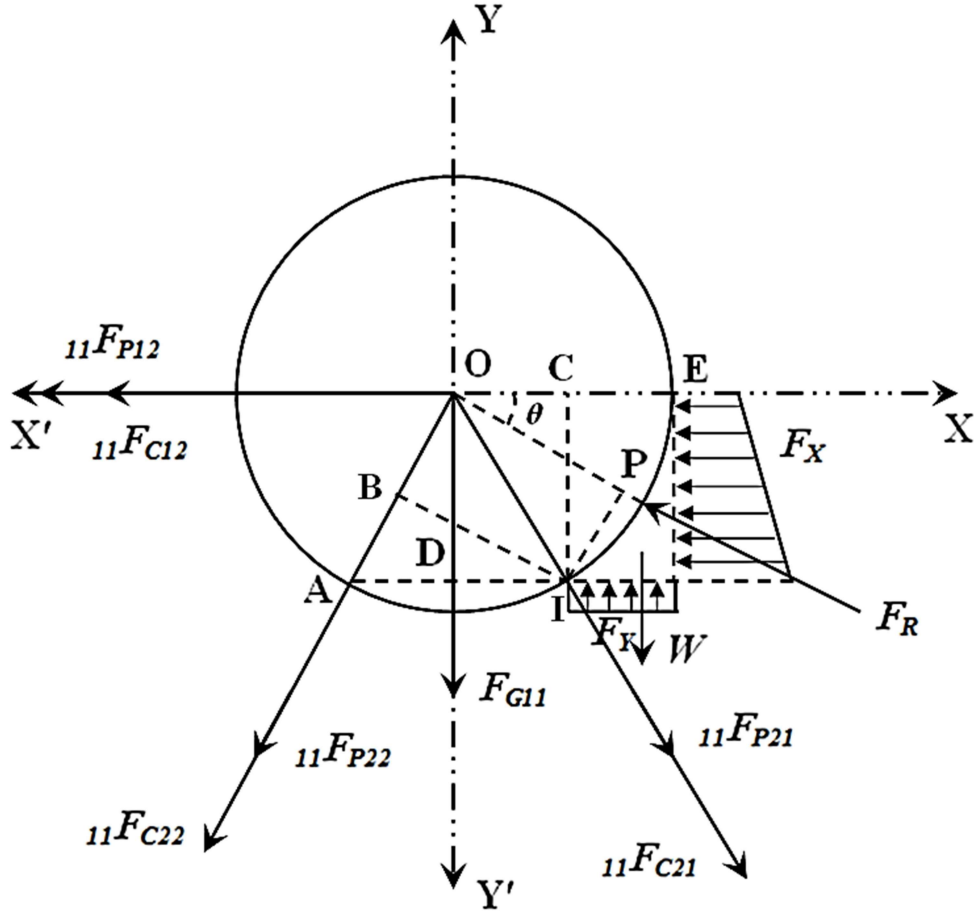


**Fig. 2.4** Particle 11's Free-body diagram under different force conditions with moments about Instantaneous Centre  $I$ .

## 2.4 Escape Velocity Calculation

The hydrostatic force expressions, when unit length is taken into account in the  $z$ -direction, are as follows:

Per unit length, hydrostatic force in a horizontal plane

$$F_X = F_H = A_X \times P_{avg} = A_X \times \rho \times g \times H_c \quad (2.6)$$

$$F_X = F_H = \rho \times g \times \frac{2}{3} \times \overline{IC} \times \overline{IC} \quad (2.7)$$

Per unit length, hydrostatic force moving upward in a vertical plane

$$F_Y = P \times A_Y = \rho \times g \times H \times A_Y \quad (2.8)$$

$$F_Y = \rho \times g \times \overline{IC} \times \overline{EC} \quad (2.9)$$

Per unit length, the fluid block's weight moving downward

$$W = m \times g = \rho \times V \times g \quad (2.10)$$

$$W = 1000 \times 9.81 \times \left[ \overline{EC} \times \overline{IC} - \frac{1}{2} \times \overline{EC} \times \overline{IE} \right] \quad (2.11)$$

(Assuming the triangle shape of AEC)

Per unit length, net hydrostatic force acting upward in a vertical plane

$$F_V = F_Y - W \quad (2.12)$$

Per unit length, resultant hydrostatic force

$$F_R = \sqrt{(F_H)^2 + (F_V)^2} \quad (2.13)$$

Furthermore, the hydrostatic force's horizontal direction subsequent to the result

$$\theta = \tan^{-1} \left( \frac{F_V}{F_H} \right) \quad (2.14)$$

Applying the theorem of conservation of angular momentum about the instantaneous centre  $I$

$$F_{G11} \times \overline{ID} + {}_{11}F_{C12} \times \overline{IC} + {}_{11}F_{C22} \times \overline{IB} + F_R \times \overline{IP} + {}_{11}F_{P12} \times \overline{IC} + {}_{11}F_{P22} \times \overline{IB} = I_I \times \alpha \quad (2.15)$$

Since  $F_C$  and  $F_p$  depend on the size of the particle, they will be the same for the same particle. Therefore, the equation above can be modified as

$$F_G \times \overline{ID} + F_C \times [\overline{IC} + \overline{IB}] + F_R \times \overline{IP} + F_P \times [\overline{IC} + \overline{IB}] = I_I \times \alpha \quad (2.16)$$

$$\Rightarrow \left[ \begin{array}{l} F_G \times \frac{R}{2} + F_C \times \left( \frac{\sqrt{3}R}{2} + \frac{\sqrt{3}R}{2} \right) + F_R \times R \sin(60 - \theta) \\ + F_P \times \left( \frac{\sqrt{3}R}{2} + \frac{\sqrt{3}R}{2} \right) \end{array} \right] = \frac{7}{5} \left( \frac{4}{3} \pi R^3 \rho_s \right) \times R^2 \times \alpha \quad (2.17)$$

The expression for angular acceleration obtained by solving the preceding equation is

$$\alpha = \left[ \frac{\frac{F_G}{2} + (F_C + F_P) \times \sqrt{3} + F_R \times \sin(60 - \theta)}{\frac{7}{5} \times \left( \frac{4}{3} \pi R^3 \rho_s \right) \times R} \right] \quad (2.18)$$

The impending acceleration expression (in m/s<sup>2</sup>) will also be

$$f = \alpha \times R \quad (2.19)$$

Also, the escape velocity expression in m/s

$$V_{esc} = [2 \times R \times f]^{0.5} \quad (2.20)$$

Here,  $R$  is expressed in m and  $f$  is expressed in m/s<sup>2</sup>.

## 2.5 Results

The parameters for rising and falling water levels have been analysed in various ways for this part. Firstly, analysis has been done for five different particle radius (0.390, 0.395, 0.400, 0.405 and 0.410 mm) keeping liquid-bridge volumes at fixed value (20 nl) depending on the degree of particle exposure (Fully submerged, Half submerged, and Fully exposed scenarios). Secondly, the analysis has been made for different liquid-bridge volumes (10, 15, 20, 25 and 30 nl) keeping particle radius at fixed value (0.400 mm) depending on the degree of particle exposure (Fully submerged, Half submerged, and Fully exposed scenarios) to analyse the dynamic effect of the river flow. In both the cases rising and falling conditions have been investigated and the escape velocity was plotted as a function of the inter-particle distance (also called inter-particle spacing).

### 2.5.1 Escape Velocity Variation for Particles of Different Sizes

Using a fixed liquid-bridge volume of 20 nl and three different degrees of particle exposure (Fully exposed [ $e = 1.0$ ] scenario, Half submerged [ $e = 0.5$ ] scenario and Fully submerged [ $e = 0.0$ ] scenario), escape velocities are plotted for five different particle radiuses (0.390 mm, 0.395 mm, 0.400 mm, 0.405 mm, and 0.410 mm). Water level variations are shown for two different varying conditions, namely rising and falling water levels.

#### 2.5.1.1 *Escape Velocity Variation for Water Level Rising*

Plot of the variation with regard to inter-particle distance for water level rising is shown. Inter-particle distance ranges from 0.145 to 0.170 mm at intervals of 0.005

mm. First five graphs are for fully exposed [ $e = 1.0$ ] scenario, next five are for half submerged [ $e = 0.5$ ] scenario and last five are for fully submerged [ $e = 0.0$ ] scenario. The related table (Table 2.1) is also provided in order to display the results in tabular form.

**Table 2.1: Escape velocity variation for different particle sizes with inter-particle distance for water level rising**

Particle Radius (mm)	Inter-Particle Distance (mm)	Escape Velocity for Fully Exposed (m/s)	Escape Velocity for Half Exposed (m/s)	Escape Velocity for Fully Submerged (m/s)
0.390	0.145	0.396704986	1.378577408	2.172640357
	0.150	0.392275635	1.377309333	2.172051529
	0.155	0.387907336	1.376071556	2.171477138
	0.160	0.383599377	1.374863377	2.170916834
	0.165	0.379351055	1.373684115	2.170370276
	0.170	0.375161676	1.372533099	2.169837129
0.395	0.145	0.393346293	1.377105507	2.17197169
	0.150	0.38892559	1.375849332	2.17138883
	0.155	0.384566323	1.374623413	2.17082037
	0.160	0.38026777	1.373427045	2.170265958
	0.165	0.37602922	1.37225954	2.169725251
	0.170	0.371849969	1.371120224	2.169197913

<b>Particle Radius (mm)</b>	<b>Inter-Particle Distance (mm)</b>	<b>Escape Velocity for Fully Exposed (m/s)</b>	<b>Escape Velocity for Half Exposed (m/s)</b>	<b>Escape Velocity for Fully Submerged (m/s)</b>
0.400	0.145	0.390054006	1.375671802	2.171320948
	0.150	0.385641965	1.374427337	2.170743948
	0.155	0.381291741	1.373213083	2.170181311
	0.160	0.377002603	1.372028331	2.169632683
	0.165	0.372773828	1.370872389	2.169097718
	0.170	0.368604705	1.369744578	2.16857608
0.405	0.145	0.386826098	1.374274894	2.170687454
	0.150	0.382422733	1.373041952	2.170116209
	0.155	0.378081562	1.371839175	2.169559289
	0.160	0.373801845	1.37066585	2.169016339
	0.165	0.369582849	1.36952128	2.168487012
	0.170	0.365423853	1.368404782	2.167970969
0.410	0.145	0.383660627	1.372913448	2.170070564
	0.150	0.379265951	1.371691846	2.169504972
	0.155	0.374933843	1.370500363	2.168953667
	0.160	0.370663552	1.369338281	2.168416293
	0.165	0.366454338	1.368204897	2.167892501
	0.170	0.36230547	1.367099526	2.167381951



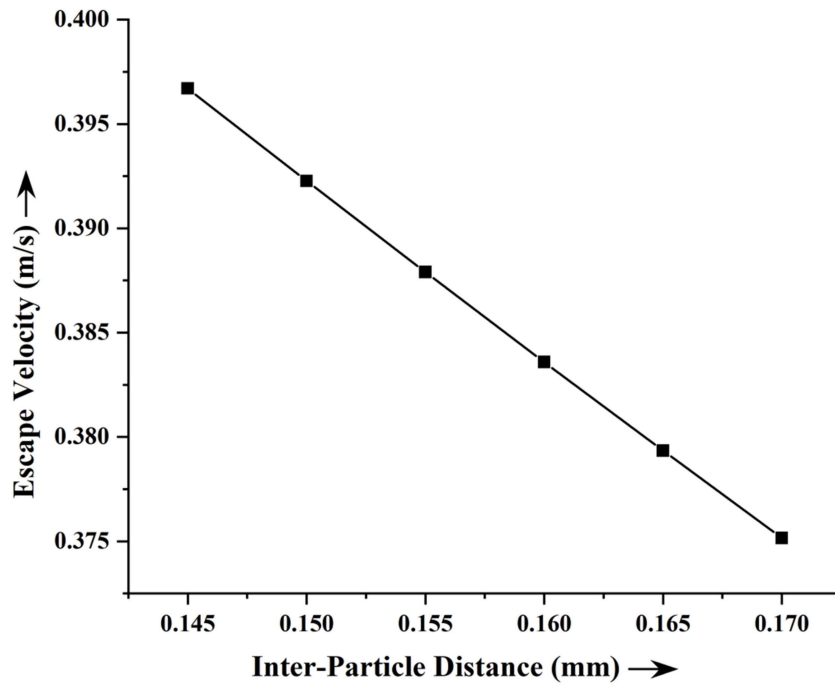


**Fig. 2.5** Changes in escape velocity with inter-particle spacing for 0.390 mm particle

radius in a fully exposed [ $e = 1.0$ ] scenario for rising river-water level

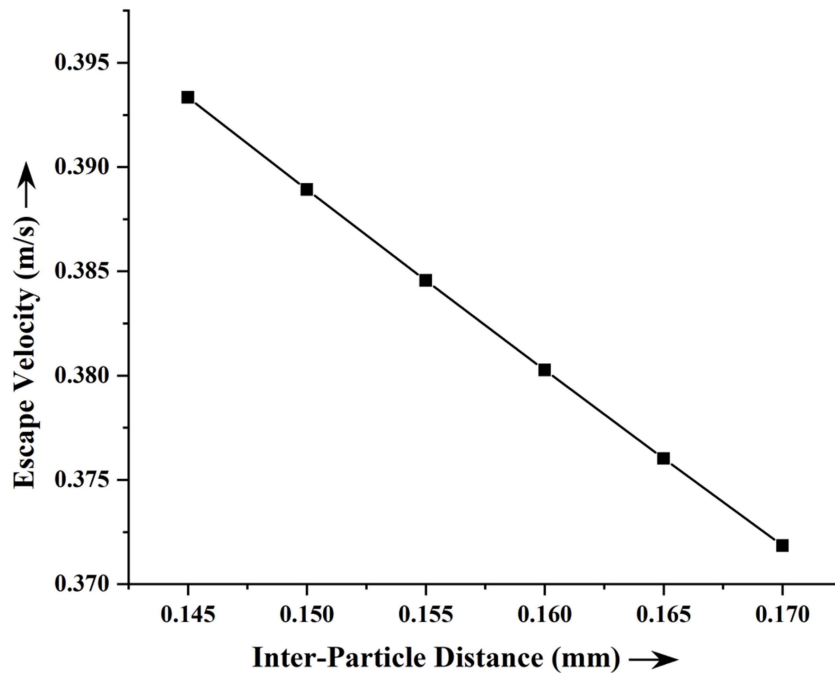


**Fig. 2.6** Changes in escape velocity with inter-particle spacing for 0.395 mm particle

radius in a fully exposed [ $e = 1.0$ ] scenario for rising river-water level

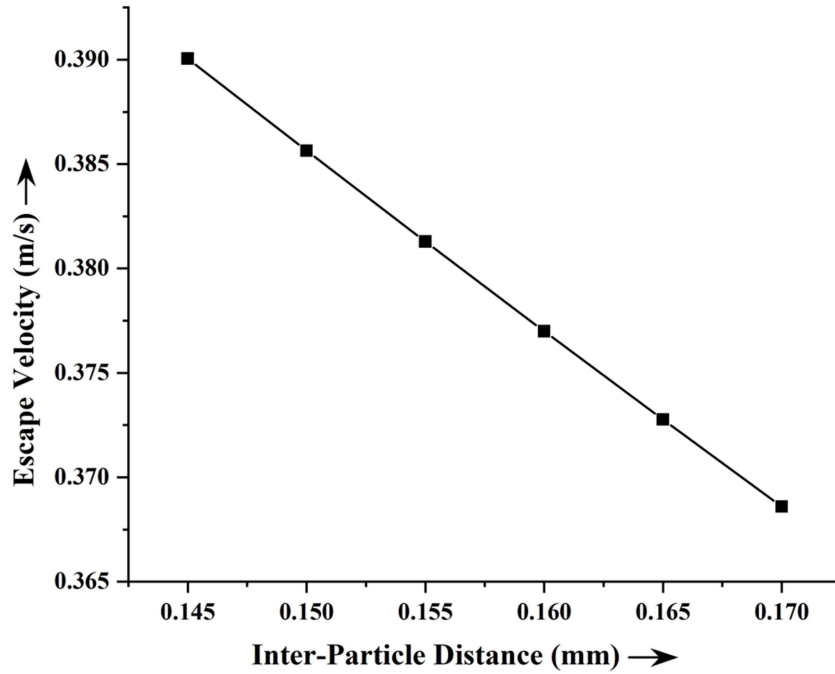


**Fig. 2.7** Changes in escape velocity with inter-particle spacing for 0.400 mm particle radius in a fully exposed [ $e = 1.0$ ] scenario for rising river-water level

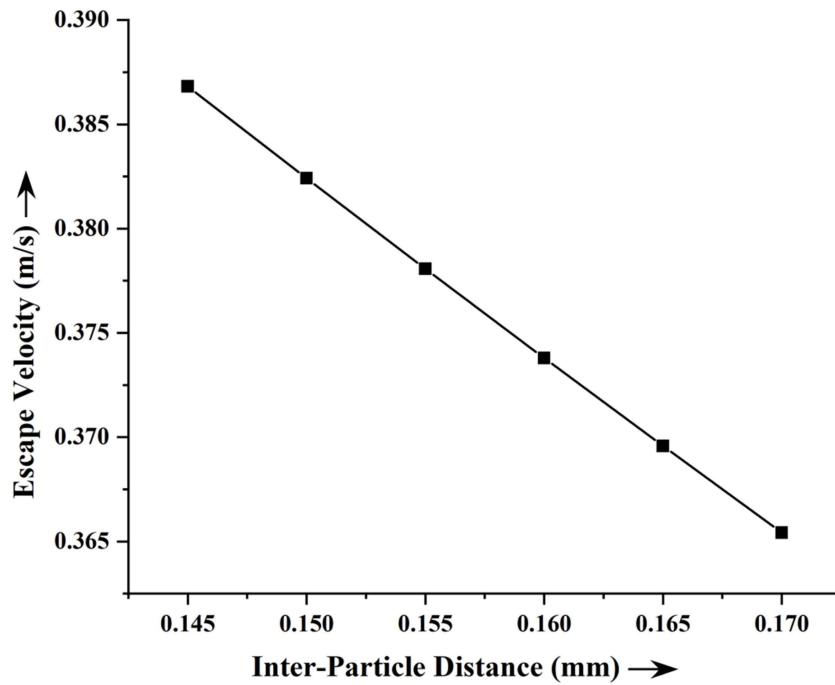


**Fig. 2.8** Changes in escape velocity with inter-particle spacing for 0.405 mm particle radius in a fully exposed [ $e = 1.0$ ] scenario for rising river-water level

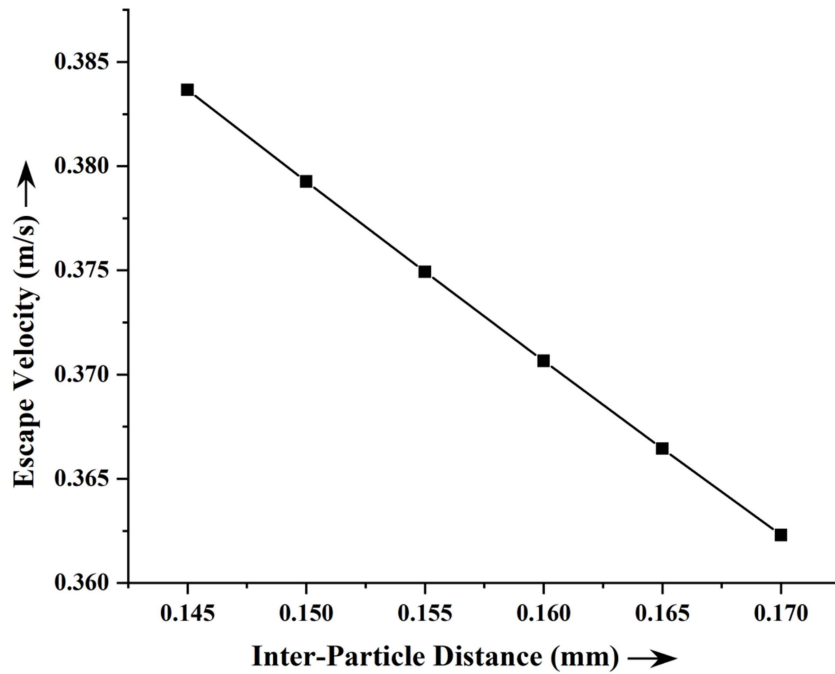


**Fig. 2.9** Changes in escape velocity with inter-particle spacing for 0.410 mm particle radius in a fully exposed [ $e = 1.0$ ] scenario for rising river-water level

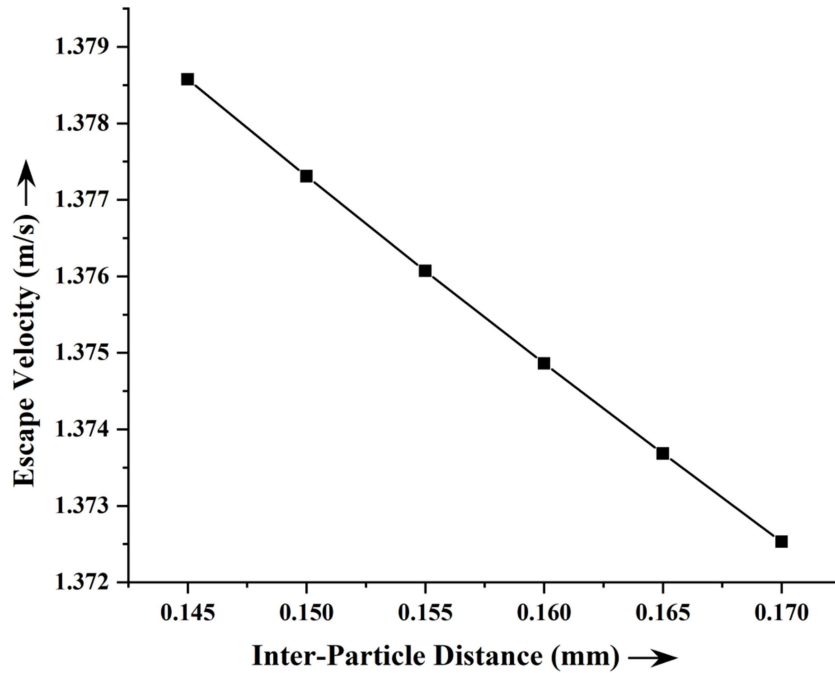


**Fig. 2.10** Changes in escape velocity with inter-particle spacing for 0.390 mm particle radius in a half submerged [ $e = 0.5$ ] scenario for rising river-water level

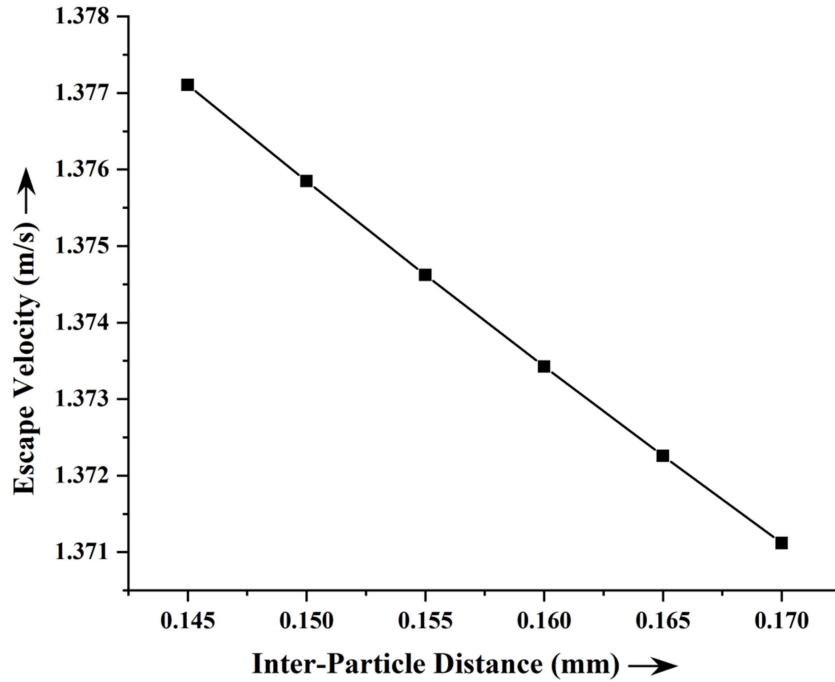


**Fig. 2.11** Changes in escape velocity with inter-particle spacing for 0.395 mm particle radius in a half submerged [ $e = 0.5$ ] scenario for rising river-water level

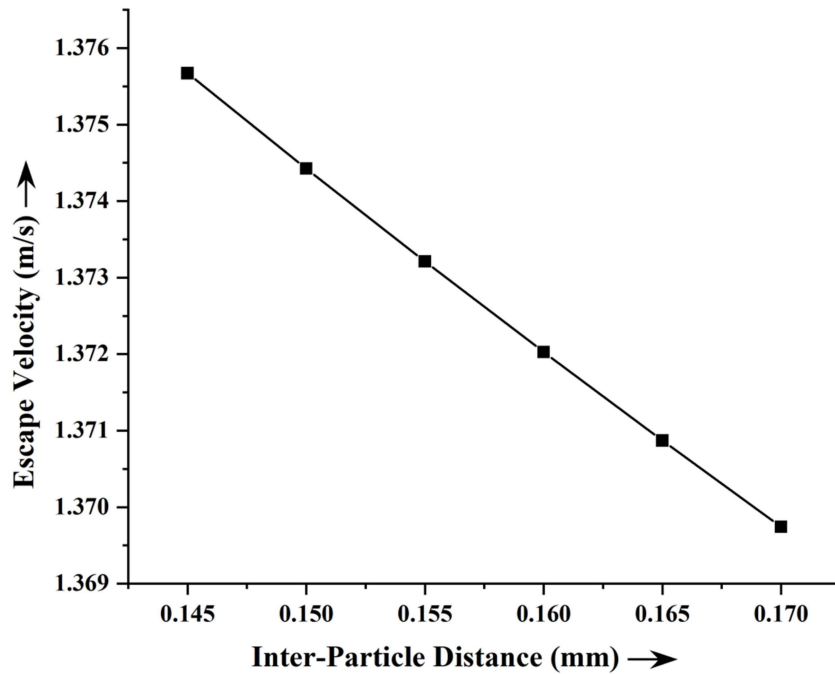


**Fig. 2.12** Changes in escape velocity with inter-particle spacing for 0.400 mm particle radius in a half submerged [ $e = 0.5$ ] scenario for rising river-water level

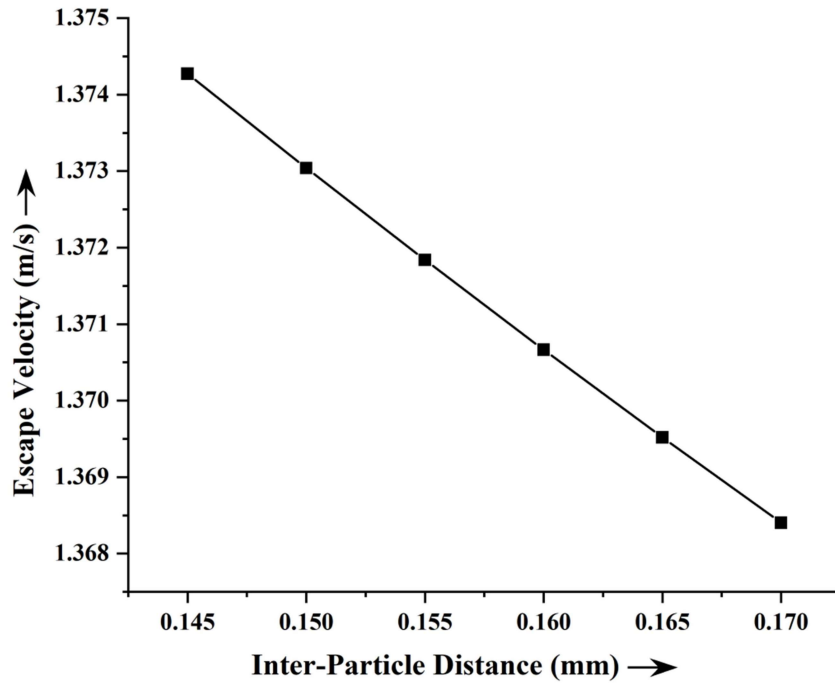


**Fig. 2.13** Changes in escape velocity with inter-particle spacing for 0.405 mm particle radius in a half submerged [ $e = 0.5$ ] scenario for rising river-water level

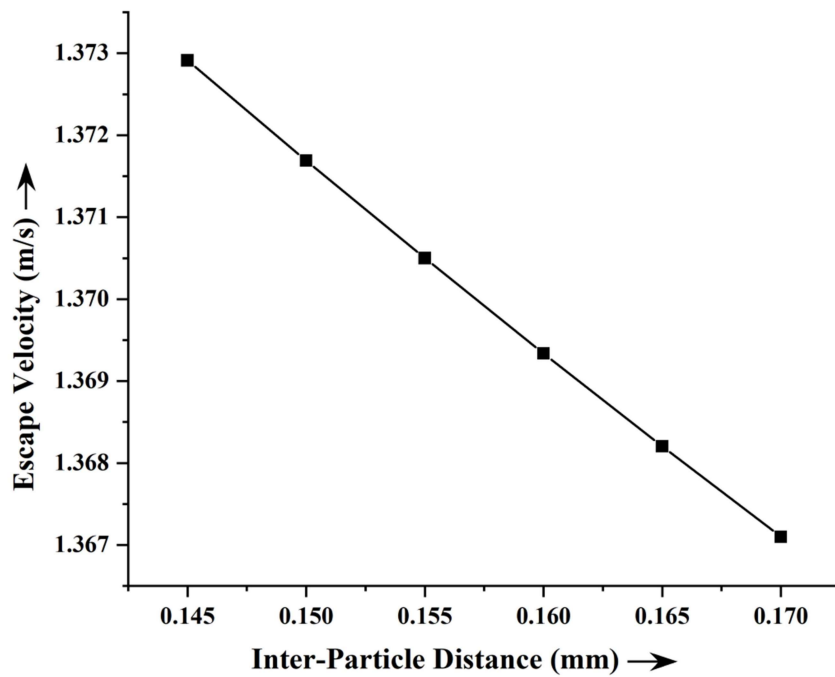


**Fig. 2.14** Changes in escape velocity with inter-particle spacing for 0.410 mm particle radius in a half submerged [ $e = 0.5$ ] scenario for rising river-water level

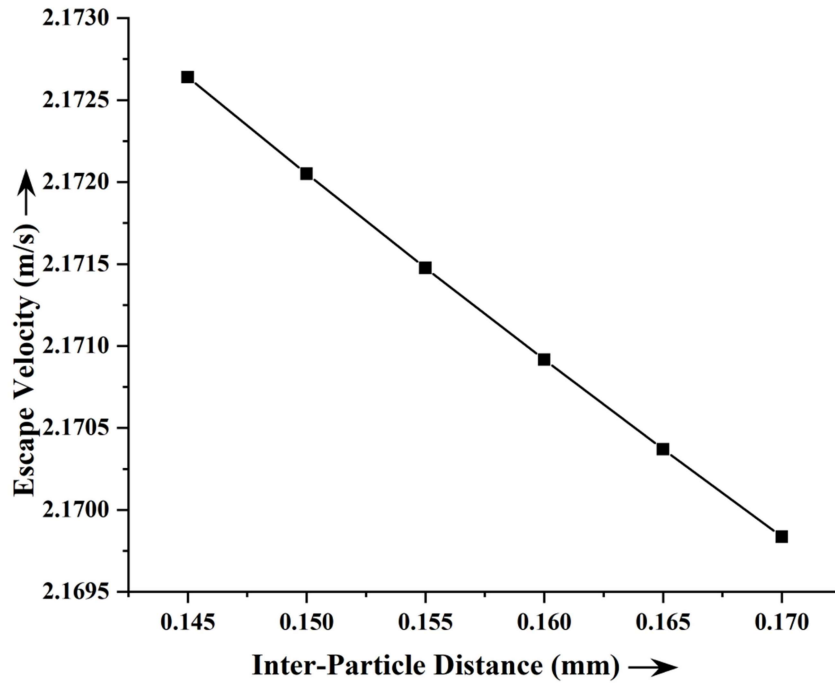


**Fig. 2.15** Changes in escape velocity with inter-particle spacing for 0.390 mm particle radius in a fully submerged [ $e = 0.0$ ] scenario for rising river-water level

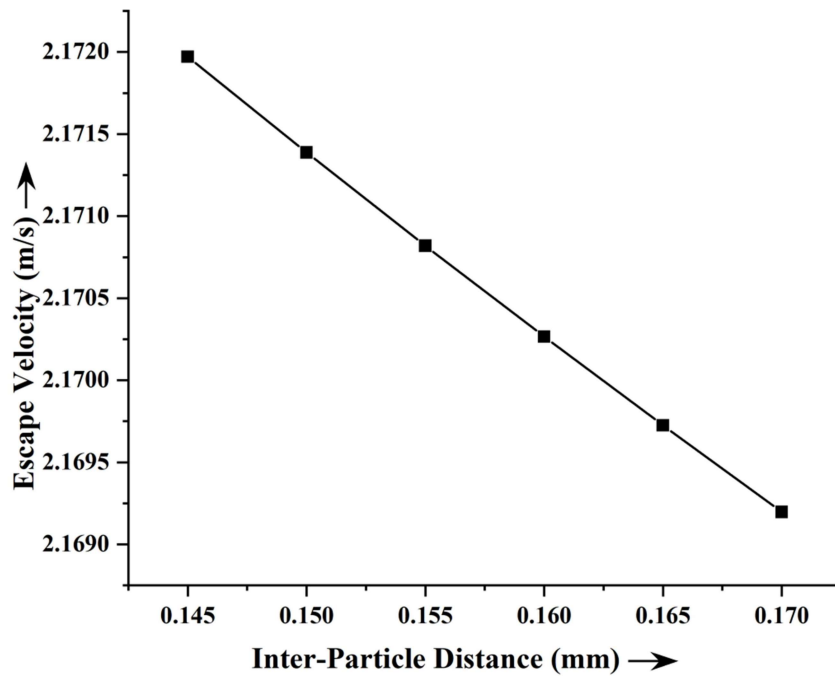


**Fig. 2.16** Changes in escape velocity with inter-particle spacing for 0.395 mm particle radius in a fully submerged [ $e = 0.0$ ] scenario for rising river-water level

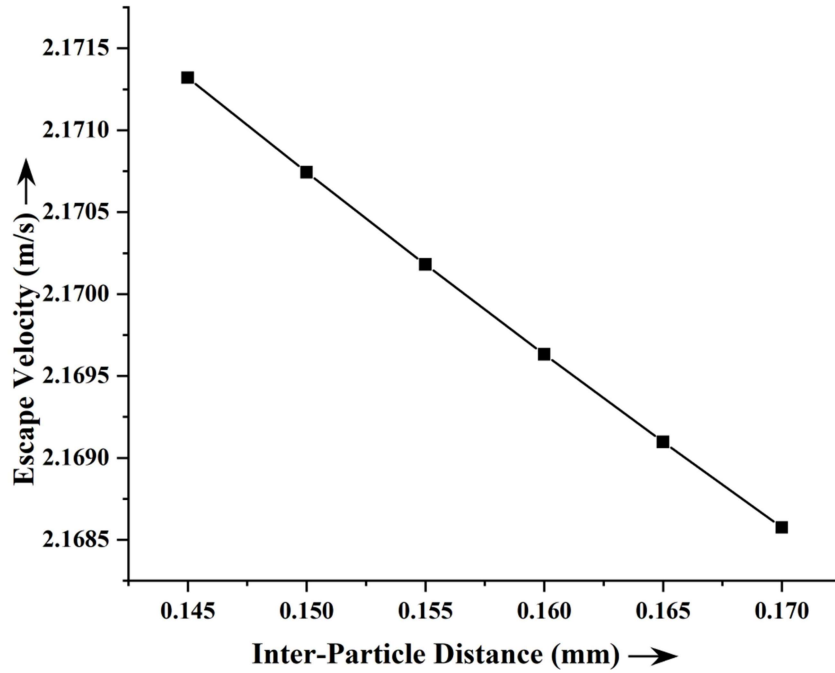


**Fig. 2.17** Changes in escape velocity with inter-particle spacing for 0.400 mm particle

radius in a fully submerged [ $e = 0.0$ ] scenario for rising river-water level

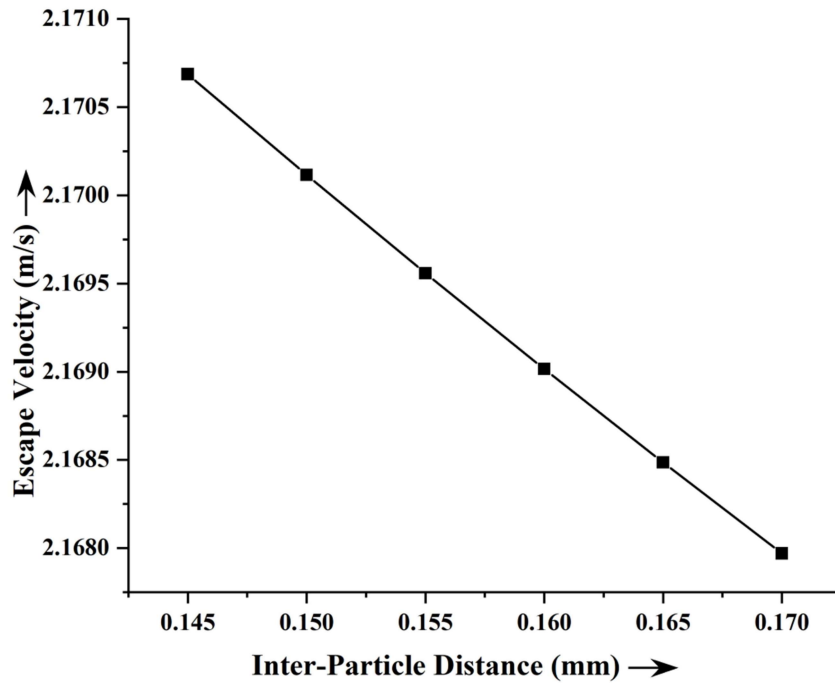


**Fig. 2.18** Changes in escape velocity with inter-particle spacing for 0.405 mm particle

radius in a fully submerged [ $e = 0.0$ ] scenario for rising river-water level

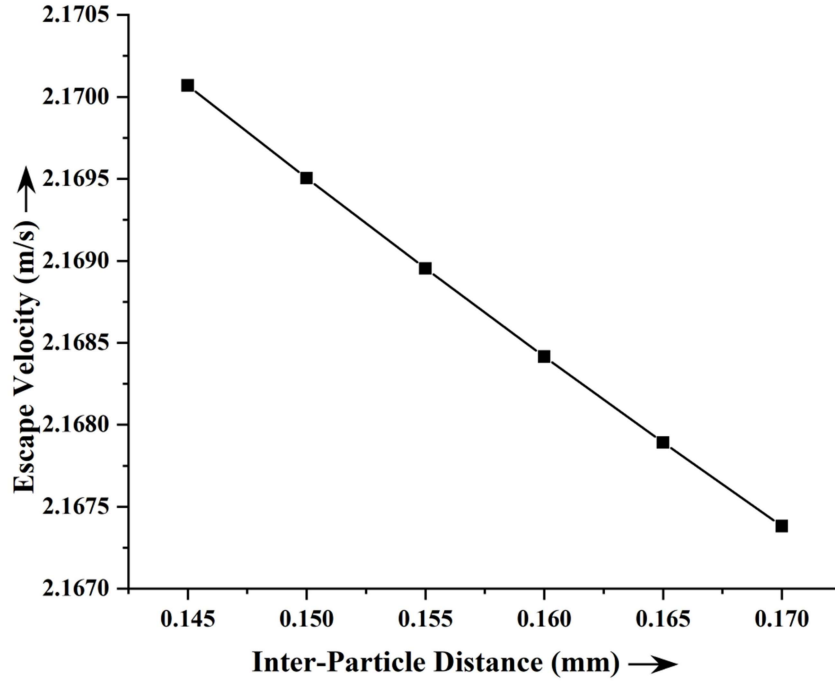


**Fig. 2.19** Changes in escape velocity with inter-particle spacing for 0.410 mm particle radius in a fully submerged [ $e = 0.0$ ] scenario for rising river-water level

#### 2.5.1.2 *Escape Velocity Variation for Water Level Falling*

Plot of the variation with regard to inter-particle distance for water level falling is depicted. Inter-particle distance ranges from 0.145 to 0.170 mm at intervals of 0.005 mm. First five graphs are for fully exposed [ $e = 1.0$ ] scenario, next five are for half submerged [ $e = 0.5$ ] scenario and last five are for fully submerged [ $e = 0.0$ ] scenario. The related table (Table 2.2) is also provided in order to display the results in tabular form.



**Table 2.2: Escape velocity variation for different particle sizes with inter-particle distance for water level falling**

<b>Particle Radius (mm)</b>	<b>Inter-Particle Distance (mm)</b>	<b>Escape Velocity for Fully Exposed (m/s)</b>	<b>Escape Velocity for Half Exposed (m/s)</b>	<b>Escape Velocity for Fully Submerged (m/s)</b>
0.390	0.145	0.340497623	0.70518785	1.496851898
	0.150	0.336719993	0.703371614	1.495997102
	0.155	0.332994701	0.701595856	1.495163016
	0.160	0.329321139	0.699859762	1.494349152
	0.165	0.325698705	0.698162531	1.493555028
	0.170	0.322126804	0.696503375	1.492780176
0.395	0.145	0.337646994	0.703815861	1.496206024
	0.150	0.333877104	0.702015095	1.495359788
	0.155	0.330159884	0.700254827	1.494534216
	0.160	0.326494718	0.698534233	1.493728816
	0.165	0.322880995	0.696852502	1.492943104
	0.170	0.319318112	0.695208839	1.492176609
0.400	0.145	0.334853387	0.702479939	1.495578071
	0.150	0.331091254	0.700694435	1.494740243
	0.155	0.327382121	0.698949445	1.493923033
	0.160	0.323725361	0.697244134	1.493125944

<b>Particle Radius (mm)</b>	<b>Inter-Particle Distance (mm)</b>	<b>Escape Velocity for Fully Exposed (m/s)</b>	<b>Escape Velocity for Half Exposed (m/s)</b>	<b>Escape Velocity for Fully Submerged (m/s)</b>
0.400	0.165	0.320120357	0.695577685	1.492348491
	0.170	0.316566499	0.693949293	1.491590199
0.405	0.145	0.332115065	0.701178786	1.494967355
	0.150	0.328360706	0.69940834	1.494137787
	0.155	0.324659672	0.697678419	1.493328791
	0.160	0.32101133	0.69598818	1.492539865
	0.165	0.317415053	0.694336798	1.491770522
0.410	0.170	0.313870224	0.692723459	1.491020286
	0.145	0.329430367	0.699911166	1.494373227
	0.150	0.325683797	0.698155576	1.493551777
	0.155	0.321990876	0.69644052	1.49275085
	0.160	0.318350961	0.694765146	1.491969943
	0.165	0.31476342	0.69312862	1.491208565
	0.170	0.311227624	0.69153012	1.490466239

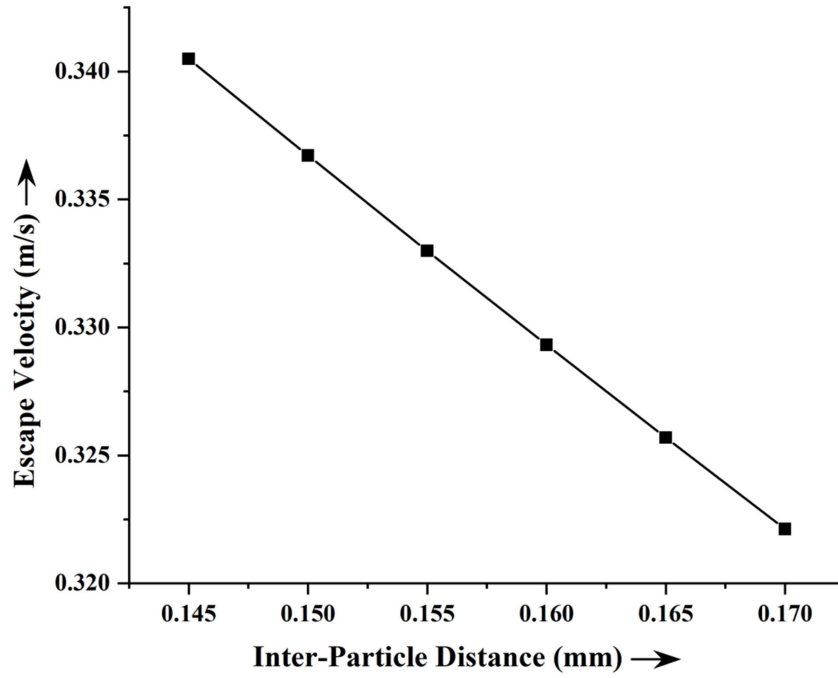


**Fig. 2.20** Changes in escape velocity with inter-particle spacing for 0.390 mm particle radius in a fully exposed [ $e = 1.0$ ] scenario for falling river-water level

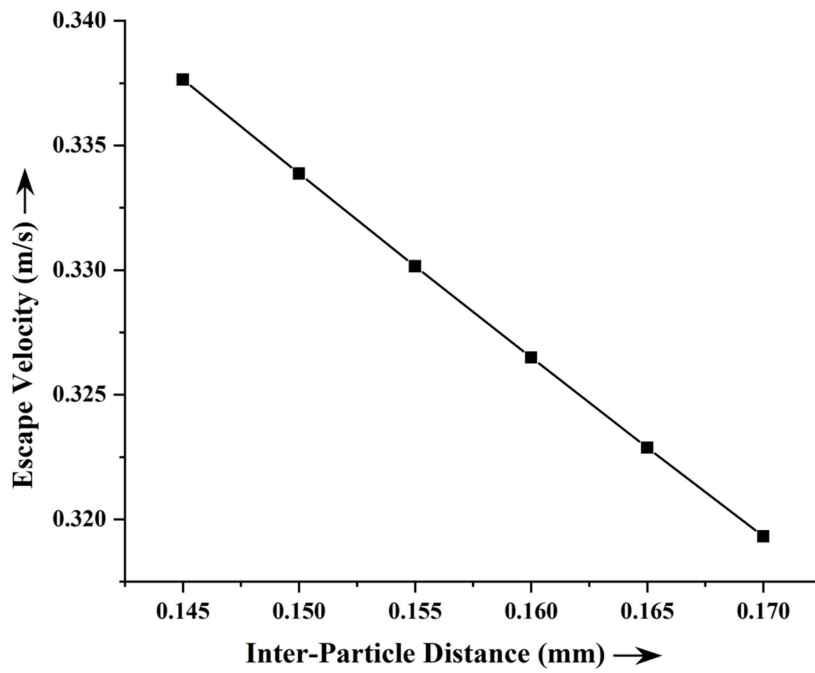


**Fig. 2.21** Changes in escape velocity with inter-particle spacing for 0.395 mm particle radius in a fully exposed [ $e = 1.0$ ] scenario for falling river-water level

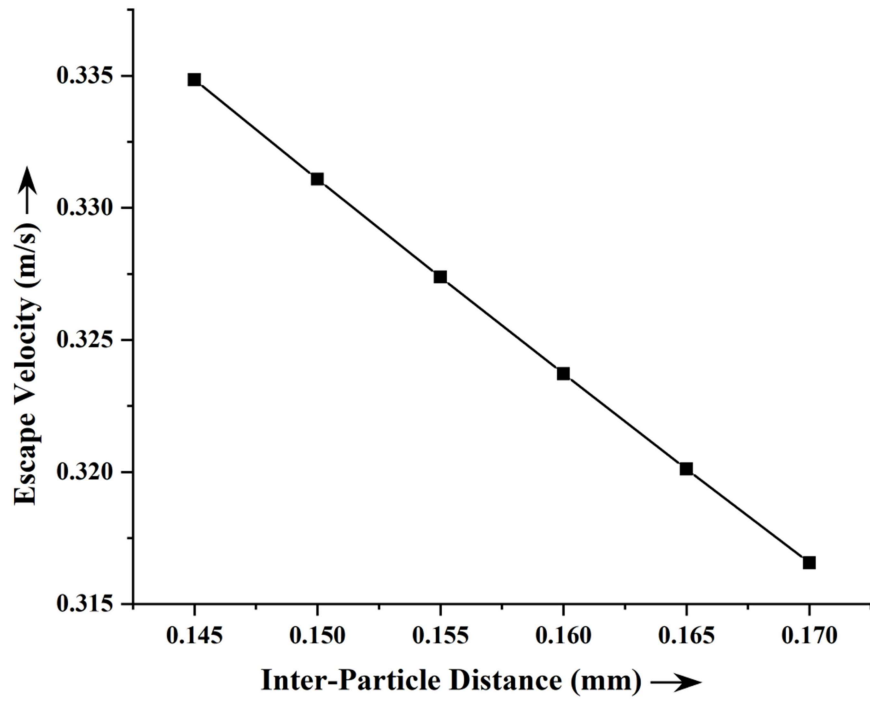


**Fig. 2.22** Changes in escape velocity with inter-particle spacing for 0.400 mm particle radius in a fully exposed [ $e = 1.0$ ] scenario for falling river-water level

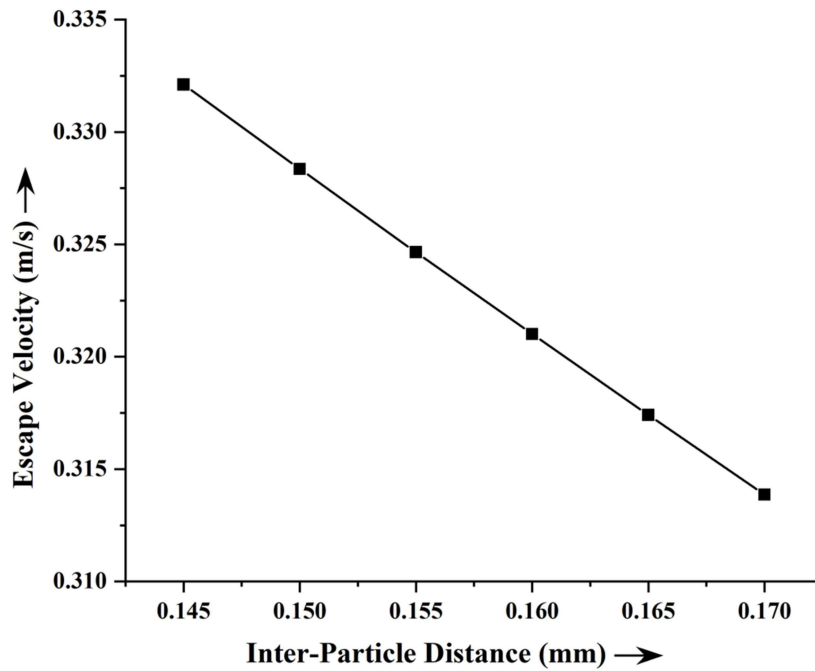


**Fig. 2.23** Changes in escape velocity with inter-particle spacing for 0.405 mm particle radius in a fully exposed [ $e = 1.0$ ] scenario for falling river-water level

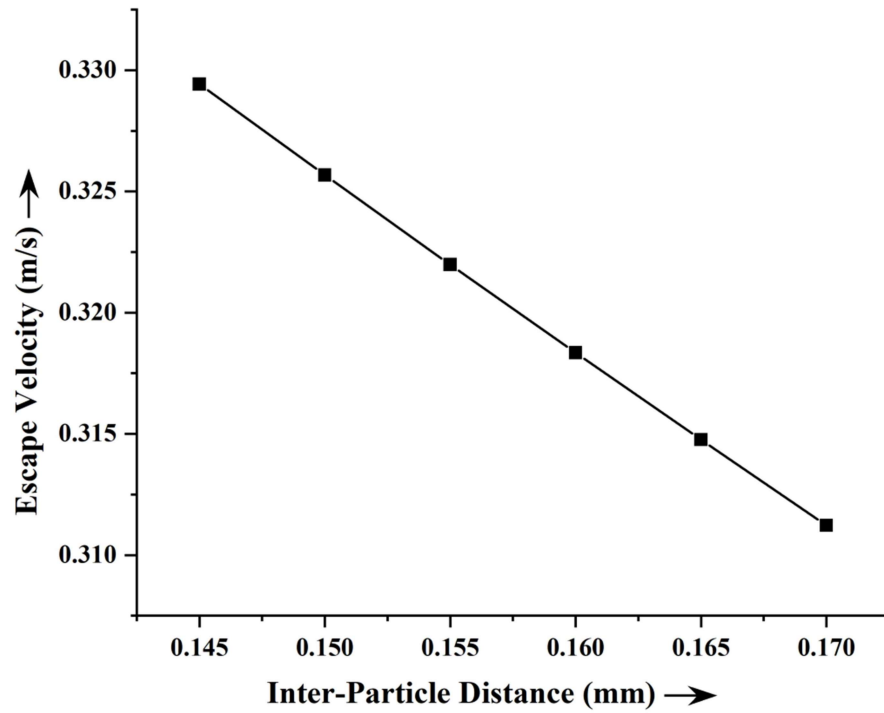


**Fig. 2.24** Changes in escape velocity with inter-particle spacing for 0.410 mm particle radius in a fully exposed [ $e = 1.0$ ] scenario for falling river-water level

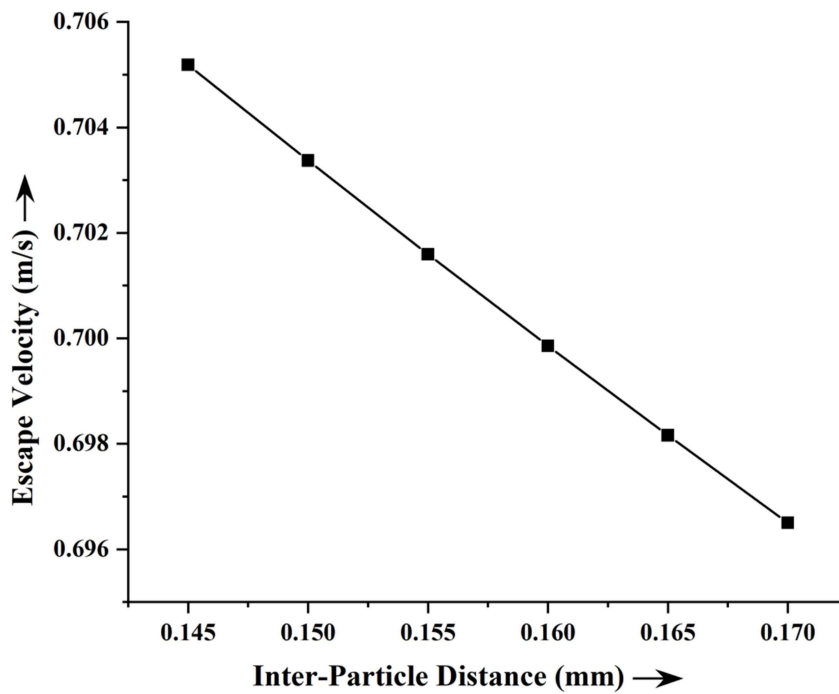


**Fig. 2.25** Changes in escape velocity with inter-particle spacing for 0.390 mm particle radius in a half submerged [ $e = 0.5$ ] scenario for falling river-water level

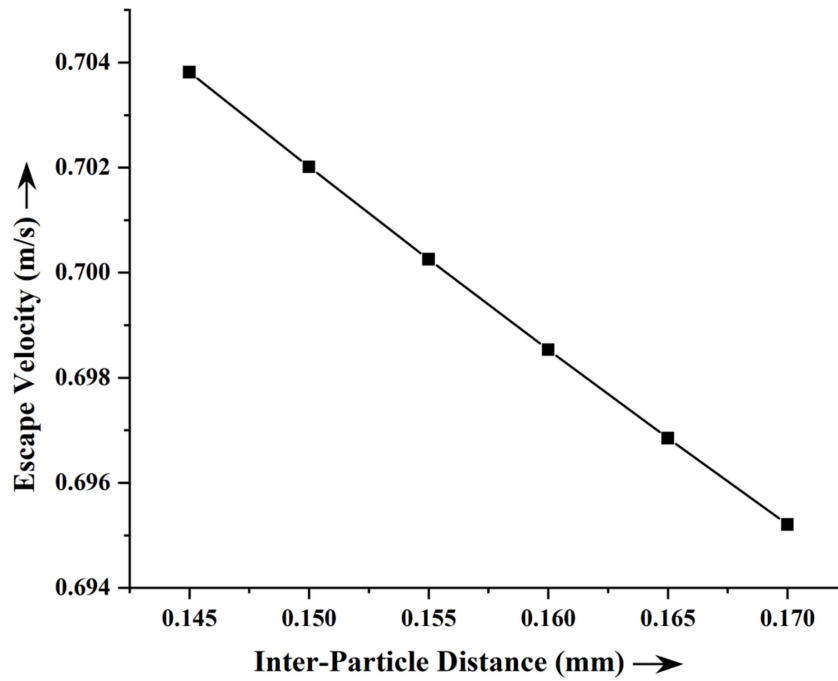


**Fig. 2.26** Changes in escape velocity with inter-particle spacing for 0.395 mm particle radius in a half submerged [ $e = 0.5$ ] scenario for falling river-water level

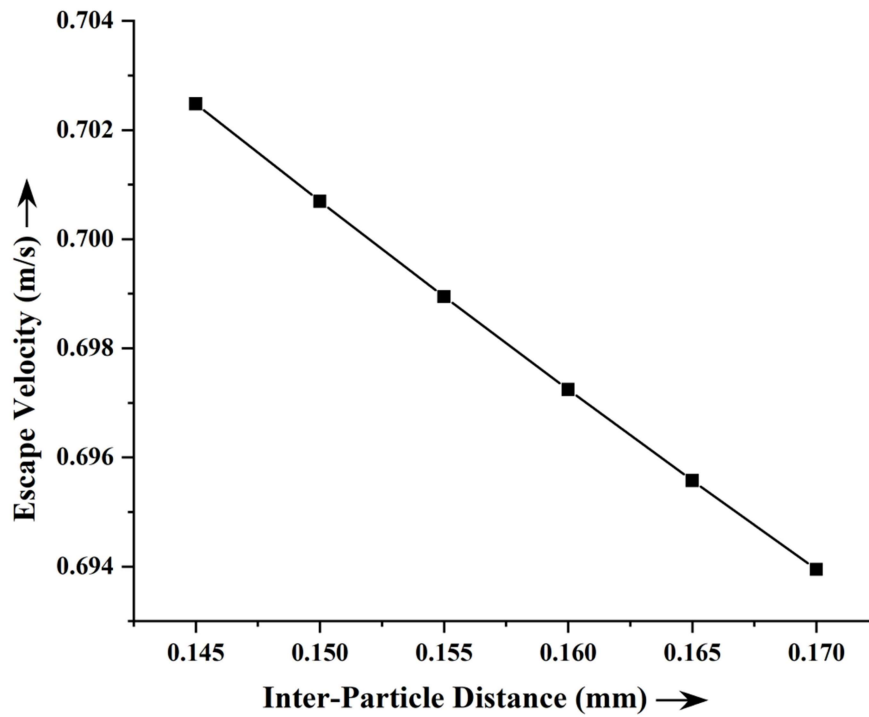


**Fig. 2.27** Changes in escape velocity with inter-particle spacing for 0.400 mm particle radius in a half submerged [ $e = 0.5$ ] scenario for falling river-water level

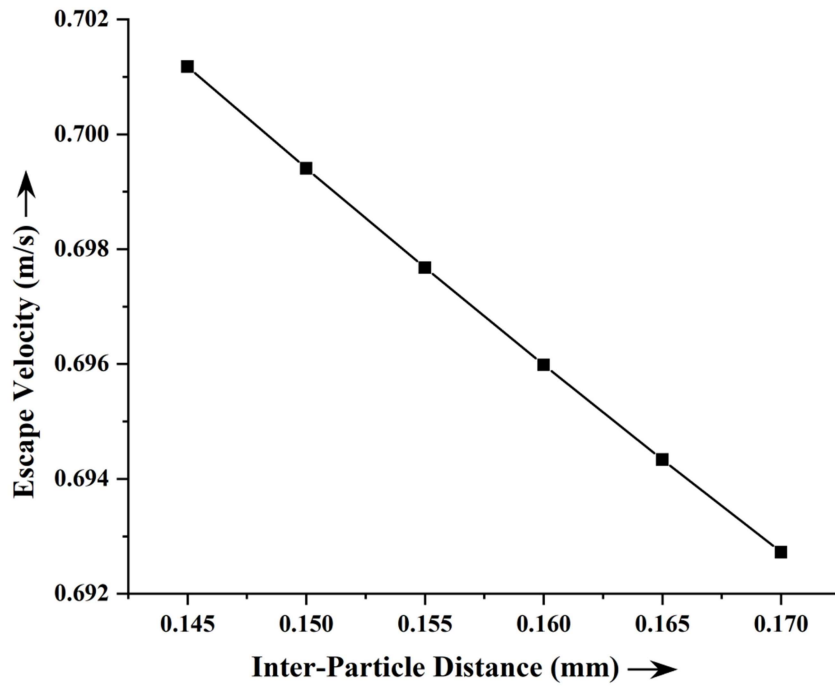


**Fig. 2.28** Changes in escape velocity with inter-particle spacing for 0.405 mm particle radius in a half submerged [ $e = 0.5$ ] scenario for falling river-water level

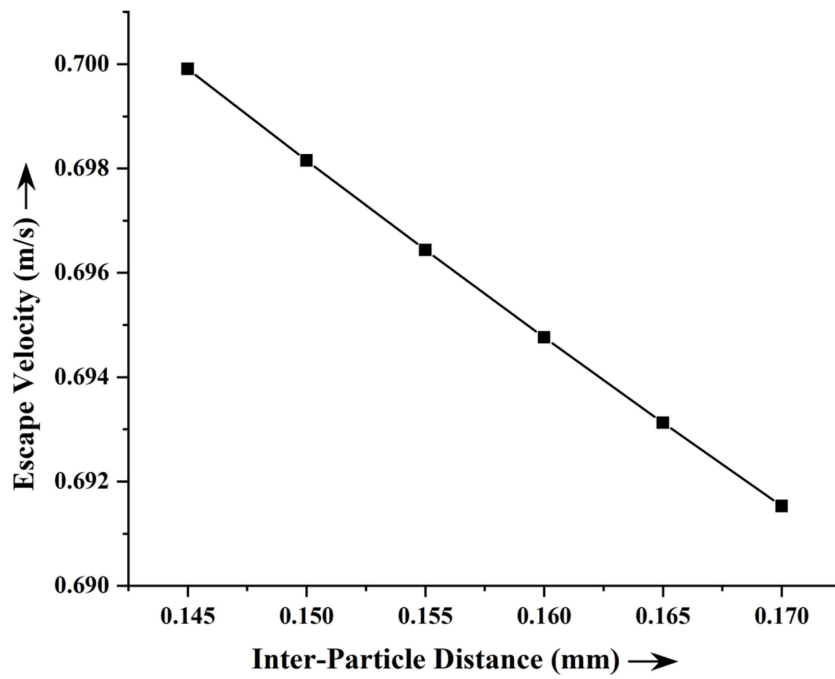


**Fig. 2.29** Changes in escape velocity with inter-particle spacing for 0.410 mm particle radius in a half submerged [ $e = 0.5$ ] scenario for falling river-water level

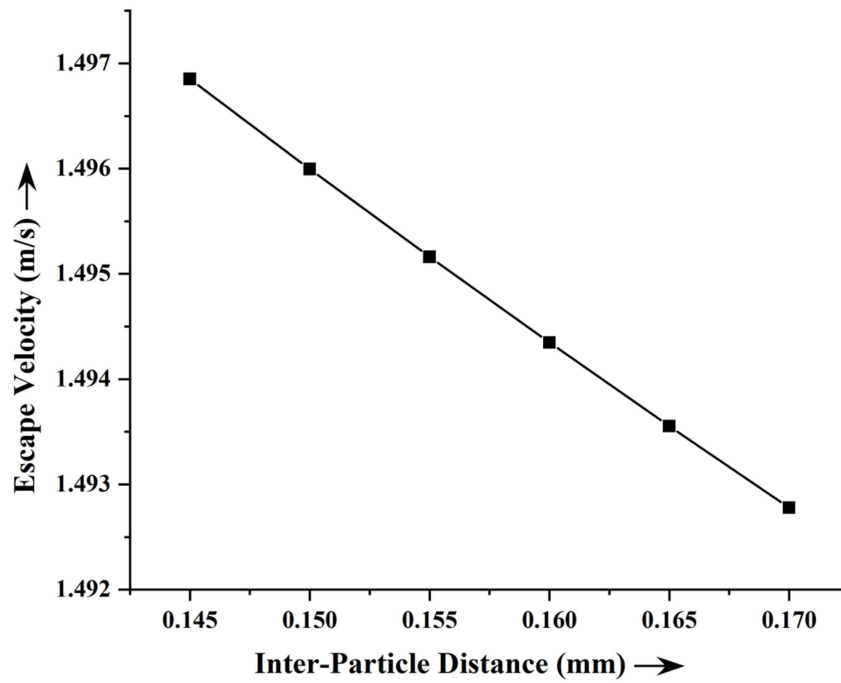


**Fig. 2.30** Changes in escape velocity with inter-particle spacing for 0.390 mm particle radius in a fully submerged [ $e = 0.0$ ] scenario for falling river-water level

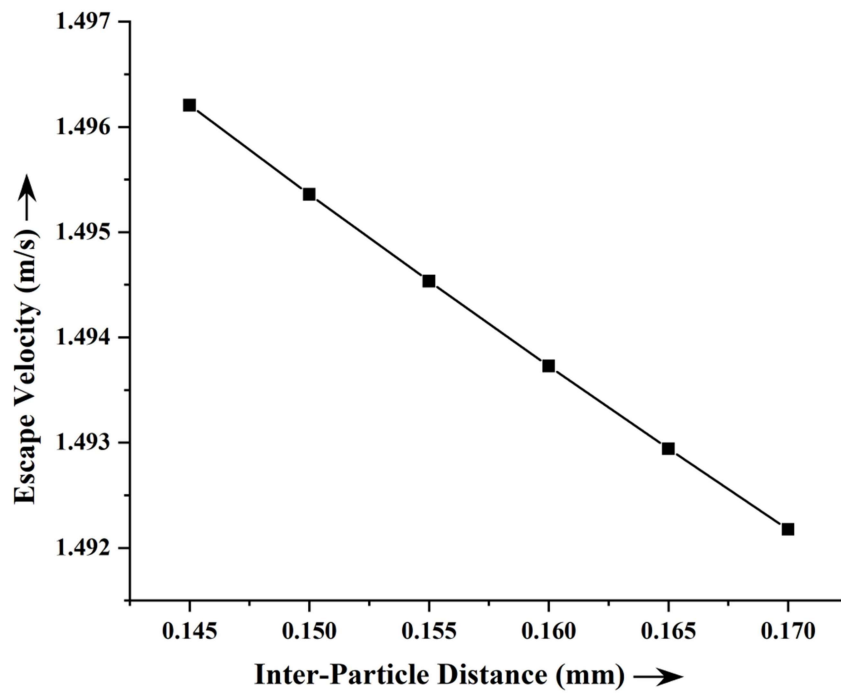


**Fig. 2.31** Changes in escape velocity with inter-particle spacing for 0.395 mm particle radius in a fully submerged [ $e = 0.0$ ] scenario for falling river-water level



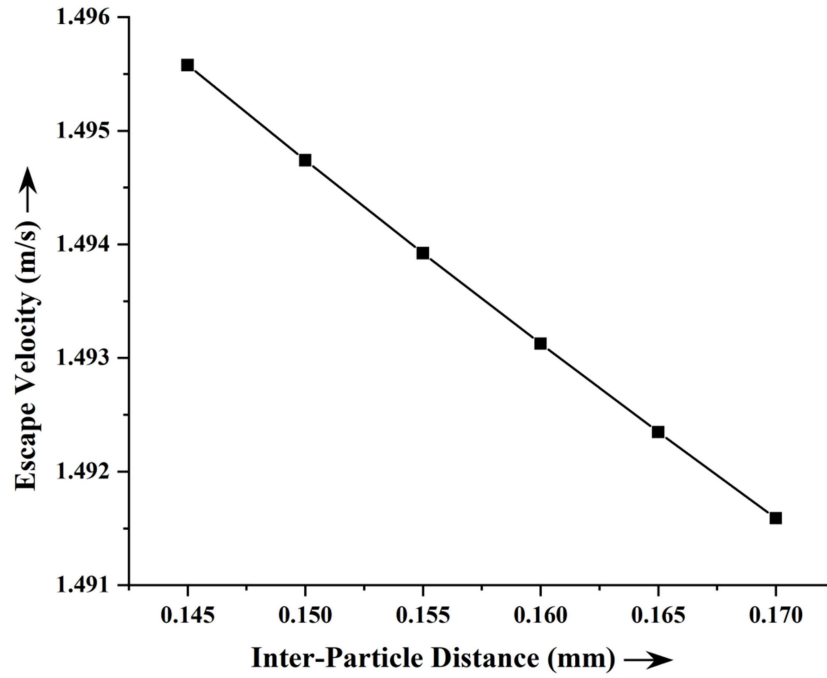


**Fig. 2.32** Changes in escape velocity with inter-particle spacing for 0.400 mm particle radius in a fully submerged [ $e = 0.0$ ] scenario for falling river-water level

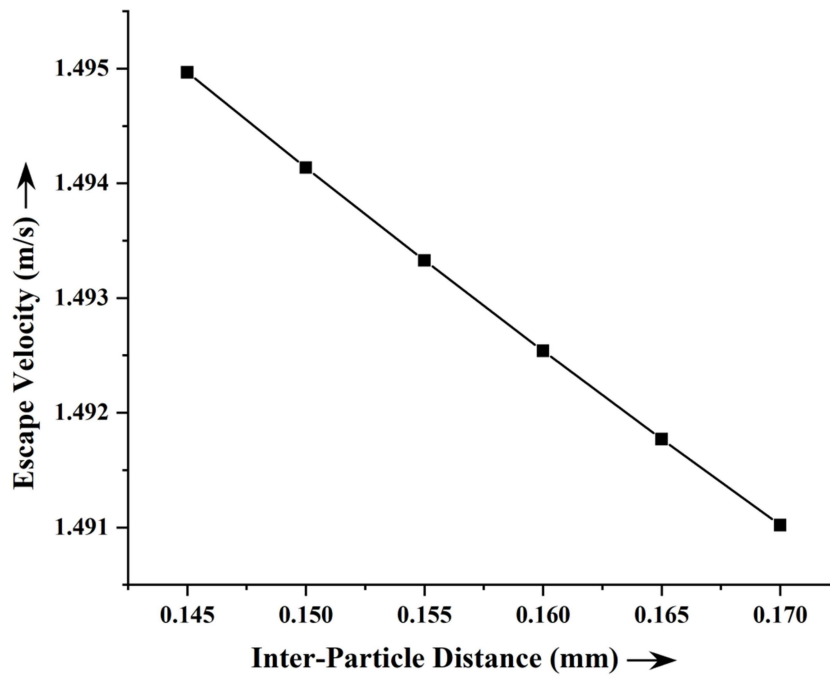


**Fig. 2.33** Changes in escape velocity with inter-particle spacing for 0.405 mm particle radius in a fully submerged [ $e = 0.0$ ] scenario for falling river-water level

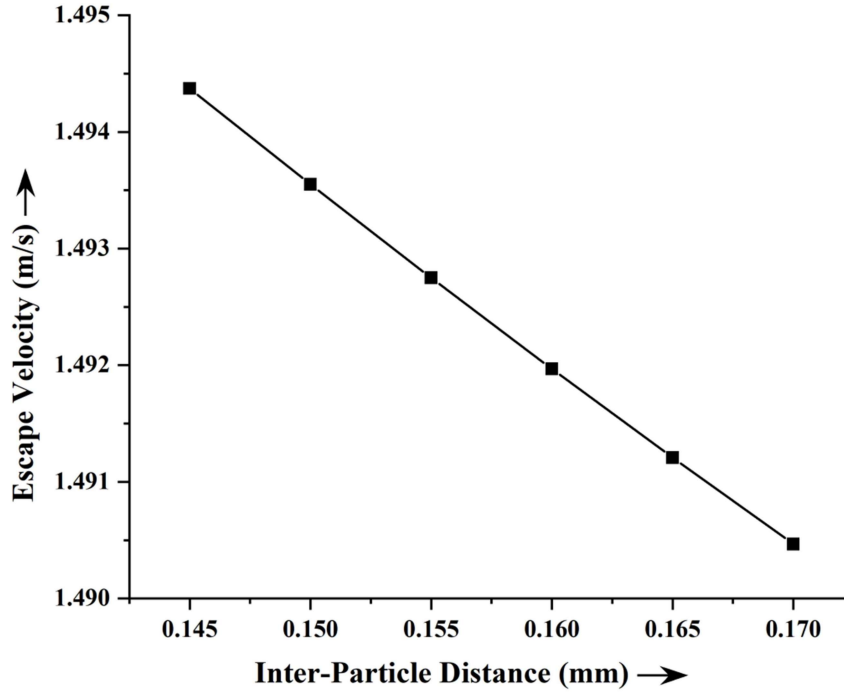


**Fig. 2.34** Changes in escape velocity with inter-particle spacing for 0.410 mm particle radius in a fully submerged [ $e = 0.0$ ] scenario for falling river-water level

## 2.5.2 Escape Velocity Variation for Different Liquid-Bridge Volumes

Here, escape velocities are plotted for five different liquid-bridge volume (10 nl, 15 nl, 20 nl, 25 nl and 30 nl) for the fixed value of particle radius of 0.400 mm for three different degrees of particle exposure ( $e$ ) in the free surface water (Fully exposed [ $e = 1.0$ ] scenario, Half submerged [ $e = 0.5$ ] scenario and Fully submerged [ $e = 0.0$ ] scenario). To study the dynamic behaviour, variations are shown for two different varying conditions, such as, for water level rising and water level falling.

### 2.5.2.1 *Escape Velocity Variation for Water Level Rising*

Plot of the variation with regard to inter-particle distance for water level rising is shown here. Inter-particle distance ranges from 0.145 to 0.170 mm at intervals of 0.005 mm. First five graphs are for fully exposed [ $e = 1.0$ ] scenario, next five are for half submerged [ $e = 0.5$ ] scenario and last five are for fully submerged [ $e = 0.0$ ] scenario. The related table (Table 2.3) is also provided in order to display the results in tabular form.

**Table 2.3: Escape velocity variation for different liquid-bridge volumes with inter-particle distance for water level rising**

<b>Liquid-Bridge Volume (nl)</b>	<b>Inter-Particle Distance (mm)</b>	<b>Escape Velocity for Fully Exposed (m/s)</b>	<b>Escape Velocity for Half Exposed (m/s)</b>	<b>Escape Velocity for Fully Submerged (m/s)</b>
10	0.145	0.338286417	1.361898851	2.164955681
	0.150	0.332982456	1.360591083	2.16435365
	0.155	0.327788795	1.359329347	2.163773198
	0.160	0.322703567	1.358112062	2.163213559
	0.165	0.317724937	1.356937698	2.16267399
	0.170	0.312851101	1.355804776	2.162153778
15	0.145	0.369793733	1.370065029	2.168724266
	0.150	0.364988981	1.368775999	2.168128334
	0.155	0.360263377	1.367523485	2.167549664
	0.160	0.355615837	1.366306482	2.166987761

<b>Liquid-Bridge Volume (nl)</b>	<b>Inter-Particle Distance (mm)</b>	<b>Escape Velocity for Fully Exposed (m/s)</b>	<b>Escape Velocity for Half Exposed (m/s)</b>	<b>Escape Velocity for Fully Submerged (m/s)</b>
15	0.165	0.351045289	1.365124014	2.166442143
	0.170	0.34655068	1.363975129	2.165912341
20	0.145	0.390054006	1.375671802	2.171320948
	0.150	0.385641965	1.374427337	2.170743948
	0.155	0.381291741	1.373213083	2.170181311
	0.160	0.377002603	1.372028331	2.169632683
	0.165	0.372773828	1.370872389	2.169097718
	0.170	0.368604705	1.369744578	2.16857608
25	0.145	0.404510618	1.379840433	2.173256431
	0.150	0.400410317	1.378643972	2.172700495
	0.155	0.396360758	1.377473278	2.172156861
	0.160	0.392361408	1.376327815	2.171625259
	0.165	0.388411737	1.37520706	2.171105425
	0.170	0.384511224	1.374110498	2.170597103
30	0.145	0.415503375	1.383102973	2.174774098
	0.150	0.411656869	1.381952299	2.17423854
	0.155	0.407853407	1.380824095	2.173713745

Liquid-Bridge Volume (nl)	Inter-Particle Distance (mm)	Escape Velocity for Fully Exposed (m/s)	Escape Velocity for Half Exposed (m/s)	Escape Velocity for Fully Submerged (m/s)
30	0.170	0.312851101	1.355804776	2.162153778
	0.165	0.400373968	1.378633415	2.172695592
	0.170	0.396697178	1.377570118	2.172201818

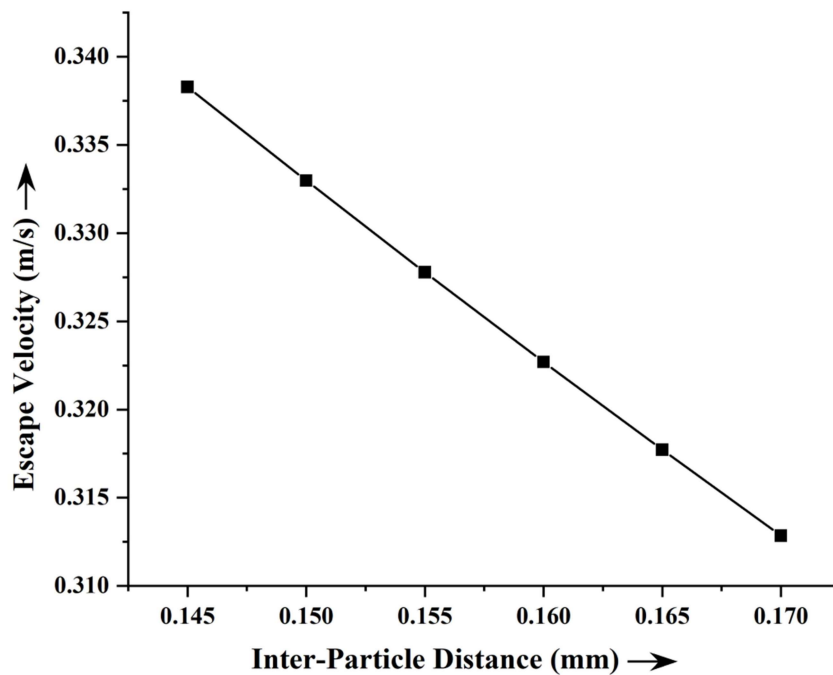


**Fig. 2.35** Changes in escape velocity with inter-particle spacing for 10 nl liquid-bridge volume in a fully exposed [ $e = 1.0$ ] scenario for rising river-water level

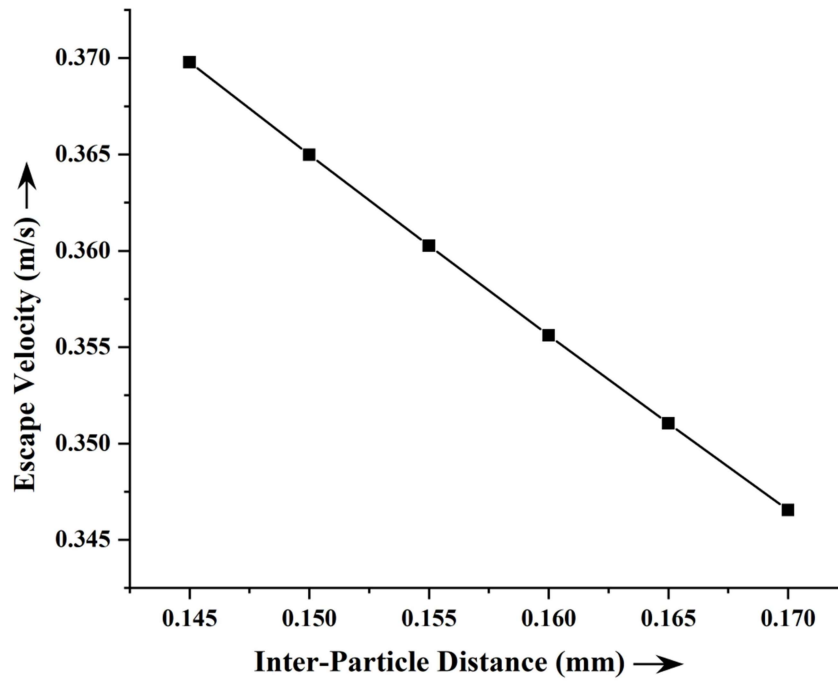


**Fig. 2.36** Changes in escape velocity with inter-particle spacing for 15 nl liquid-bridge volume in a fully exposed [ $e = 1.0$ ] scenario for rising river-water level

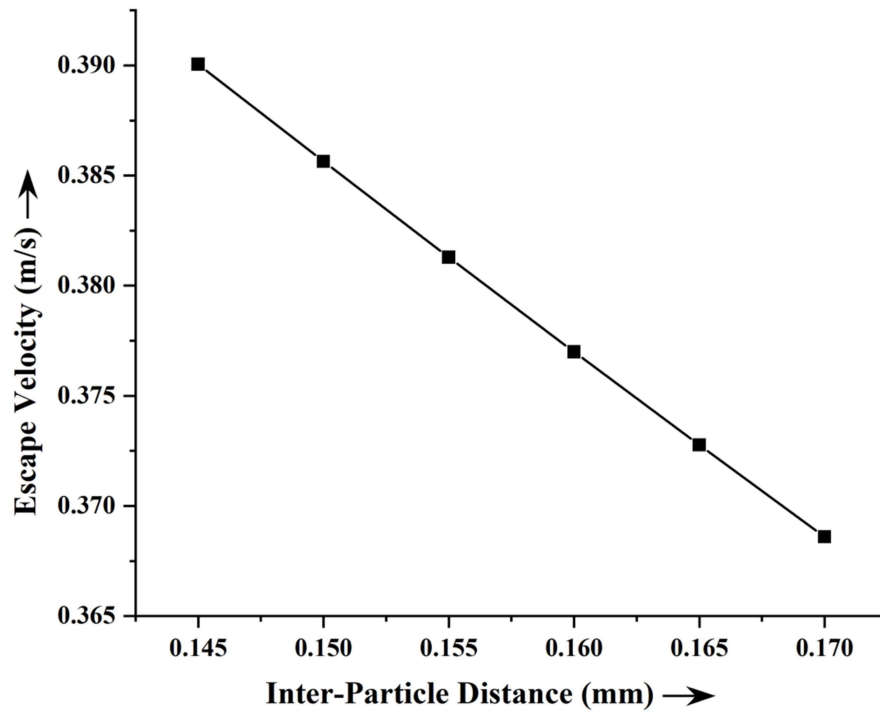


**Fig. 2.37** Changes in escape velocity with inter-particle spacing for 20 nl liquid-bridge volume in a fully exposed [ $e = 1.0$ ] scenario for rising river-water level

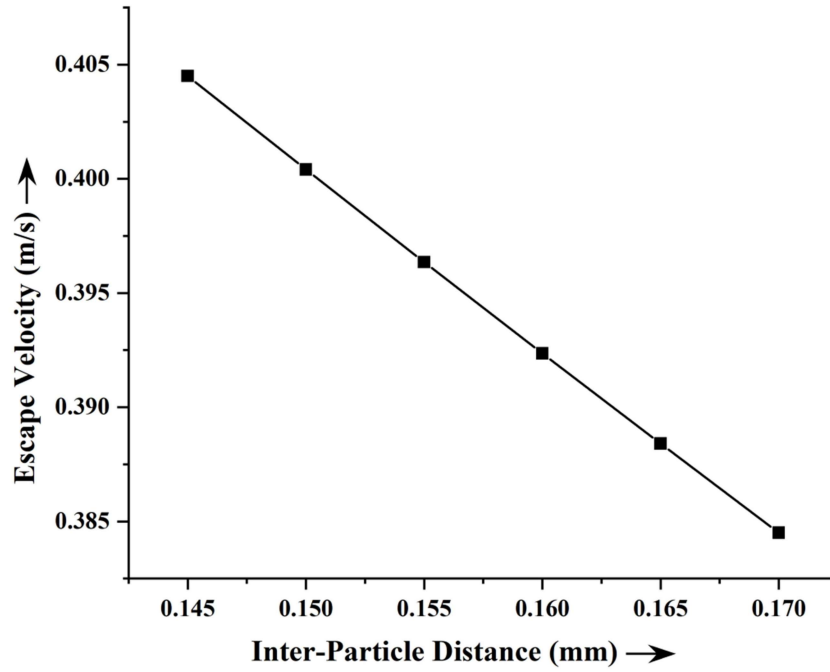


**Fig. 2.38** Changes in escape velocity with inter-particle spacing for 25 nl liquid-bridge volume in a fully exposed [ $e = 1.0$ ] scenario for rising river-water level

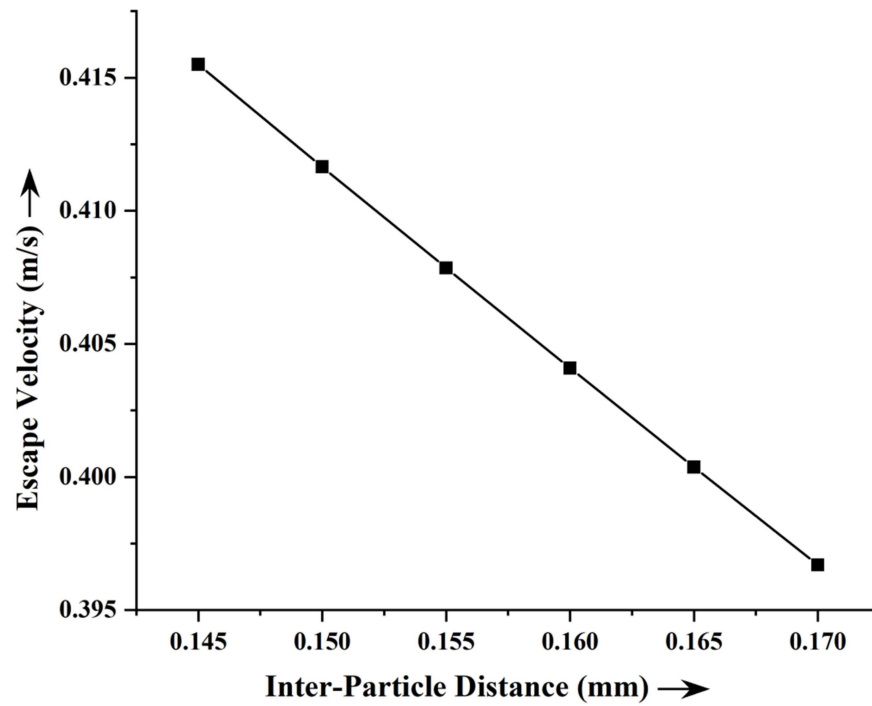


**Fig. 2.39** Changes in escape velocity with inter-particle spacing for 30 nl liquid-bridge volume in a fully exposed [ $e = 1.0$ ] scenario for rising river-water level

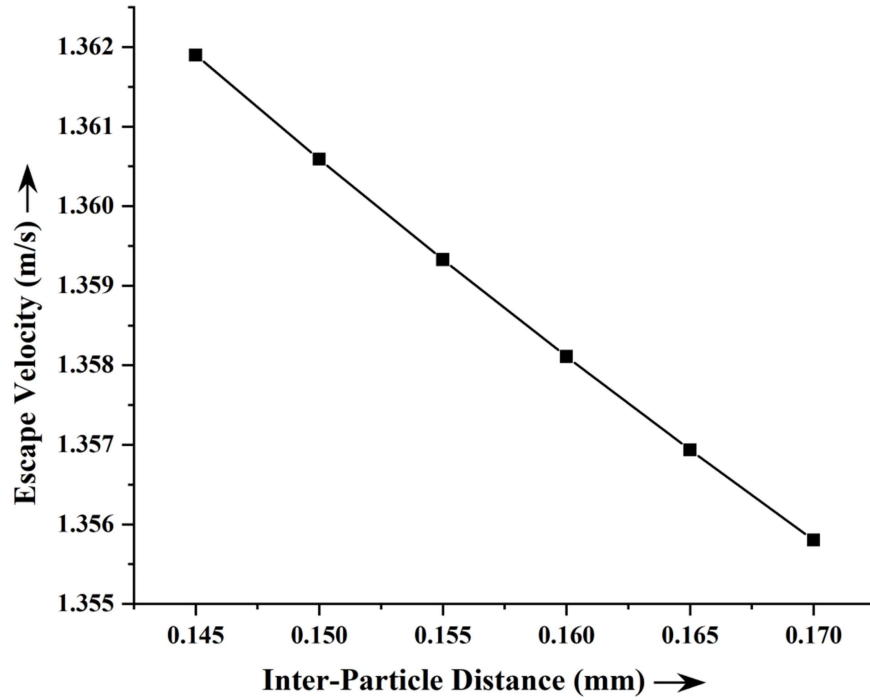


**Fig. 2.40** Changes in escape velocity with inter-particle spacing for 10 nl liquid-bridge volume in a half submerged [ $e = 0.5$ ] scenario for rising river-water level

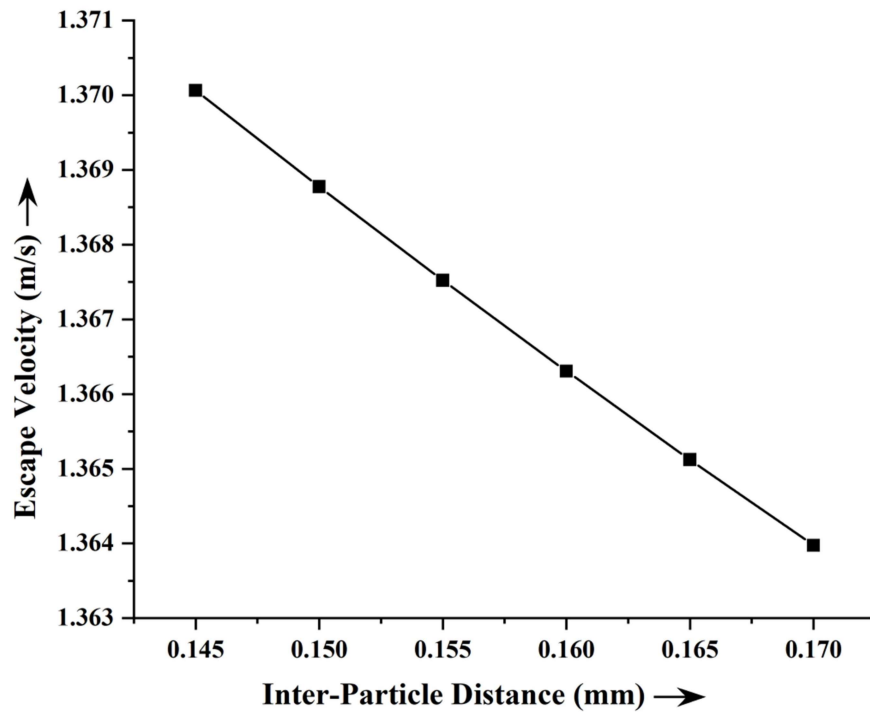


**Fig. 2.41** Changes in escape velocity with inter-particle spacing for 15 nl liquid-bridge volume in a half submerged [ $e = 0.5$ ] scenario for rising river-water level



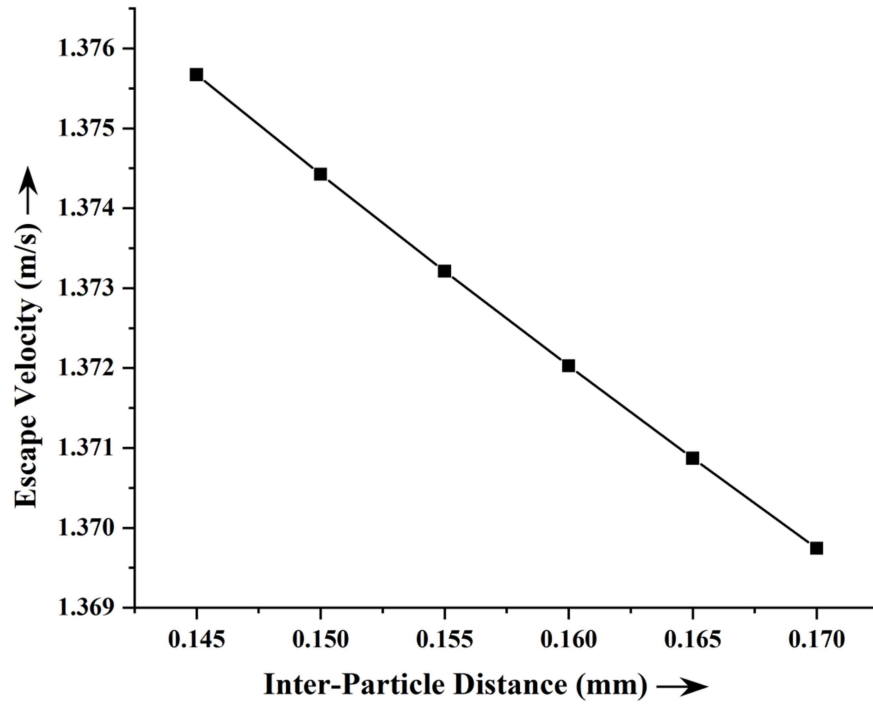


**Fig. 2.42** Changes in escape velocity with inter-particle spacing for 20 nl liquid-bridge volume in a half submerged [ $e = 0.5$ ] scenario for rising river-water level

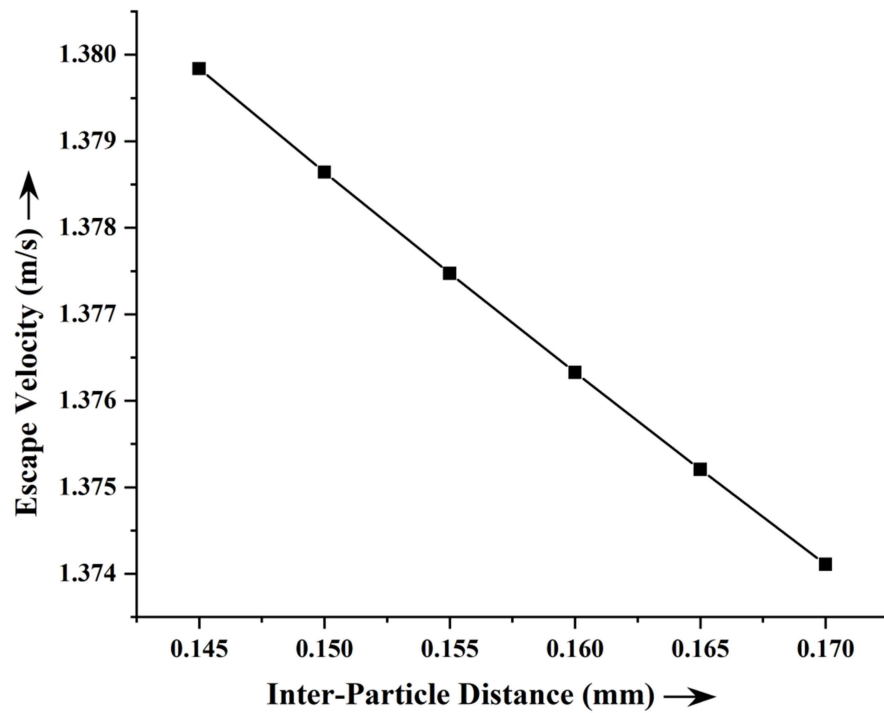


**Fig. 2.43** Changes in escape velocity with inter-particle spacing for 25 nl liquid-bridge volume in a half submerged [ $e = 0.5$ ] scenario for rising river-water level

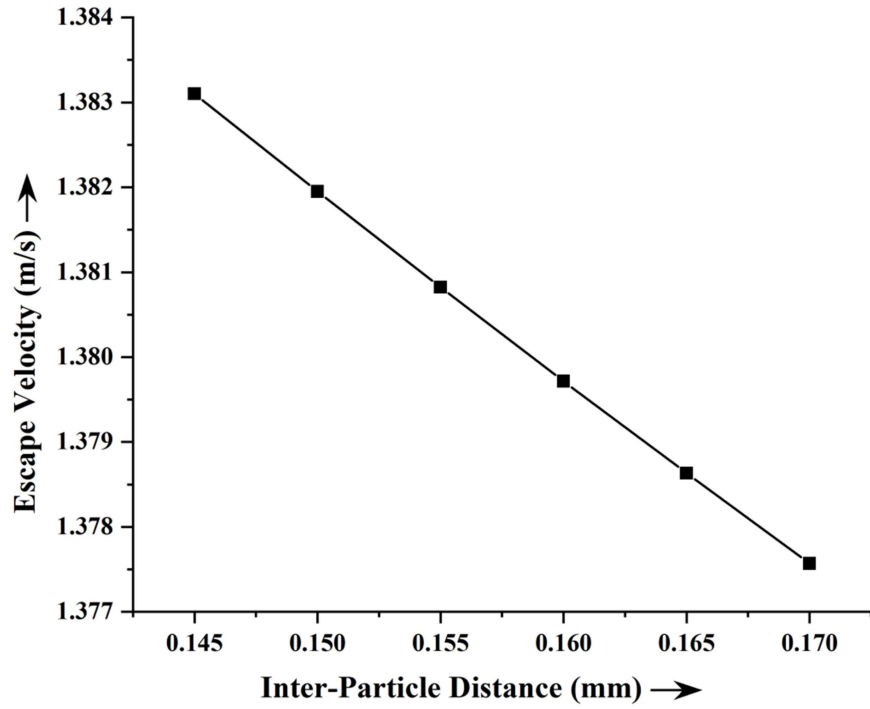


**Fig. 2.44** Changes in escape velocity with inter-particle spacing for 30 nl liquid-bridge volume in a half submerged [ $e = 0.5$ ] scenario for rising river-water level

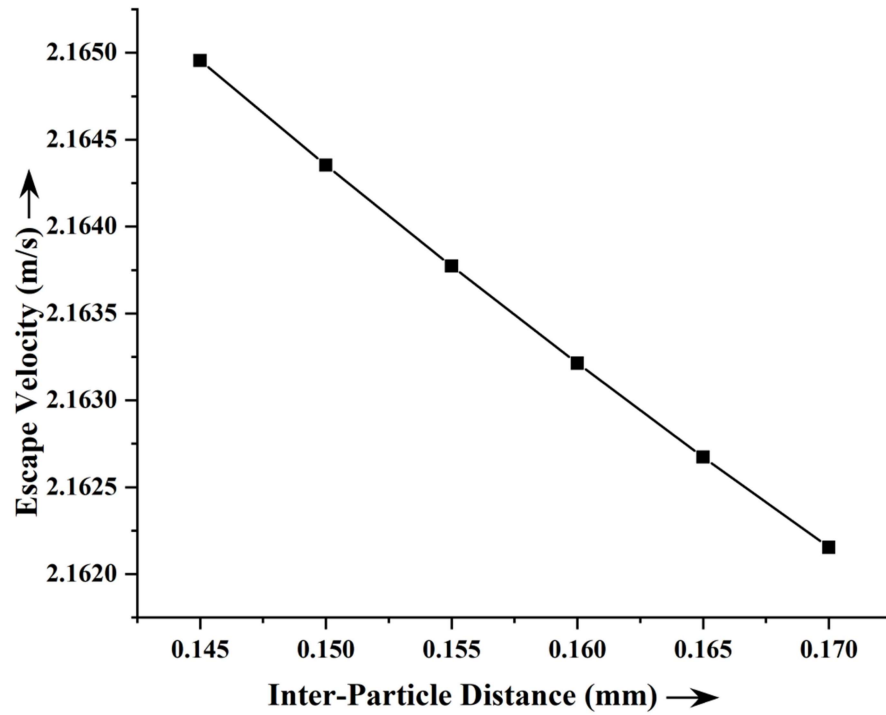


**Fig. 2.45** Changes in escape velocity with inter-particle spacing for 10 nl liquid-bridge volume in a fully submerged [ $e = 0.0$ ] scenario for rising river-water level

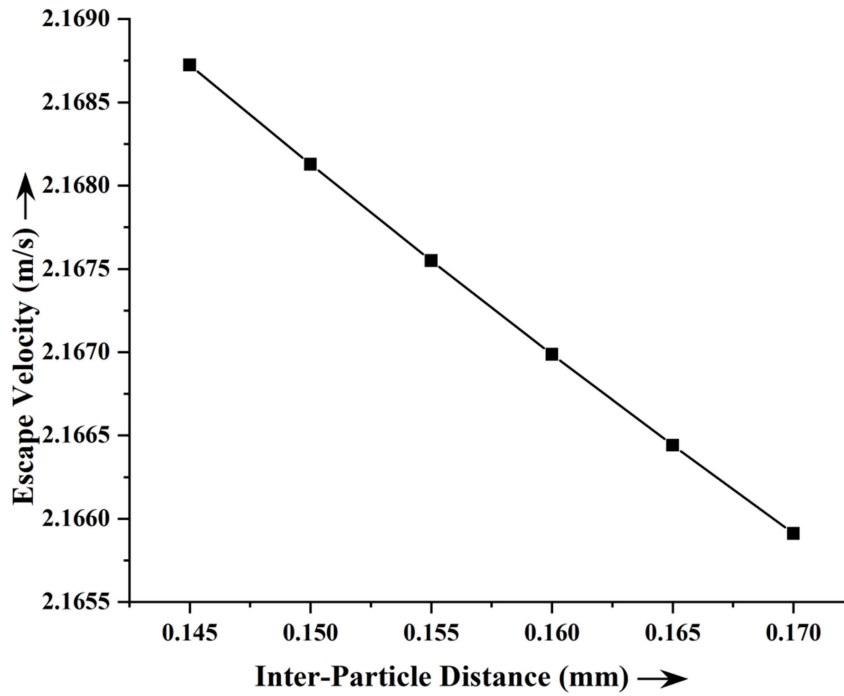


**Fig. 2.46** Changes in escape velocity with inter-particle spacing for 15 nl liquid-bridge volume in a fully submerged [ $e = 0.0$ ] scenario for rising river-water level

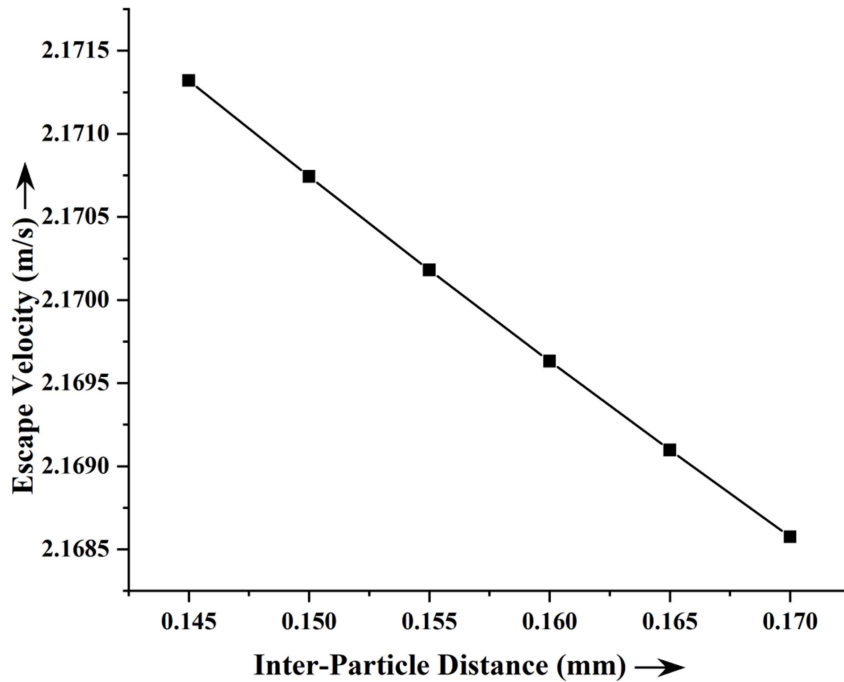


**Fig. 2.47** Changes in escape velocity with inter-particle spacing for 20 nl liquid-bridge volume in a fully submerged [ $e = 0.0$ ] scenario for rising river-water level

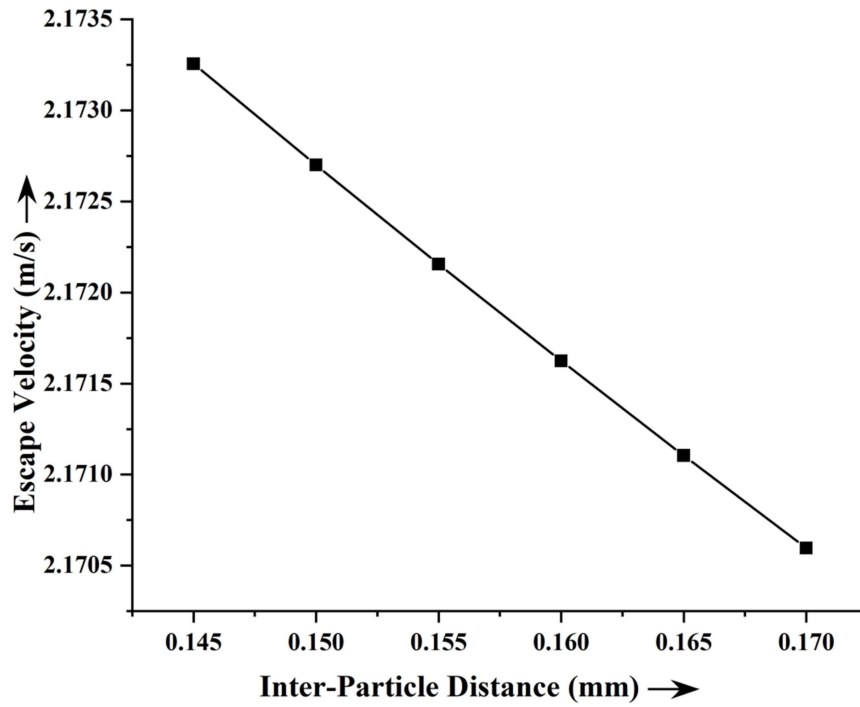


**Fig. 2.48** Changes in escape velocity with inter-particle spacing for 25 nl liquid-bridge volume in a fully submerged [ $e = 0.0$ ] scenario for rising river-water level

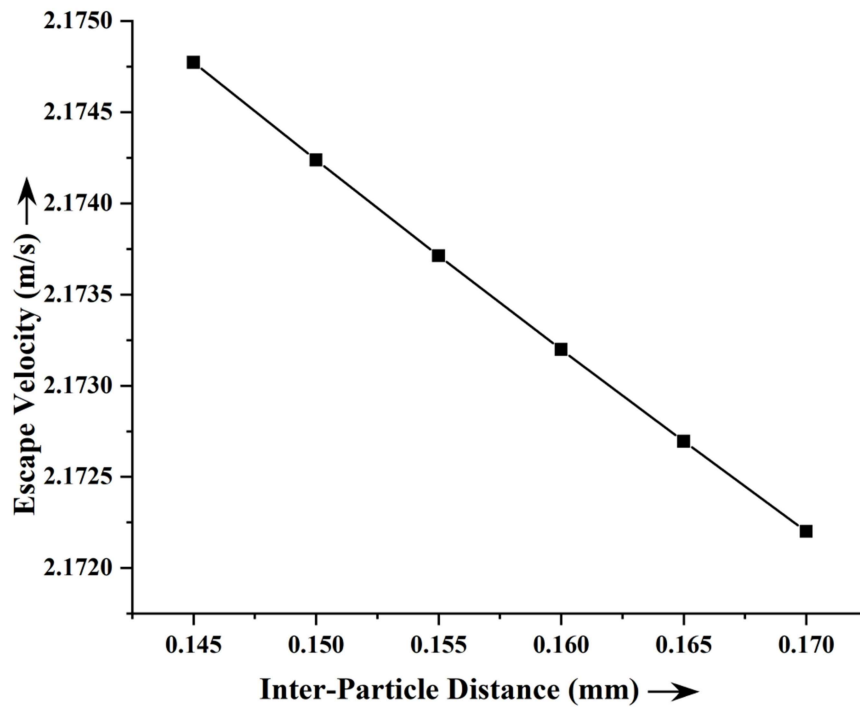


**Fig. 2.49** Changes in escape velocity with inter-particle spacing for 30 nl liquid-bridge volume in a fully submerged [ $e = 0.0$ ] scenario for rising river-water level

### 2.5.2.2 *Escape Velocity Variation for Water Level Falling*

Graph of the variation with regard to inter-particle distance for water level falling is presented here. Inter-particle distance ranges from 0.145 to 0.170 mm at intervals of 0.005 mm. First five graphs are for fully exposed [ $e = 1.0$ ] scenario, next five are for half exposed [ $e = 0.5$ ] scenario and last five are for fully submerged [ $e = 0.0$ ] scenario. The related table (Table 2.4) is also provided in order to display the results in tabular form.

**Table 2.4: Escape velocity variation with inter-particle distance for different liquid-bridge volumes for water level falling**

<b>Liquid-Bridge Volume (nl)</b>	<b>Inter-Particle Distance (mm)</b>	<b>Escape Velocity for Fully Exposed (m/s)</b>	<b>Escape Velocity for Half Exposed (m/s)</b>	<b>Escape Velocity for Fully Submerged (m/s)</b>
10	0.145	0.290732238	0.682551469	1.486321704
	0.150	0.286214696	0.680639497	1.485444656
	0.155	0.281791739	0.678791468	1.484598787
	0.160	0.277461767	0.677005395	1.483783005
	0.165	0.273223205	0.675279344	1.482996256
	0.170	0.269074507	0.673611434	1.48223752
15	0.145	0.317580024	0.69441223	1.491805633
	0.150	0.313484615	0.692548826	1.49093916
	0.155	0.309457071	0.690735081	1.490097532

<b>Liquid-Bridge Volume (nl)</b>	<b>Inter-Particle Distance (mm)</b>	<b>Escape Velocity for Fully Exposed (m/s)</b>	<b>Escape Velocity for Half Exposed (m/s)</b>	<b>Escape Velocity for Fully Submerged (m/s)</b>
15	0.160	0.305496463	0.688969783	1.489280049
	0.165	0.301601874	0.687251747	1.488486031
	0.170	0.297772401	0.68557981	1.487714817
20	0.145	0.334853387	0.702479939	1.495578071
	0.150	0.331091254	0.700694435	1.494740243
	0.155	0.327382121	0.698949445	1.493923033
	0.160	0.323725361	0.697244134	1.493125944
	0.165	0.320120357	0.695577685	1.492348491
	0.170	0.316566499	0.693949293	1.491590199
25	0.145	0.347182442	0.70843978	1.498386673
	0.150	0.343685283	0.706732515	1.497580231
	0.155	0.340231627	0.705059454	1.496791413
	0.160	0.336821015	0.703419981	1.496019843
	0.165	0.333452996	0.701813489	1.495265152
	0.170	0.330127121	0.70023938	1.494526979
30	0.145	0.356559267	0.713081892	1.500587047
	0.150	0.353278023	0.71144686	1.499810767

Liquid-Bridge Volume (nl)	Inter-Particle Distance (mm)	Escape Velocity for Fully Exposed (m/s)	Escape Velocity for Half Exposed (m/s)	Escape Velocity for Fully Submerged (m/s)
30	0.155	0.35003368	0.709841426	1.499049883
	0.160	0.346825883	0.70826511	1.498304097
	0.165	0.343654282	0.706717439	1.497573117
	0.170	0.340518533	0.705197947	1.496856655

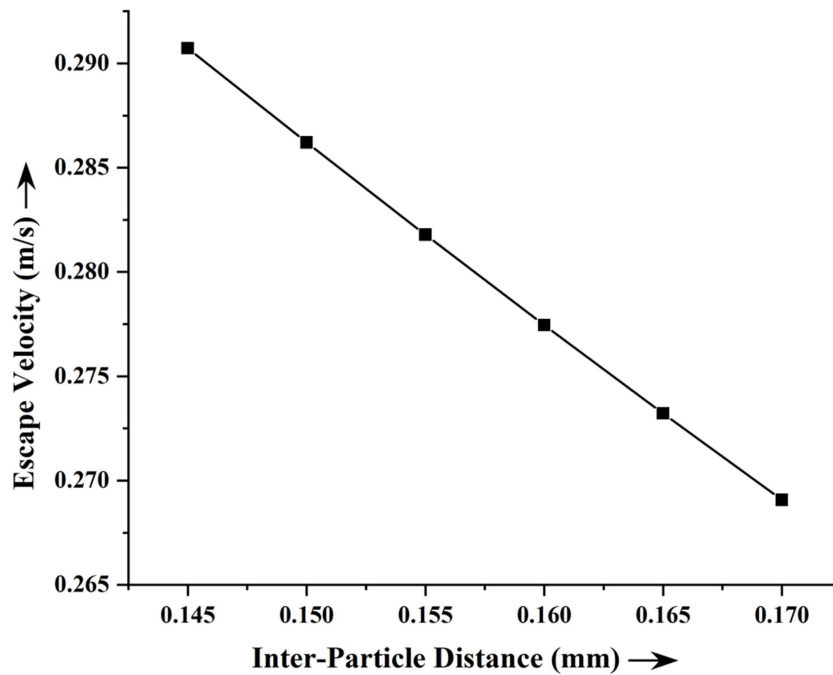


**Fig. 2.50** Changes in escape velocity with inter-particle spacing for 10 nl liquid-bridge volume in a fully exposed [ $e = 1.0$ ] scenario for falling river-water level

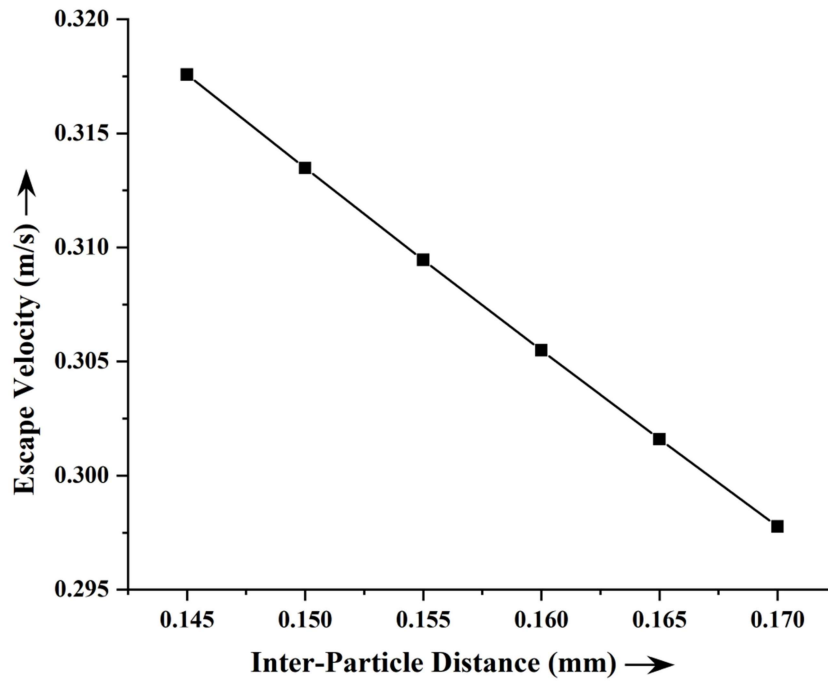


**Fig. 2.51** Changes in escape velocity with inter-particle spacing for 15 nl liquid-bridge volume in a fully exposed [ $e = 1.0$ ] scenario for falling river-water level

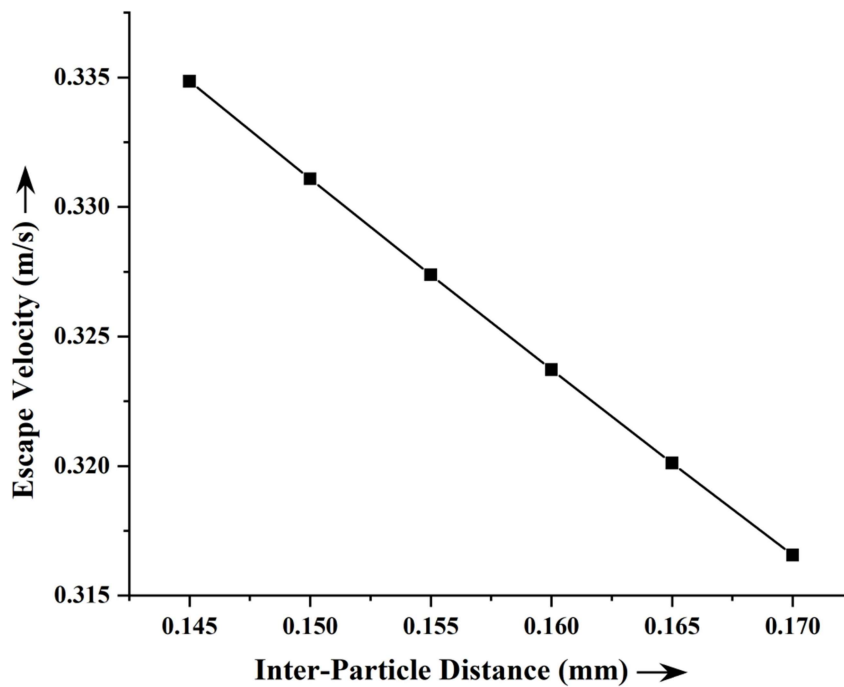


**Fig. 2.52** Changes in escape velocity with inter-particle spacing for 20 nl liquid-bridge volume in a fully exposed [ $e = 1.0$ ] scenario for falling river-water level



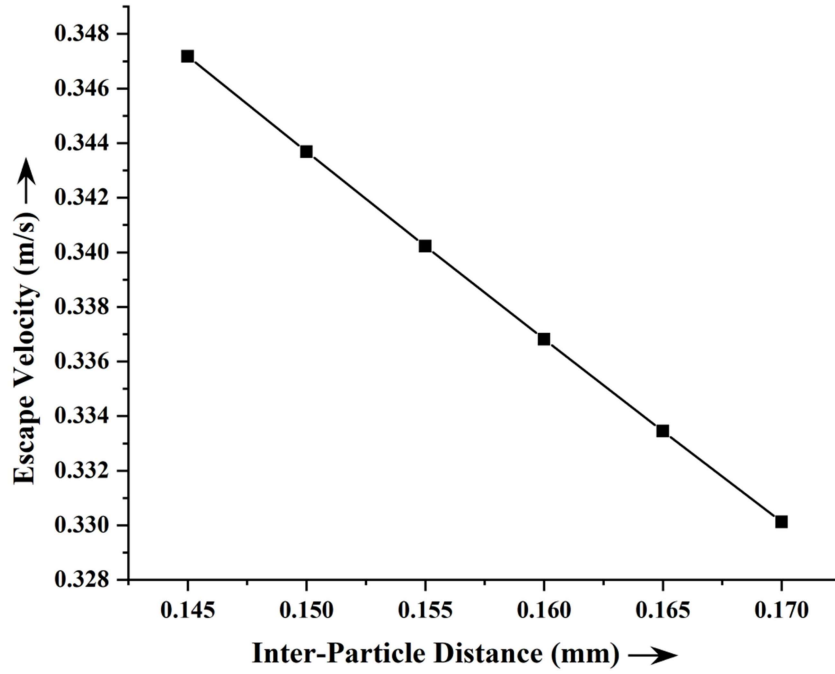


**Fig. 2.53** Changes in escape velocity with inter-particle spacing for 25 nl liquid-bridge volume in a fully exposed [ $e = 1.0$ ] scenario for falling river-water level

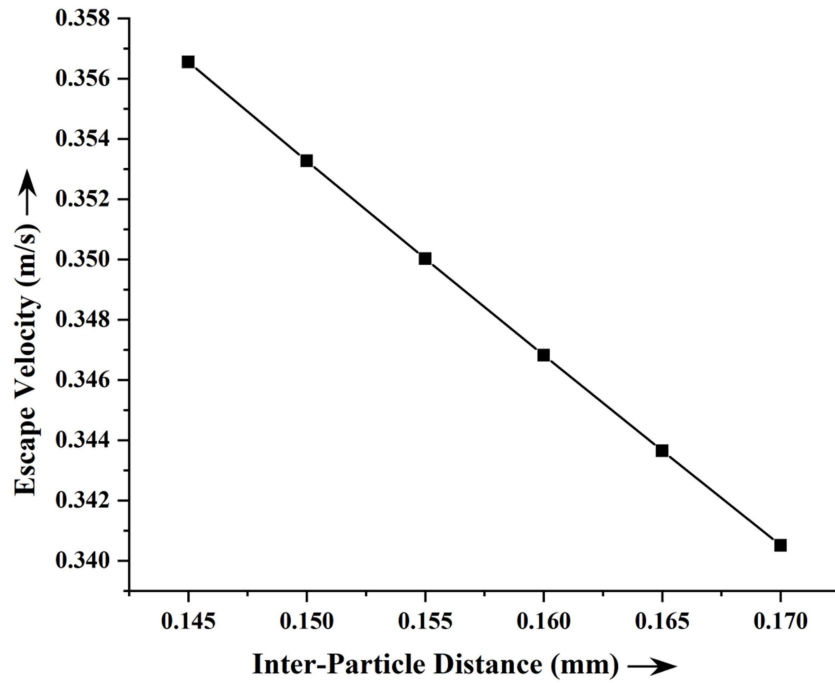


**Fig. 2.54** Changes in escape velocity with inter-particle spacing for 30 nl liquid-bridge volume in a fully exposed [ $e = 1.0$ ] scenario for falling river-water level

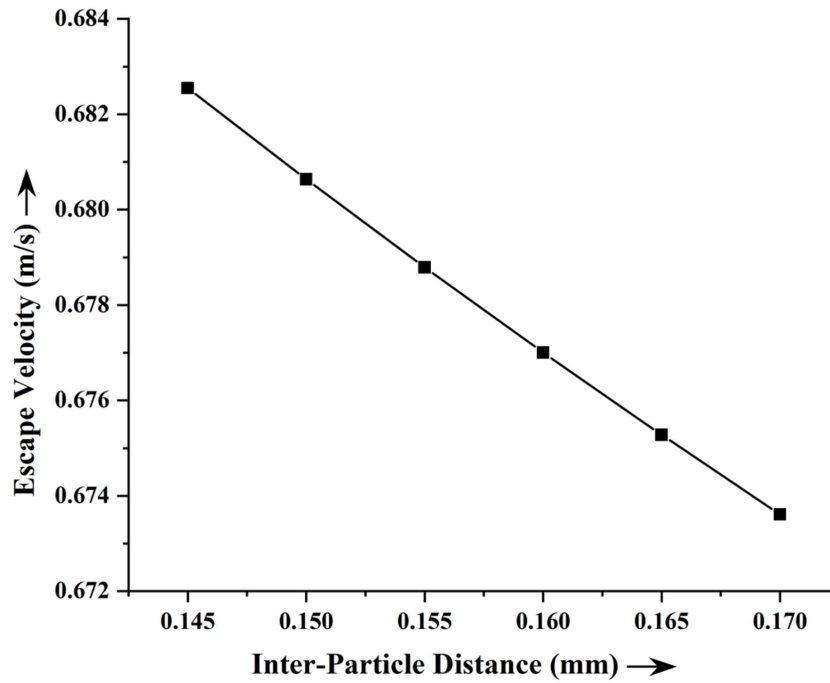


**Fig. 2.55** Changes in escape velocity with inter-particle spacing for 10 nl liquid-bridge volume in a half submerged [ $e = 0.5$ ] scenario for falling river-water level

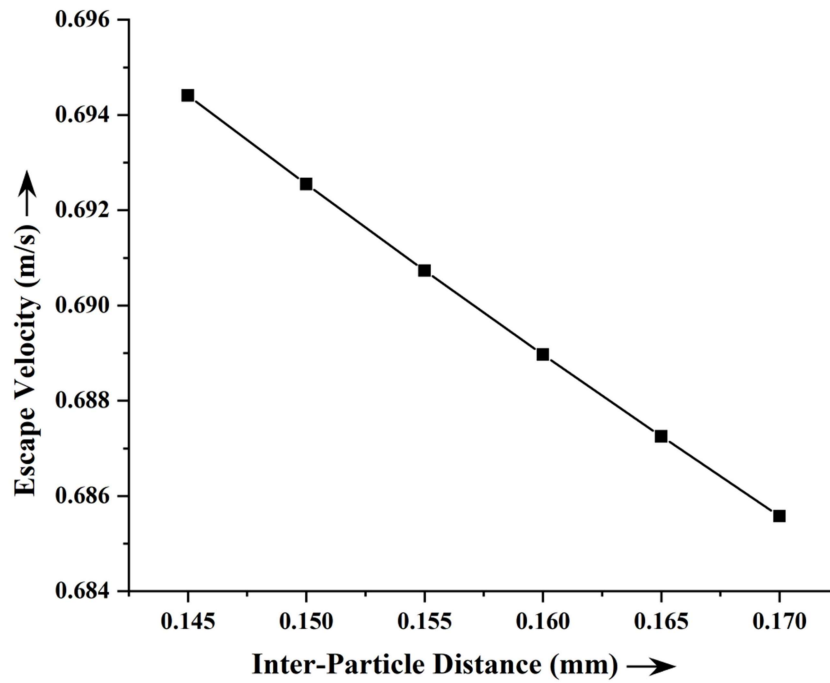


**Fig. 2.56** Changes in escape velocity with inter-particle spacing for 15 nl liquid-bridge volume in a half submerged [ $e = 0.5$ ] scenario for falling river-water level

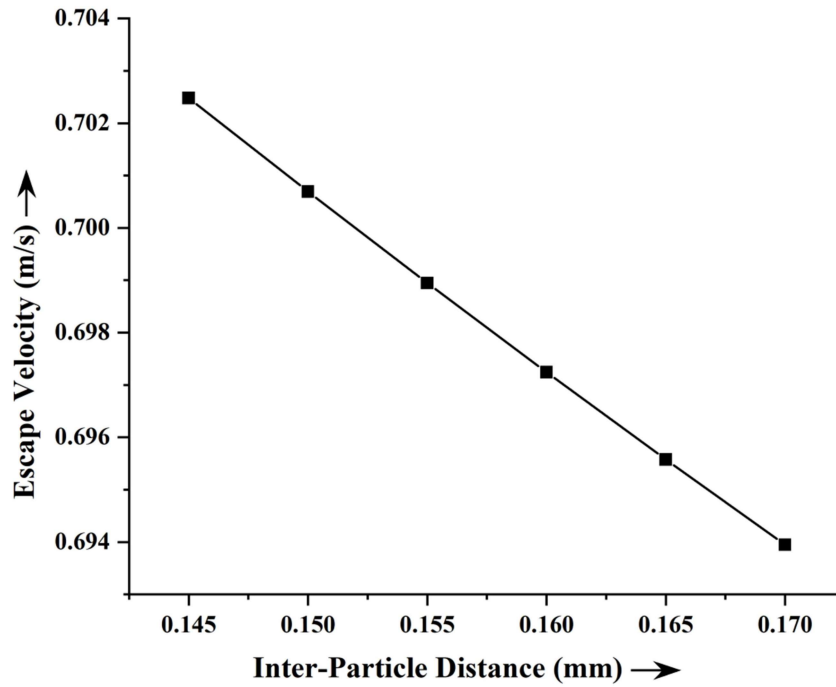


**Fig. 2.57** Changes in escape velocity with inter-particle spacing for 20 nl liquid-bridge volume in a half submerged [ $e = 0.5$ ] scenario for falling river-water level

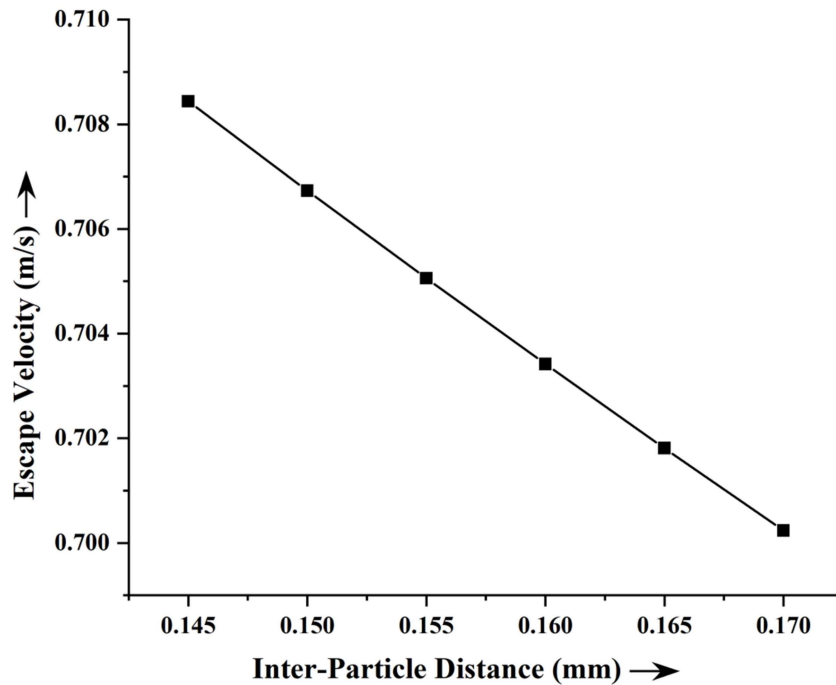


**Fig. 2.58** Changes in escape velocity with inter-particle spacing for 25 nl liquid-bridge volume in a half submerged [ $e = 0.5$ ] scenario for falling river-water level

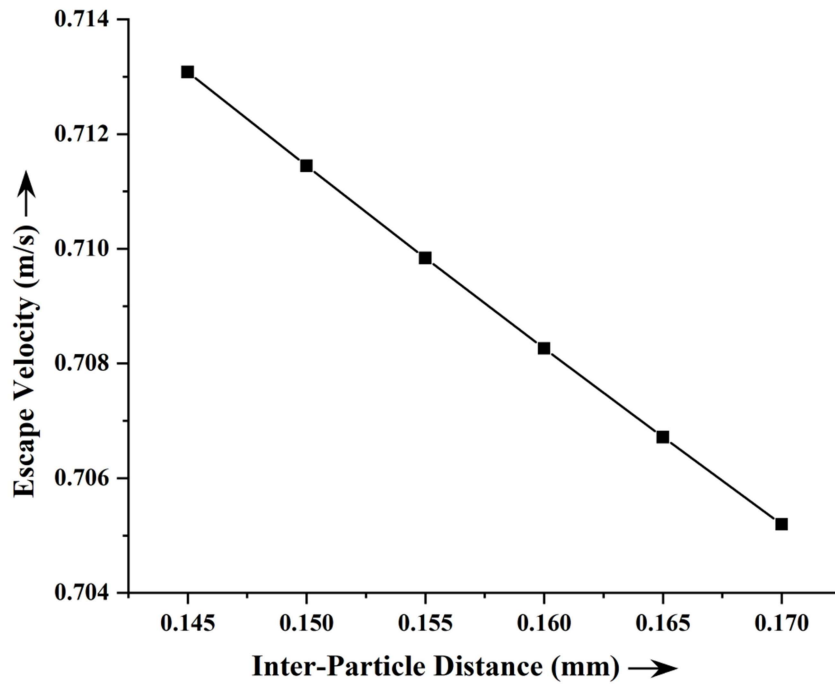


**Fig. 2.59** Changes in escape velocity with inter-particle spacing for 30 nl liquid-bridge volume in a half submerged [ $e = 0.5$ ] scenario for falling river-water level

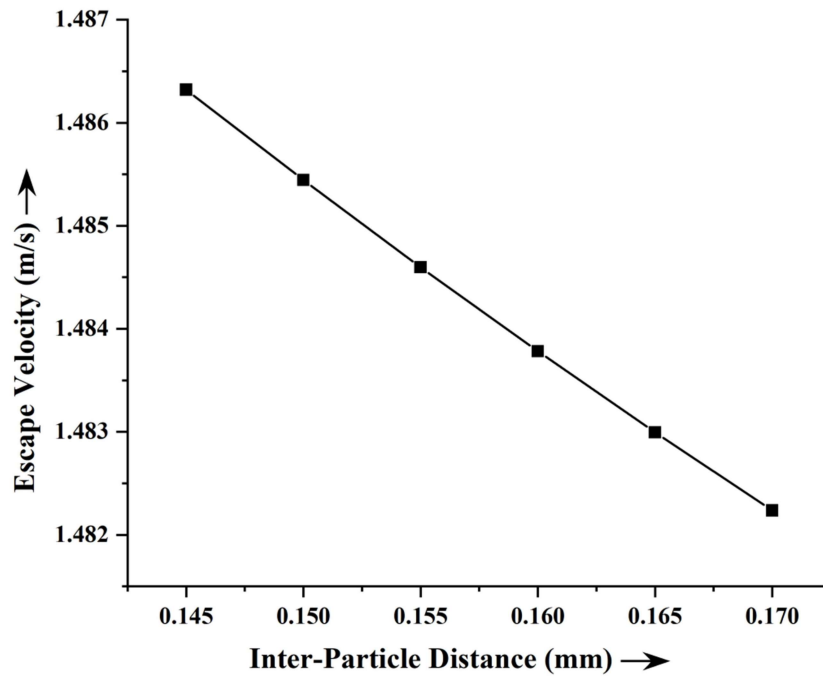


**Fig. 2.60** Changes in escape velocity with inter-particle spacing for 10 nl liquid-bridge volume in a fully submerged [ $e = 0.0$ ] scenario for falling river-water level

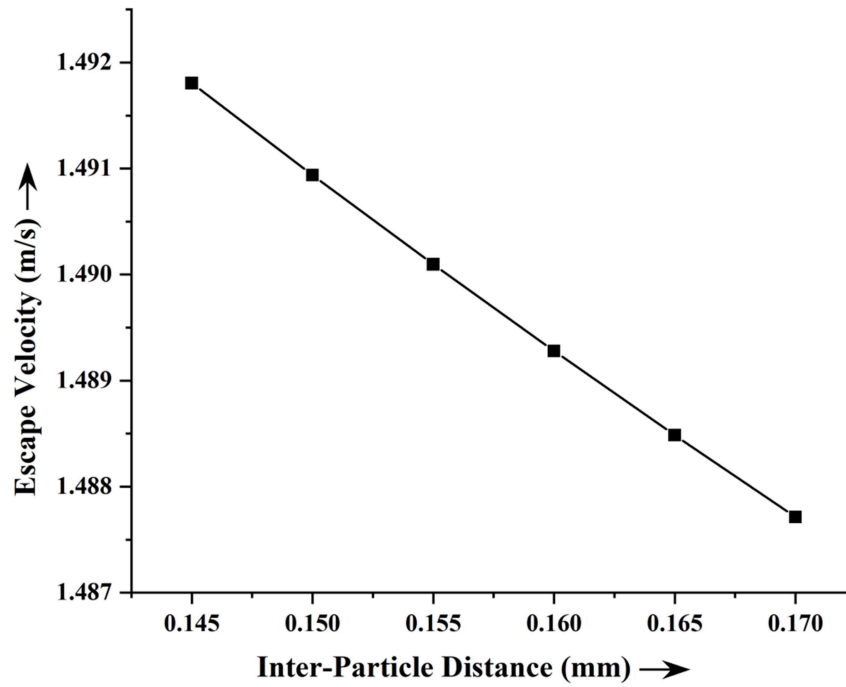


**Fig. 2.61** Changes in escape velocity with inter-particle spacing for 15 nl liquid-bridge volume in a fully submerged [ $e = 0.0$ ] scenario for falling river-water level

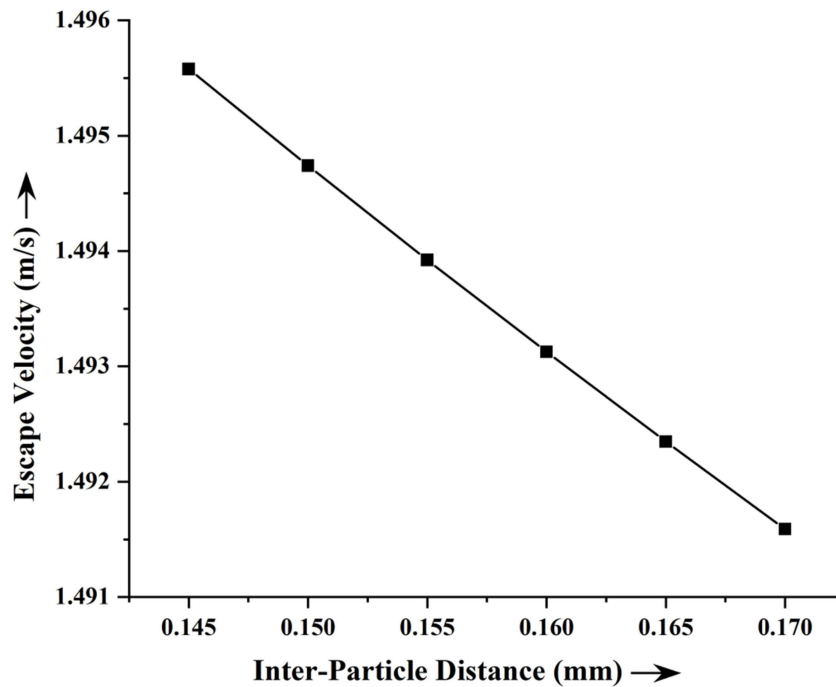


**Fig. 2.62** Changes in escape velocity with inter-particle spacing for 20 nl liquid-bridge volume in a fully submerged [ $e = 0.0$ ] scenario for falling river-water level

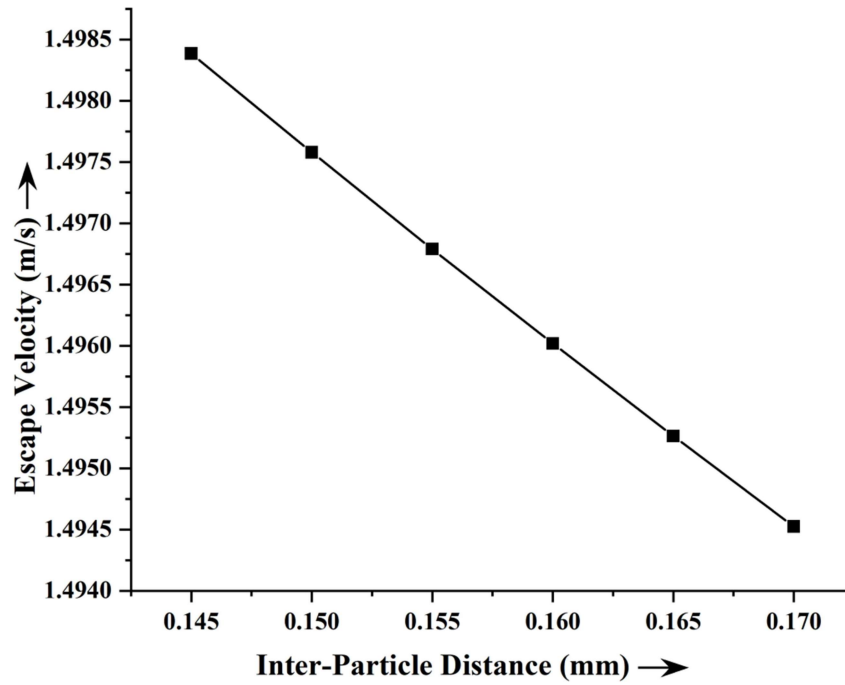


**Fig. 2.63** Changes in escape velocity with inter-particle spacing for 25 nl liquid-bridge volume in a fully submerged [ $e = 0.0$ ] scenario for falling river-water level

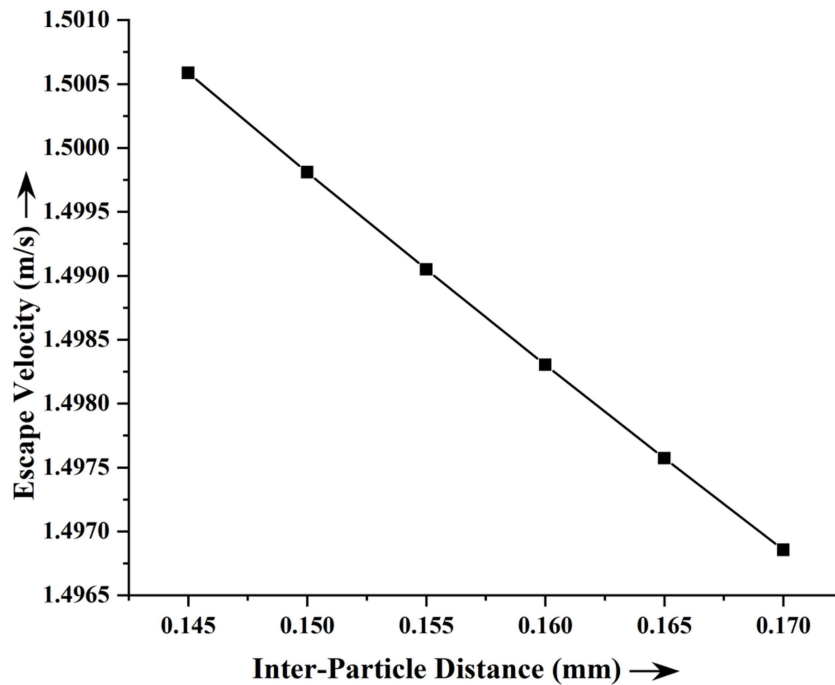


**Fig. 2.64** Changes in escape velocity with inter-particle spacing for 30 nl liquid-bridge volume in a fully submerged [ $e = 0.0$ ] scenario for falling river-water level

## 2.6 Discussions

Analyses are made with varying parameters various parameter corresponding to rise and fall of water levels. Firstly, the liquid-bridge volume is kept constant while various particle sizes are analysed, and the escape velocity variations are plotted against the inter-particle distance both conditions of water level rising (Fig. 2.5 to Fig. 2.19) and falling (Fig. 2.20 to Fig. 2.34), for three different degrees of particle exposure ( $e$ ) scenarios (Fully exposed [ $e = 1.0$ ] scenario, Half submerged [ $e = 0.5$ ] scenario and Fully submerged [ $e = 0.0$ ] scenario). As the distance between particles grows, the escape velocity gradually decreases. The graph clearly shows that as particle size grows, the escape velocity gradually drops. As the degree of exposure increases, the escape velocity drops. When entirely submerged, escape velocity has the maximum value; when fully exposed, it has the minimum value. This is because water binds the particle together. Therefore, a totally submerged particle has the greatest stability, whereas a fully exposed particle has the minimum stability. Moreover, while comparing a situation when the water level is rising to the one when it is decreasing, the escape velocity in the falling water scenario is smaller. This demonstrates how the riverbank erodes when the water level drops as opposed to when it rises.

Secondly, the particle size is kept constant while various liquid-bridge volumes are analysed, and the escape velocity graphs are plotted vis-à-vis the inter-particle distance. This is done for both the situations – rising (Fig. 2.35 to Fig. 2.49) and falling water level (Fig. 2.50 to Fig. 2.64), for three different degrees of particle exposure ( $e$ ) scenarios (Fully exposed [ $e = 1.0$ ] scenario, Half exposed [ $e = 0.5$ ]

scenario and Fully submerged [ $e = 0.0$ ] scenario). The escape velocity decreases as the distance between particles grows. The greater is the degree of exposure, the lower the escape velocity. Escape velocity has the maximum value when completely submerged and the minimum value when fully exposed. Again, this happens due to binding ability of water. Consequently, the particle that is fully immersed is the most stable, whereas the particle that is fully exposed is the least stable. There is a positive correlation between the escape velocity and the liquid-bridge volume. This is due to the fact that the water that has been trapped is essential to the particle's cohesiveness. Therefore, as the liquid-bridge volume grows, the stability improves. This is why, moist sand is more stable than dry sand.



**CHAPTER 3**

**MACROSCOPIC ANALYSIS**

# Chapter 3

## Macroscopic Analysis

### 3.1 Introduction

From the days of yore to the present era, human civilization has mostly been affected by the river system and flood defence. Most of the civilization has been developed based on the river stream as to grow their basic need like agriculture. Man-made infrastructure has been destroyed due to riverbank failure as it is associated loss of lands. From the page of history there is a clear picture that the civilization has been destroyed most of the cases due to either flood or riverbank erosion. So, from the primitive era there is a great interest for the researchers to analyse the riverbank stability.

Most of the research works in the field of riverbank stability are based on the experimental results which have been basically different case studies associated with particular river system. The results obtained in that manner are not any physically significant for the other river system. On the other hand these types of experiment consume lots of time as well as huge money. So, it is quite obvious to find out general expressions for riverbank stability with less time and less investigation cost which are applicable for any kind of river system. So, the necessity of the analytical approach is very important. Many researchers have tried to find out an analytical solution in microscopic level. But macroscopic approach to find out the riverbank stability is yet to be investigated. Here, in this section transformation of well-established microscopic force analysis into macroscopic force analysis has been implemented which are more practical and comparable with the filed data analysis. By transforming

microscopic analysis into macroscopic analysis volumetric rate of erosion has been found out in terms of escape velocity, as the escape velocity is considered to be the most significant parameter to measure the stability of the bank surfaces. Lower escape velocity implies higher the value of volumetric erosion rate which indicates less stability of the riverbank.

Right-angled trapezoidal failure block has been considered to find out the escape velocity. The common bank angle considered here is of  $60^\circ$  which is in line with Darby and Thorne (1996). Each particle will be positioned on top of two adjacent particles with a small volume of liquid entrapment in the microscopic arrangement of the particles. This type of arrangement of the particles is considered as most stable particle arrangement which has been established by Mukherjee and Mazumdar (2010).

Different kinds of microscopic forces considered in this analysis are particle pore pressure force, inter-molecular force of cohesion, hydrostatic pressure force due to water entrapment and the force which is induced due to net weight of the block. To assess the particle's escape velocity, the overall effect of these forces on the trapezoidal tension crack has been analysed.

Both the situations comprising of rising and falling water level have been studied to see the manifestation of the dynamic nature of the river system. For both the situations, results have been plotted for various free surface heights of the water level. The dynamic nature of the river system has been observed in both rising and falling water level scenarios that have been examined. The outcomes for each scenario have been plotted at different water level free surface heights.

This study examines how the dynamic behaviour of confined water affects bank soil particle erosion as a function of rising and falling water levels. Water level fluctuations have a direct impact on the rate of bank erosion in terms of escape velocity at the macro and micro-levels, which is ultimately a major contributing factor to mass failure. As a result, the hydraulic natures of the river and bank erosion are directly correlated in this study.

### 3.2 Force Calculation

Here, both the microscopic and macroscopic forces have been analysed. Microscopic forces are the particle level forces which are particle cohesive force and particle pore pressure force whereas macroscopic forces act on the failure block as a whole. Hydroscopic pressure force and the force induced due to the weight of the failure block are considered as macroscopic forces. Transformation of the microscopic forces into macroscopic force has been depicted here.

Right-angle trapezoidal failure block has been considered in this present work with similar size particle. Considering different macroscopic forces, the free-body diagram of the block has been shown in the Fig. 3.1. Trapezoidal failure block has been represented by ABDE. The centre of gravity of the block in the Fig. 3.1 is point O and  $\frac{2}{3}rd$  distance from the base AB has been shown by the line CF. Free surface water level has been represented by line MN which is varying from 0 to height of the block to study the dynamic behaviour the riverbank system.

The height of the failure block is represented by  $H$  whereas free surface water column height is represented by  $H_w$  in the Fig. 3.1 with the base of  $b$  and width of  $w$ . Hydrostatic confining pressure force is represented by  $F_{cp}$  with two components of

$F_{cpx}$  and  $F_{cpy}$ . And the net weight of the failure block is represented by  $F_g$ . The centre of gravity of the right-angled trapezoidal failure block

$$[x_o, y_o] = \left[ \frac{H}{2}, \frac{(w+2b)}{3 \times (w+b)} \times H \right] \quad (3.1)$$

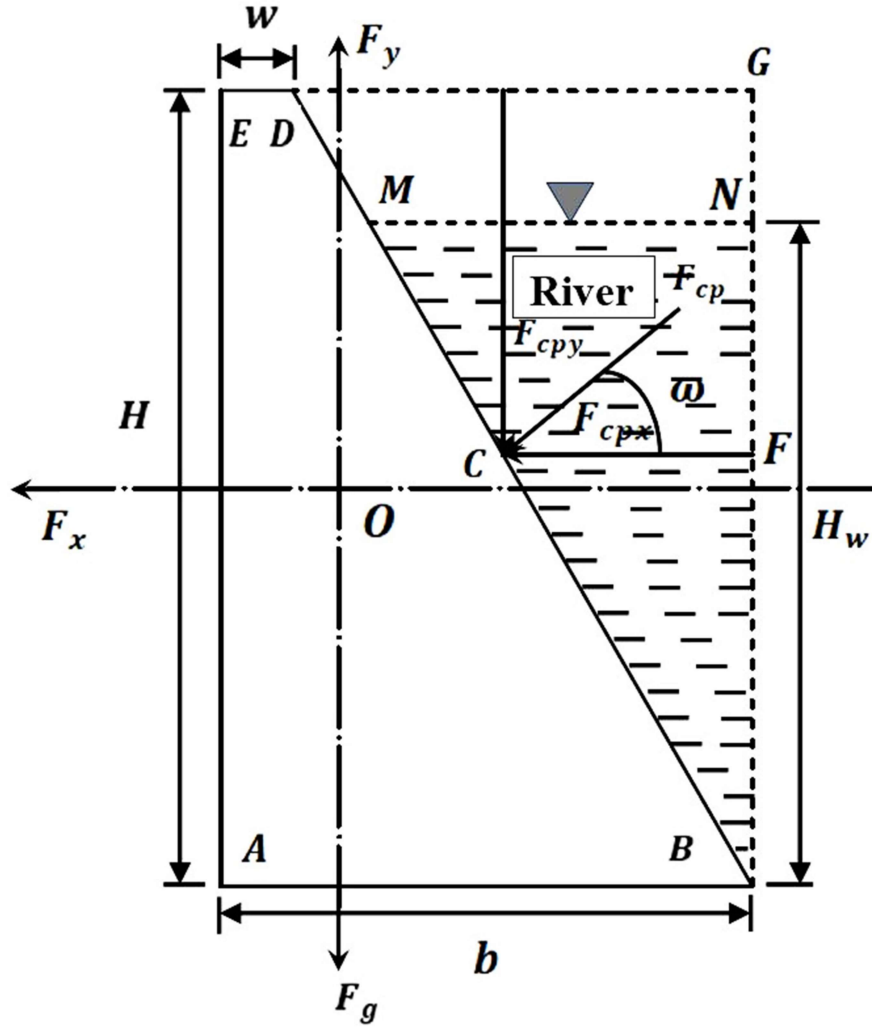


**Fig. 3.1** Free-body diagram of trapezoidal failure block alongside river water

Here, Base  $b = 2 \times P \times (n-1)$  and Width  $w = 2 \times P$ , and Height

$$H = 2 \times \frac{\sqrt{3}}{2} \times P \times (n-2) \text{ and } P = \left[ R + \frac{d_p}{2} \right], \text{ } n \text{ represents the number of base particles}$$

in the block,  $R$  represents the radius of the spherical soil grains and  $d_p$  represents the

inter-particle distance. The total number of particles in the block can be calculated as a function of  $n$  as  $N = [n^2 - 2]$ . The hydrostatic confining pressure force will act on the block at a height  $\frac{2}{3}rd$  of the free surface water depth through the point  $C$ . Hence the distance  $x_c$  and  $y_c$  can be calculated as follows

$$x_c = b - \frac{2}{3} \times \frac{H_w}{H} \times (b - w) \quad (3.2a)$$

$$y_c = \overline{BF} = \frac{2}{3} \times H_w \quad (3.2b)$$

### 3.2.1 Particle Cohesive Force

Considering toroidal or parabolic structured liquid-bridge between the two adjacent grains, an expression for the calculation of cohesive force has been developed by Soulie et al. (2006)<sup>25</sup> for two dissimilar grains. Two different sized particles with radii  $R_1$  and  $R_2$  and the inter-particle gap of  $d_p$  have been shown in Fig. 3.2 and the expression developed by them is as follows (Eq. 2.1 to Eq. 2.3c are written once again for ready reference)

$$F_c = \sigma \times \pi \times \sqrt{R_1 \times R_2} \times \left[ \exp \left\{ A \times \left( \frac{d_p}{R_{max}} \right) + B \right\} + C \right] \quad (2.1)$$

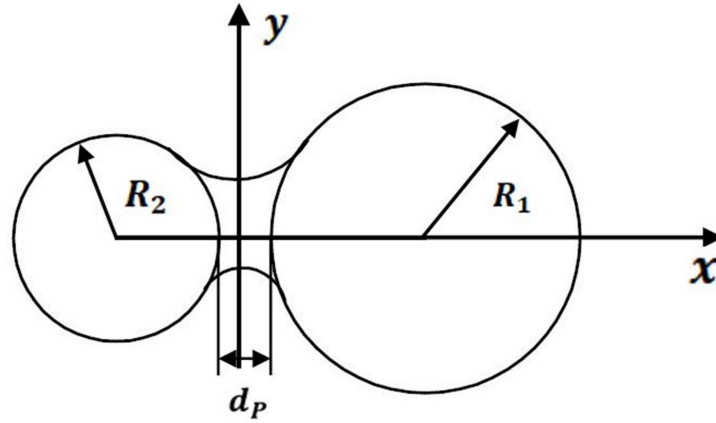


**Fig. 3.2** Dissimilar soil grains with toroid shaped entrapped inter-granular liquid-bridge [Soulie et al. (2006)<sup>25</sup>]

Here, capillary cohesive force between two dissimilar grains has been represented by  $F_c$ . And the surface tension coefficient has been represented by  $\sigma = 0.073 \text{ N/m}$  (pure water). By considering similar sized particles, above expression can be reduced

$$F_c = \sigma \times \pi \times R \times \left[ \exp \left\{ A \times \left( \frac{d_p}{R} \right) + B \right\} + C \right] \quad (2.2)$$

The parameters  $A$ ,  $B$  and  $C$  in the above expression depend upon grain radius ( $R$ ) and inter-granular liquid-bridge volume ( $\forall_l$ ). And the expressions to evaluate  $A$ ,  $B$  and  $C$  are as follows

$$A = -1.1 \times (\forall_l / R^3)^{(-0.53)} \quad (2.3a)$$

$$B = \left[ \left\{ -0.148 \ln \left( \frac{\forall_l}{R^3} \right) - 0.96 \right\} \times \varnothing^2 - 0.0082 \ln \left( \frac{\forall_l}{R^3} \right) + 0.48 \right] \quad (2.3b)$$

$$C = \left[ 0.0018 \times \ln \left( \frac{\forall_l}{R^3} \right) + 0.078 \right] \quad (2.3c)$$

Here,  $\theta$  represents the angle of contact. It has been considered to be  $0^\circ$  for pure water.

### 3.2.2 Particle Pore Pressure Force

In order to ascertain the situation of saturated or unsaturated, it is necessary to determine the capillary rise height. For finding the capillary rise through the tube the generalized expression is

$$h_{CR} = \frac{4 \times \sigma \times \cos \theta}{\gamma_w \times d_t} \quad (3.3)$$

$\theta$  represents the angle of contact between solid and liquid interface and  $d_t$  and  $\gamma_w$  represent the average diameter of the tube and specific weight of water respectively. For identifying average diameter of the tube an approximation has been given by Bowles (1979)<sup>50</sup> as follows

$$d_t \cong 0.2 \times D_{10} \quad (3.4)$$

$D_{10}$  has been considered in the order of 0.15 mm for the soil grains. Therefore, Considering above value of  $D_{10}$  the diameter of the tube will be in the range of 0.03 mm and hence capillary rise will be in order of 10 m. In general situation the bank height is less than 10 m. So, it can be considered fully saturated condition to calculate pore water pressure. Likos and Lu (2002)<sup>15</sup> have suggested a series of equations to calculate the induced pore pressure force for fully saturated soil grains, which are as follows (Eq. 2.4 and Eq. 2.5 are written once again for ready reference):

$$F_p = \pi \times P_w \times r_2^2 + 2 \times \pi \times \sigma \times r_2 \quad (2.4)$$



Here, the pore water pressure  $P_w$  has been considered as 10  $kPa$  by Likos and Lu (2002)<sup>15</sup> and

$$r_2 = R \times [\tan \beta - \sec \beta + 1] \quad (2.5)$$

Here,  $\beta$  = Water content index angle =  $45^\circ$  for fully saturated particles by Likos and Lu (2002)<sup>15</sup>.

### 3.2.3 Hydrostatic Confining Pressure Force

**H**ydrostatic confining pressure force exerted on the failure block can be determined by resolving it into two components, such as vertical component and horizontal component. The force will act on the block by considering triangle entrapped area which will act through the height  $\frac{2}{3}rd$  of the depth of free surface water. The hydrostatic confining pressure force in horizontal direction can be evaluated through the expression by Douglas et al. (1995)<sup>51</sup> as

$$F_x = \frac{1}{2} \times H_w^2 \times \gamma_w \quad (3.5)$$

Here,  $\gamma_w$  represents the specific weight of water =  $\rho g$

$\rho$  represents the density of water.

The hydrostatic confining pressure force in vertical direction can be calculated by measuring the water entrapped on the sloped bank face through the following expression

$$F_y = \rho g V_w = \rho g A_w \quad (3.6)$$

Where  $F_y$  = Weight of the water alongside the sloped bank face

Now, from the Fig. 3.1

$$A_w = \frac{1}{2} \times (b - w) \times \frac{H_w}{H} \times H_w \quad (3.7)$$

Hence, the final expression will be

$$F_y = \rho \times g \times \left[ \frac{1}{2} \times (b - w) \times \frac{H_w^2}{H} \right] \quad (3.8)$$

### 3.2.4 Weight of the failure block

Two opposite direction forces are acting on the failure block. They are upward directed buoyancy force and downward directed gravitational force. Hence, the difference between these forces is the net weight of the failure block which has been determined by following expression

$$F_g = A_s \times (\rho_s - \rho) \times g \quad (3.9)$$

Here,  $A_s$  represents the total particles surface area  $= N \times a_s = N \times \pi R^2$ .

Density of the soil grain is  $\rho_s = 2650 \text{ kg/m}^3$  and  $\rho = 1000 \text{ kg/m}^3$  (Duan, 2005)<sup>23</sup>.

## 3.3 Transformation of Microscopic Force System into

### Macroscopic Force System

The concept of momentum principle has been adopted for transforming micro-level force system into a generalized macro-level force. The moment has been taken about the left most base particles which has been considered most stable particle. The direction of the different micro-level forces are different for rising and falling situation, separate approach has to be considered for rising and falling situation for transforming of micro into macro system.

### 3.3.1 For Water Level Rising

Trapezoidal failure block with the particle arrangement and the different micro-level forces acting on it for water level rising has been depicted in the Fig. 3.3. The riverside has been shown in the right side of the block. Here, in this figure the different micro-level forces are mentioned and calculated by the expressions which have been discussed previously. For the simplicity of the analysis the assumptions are made as 1. Spherical shaped particles, 2. Materially homogeneous and 3. Equal in diameter.

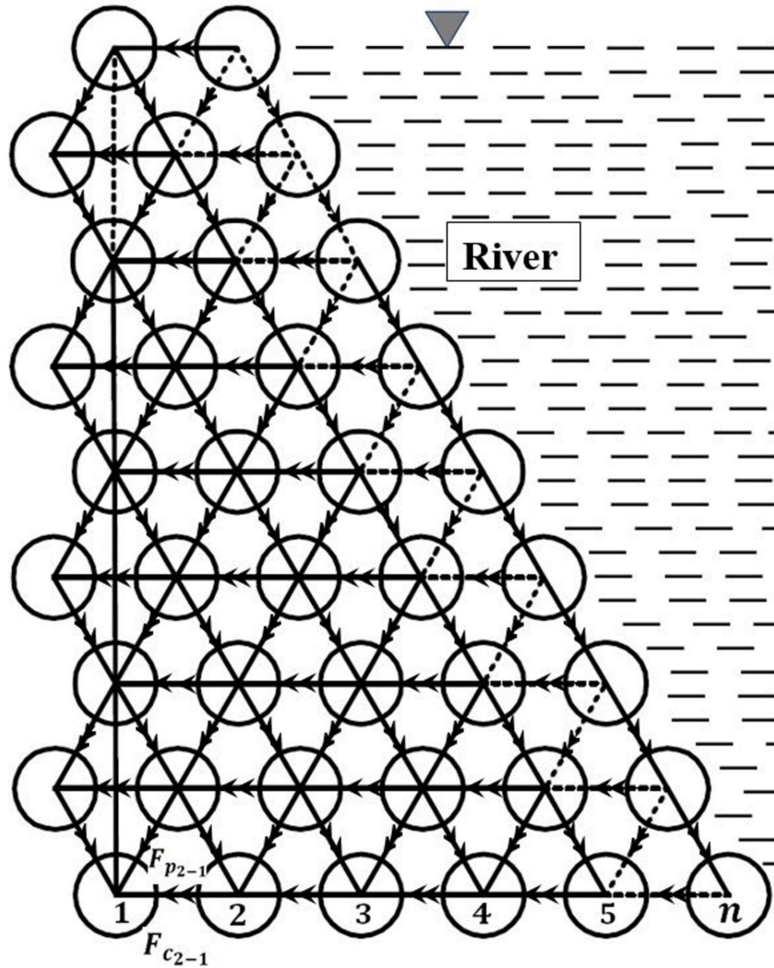


**Fig. 3.3** Particle arrangement with the different micro-level forces direction in trapezoidal failure block with  $n$  number of base particles for water level rising

By applying conservation of momentum principle both  $x$ -directional and  $y$ -directional forces have been calculated for water level rising. To start with, calculations have been done for  $n = 3$ .

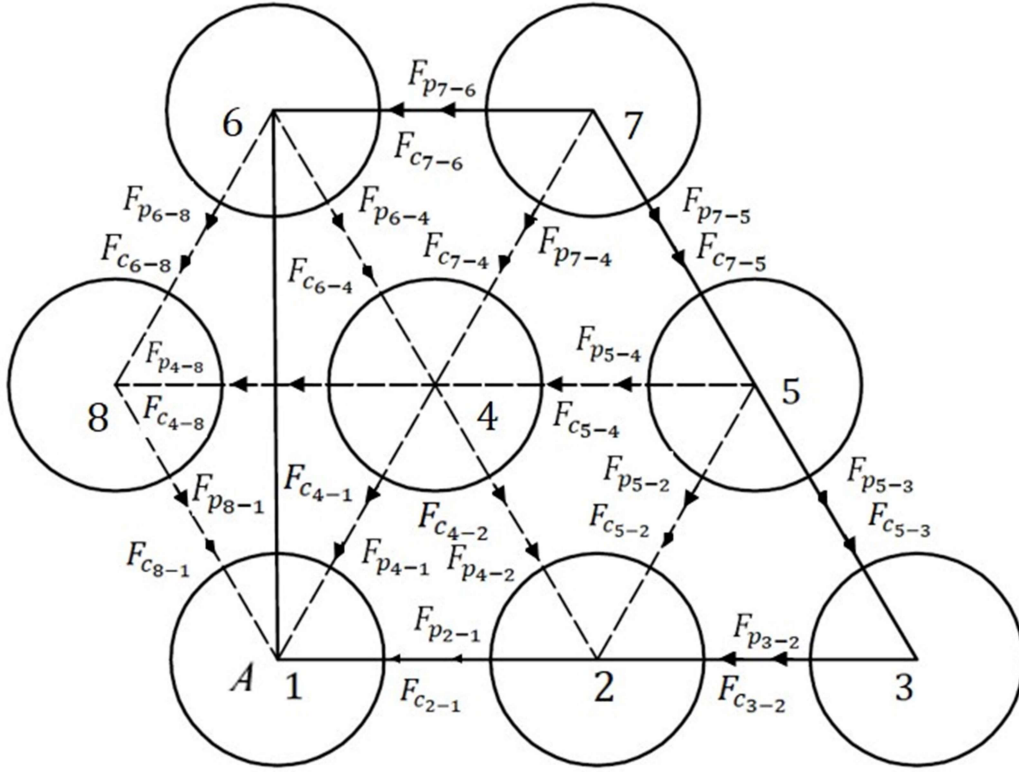


**Fig. 3.4** Various micro-level forces with directions for water level rising for  $n = 3$

### 3.3.1.1 $F_x$ Calculation

Now, taking moment about point A,  $x$ -directional component of force can be calculated as follows

$$\begin{aligned}
& \left[ \left\{ F_x \times y_O \right\} + \left\{ F_{cpx} \times y_C \right\} + \right. \\
& \left. \left\{ \begin{aligned} & \left( F_{c_{4-8}} \times \sqrt{3} \times P \right) + \left( F_{c_{5-4}} \times \sqrt{3} \times P \right) + \left( F_{c_{7-6}} \times \sqrt{3} \times P \times 2 \right) + \left( F_{c_{4-1}} \times \cos 60^\circ \times \sqrt{3} \times P \right) \\ & - \left( F_{c_{4-2}} \times \cos 60^\circ \times \sqrt{3} \times P \right) + \left( F_{c_{5-2}} \times \cos 60^\circ \times \sqrt{3} \times P \right) - \left( F_{c_{5-3}} \times \cos 60^\circ \times \sqrt{3} \times P \right) \\ & + \left( F_{c_{6-8}} \times \cos 60^\circ \times \sqrt{3} \times 2 \right) - \left( F_{c_{6-4}} \times \cos 60^\circ \times \sqrt{3} \times 2 \right) + \left( F_{c_{7-4}} \times \cos 60^\circ \times \sqrt{3} \times 2 \right) \\ & - \left( F_{c_{7-5}} \times \cos 60^\circ \times \sqrt{3} \times 2 \right) \end{aligned} \right\} + \right. \\
& \left. \left\{ \begin{aligned} & \left( F_{p_{4-8}} \times \sqrt{3} \times P \right) + \left( F_{p_{5-4}} \times \sqrt{3} \times P \right) + \left( F_{p_{7-6}} \times \sqrt{3} \times P \times 2 \right) + \left( F_{p_{4-1}} \times \cos 60^\circ \times \sqrt{3} \times P \right) \\ & - \left( F_{p_{4-2}} \times \cos 60^\circ \times \sqrt{3} \times P \right) + \left( F_{p_{5-2}} \times \cos 60^\circ \times \sqrt{3} \times P \right) - \left( F_{p_{5-3}} \times \cos 60^\circ \times \sqrt{3} \times P \right) \\ & + \left( F_{p_{6-8}} \times \cos 60^\circ \times \sqrt{3} \times 2 \right) - \left( F_{p_{6-4}} \times \cos 60^\circ \times \sqrt{3} \times 2 \right) + \left( F_{p_{7-4}} \times \cos 60^\circ \times \sqrt{3} \times 2 \right) \\ & - \left( F_{p_{7-5}} \times \cos 60^\circ \times \sqrt{3} \times 2 \right) \end{aligned} \right\} \right] = 0 \\
& - \left\{ \left( F_{c_{8-1}} \times \sqrt{3} \times P \right) + \left( F_{p_{8-1}} \times \sqrt{3} \times P \right) \right\}
\end{aligned} \tag{3.10}$$

As the cohesive forces and pore pressure forces are functions of radius only, so, for equally sized particles all cohesive forces will be equal in magnitude and so will be all pore pressure forces. Hence, the above expression can be reduced to

$$F_x = -\frac{1}{y_O} \times \left[ F_{cpx} \times y_C + \left\{ (F_c + F_p) \times \sqrt{3} \times P \times (1+1+2) \right\} \right] - \left\{ (F_c + F_p) \cos 60^\circ \times \sqrt{3} \times P \times (1) \right\} \tag{3.11}$$

Now, from the similarity analysis and by analysing the Fig. 3.4 it can be calculated for different numbers of base particles in the following way:

For  $n = 4$  the expression will be

$$F_x = -\frac{1}{y_O} \times \left[ F_{cpx} \times y_C + \left\{ \begin{aligned} & (F_c + F_p) \times \sqrt{3} \times P \times \\ & (1+1+1+2+2+3+3+4) \end{aligned} \right\} \right] - \left\{ (F_c + F_p) \cos 60^\circ \times \sqrt{3} \times P \times (1+3) \right\} \tag{3.12}$$

For  $n = 5$  the expression will be

$$F_x = -\frac{1}{y_O} \times \left[ \begin{aligned} &F_{cpx} \times y_C + \left\{ \left( F_c + F_p \right) \times \sqrt{3} \times P \times \right. \\ &\quad \left. \left( \begin{aligned} &1+1+1+1+2+2+2+ \\ &3+3+3+4+4+5+5+6 \end{aligned} \right) \right\} \\ &- \left\{ \left( F_c + F_p \right) \cos 60^\circ \times \sqrt{3} \times P \times (1+3+5) \right\} \end{aligned} \right] \quad (3.13)$$

For  $n = 6$  the expression will be

$$F_x = -\frac{1}{y_O} \times \left[ \begin{aligned} &F_{cpx} \times y_C + \left\{ \left( F_c + F_p \right) \times \sqrt{3} \times P \times \right. \\ &\quad \left( \begin{aligned} &1+1+1+1+1+2+2+2+2+3 \\ &+3+3+3+4+4+4+5+5+5 \\ &+6+6+7+7+8 \end{aligned} \right) \right\} \\ &+ \left\{ \left( F_c + F_p \right) \cos 60^\circ \times \sqrt{3} \times P \times (1+3+5+7) \right\} \end{aligned} \right] \quad (3.14)$$

Now, for x-directional force, from Eq. 3.11, Eq. 3.12, Eq. 3.13 and Eq. 3.14 have two series values which are as follows:

**Table 3.1: x-directional series values for first series**

$n$	3	4	5	6
$f(n)$	4	17	43	86

**Table 3.2: Newton's Forward Interpolation Chart for first series of x-direction**

$n$	$f(n)$	$\Delta f(n)$	$\Delta^2 f(n)$	$\Delta^3 f(n)$	$\Delta^4 f(n)$
3	4	13	13	4	0
4	17	26	17	4	

$n$	$f(n)$	$\Delta f(n)$	$\Delta^2 f(n)$	$\Delta^3 f(n)$	$\Delta^4 f(n)$
5	43	43	21		
6	86	64			

By using Newton's Forward Interpolation Formula

$$f(n) = \left[ f_0(n) + u \times \Delta f_0(n) + \left[ \frac{\{u \times (u-1)\}}{2!} \times \Delta^2 f_0(n) \right] + \left[ \frac{\{u \times (u-1) \times (u-2)\}}{3!} \times \Delta^3 f_0(n) \right] + \dots \right] \quad (3.15)$$

$$f(n) = 4 + u \times 13 + \frac{u \times (u-1)}{2} \times 13 + \frac{u \times (u-1) \times (u-2)}{6} \times 4 \quad (3.16)$$

$$f(n) = \frac{2}{3}u^3 + \frac{9}{2}u^2 + \frac{47}{6}u + 4 \quad (3.17)$$

$$f(n) = \frac{1}{6} [4u^3 + 27u^2 + 47u + 24] \quad (3.18)$$

Now,

$$u = \frac{n - n_0}{\Delta n} = \frac{n - 3}{1} = (n - 3) \quad (3.19)$$

$$f(n) = \frac{1}{6} [4 \times (n-3)^3 + 27 \times (n-3)^2 + 47 \times (n-3) + 24] \quad (3.20)$$

$$f(n) = \frac{1}{6} [4n^3 - 9n^2 - 7n + 18] \quad (3.21)$$

**Table 3.3: x-directional series values for second series**

$n$	3	4	5	6
$f(n)$	1	4	9	16

**Table 3.4: Newton's Forward Interpolation Chart second series of x-direction**

$n$	$f(n)$	$\Delta f(n)$	$\Delta^2 f(n)$	$\Delta^3 f(n)$	$\Delta^4 f(n)$
3	1	3	2	0	0
4	4	5	2		
5	9	7	2		
6	16	9			
7	25				

By using Newton's Forward Interpolation Formula

$$f(n) = f_0(n) + u \times \Delta f_0(n) + \frac{u(u-1)}{2!} \times \Delta^2 f_0(n) \quad (3.22)$$

$$f(n) = 1 + u \times 3 + \frac{u(u-1)}{2} \times 2 \quad (3.23)$$

$$f(n) = (n-2)^2 \quad (3.24)$$



So, by putting the series values, the final expression of  $x$ -directional macroscopic force

$$F_x = -\frac{1}{y_O} \times \left[ F_{cpx} \times y_C + \left\{ (F_c + F_p) \times \sqrt{3} \times P \times \frac{1}{6} \times (4n^3 - 9n^2 - 7n + 18) \right\} + \left\{ (F_c + F_p) \cos 60^\circ \times \sqrt{3} \times P \times (n-2)^2 \right\} \right] \quad (3.25)$$

### 3.3.1.2 $F_y$ Calculation:

Now, taking moment about point A,  $y$ -directional component of force can be calculated as follows

For  $n = 3$  the expression will be

$$\left[ \begin{aligned} & \left\{ F_y \times x_O - F_g \times x_O - F_{cpy} \times x_C \right\} \\ & - \left\{ \begin{aligned} & F_{c_{4-1}} \times \sin 60^\circ \times P + F_{c_{4-2}} \times \sin 60^\circ \times P + F_{c_{7-4}} \times \sin 60^\circ \times P \times 2 \\ & + F_{c_{7-5}} \times \sin 60^\circ \times P \times 2 + F_{c_{5-2}} \times \sin 60^\circ \times P \times 3 \\ & + F_{c_{5-3}} \times \sin 60^\circ \times P \times 3 \end{aligned} \right\} \\ & - \left\{ \begin{aligned} & F_{p_{4-1}} \times \sin 60^\circ \times P + F_{p_{4-2}} \times \sin 60^\circ \times P + F_{p_{7-4}} \times \sin 60^\circ \times P \times 2 \\ & + F_{p_{7-5}} \times \sin 60^\circ \times P \times 2 + F_{p_{5-2}} \times \sin 60^\circ \times P \times 3 \\ & + F_{p_{5-3}} \times \sin 60^\circ \times P \times 3 \end{aligned} \right\} \\ & - \left\{ F_{c_{8-1}} \times \sin 60^\circ \times P + F_{p_{8-1}} \times \sin 60^\circ \times P \right\} \end{aligned} \right] = 0 \quad (3.26)$$

As the cohesive forces and pore pressure forces are functions of radius only, so, for equally sized particles all cohesive forces will be equal in magnitude and will be all pore pressure forces. Hence, the above expression can be reduced to

$$F_y = F_g + \frac{x_C}{x_O} \times F_{cpy} + \frac{1}{x_O} \times \left[ \begin{aligned} &\left\{ \left( F_c + F_p \right) \sin 60^\circ \times P \times \right. \\ &\left. \left( 1+1+2+2+3+3 \right) \right\} \\ &\left. - \left\{ \left( F_c + F_p \right) \sin 60^\circ \times P \times 1 \right\} \right] \end{aligned} \right] \quad (3.27)$$

For  $n = 4$  the expression will be

$$F_y = F_g + \frac{x_C}{x_O} \times F_{cpy} + \frac{1}{x_O} \times \left[ \begin{aligned} &\left\{ \left( F_c + F_p \right) \sin 60^\circ \times P \times \right. \\ &\left. \left( 1+1+1+1+2+2+2+2 \right. \right. \\ &\left. \left. +3+3+3+3+4+4+5+5 \right) \right\} \\ &\left. - \left\{ \left( F_c + F_p \right) \sin 60^\circ \times P \times 2 \right\} \right] \end{aligned} \right] \quad (3.28)$$

For  $n = 5$  the expression will be

$$F_y = F_g + \frac{x_C}{x_O} \times F_{cpy} + \frac{1}{x_O} \times \left[ \begin{aligned} &\left\{ \left( F_c + F_p \right) \sin 60^\circ \times P \times \right. \\ &\left( 1+1+1+1+1+1+2+2+2+2+2 \right. \\ &\left. +2+3+3+3+3+3+3+4+4+4 \right. \\ &\left. +4+5+5+5+5+6+6+7+7 \right) \right\} \\ &\left. - \left\{ \left( F_c + F_p \right) \sin 60^\circ \times P \times 3 \right\} \right] \end{aligned} \right] \quad (3.29)$$

For  $n = 6$  the expression will be

$$F_y = F_g + \frac{x_C}{x_O} \times F_{cpy} + \frac{1}{x_O} \times \left[ \begin{aligned} &\left\{ \left( F_c + F_p \right) \sin 60^\circ \times P \times \right. \\ &\left( 1+1+1+1+1+1+1+1+2+2+2 \right. \\ &\left. +2+2+2+2+2+3+3+3+3+3 \right. \\ &\left. +3+3+3+4+4+4+4+4+4+5 \right. \\ &\left. +5+5+5+5+5+6+6+6+6+7 \right. \\ &\left. +7+7+7+8+8+9+9 \right) \right\} \\ &\left. - \left\{ \left( F_c + F_p \right) \sin 60^\circ \times P \times 4 \right\} \right] \end{aligned} \right] \quad (3.30)$$

Now, for y-directional force, from Eq. 3.27, Eq. 3.38, Eq. 3.29 and Eq. 3.30 it can be observed that it has only one series value as following manner:

**Table 3.5: y-directional series values**

$n$	3	4	5	6
$f(n)$	12	42	98	188

**Table 3.6: Newton's Forward Interpolation Chart of y-direction**

$n$	$f(n)$	$\Delta f(n)$	$\Delta^2 f(n)$	$\Delta^3 f(n)$	$\Delta^4 f(n)$
3	12	30	26	8	0
4	42	56	34	8	
5	98	90	42		
6	188	132			
7	320				

By using Newton's Forward Interpolation Formula

$$f(n) = f_0(n) + u \times \Delta f_0(n) + \frac{u(u-1)}{2!} \times \Delta^2 f_0(n) + \frac{u(u-1)(u-2)}{3!} \times \Delta^3 f_0(n) + \dots \quad (3.31)$$

$$f(n) = 12 + u \times 30 + \frac{u(u-1)}{2} \times 26 + \frac{u(u-1)(u-2)}{6} \times 8 \quad (3.32)$$

$$f(n) = \frac{4}{3}u^3 + \frac{9}{2}u^2 + \frac{59}{3}u + 12 \quad (3.33)$$

$$f(n) = \frac{1}{3} [4u^3 + 27u^2 + 59u + 36] \quad (3.34)$$

Now,

$$u = \frac{n - n_0}{\Delta n} = \frac{n - 3}{1} = (n - 3) \quad (3.35)$$

$$f(n) = \frac{1}{3} \left[ 4(n - 3)^3 + 27(n - 3)^2 + 59(n - 3) + 36 \right] \quad (3.36)$$

$$f(n) = \frac{1}{3} \left[ 4n^3 - 9n^2 + 5n - 6 \right] \quad (3.37)$$

So, putting above series value, the final expression of  $y$ -directional macroscopic force

$$F_y = F_g + \frac{x_c}{x_o} \times F_{cpy} + \frac{1}{x_A} \times \left[ \begin{array}{l} \left\{ (F_c + F_p) \sin 60^\circ \times P \times \frac{1}{3} \times \right. \\ \left. (4n^3 - 9n^2 + 5n - 6) \right\} \\ \left. - \left\{ (F_c + F_p) \sin 60^\circ \times P \times (n - 2) \right\} \right] \quad (3.38)$$

### 3.3.2 For Water Level Falling

Trapezoidal failure block with the particle arrangement and the different micro-level forces acting on it for water level falling has been depicted in the Fig. 3.5. The riverside has been shown in the right side of the block. Here, in this figure the different micro-level forces are mentioned and calculated by the expressions which have been discussed previously. For the simplicity of the analysis the assumptions are made as 1. Spherical shaped particles, 2. Materially homogeneous and 3. Equal in diameter.

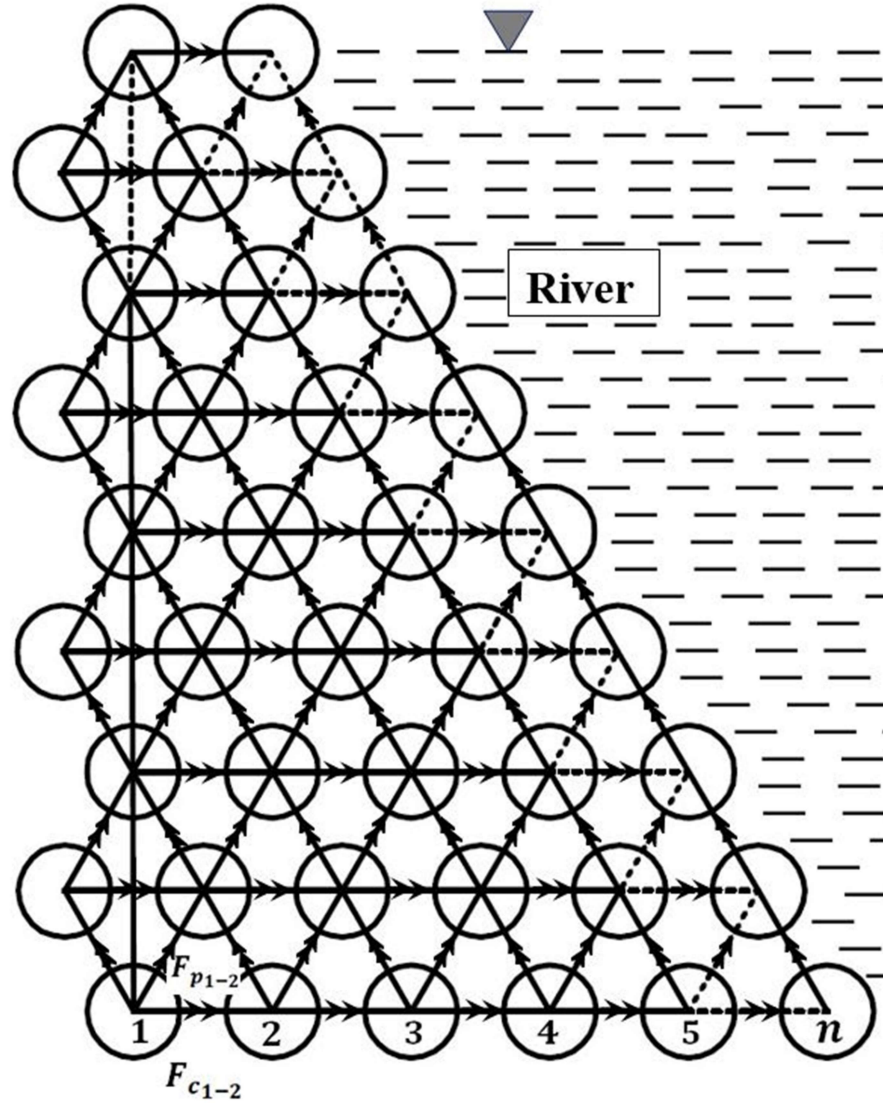


**Fig. 3.5** Particle arrangement with the different micro-level forces direction in trapezoidal failure block with  $n$  number of base particles for water level falling

Applying conservation of momentum principle both  $x$ -directional and  $y$ -directional forces have been calculated for water level falling. To start with, calculations have been done for  $n = 3$ .

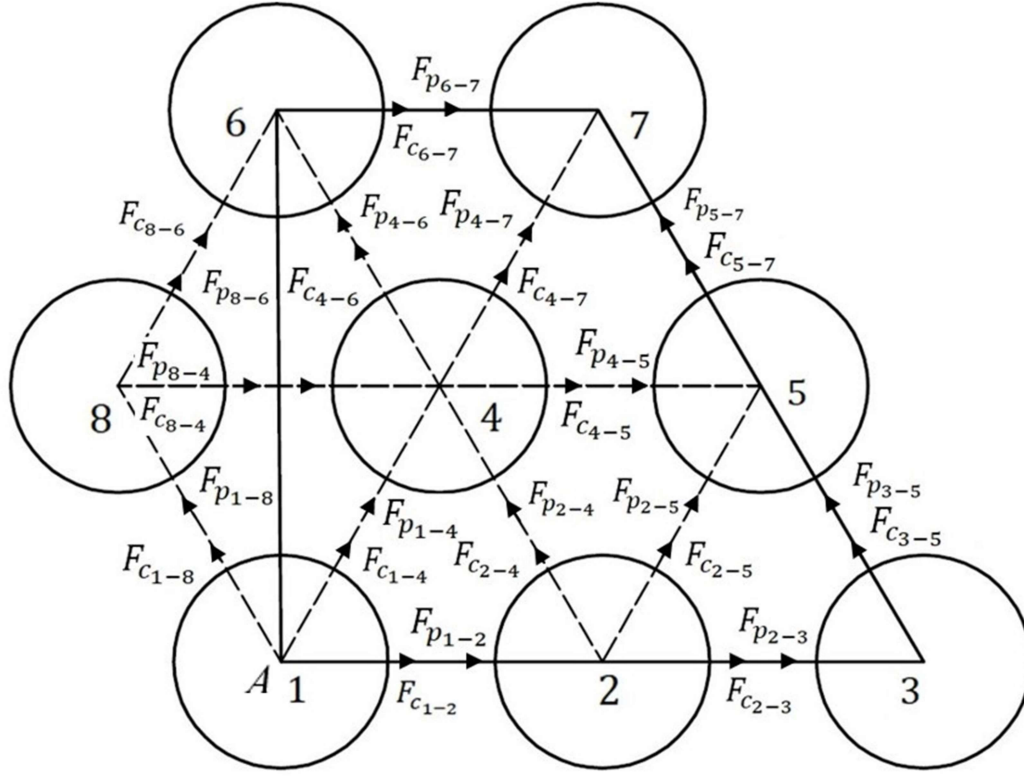


**Fig. 3.6** Various micro-level forces with directions for water level falling for  $n = 3$

### 3.3.2.1 $F_x$ Calculation

Now, taking moment about point A,  $x$ -directional component of force can be calculated as follows

For  $n = 3$  the expression will be

$$\left[ \begin{aligned}
 & \left\{ F_x \times y_O + F_{cpx} \times y_C \right\} \\
 & + \left\{ F_c \times \sqrt{3} \times P + F_c \times \sqrt{3} \times P + F_c \times \cos 60 \times \sqrt{3} \times P - F_c \times \cos 60 \times \sqrt{3} \times P + \right. \\
 & \quad \left. F_c \times \sqrt{3} \times P \times 2 + F_c \times \cos 60 \times \sqrt{3} \right\} \\
 & + \left\{ F_p \times \sqrt{3} \times P + F_p \times \sqrt{3} \times P + F_p \times \cos 60 \times \sqrt{3} \times P - F_p \times \cos 60 \times \sqrt{3} \times P \right. \\
 & \quad \left. + F_p \times \sqrt{3} \times P \times 2 + F_p \times \cos 60 \times \sqrt{3} \right\} \\
 & - \left\{ F_c \times \cos 60 \times \sqrt{3} + F_p \times \cos 60 \times \sqrt{3} \right\}
 \end{aligned} \right] = 0 \quad (3.39)$$

$$F_x = -\frac{1}{y_O} \times \left[ F_{cpx} \times y_C + \left\{ F_c \times \sqrt{3} \times P \times (1+1+2) \right\} + \left\{ F_p \times \sqrt{3} \times P \times (1+1+2) \right\} \right] \quad (3.40)$$

For  $n = 4$  the expression will be

$$F_x = -\frac{1}{y_O} \times \left[ F_{cpx} \times y_C + \left\{ F_c \times \sqrt{3} \times P \times (1+1+1+2+2+3+3+4) \right\} + \left\{ F_p \times \sqrt{3} \times P \times (1+1+1+2+2+3+3+4) \right\} \right] \quad (3.41)$$

For  $n = 5$  the expression will be

$$F_x = -\frac{1}{y_O} \times \left[ F_{cpx} \times y_C + \left\{ F_c \times \sqrt{3} \times P \times \left( \begin{array}{l} 1+1+1+1+2+2+2+3 \\ +3+3+4+4+5+5+6 \end{array} \right) \right\} + \left\{ F_p \times \sqrt{3} \times P \times \left( \begin{array}{l} 1+1+1+1+2+2+2+3+3+3 \\ +4+4+5+5+6 \end{array} \right) \right\} \right] \quad (3.42)$$

For  $n = 6$  the expression will be

$$F_x = -\frac{1}{y_O} \times \left[ F_{cpx} \times y_C + \left\{ F_c \times \sqrt{3} \times P \times \left( \begin{array}{l} 1+1+1+1+1+2+2+2+2+3+3+3+3 \\ +4+4+4+5+5+5+6+6+7+7+8 \end{array} \right) \right\} + \left\{ F_p \times \sqrt{3} \times P \times \left( \begin{array}{l} 1+1+1+1+1+2+2+2+2+3+3+3+3 \\ +4+4+4+5+5+5+6+6+7+7+8 \end{array} \right) \right\} \right] \quad (3.43)$$

Now, for  $x$ -directional force, from Eq. 3.40, Eq. 3.41, Eq. 3.42 and Eq. 3.43, it can be observed that, it has two series values which are as follows:

**Table 3.7:  $x$ -directional series values**

$n = 3$	$n = 4$	$n = 5$	$n = 6$
$f(n) = 4$	$f(n) = 17$	$f(n) = 43$	$f(n) = 86$

**Table 3.8: Newton's Forward Interpolation Chart of x-direction**

$n$	$f(n)$	$\Delta f(n)$	$\Delta^2 f(n)$	$\Delta^3 f(n)$	$\Delta^4 f(n)$
3	4	13	13	4	0
4	17	26	17	4	
5	43	43	21	4	
6	86	64	25		
7	150				

By using Newton's Forward Interpolation Formula

$$f(n) = f_0(n) + u \times \Delta f_0(n) + \frac{u(u-1)}{2!} \times \Delta^2 f_0(n) + \frac{u(u-1)(u-2)}{3!} \times \Delta^3 f_0(n) + \dots \quad (3.44)$$

$$f(n) = 4 + u \times 13 + \frac{u(u-1)}{2} \times 13 + \frac{u(u-1)(u-2)}{6} \times 4 \quad (3.45)$$

$$f(n) = \frac{2}{3}u^3 + \frac{9}{2}u^2 + \frac{47}{6}u + 4 \quad (3.46)$$

$$f(n) = \frac{1}{6} [4u^3 + 27u^2 + 47u + 24] \quad (3.47)$$

Now,

$$u = \frac{n - n_0}{\Delta n} = \frac{n - 3}{1} = (n - 3) \quad (3.48)$$

$$f(n) = \frac{1}{6} [4(n-3)^3 + 27(n-3)^2 + 47(n-3) + 24] \quad (3.49)$$



$$f(n) = \frac{1}{6} [4n^3 - 9n^2 - 7n + 18] \quad (3.50)$$

So, by putting the series values, the final expression of x-directional macroscopic force

$$F_x = -\frac{1}{y_O} \times \left[ F_{cpx} \times y_C - \left\{ (F_c + F_p) \times \sqrt{3} \times P \times \frac{1}{6} (4n^3 - 9n^2 - 7n + 18) \right\} \right] \quad (3.51)$$

### 3.3.2.2 $F_y$ Calculation:

Now, taking moment about point A, y-directional component of force can be calculated as follows

For  $n = 3$  the expression will be

$$\left[ \begin{aligned} & \{ F_y \times x_O - F_g \times x_O - F_{cpy} \times x_C \} \\ & + \left\{ F_c \sin 60 \times P + F_c \sin 60 \times P + F_c \sin 60 \times P \times 2 + F_c \sin 60 \times P \times 2 \right\} \\ & + \left\{ F_c \sin 60 \times P \times 3 + F_c \sin 60 \times P \times 4 \right\} \\ & + \left\{ F_p \sin 60 \times P + F_p \sin 60 \times P + F_p \sin 60 \times P \times 2 + F_p \sin 60 \times P \times 2 \right\} \\ & + \left\{ F_p \sin 60 \times P \times 3 + F_p \sin 60 \times P \times 4 \right\} \\ & - \{ F_c \sin 60 \times P + F_p \sin 60 \times P \} \end{aligned} \right] = 0 \quad (3.52)$$

$$F_y = F_g + \frac{x_C}{x_O} \times F_{cpy} - \frac{1}{x_O} \times \left[ \begin{aligned} & \{ (F_c + F_p) \sin 60 \times P \times (1 + 1 + 2 + 2 + 3 + 4) \} \\ & - \{ (F_c + F_p) \sin 60 \times P \} \end{aligned} \right] \quad (3.53)$$

For  $n = 4$  the expression will be

$$F_y = F_g + \frac{x_C}{x_O} \times F_{cpy} - \frac{1}{x_O} \times \left[ \begin{aligned} & \left\{ (F_c + F_p) \sin 60 \times P \times \right. \\ & \left. \left( \begin{aligned} & 1 + 1 + 1 + 1 + 2 + 2 + 2 + 2 \\ & + 3 + 3 + 3 + 4 + 4 + 4 + 5 + 6 \end{aligned} \right) \right\} \\ & - \{ (F_c + F_p) \sin 60 \times P \times 2 \} \end{aligned} \right] \quad (3.54)$$

For  $n = 5$  the expression will be

$$F_y = F_g + \frac{x_C}{x_O} \times F_{cpy} - \frac{1}{x_O} \times \left[ \left\{ \begin{aligned} &(F_c + F_p) \sin 60 \times P \times \\ &\left( \begin{aligned} &1+1+1+1+1+1+2+2+2+2+2 \\ &+2+3+3+3+3+3+4+4+4+4 \\ &+4+5+5+5+6+6+6+7+8 \end{aligned} \right) \end{aligned} \right\} \right] - \left\{ (F_c + F_p) \sin 60 \times P \times 3 \right\} \right] \quad (3.55)$$

For  $n = 6$  the expression will be

$$F_y = F_g + \frac{x_C}{x_O} \times F_{cpy} - \frac{1}{x_O} \times \left[ \left\{ \begin{aligned} &(F_c + F_p) \sin 60 \times P \times \\ &\left( \begin{aligned} &1+1+1+1+1+1+1+1+2+2+2 \\ &+2+2+2+2+2+3+3+3+3+3 \\ &+3+3+4+4+4+4+4+4+4+5 \\ &+5+5+5+5+6+6+6+6+6+7 \\ &+7+7+8+8+8+9+10 \end{aligned} \right) \end{aligned} \right\} \right] - \left\{ (F_c + F_p) \sin 60 \times P \times 4 \right\} \right] \quad (3.56)$$

Now, for  $y$ -directional force, Eq. 3.53, Eq. 3.54, Eq. 3.55 and Eq. 3.56, have been solved to get the series values

**Table 3.9:  $y$ -directional series values**

$n = 3$	$n = 4$	$n = 5$	$n = 6$
$f(n) = 13$	$f(n) = 44$	$f(n) = 101$	$f(n) = 192$

**Table 3.10: Newton's Forward Interpolation Chart of  $y$ -direction**

$n$	$f(n)$	$\Delta f(n)$	$\Delta^2 f(n)$	$\Delta^3 f(n)$	$\Delta^4 f(n)$
3	13	31	26	8	0

$n$	$f(n)$	$\Delta f(n)$	$\Delta^2 f(n)$	$\Delta^3 f(n)$	$\Delta^4 f(n)$
4	44	57	34	8	
5	101	91	42	8	
6	192	133			
7	325				

By using Newton's Forward Interpolation Formula

$$f(n) = f_0(n) + u \times \Delta f_0(n) + \frac{u(u-1)}{2!} \times \Delta^2 f_0(n) + \frac{u(u-1)(u-2)}{3!} \times \Delta^3 f_0(n) + \dots \quad (3.57)$$

$$f(n) = 13 + u \times 31 + \frac{u(u-1)}{2} \times 26 + \frac{u(u-1)(u-2)}{6} \times 8 \quad (3.58)$$

$$f(n) = \frac{4}{3}u^3 + 9u^2 + \frac{62}{3}u + 13 \quad (3.59)$$

$$f(n) = \frac{1}{3} [4u^3 + 27u^2 + 62u + 39] \quad (3.60)$$

Now,

$$u = \frac{n - n_0}{\Delta n} = \frac{n - 3}{1} = (n - 3) \quad (3.61)$$

$$f(n) = \frac{1}{3} [4(n-3)^3 + 27(n-3)^2 + 62(n-3) + 39] \quad (3.62)$$

$$f(n) = \frac{1}{3} [4n^3 - 9n^2 + 8n - 12] \quad (3.63)$$

So, by putting the series values, the final expression of  $y$ -directional macroscopic force

$$F_y = F_g + \frac{x_c}{x_o} \times F_{cpy} - \frac{1}{x_o} \times \left[ \begin{aligned} &\left\{ (F_c + F_p) \sin 60^\circ \times P \times \frac{1}{3} \times \right. \\ &\left. (4n^3 - 9n^2 + 8n - 12) \right\} \\ &\left. - \left\{ (F_c + F_p) \sin 60^\circ \times P \times (n - 2) \right\} \right] \end{aligned} \right] \quad (3.64)$$

So, the expressions for both  $x$ -directional and  $y$ -directional macroscopic forces are known now for both water level rising and falling situation. Hence, the resultant force will be

$$F = \sqrt{(F_x)^2 + (F_y)^2} \quad (3.65)$$

Correspondingly, the expression for resultant impending acceleration will be

$$f = \frac{F}{A_p \times (\rho_s - \rho)} \quad (3.66)$$

And the expression for escape velocity in m/s (Duan, 2005)<sup>23</sup>

$$V_{esc} = [2 \times R \times f]^{0.5} \quad (3.67)$$

Here,  $R$  is expressed in m and  $f$  is expressed in  $\text{m/s}^2$ .

### **3.4 Results**

**D**ifferent types of analysis have been made in this section by varying different parameters for both water level rising and falling conditions. Firstly, analysis has been done for different inter-particle distances keeping particle size and liquid-bridge volume at fixed value. Secondly, analysis has been done for different liquid-bridge volumes keeping inter-particle distance and particle size at fixed value. Thirdly, analysis has been done for different particle sizes keeping inter-particle distance and liquid-bridge volume at fixed value. For all the cases escape velocity graphs have plotted with respect to number of base particles and number of total particles for water level rising as well as falling situations and comparative studies have been made. Lastly, escape velocity has been calculated for different free surface heights for different number of total particles in the block to study the dynamic behaviour and its effect on the stability of the riverbank. Here, in this case the escape velocity graphs have been plotted against free surface height of the water level for both water level rising and falling situation to identify vulnerable effect of the dynamic behaviour of the river system.

#### **3.4.1 Escape Velocity Variation for Different Inter-Particle Distances**

**H**ere, escape velocity variation is plotted for five different inter-particle distances (0.145 mm, 0.150 mm, 0.155 mm, 0.160 mm and 0.165 mm) for the fixed value liquid-bridge volume of 20 nl and particle radius of 0.4 mm. Variations are shown for two different varying conditions, such as, number of base particles and number of total particles.

### 3.4.1.1 *Escape Velocity Variation with Number of Base Particles*

Here, the variation is plotted with respect to number of base particles. The numbers of base particle have been varied from 10 to 100 with the intervals of 10. The first five graphs are for water level falling and next five are for water level rising. For showing the results in a tabular form, the corresponding table (Table 3.11) is also added.

**Table 3.11: Escape velocity variation with number of base particles for different inter-particle distances**

Inter-Particle Distance (mm)	Number of Base Particles	Escape Velocity for Rising Water Level (m/s)	Escape Velocity for Falling Water Level (m/s)
0.145	10	0.122699098	0.109548733
	20	0.128158678	0.115772664
	30	0.130150668	0.118017503
	40	0.13117999	0.119172627
	50	0.131808404	0.119876289
	60	0.132231894	0.120349839
	70	0.132536627	0.120690275
	80	0.132766407	0.120946801
	90	0.132945855	0.121147035
	100	0.133089875	0.121307671
0.150	10	0.123017717	0.109921842
	20	0.128538507	0.116212765

Inter-Particle Distance (mm)	Number of Base Particles	Escape Velocity for Rising Water Level (m/s)	Escape Velocity for Falling Water Level (m/s)
0.150	30	0.130551633	0.118480266
	40	0.131591649	0.119646767
	50	0.132226519	0.120357269
	60	0.132654329	0.120835385
	70	0.132962155	0.121179085
	80	0.133194258	0.121438061
	90	0.133375517	0.1216402
	100	0.133520987	0.121802361
0.155	10	0.123338148	0.110296496
	20	0.128920237	0.116654363
	30	0.130954516	0.118944491
	40	0.13200523	0.120122349
	50	0.132646557	0.120839678
	60	0.133078687	0.121322351
	70	0.133389606	0.121669308
	80	0.133624034	0.121930728
	90	0.133807103	0.122134769
	100	0.133954022	0.122298453
0.160	10	0.123660372	0.110672677
	20	0.129303848	0.117097436

<b>Inter-Particle Distance (mm)</b>	<b>Number of Base Particles</b>	<b>Escape Velocity for Rising Water Level (m/s)</b>	<b>Escape Velocity for Falling Water Level (m/s)</b>
0.160	30	0.131359291	0.119410156
	40	0.132420707	0.120599352
	50	0.133068492	0.121323495
	60	0.133504943	0.121810715
	80	0.134055708	0.122424783
	90	0.134240587	0.122630722
	100	0.134388956	0.122795925
0.165	10	0.123984374	0.111050369
	20	0.129689317	0.117541966
	30	0.131765936	0.119877242
	40	0.132838057	0.121077754
	50	0.133492301	0.121808699
	60	0.133933073	0.122300458
	70	0.13425018	0.12265391
	80	0.134489256	0.122920204
	90	0.134675945	0.123128037
	100	0.134825764	0.123294756



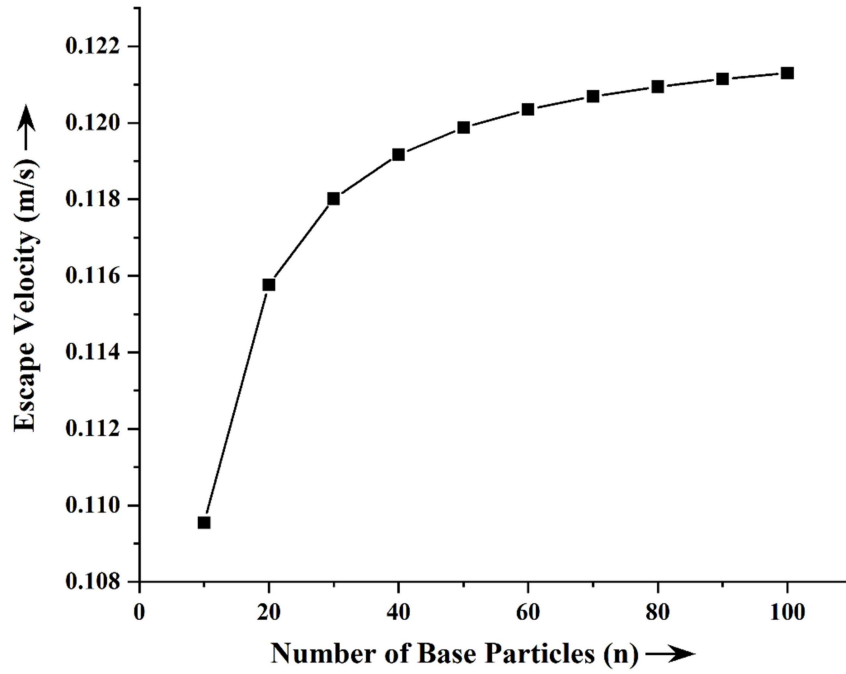


**Fig. 3.7** Escape velocity variation with number of base particles for inter-particle distance of 0.145 mm for water level falling

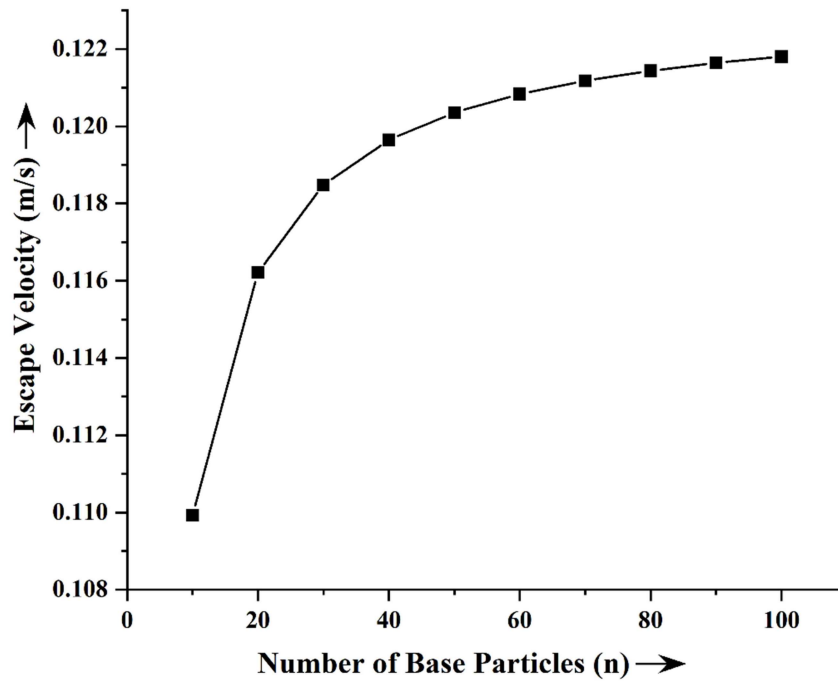


**Fig. 3.8** Escape velocity variation with number of base particles for inter-particle distance of 0.150 mm for water level falling

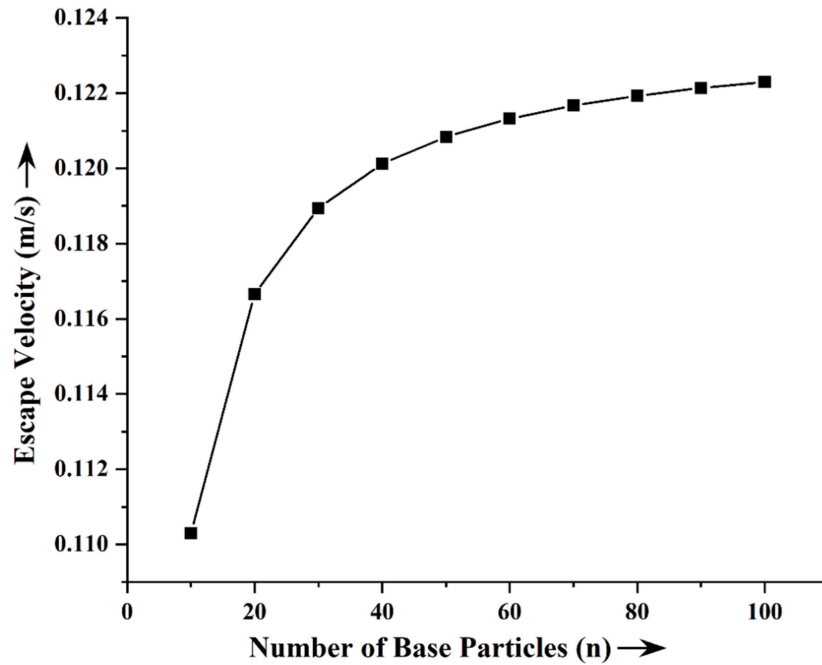


**Fig. 3.9** Escape velocity variation with number of base particles for inter-particle distance of 0.155 mm for water level falling

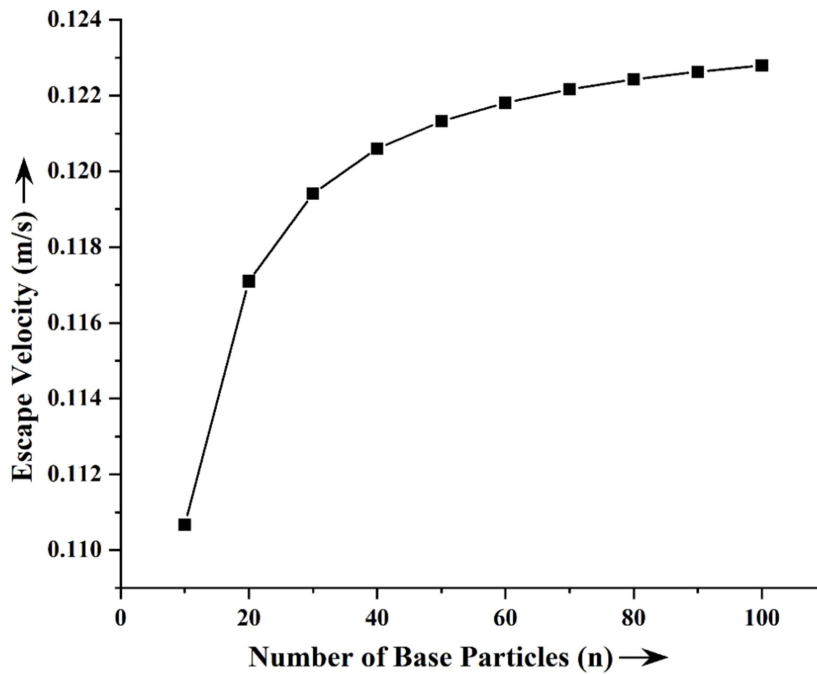


**Fig. 3.10** Escape velocity variation with number of base particles for inter-particle distance of 0.160 mm for water level falling

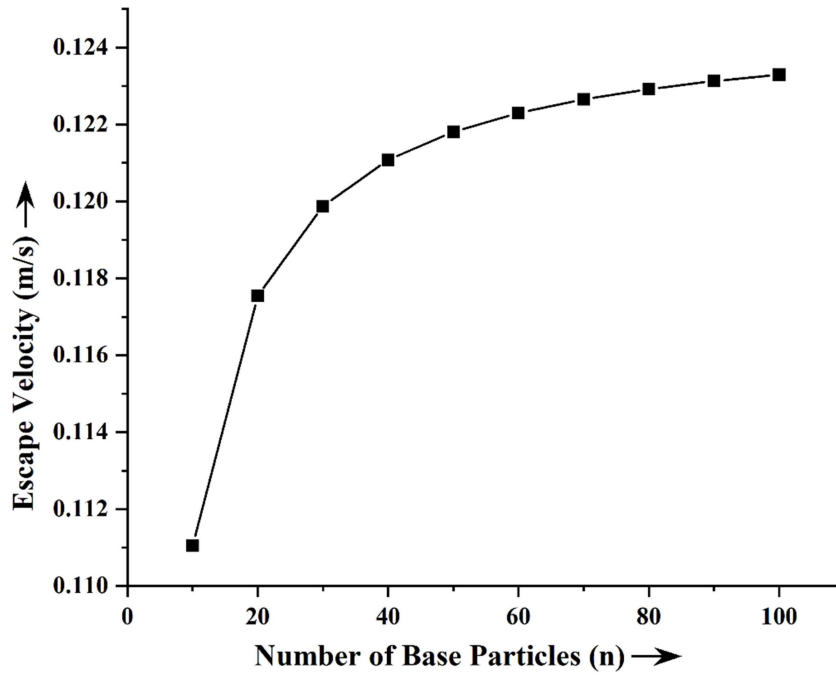


**Fig. 3.11** Escape velocity variation with number of base particles for inter-particle distance of 0.165 mm for water level falling

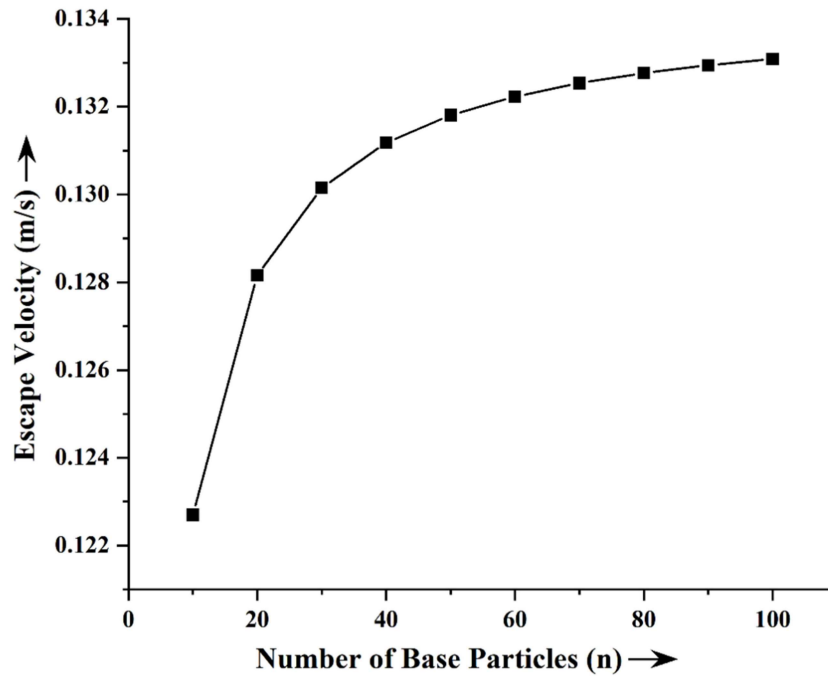


**Fig. 3.12** Escape velocity variation with number of base particles for inter-particle distance of 0.145 mm for water level rising

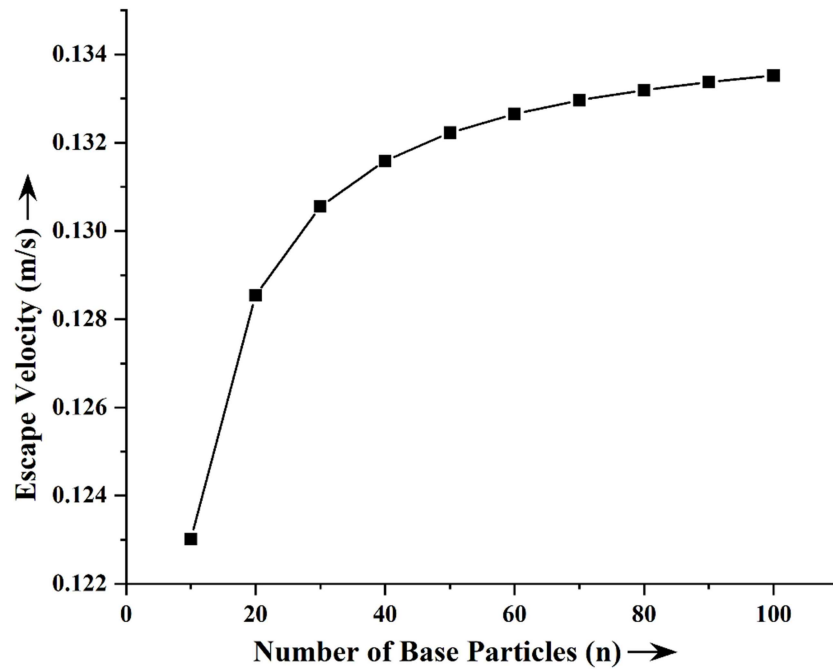


**Fig. 3.13** Escape velocity variation with number of base particles for inter-particle distance of 0.150 mm for water level rising

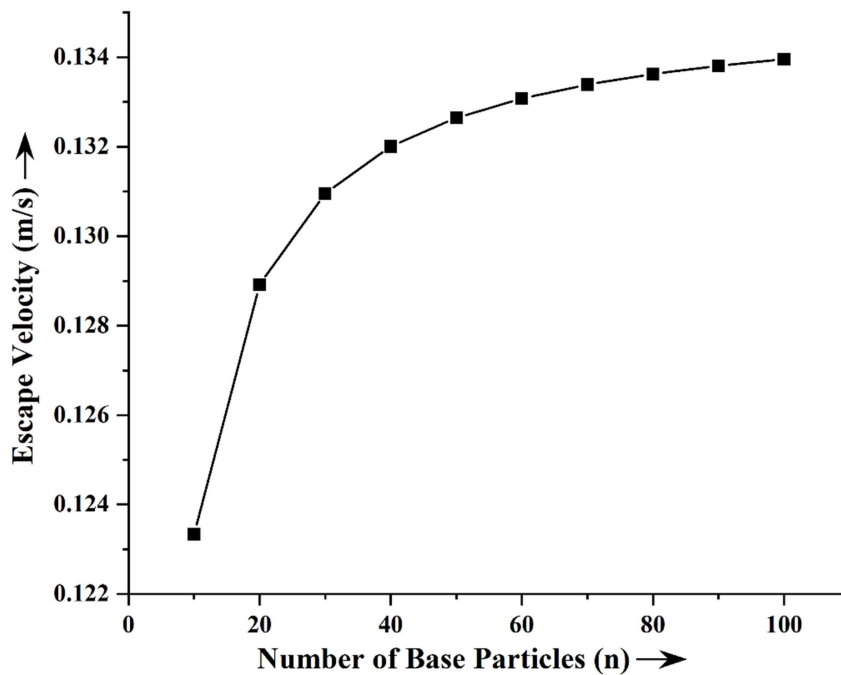


**Fig. 3.14** Escape velocity variation with number of base particles for inter-particle distance of 0.155 mm for water level rising

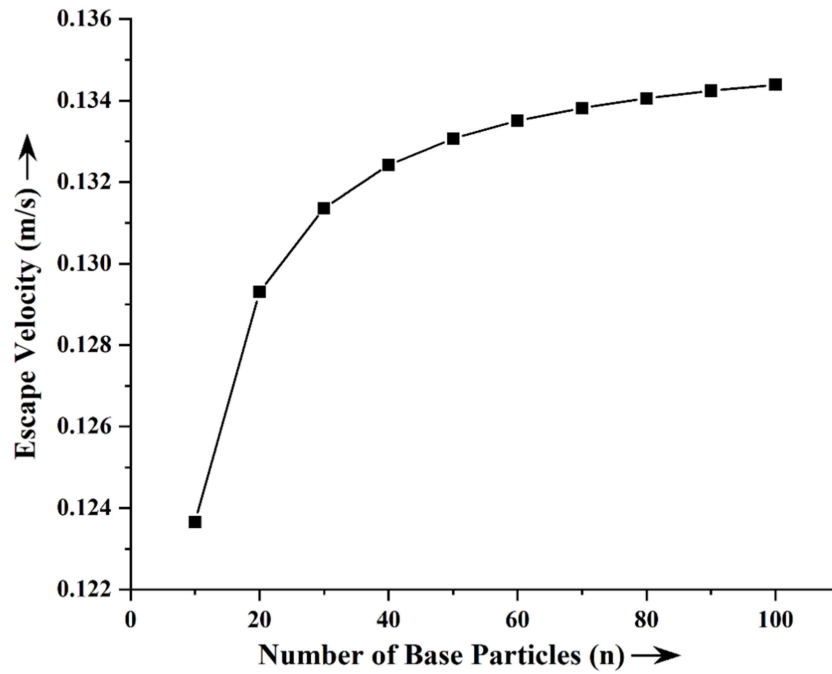


**Fig. 3.15** Escape velocity variation with number of base particles for inter-particle distance of 0.160 mm for water level rising

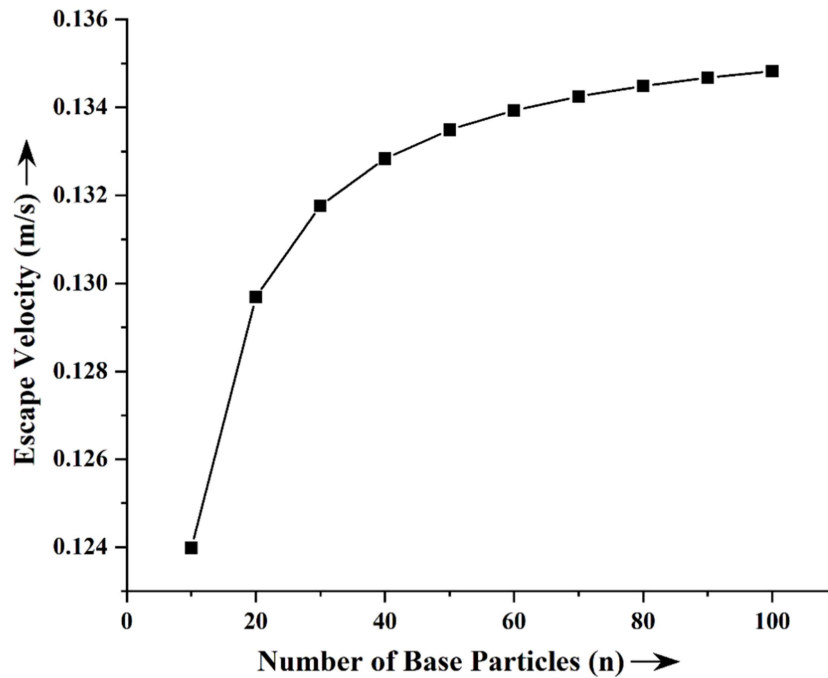


**Fig. 3.16** Escape velocity variation with number of base particles for inter-particle distance of 0.165 mm for water level rising

### 3.4.1.2 *Escape Velocity Variation with Number of Total Particles*

Here, the variation is plotted with respect to number of total particles. The numbers of total particle have been varied from 1000 to 10000 with the intervals of 1000. The first five graphs are for water level falling and next five are for water level rising. For showing the results in a tabular form, the corresponding table (Table 3.12) is also added.

**Table 3.12: Escape velocity variation with number of total particle for different inter-particles distances**

<b>Inter-Particle Distance (mm)</b>	<b>Number of Total Particles</b>	<b>Escape Velocity for Rising Water Level (m/s)</b>	<b>Escape Velocity for Falling Water Level (m/s)</b>
0.145	1000	0.130364	0.118257173
	2000	0.131512095	0.119544643
	3000	0.132030111	0.120124268
	4000	0.132341649	0.120472484
	5000	0.132555426	0.120711268
	6000	0.13271384	0.120888129
	7000	0.132837317	0.121025936
	8000	0.132937076	0.121137241
	9000	0.133019862	0.121229587
	10000	0.133090005	0.121307816
0.150	1000	0.130767195	0.118722312
	2000	0.131927173	0.120022408

<b>Inter-Particle Distance (mm)</b>	<b>Number of Total Particles</b>	<b>Escape Velocity for Rising Water Level (m/s)</b>	<b>Escape Velocity for Falling Water Level (m/s)</b>
0.150	3000	0.132450491	0.120607643
	4000	0.132765199	0.120959207
0.150	5000	0.132981144	0.121200279
	6000	0.133141161	0.121378829
	7000	0.133265884	0.121517949
	8000	0.13336665	0.121630313
	9000	0.133450269	0.121723537
	10000	0.133521118	0.121802508
0.155	1000	0.131172307	0.119188909
	2000	0.132344173	0.120501608
	3000	0.132872793	0.121092442
	4000	0.133190673	0.121447349
	5000	0.133408786	0.121690702
	6000	0.133570405	0.121870938
	7000	0.133696376	0.122011369
	8000	0.133798147	0.12212479
	9000	0.1338826	0.122218889
	10000	0.133954155	0.122298601
0.160	1000	0.131579314	0.119656942
	2000	0.13276307	0.120982222

<b>Inter-Particle Distance (mm)</b>	<b>Number of Total Particles</b>	<b>Escape Velocity for Rising Water Level (m/s)</b>	<b>Escape Velocity for Falling Water Level (m/s)</b>
0.160	3000	0.133296994	0.121578645
	4000	0.133618045	0.121936886
	5000	0.133838327	0.122182518
	6000	0.134001548	0.122364436
	7000	0.134128766	0.122506174
	8000	0.134231543	0.12262065
	9000	0.13431683	0.122715623
	10000	0.13438909	0.122796074
0.165	1000	0.13198819	0.120126392
	2000	0.133183841	0.121464229
	3000	0.133723068	0.122066229
	4000	0.134047291	0.122427799
	5000	0.134269741	0.122675704
	6000	0.134434565	0.122859301
	7000	0.134563029	0.123002344
	8000	0.134666812	0.123117872
	9000	0.134752933	0.123213717
	10000	0.134825899	0.123294906



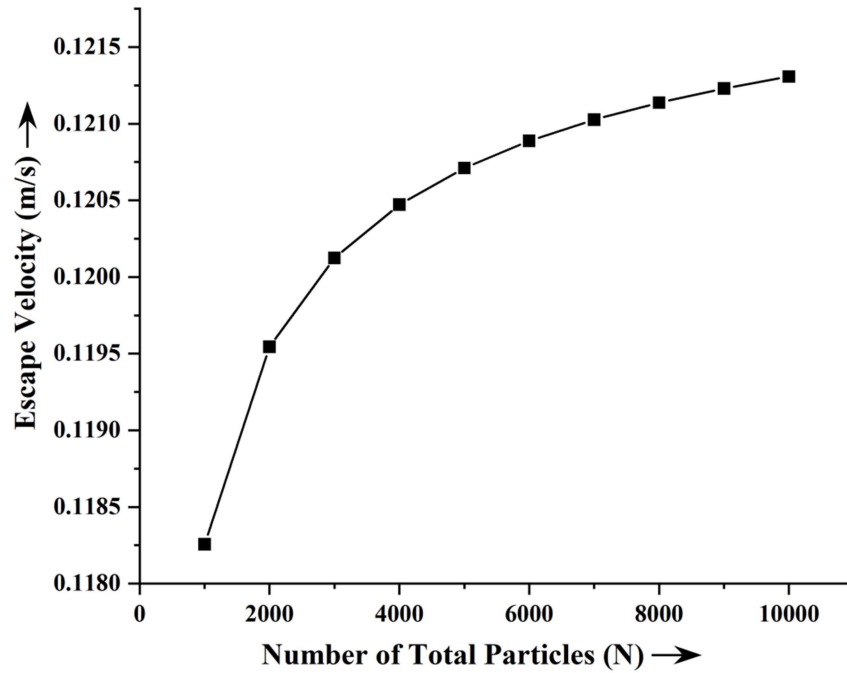


**Fig. 3.17** Escape velocity variation with number of total particles for inter-particle distance of 0.145 mm for water level falling

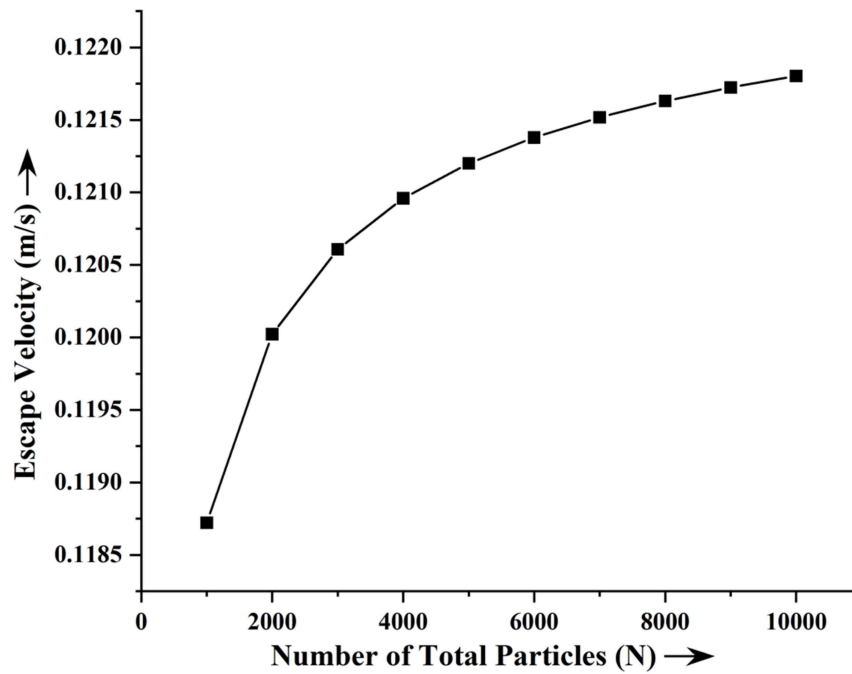


**Fig. 3.18** Escape velocity variation with number of total particles for inter-particle distance of 0.150 mm for water level falling

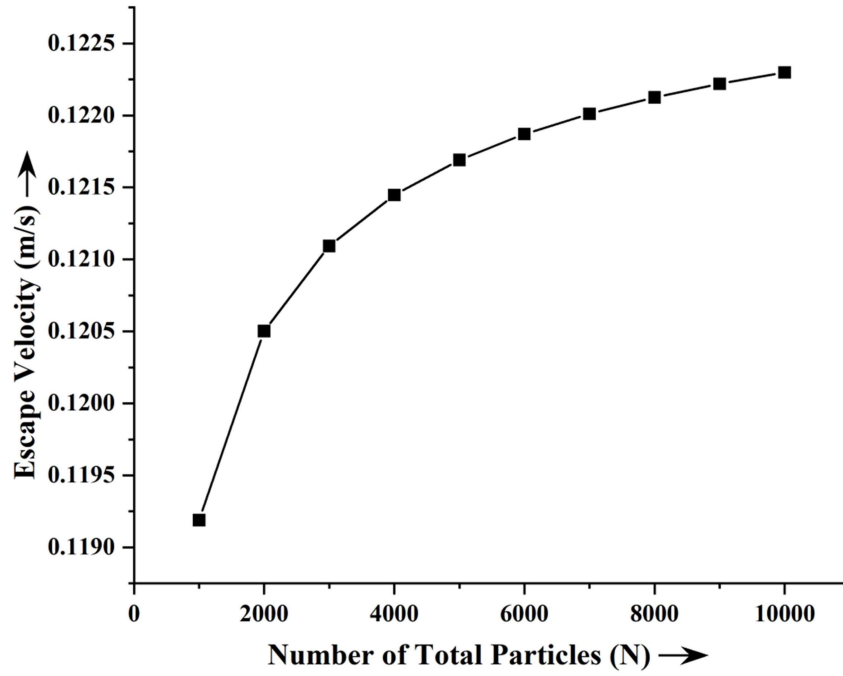


**Fig. 3.19** Escape velocity variation with number of total particles for inter-particle distance of 0.155 mm for water level falling

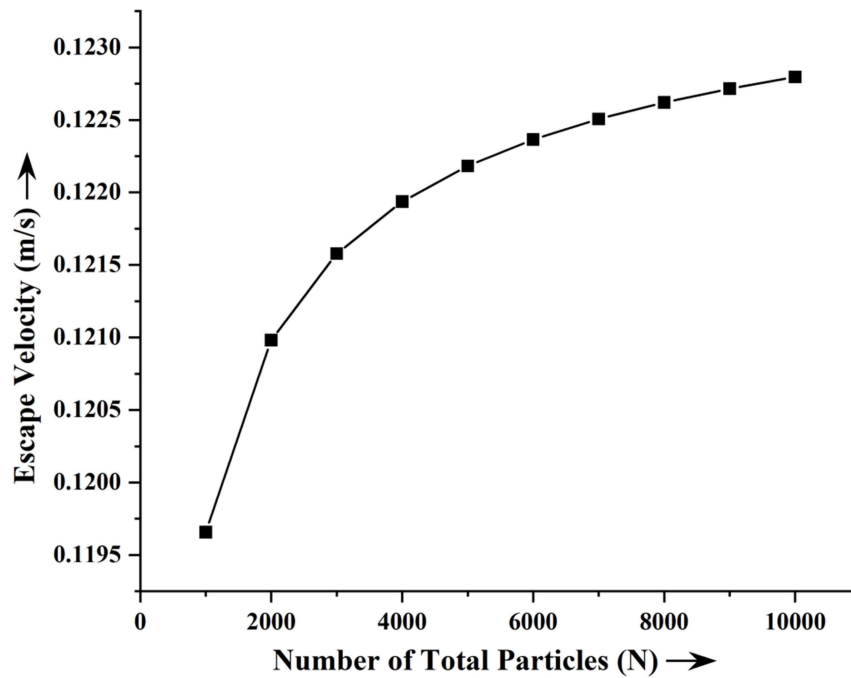


**Fig. 3.20** Escape velocity variation with number of total particles for inter-particle distance of 0.160 mm for water level falling

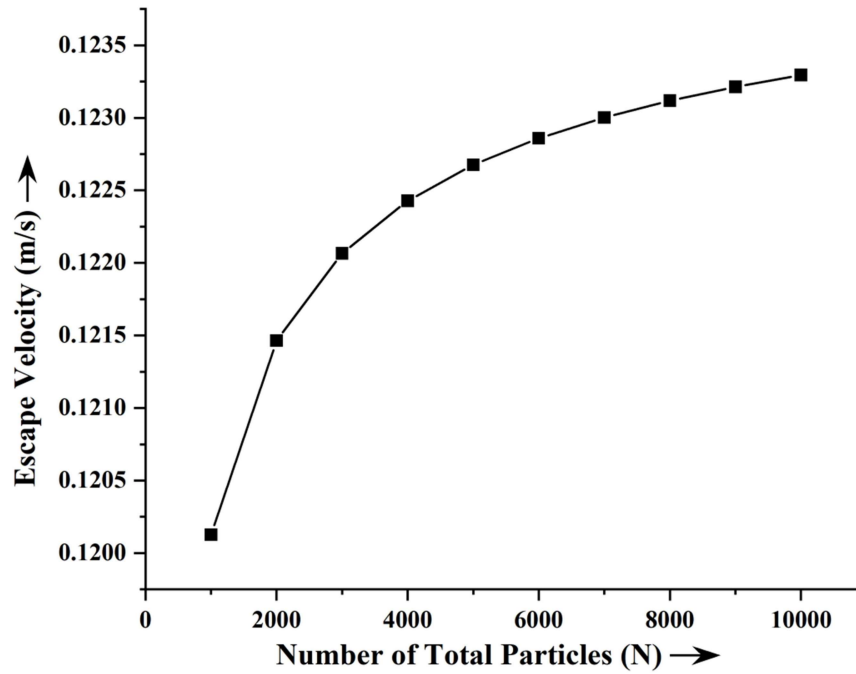


**Fig. 3.21** Escape velocity variation with number of total particles for inter-particle distance of 0.165 mm for water level falling

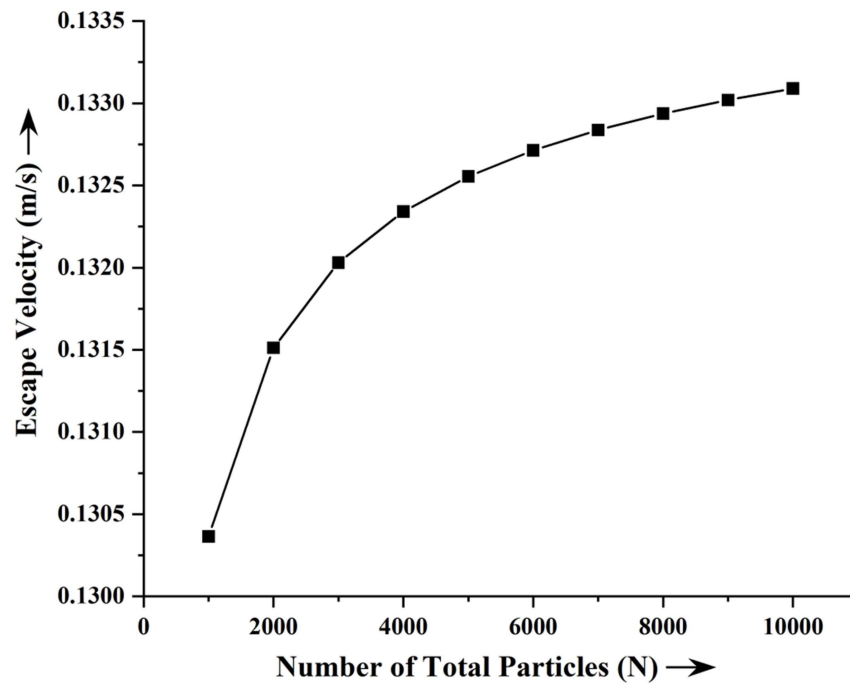


**Fig. 3.22** Escape velocity variation with number of total particles for inter-particle distance of 0.145 mm for water level rising

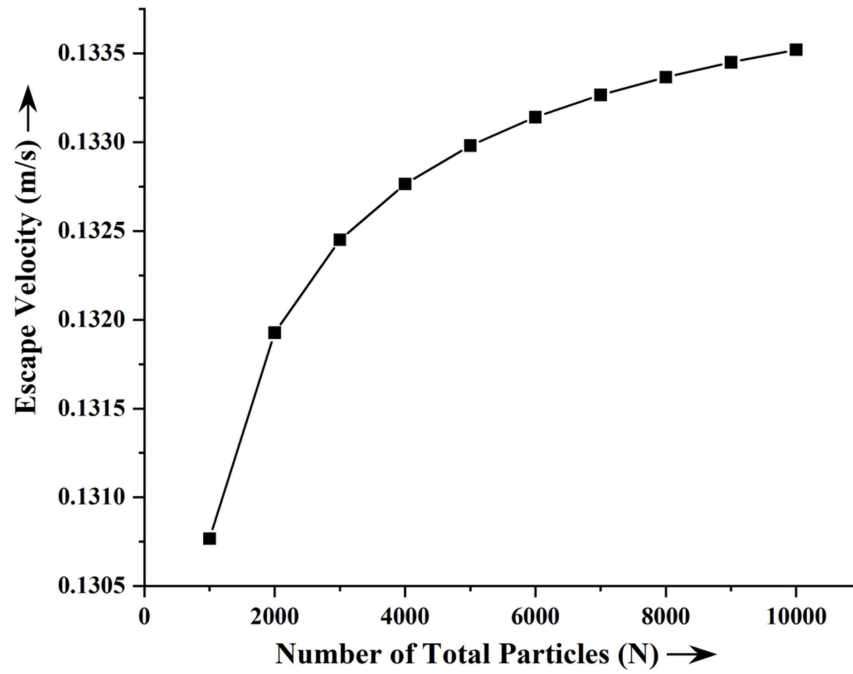


**Fig. 3.23** Escape velocity variation with number of total particles for inter-particle distance of 0.150 mm for water level rising

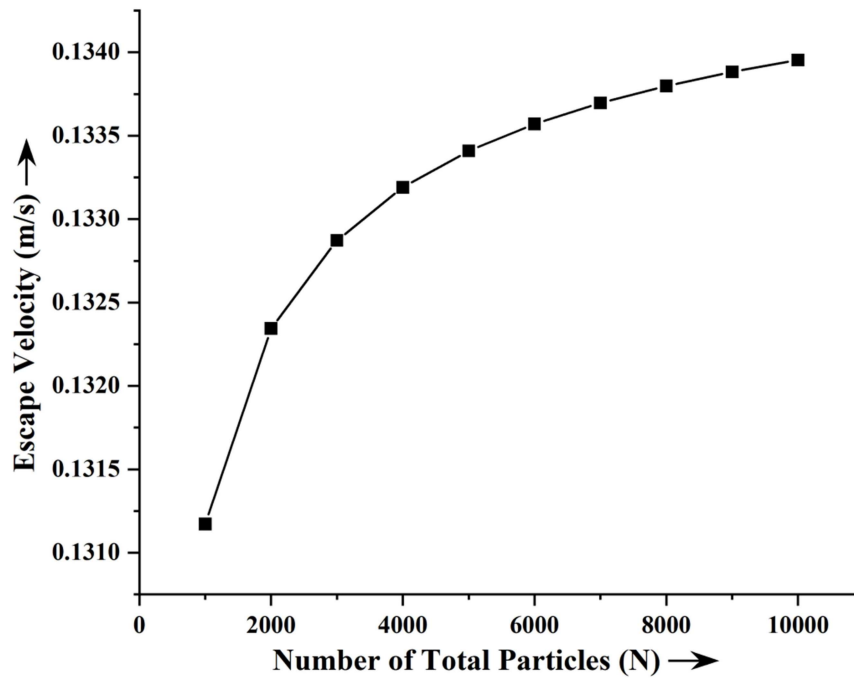


**Fig. 3.24** Escape velocity variation with number of total particles for inter-particle distance of 0.155 mm for water level rising

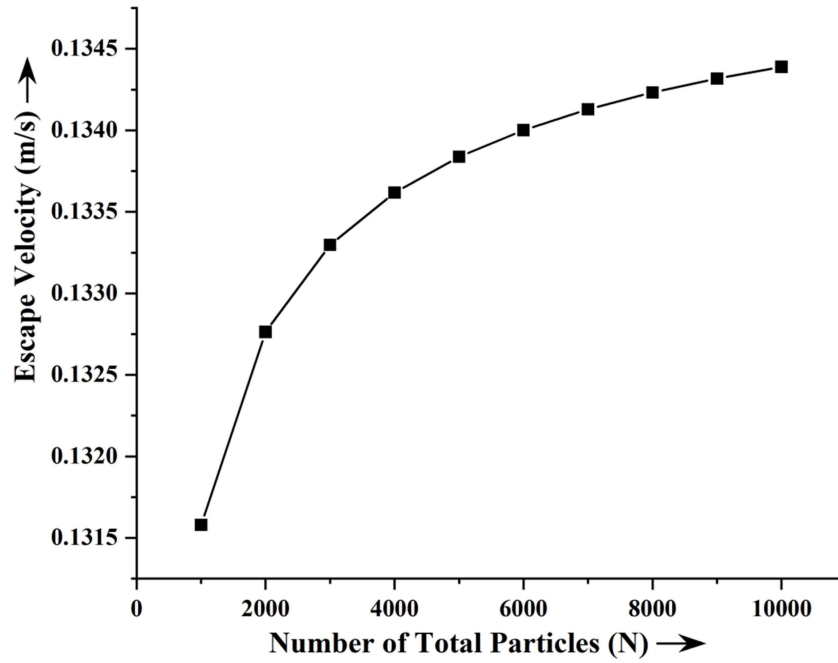


**Fig. 3.25** Escape velocity variation with number of total particles for inter-particle distance of 0.160 mm for water level rising

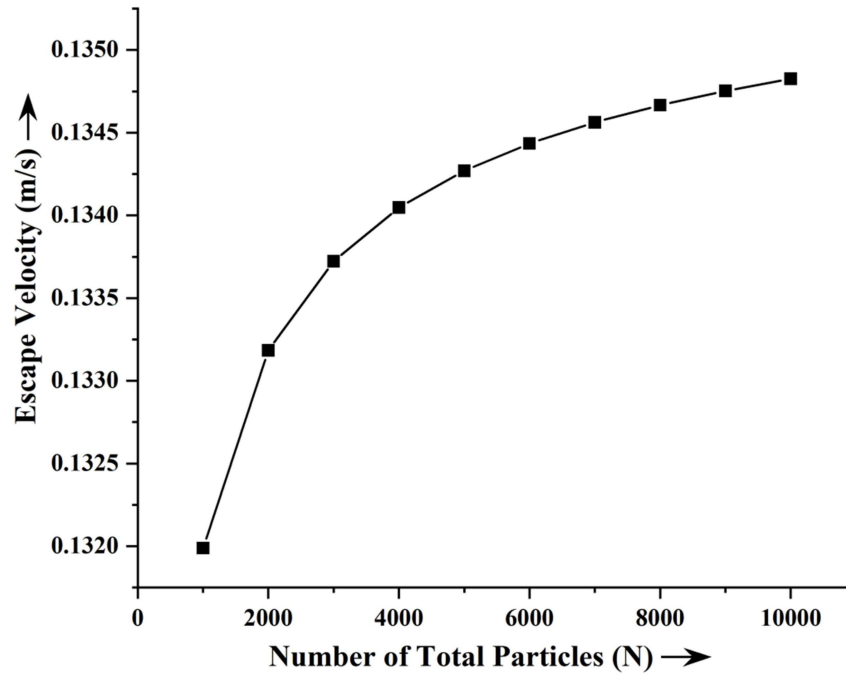


**Fig. 3.26** Escape velocity variation with number of total particles for inter-particle distance of 0.165 mm for water level rising

### 3.4.2 Escape Velocity Variation for Different Liquid-Bridge Volumes

Here, escape velocity variation is plotted for five different liquid-bridge volumes (10 nl, 15 nl, 20 nl, 25 nl and 30 nl) for the fixed values inter-particle distance of 0.145 mm and particle radius of 0.4 mm. Variations are shown for two different varying conditions, such as, number of base particles and number of total particles.

#### 3.4.2.1 Escape Velocity Variation with Number of Base Particles

Here, the variation is plotted with respect to number of base particles. The numbers of base particle have been varied from 10 to 100 with the intervals of 10. The first five graphs are for water level falling and next five are for water level rising. For showing the results in a tabular form, the corresponding table (Table 3.13) is also added.

**Table 3.13: Escape velocity variation with number of base particles for different liquid-bridge volumes**

Liquid-Bridge Volume (nl)	Number of Base Particles	Escape Velocity for Rising Water Level (m/s)	Escape Velocity for Falling Water Level (m/s)
10	10	0.122635492	0.109622024
	20	0.128097924	0.115840684
	30	0.130090851	0.118083775
	40	0.131120638	0.119238029
	50	0.131749331	0.11994117

Liquid-Bridge Volume (nl)	Number of Base Particles	Escape Velocity for Rising Water Level (m/s)	Escape Velocity for Falling Water Level (m/s)
10	60	0.132173006	0.120414374
	70	0.132477871	0.120754563
	80	0.132707749	0.121010904
	90	0.132887274	0.121210994
	100	0.133031356	0.121371515
15	10	0.122673132	0.109578663
	20	0.128133876	0.115800441
	30	0.130126247	0.118044566
	40	0.13115576	0.119199334
	50	0.131784287	0.119902784
	60	0.132207853	0.120376192
	70	0.13251264	0.120716527
	80	0.13274246	0.120972978
	90	0.132921939	0.121173153
	100	0.133065985	0.121333742
20	10	0.122699098	0.109548733
	20	0.128158678	0.115772664
	30	0.130150668	0.118017503
	40	0.13117999	0.119172627
	50	0.131808404	0.119876289
	60	0.132231894	0.120349839
	70	0.132536627	0.120690275

Liquid-Bridge Volume (nl)	Number of Base Particles	Escape Velocity for Rising Water Level (m/s)	Escape Velocity for Falling Water Level (m/s)
	80	0.132766407	0.120946801
	90	0.132945855	0.121147035
	100	0.133089875	0.121307671
25	10	0.12271847	0.109526395
	20	0.128177182	0.115751934
	30	0.130168886	0.117997306
	40	0.131198066	0.119152695
	50	0.131826396	0.119856516
	60	0.13224983	0.120330172
	70	0.132554522	0.120670683
	80	0.132784272	0.120927266
	90	0.132963697	0.121127543
	100	0.133107699	0.121288215
30	10	0.12273367	0.109508862
	20	0.128191701	0.115735663
	30	0.130183181	0.117981454
	40	0.13121225	0.119137052
	50	0.131840513	0.119840997
	60	0.132263903	0.120314736
	70	0.132568564	0.120655307
	80	0.13279829	0.120911934
	90	0.132977697	0.121112246
	100	0.133121684	0.121272945



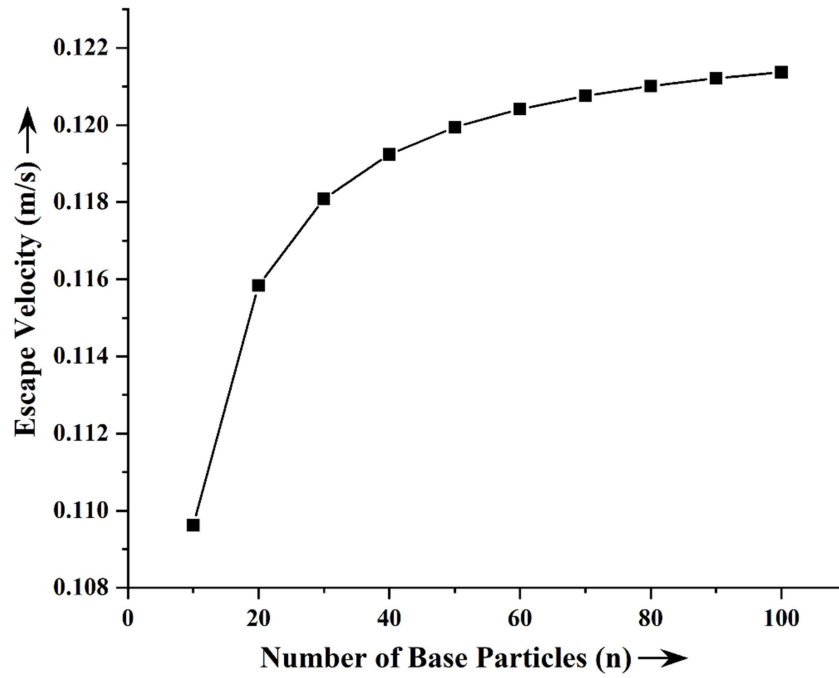


**Fig. 3.27** Escape velocity variation with number of base particles for liquid-bridge  
volume of 10 nl for water level falling

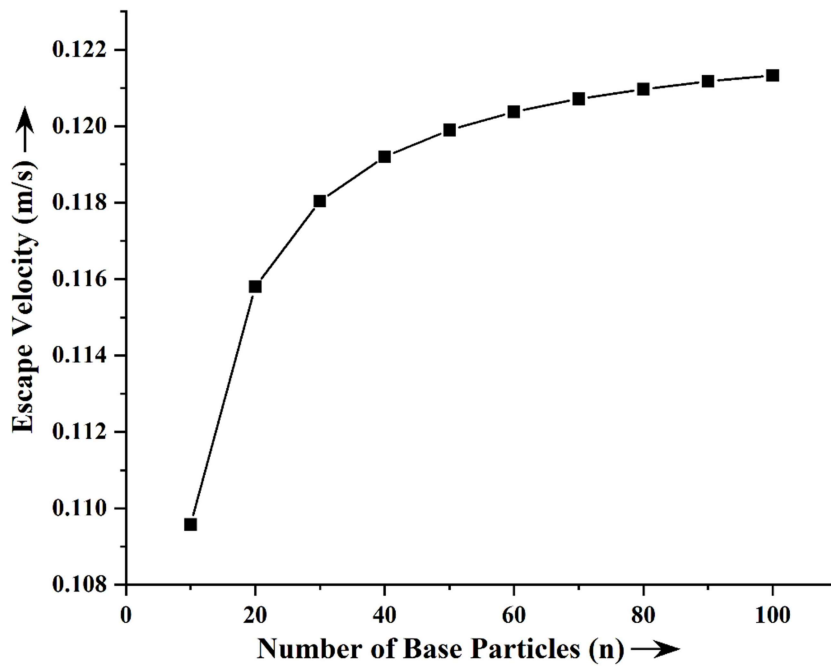


**Fig. 3.28** Escape velocity variation with number of base particles for liquid-bridge  
volume of 15 nl for water level falling

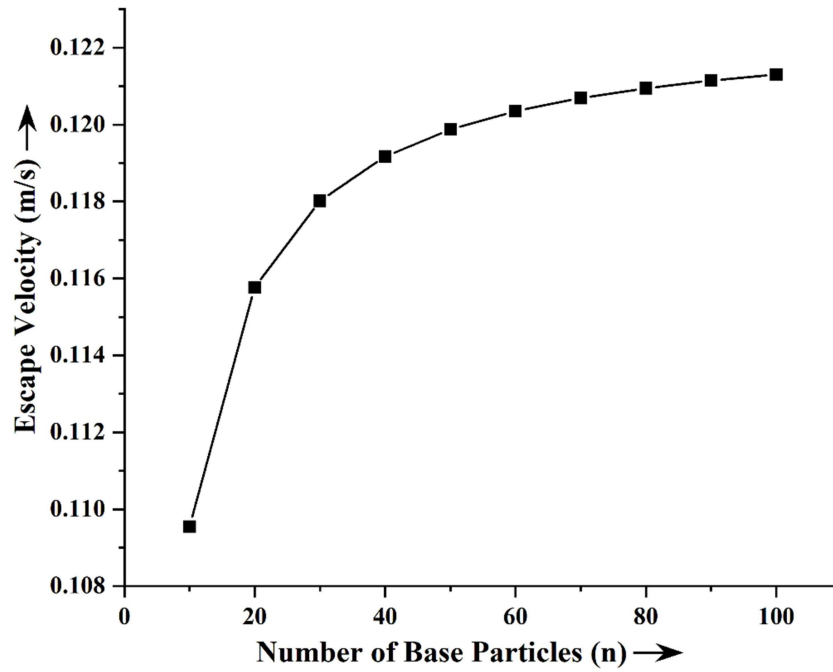


**Fig. 3.29** Escape velocity variation with number of base particles for liquid-bridge  
volume of 20 nl for water level falling

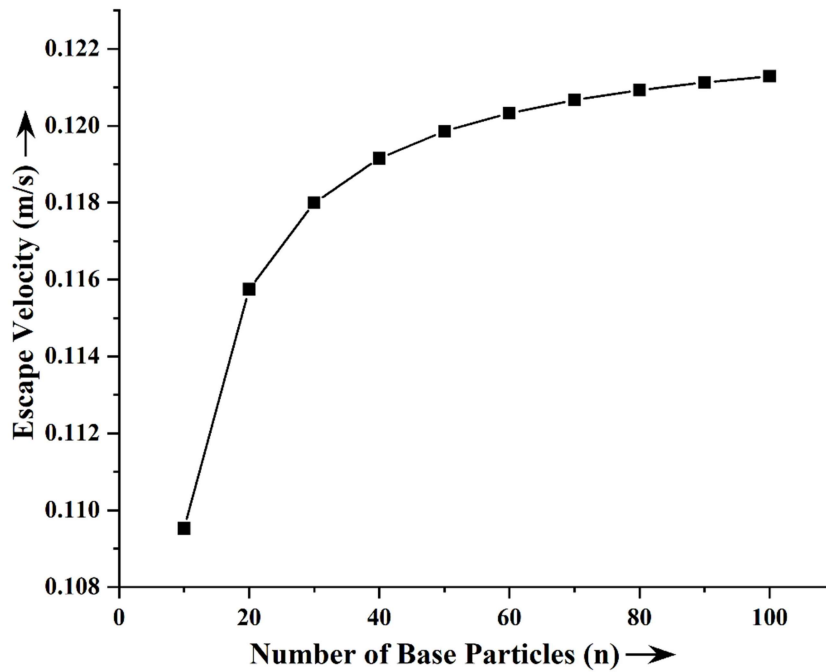


**Fig. 3.30** Escape velocity variation with number of base particles for liquid-bridge  
volume of 25 nl for water level falling

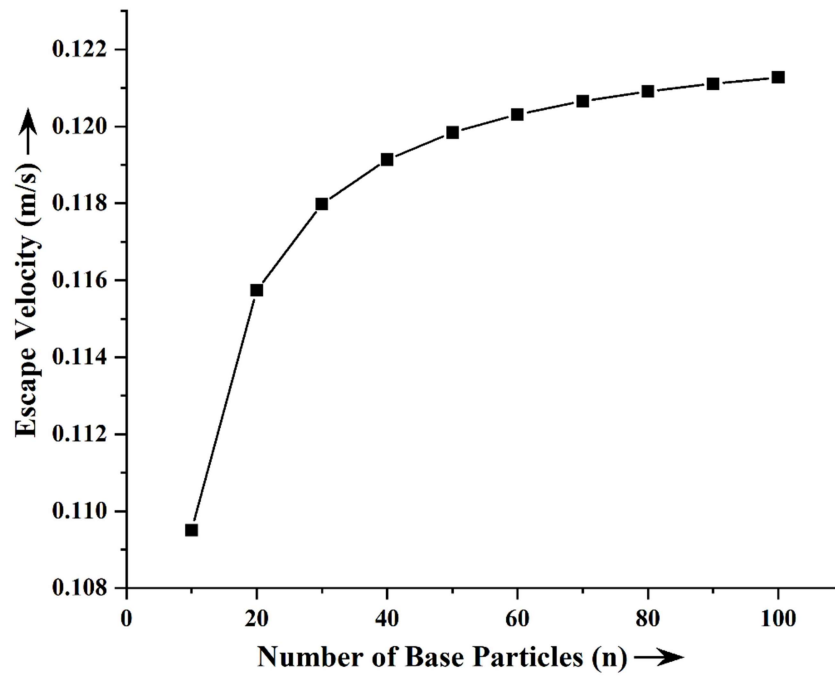


**Fig. 3.31** Escape velocity variation with number of base particles for liquid-bridge  
volume of 30 nl for water level falling

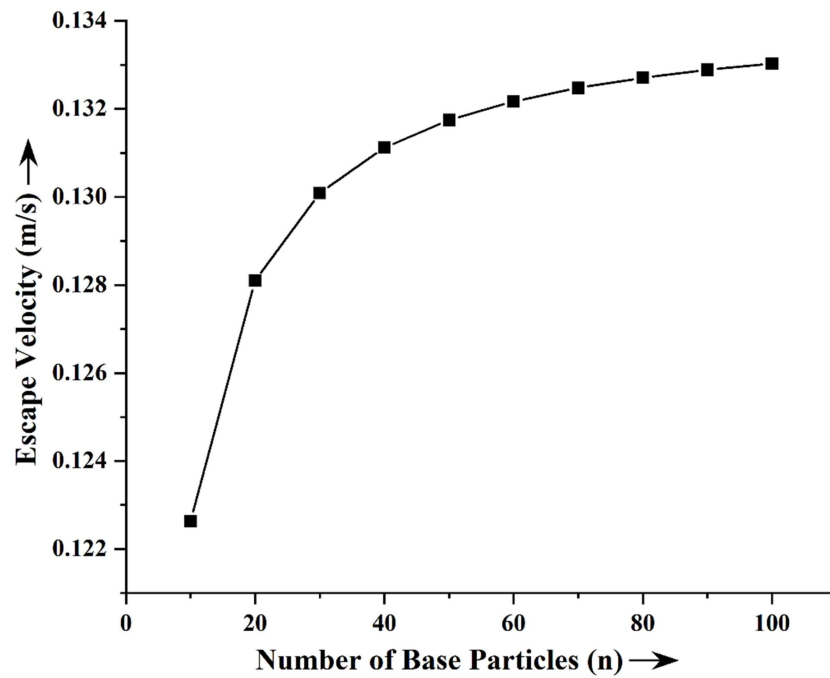


**Fig. 3.32** Escape velocity variation with number of base particles for liquid-bridge  
volume of 10 nl for water level rising

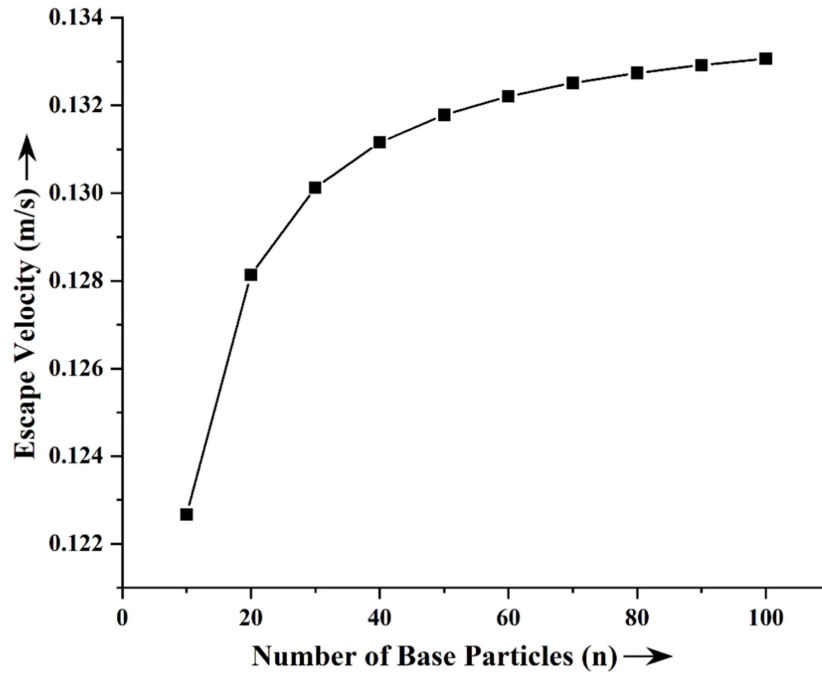


**Fig. 3.33** Escape velocity variation with number of base particles for liquid-bridge  
volume of 15 nl for water level rising

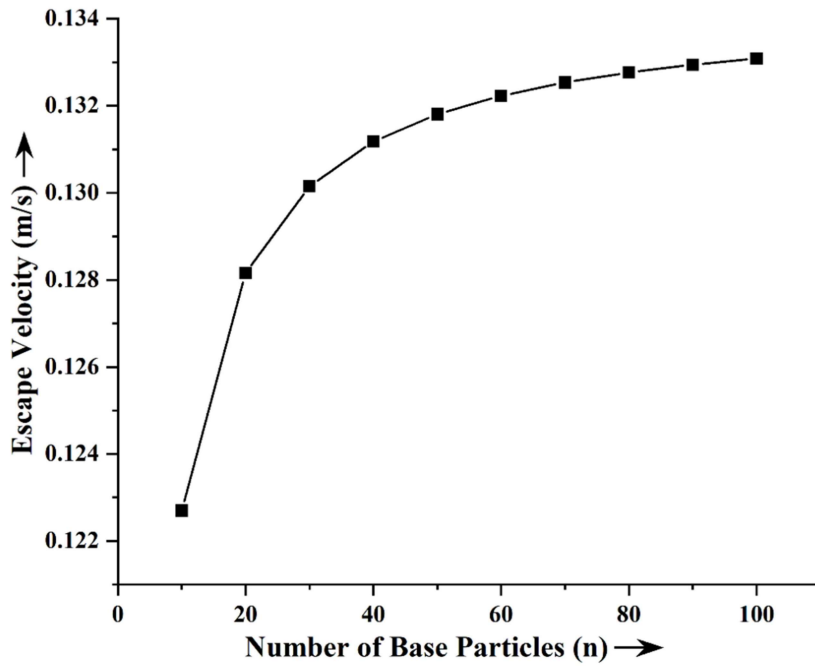


**Fig. 3.34** Escape velocity variation with number of base particles for liquid-bridge  
volume of 20 nl for water level rising

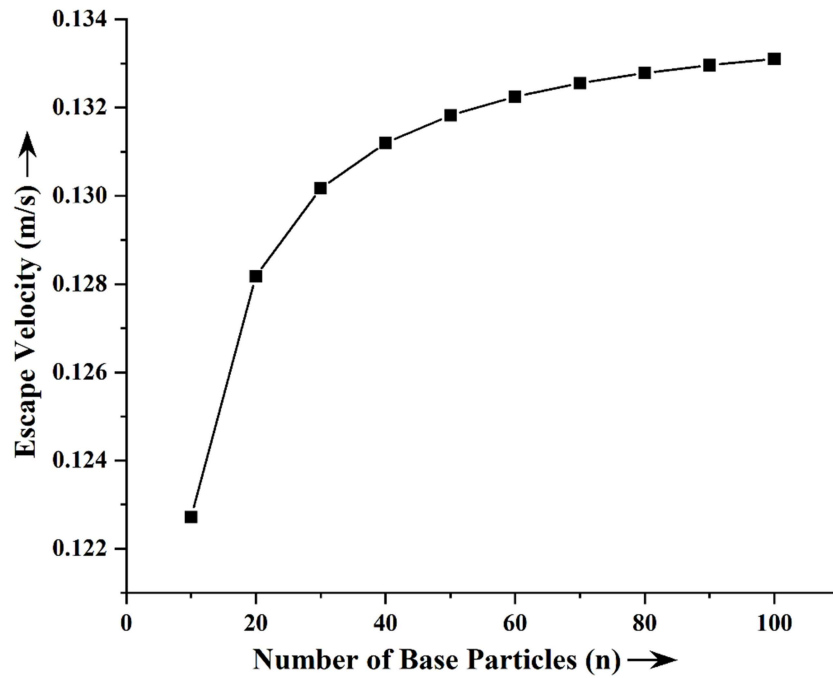


**Fig. 3.35** Escape velocity variation with number of base particles for liquid-bridge  
volume of 25 nl for water level rising

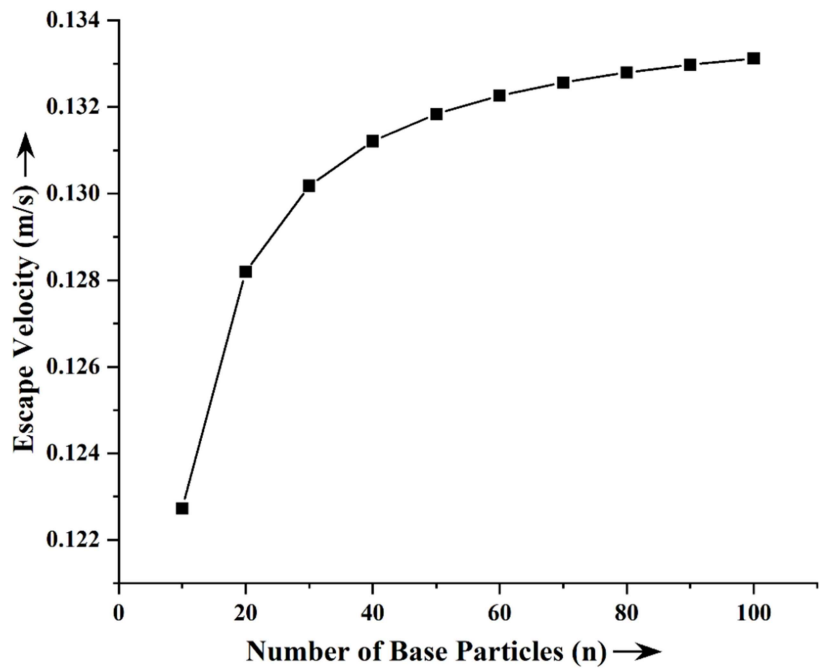


**Fig. 3.36** Escape velocity variation with number of base particles for liquid-bridge  
volume of 30 nl for water level rising

### 3.4.2.2 *Escape Velocity Variation with Number of Total Particles*

Here, variations are plotted with respect to number of total particles. The numbers of total particle vary from 1000 to 10000 with the intervals of 1000. The first five graphs are for water level falling and next five are for water level rising. For showing the results in a tabular form, the corresponding table (Table 3.14) is also added.

**Table 3.14: Escape velocity variation with number of total particles for different liquid-bridge volumes**

<b>Liquid-Bridge Volume (nl)</b>	<b>Number of Total Particles</b>	<b>Escape Velocity for Rising Water Level (m/s)</b>	<b>Escape Velocity for Falling Water Level (m/s)</b>
10	1000	0.130304281	0.118323263
	2000	0.131452891	0.119609769
	3000	0.131971135	0.120188968
	4000	0.132282809	0.12053693
	5000	0.132496678	0.120775541
	6000	0.13265516	0.120952274
	7000	0.13277869	0.121089982
	8000	0.132878492	0.121201207
	9000	0.132961313	0.121293487
	10000	0.133031486	0.12137166
15	1000	0.13033962	0.118284162
	2000	0.131487925	0.119571238
	3000	0.132006034	0.120150689
	4000	0.132317628	0.120498801

Liquid-Bridge Volume (nl)	Number of Total Particles	Escape Velocity for Rising Water Level (m/s)	Escape Velocity for Falling Water Level (m/s)
15	5000	0.132531442	0.120737514
	6000	0.132689884	0.120914323
	7000	0.132813382	0.121052089
	8000	0.132913159	0.121163362
	9000	0.132995959	0.121255681
	10000	0.133066115	0.121333887
20	1000	0.130364	0.118257173
	2000	0.131512095	0.119544643
	3000	0.132030111	0.120124268
	4000	0.132341649	0.120472484
	5000	0.132555426	0.120711268
	6000	0.13271384	0.120888129
	7000	0.132837317	0.121025936
	8000	0.132937076	0.121137241
	9000	0.133019862	0.121229587
	10000	0.133090005	0.121307816
25	1000	0.130382189	0.118237032
	2000	0.131530126	0.119524796
	3000	0.132048073	0.120104551
	4000	0.13235957	0.120452844

<b>Liquid-Bridge Volume (nl)</b>	<b>Number of Total Particles</b>	<b>Escape Velocity for Rising Water Level (m/s)</b>	<b>Escape Velocity for Falling Water Level (m/s)</b>
25	5000	0.132573319	0.120691681
	6000	0.132731712	0.120868581
	7000	0.132855173	0.121006418
	8000	0.132954919	0.121117748
	9000	0.133037694	0.121210114
	10000	0.133107829	0.12128836
30	1000	0.13039646	0.118221224
	2000	0.131544275	0.119509219
	3000	0.132062168	0.120089076
	4000	0.132373632	0.12043743
	5000	0.132587359	0.120676308
	6000	0.132745736	0.120853239
	7000	0.132869184	0.120991099
	8000	0.13296892	0.121102448
	9000	0.133051687	0.12119483
	10000	0.133121814	0.121273089



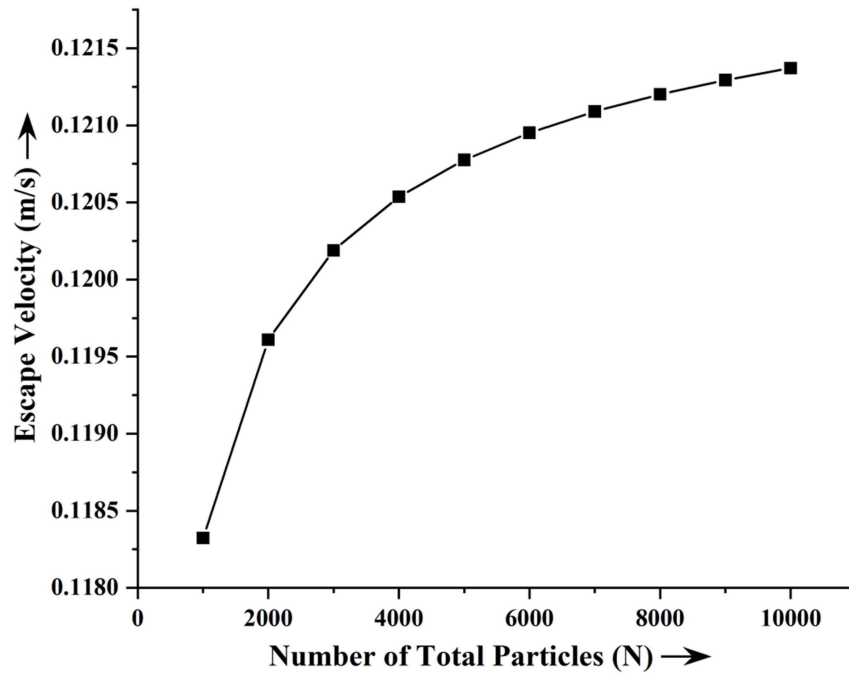


**Fig. 3.37** Escape velocity variation with number of total particles for liquid-bridge  
volume of 10 nl for water level falling

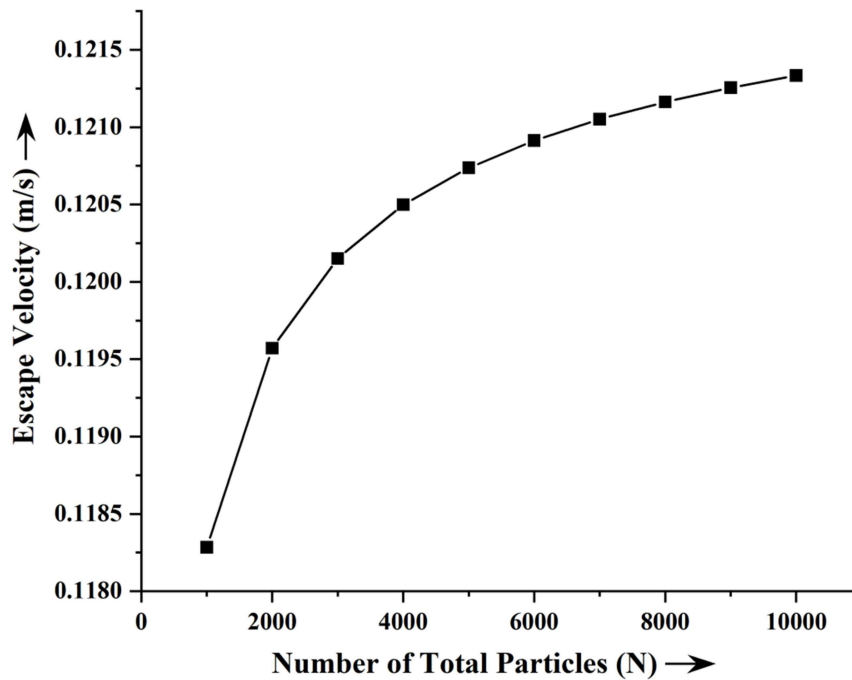


**Fig. 3.38** Escape velocity variation with number of total particles for liquid-bridge  
volume of 15 nl for water level falling

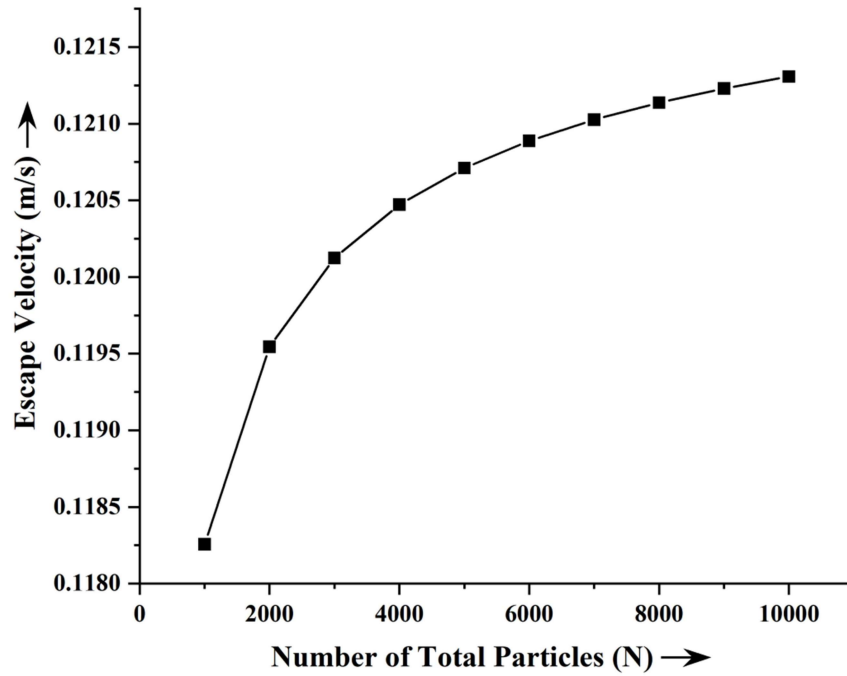


**Fig. 3.39** Escape velocity variation with number of total particles for liquid-bridge  
volume of 20 nl for water level falling

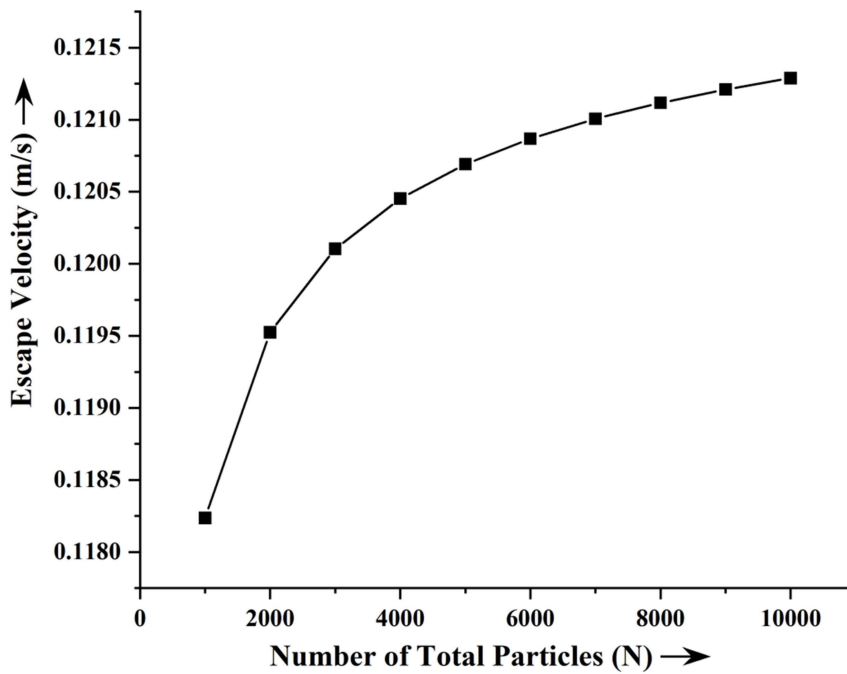


**Fig. 3.40** Escape velocity variation with number of total particles for liquid-bridge  
volume of 25 nl for water level falling

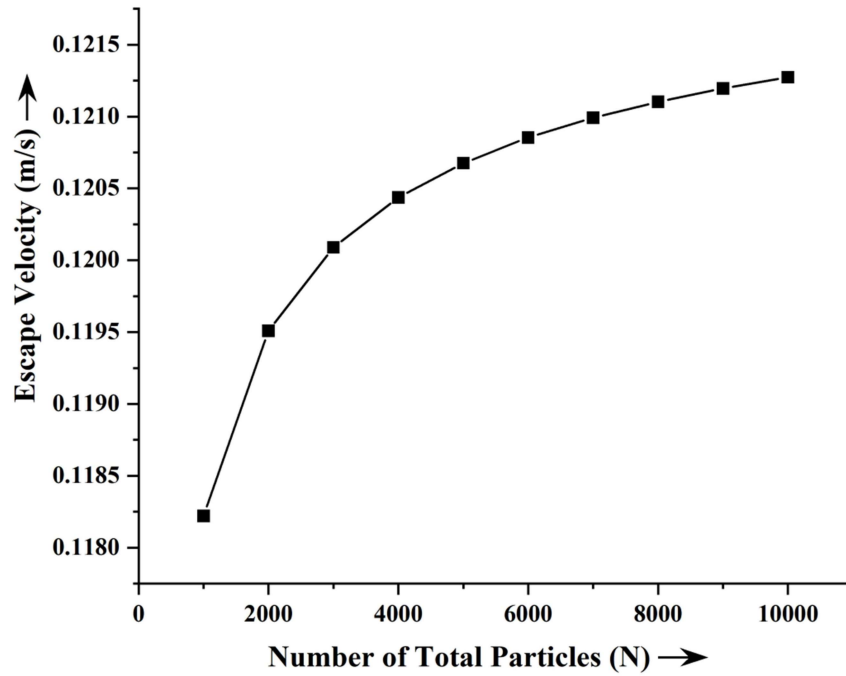


**Fig. 3.41** Escape velocity variation with number of total particles for liquid-bridge  
volume of 30 nl for water level falling

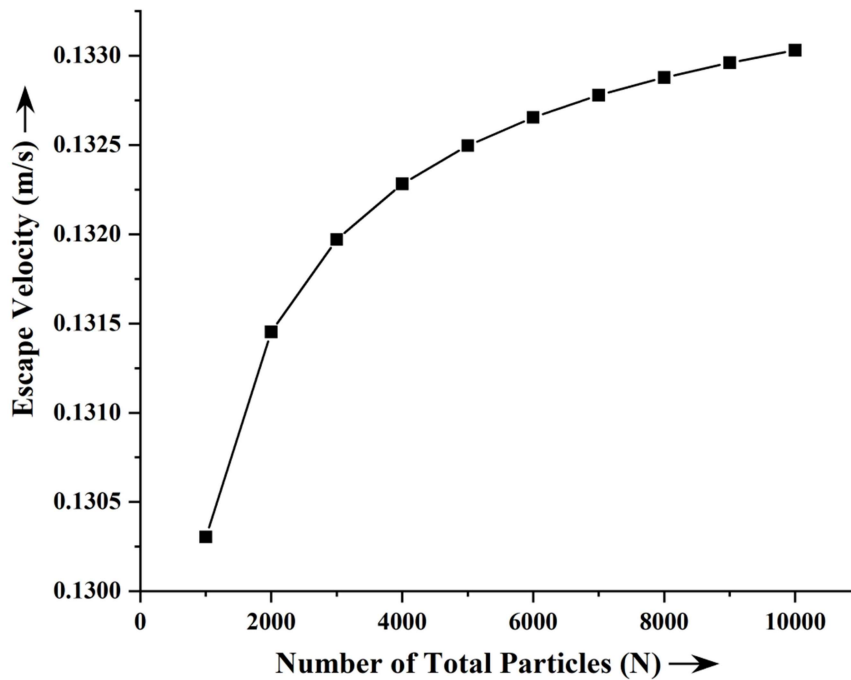


**Fig. 3.42** Escape velocity variation with number of total particles for liquid-bridge  
volume of 10 nl for water level rising

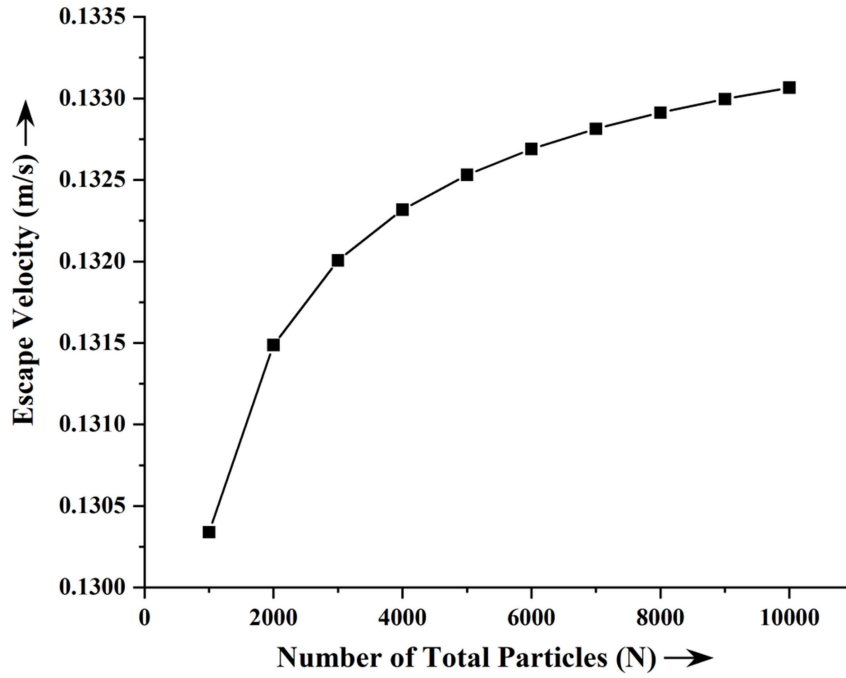


**Fig. 3.43** Escape velocity variation with number of total particles for liquid-bridge  
volume of 15 nl for water level rising

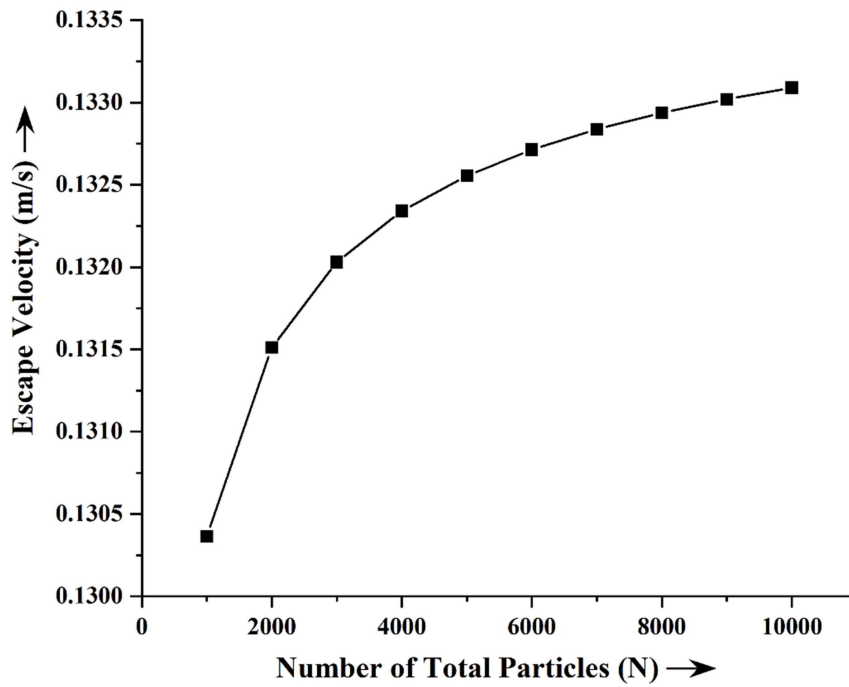


**Fig. 3.44** Escape velocity variation with number of total particles for liquid-bridge  
volume of 20 nl for water level rising

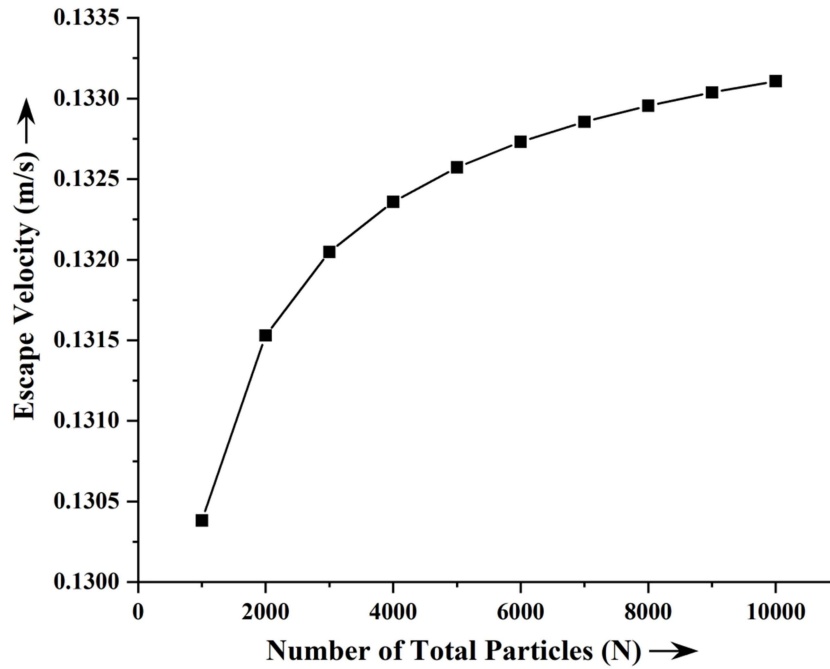


**Fig. 3.45** Escape velocity variation with number of total particles for liquid-bridge  
volume of 25 nl for water level rising

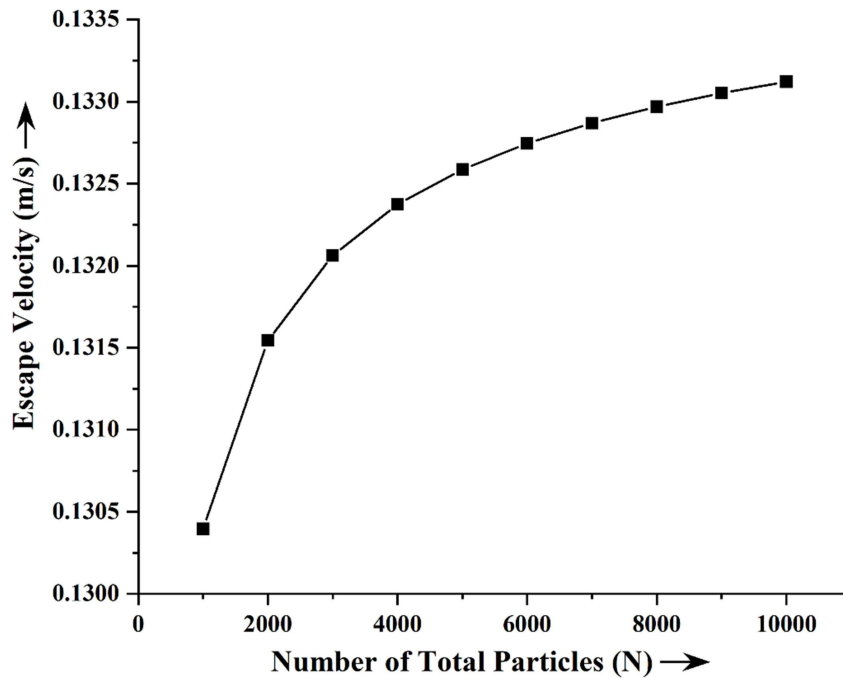


**Fig. 3.46** Escape velocity variation with number of total particles for liquid-bridge  
volume of 30 nl for water level rising

### 3.4.3 Escape Velocity Variation for Different Size of Particles

Here, escape velocities are plotted for five different particle radii (0.390 mm, 0.395 mm, 0.400 mm, 0.405 mm and 0.410 mm) for the fixed values inter-particle distance of 0.145 mm and liquid-bridge volume of 20 nl. Variations are shown for two different varying conditions, such as, number of base particles and number of total particles.

#### 3.4.3.1 *Escape Velocity Variation with Number of Base Particles*

Here, the variation is plotted with respect to number of base particles. The numbers of base particle vary from 10 to 100 with the intervals of 10. The first five graphs are for water level falling and next five are for water level rising. For showing the results in a tabular form, the corresponding table (Table 3.15) is also added.

**Table 3.15: Escape velocity variation with number of base particles for different sizes particle**

Radius of Particle (mm)	Number of Base Particles	Escape Velocity for Rising Water Level (m/s)	Escape Velocity for Falling Water Level (m/s)
0.390	10	0.121703064	0.108082053
	20	0.127124747	0.114303264
	30	0.129102547	0.116545243
	40	0.130124464	0.117698537
	50	0.130748334	0.11840097
	60	0.131168752	0.118873645
	70	0.13147127	0.119213429

Radius of Particle (mm)	Number of Base Particles	Escape Velocity for Rising Water Level (m/s)	Escape Velocity for Falling Water Level (m/s)
0.390	80	0.131699376	0.119469451
	90	0.131877516	0.119669283
	100	0.132020485	0.119829593
0.395	10	0.122200973	0.108818756
	20	0.127641665	0.115041067
	30	0.129626581	0.117284397
	40	0.130652212	0.118438568
	50	0.131278361	0.119141593
	60	0.131700319	0.119614691
	70	0.132003947	0.119954791
	80	0.132232893	0.120211057
	90	0.132411689	0.120411084
	100	0.132555185	0.120571552
0.400	10	0.122699098	0.109548733
	20	0.128158678	0.115772664
	30	0.130150668	0.118017503
	40	0.13117999	0.119172627
	50	0.131808404	0.119876289
	60	0.132231894	0.120349839
	70	0.132536627	0.120690275
	80	0.132766407	0.120946801
	90	0.132945855	0.121147035

<b>Radius of Particle (mm)</b>	<b>Number of Base Particles</b>	<b>Escape Velocity for Rising Water Level (m/s)</b>	<b>Escape Velocity for Falling Water Level (m/s)</b>
0.405	100	0.133089875	0.121307671
	10	0.123197355	0.11027218
	20	0.128675707	0.116498224
	30	0.130674727	0.118744722
	40	0.131707719	0.119900871
	50	0.132338386	0.120605211
	60	0.132763399	0.121079241
	70	0.133069231	0.121420033
	80	0.13329984	0.121676834
	90	0.133479937	0.121877286
	100	0.133624478	0.122038099
0.410	10	0.123695665	0.110989285
	20	0.129192674	0.117217909
	30	0.131198686	0.119466208
	40	0.132235328	0.120623449
	50	0.132868234	0.121328509
	60	0.133294762	0.121803045
	70	0.133601685	0.122144212
	80	0.13383312	0.122401301
	90	0.134013862	0.122601981
	100	0.134158921	0.12276298



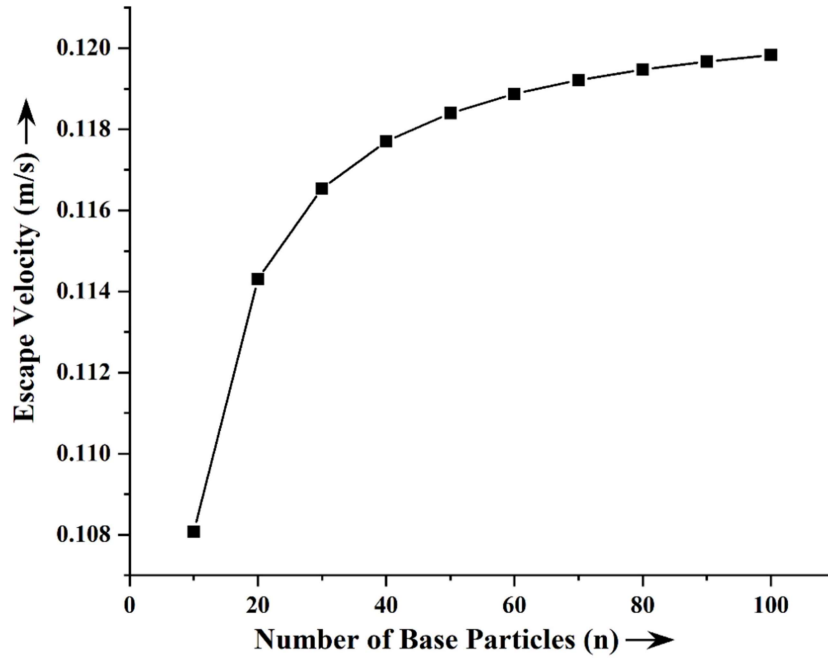


**Fig. 3.47** Escape velocity variation with number of base particles for radius of particle of 0.390 mm for water level falling

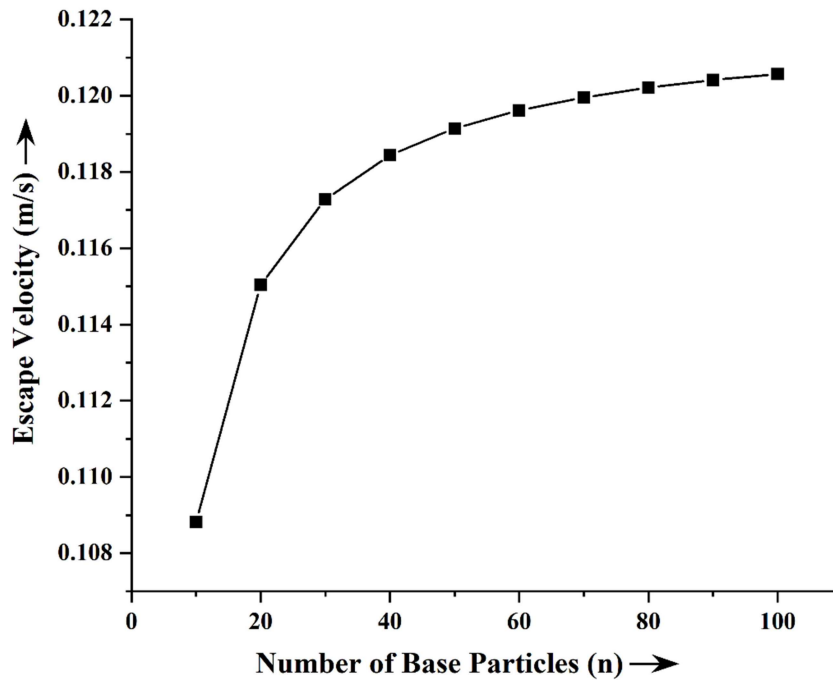


**Fig. 3.48** Escape velocity variation with number of base particles for radius of particle of 0.395 mm for water level falling

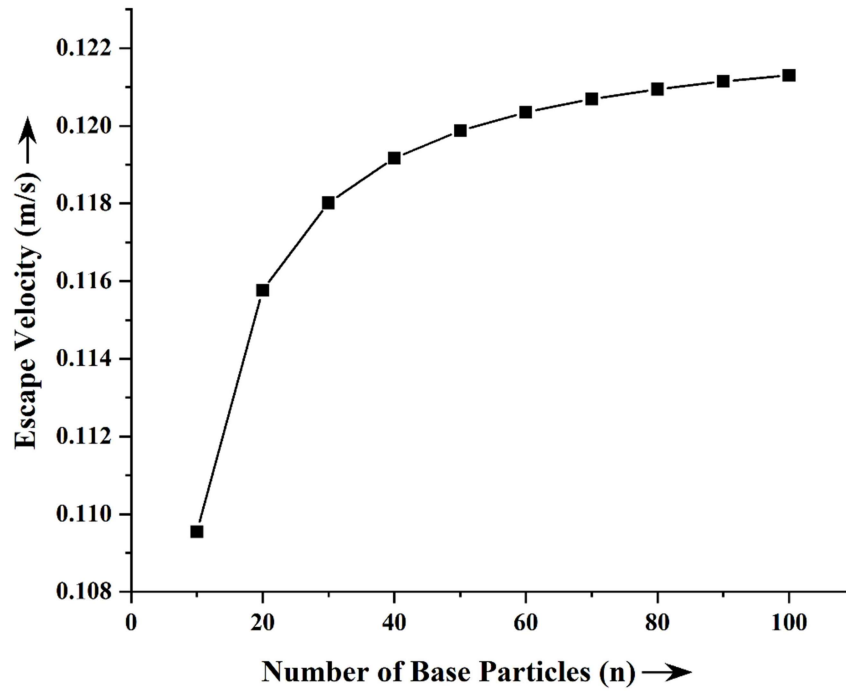


**Fig. 3.49** Escape velocity variation with number of base particles for radius of particle of 0.400 mm for water level falling

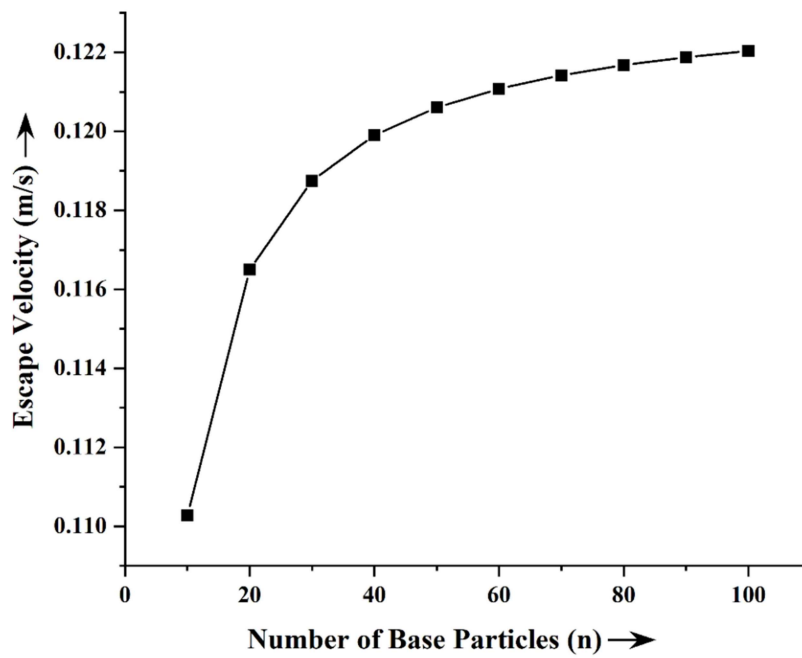


**Fig. 3.50** Escape velocity variation with number of base particles for radius of particle of 0.405 mm for water level falling

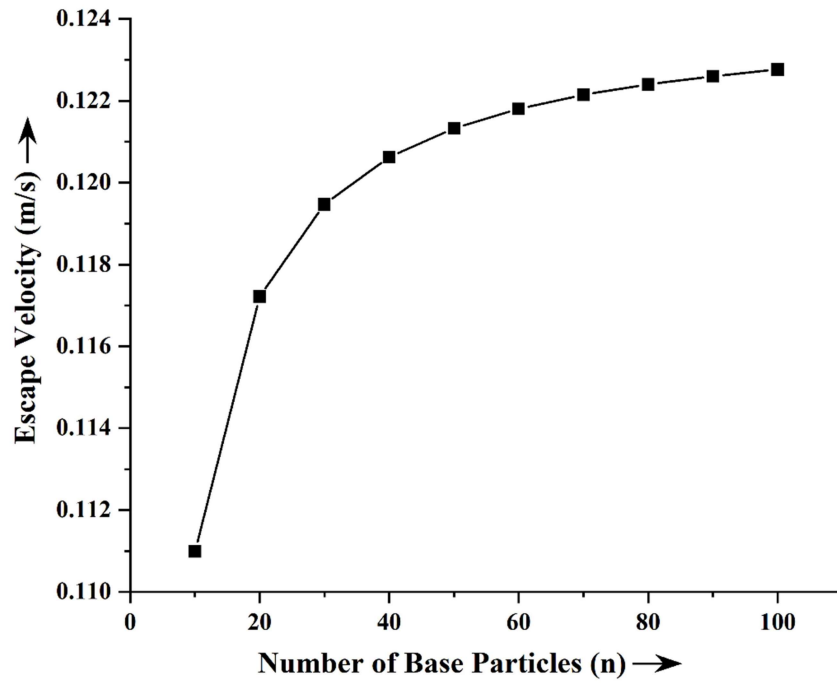


**Fig. 3.51** Escape velocity variation with number of base particles for radius of particle of 0.410 mm for water level falling

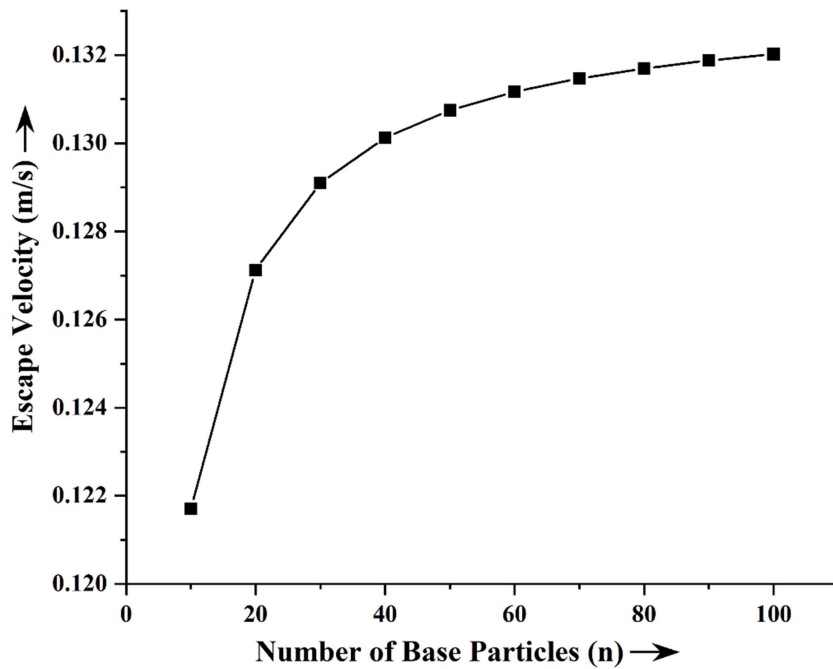


**Fig. 3.52** Escape velocity variation with number of base particles for radius of particle of 0.390 mm for water level rising

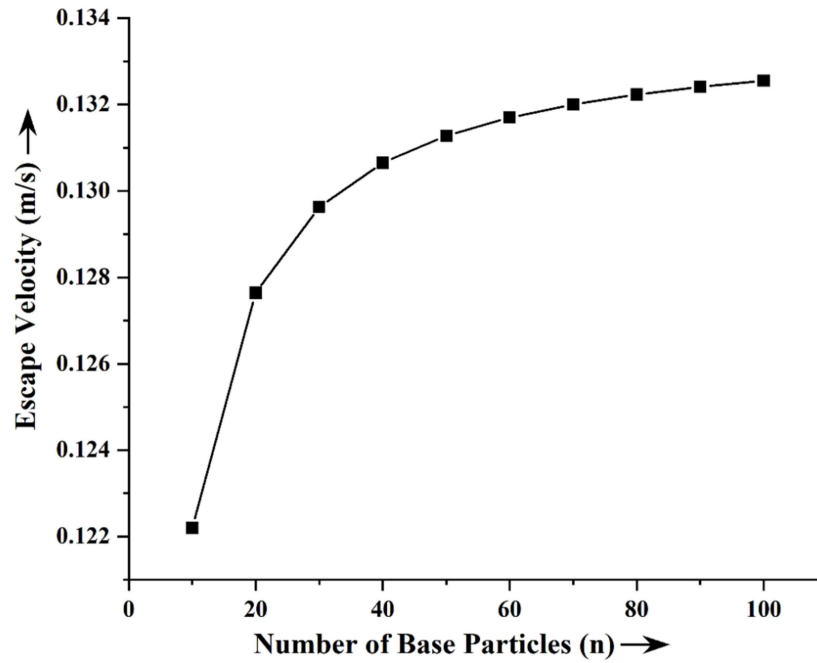


**Fig. 3.53** Escape velocity variation with number of base particles for radius of particle of 0.395 mm for water level rising

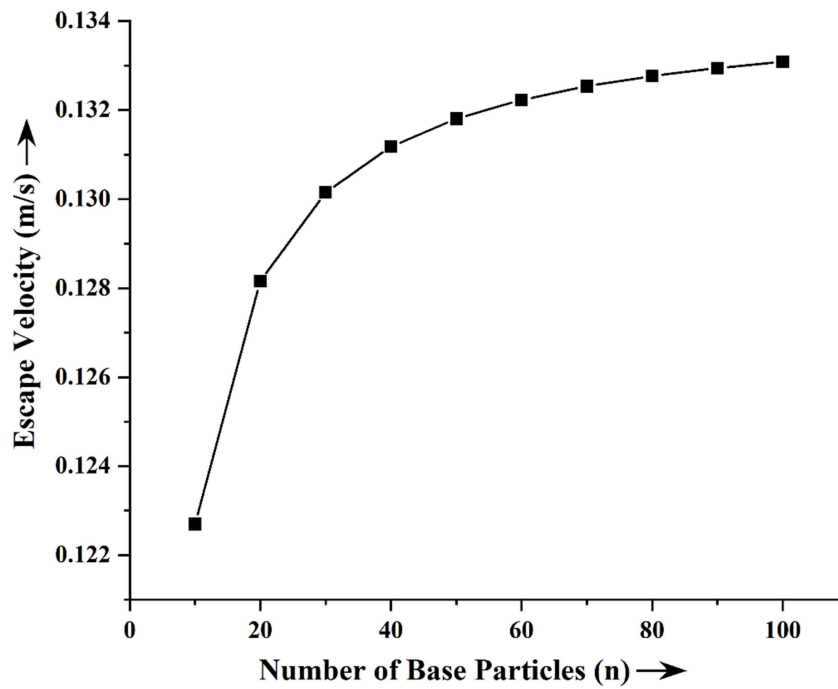


**Fig. 3.54** Escape velocity variation with number of base particles for radius of particle of 0.400 mm for water level rising

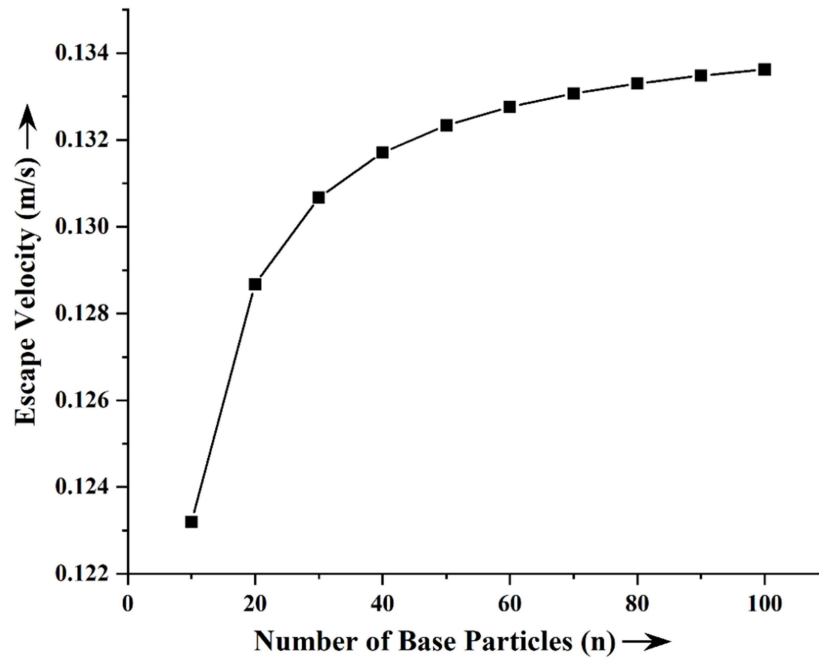


**Fig. 3.55** Escape velocity variation with number of base particles for radius of particle of 0.405 mm for water level rising

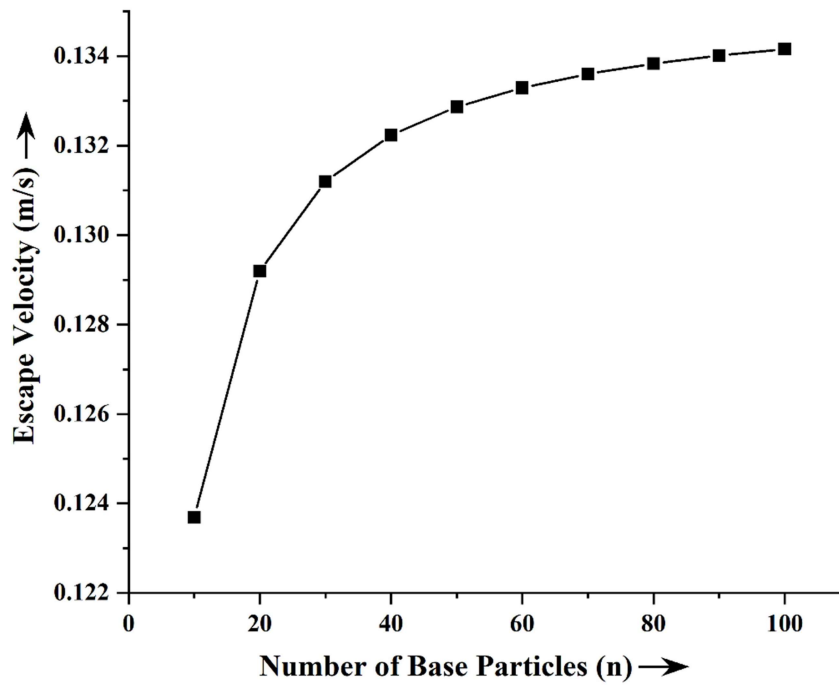


**Fig. 3.56** Escape velocity variation with number of base particles for radius of particle of 0.410 mm for water level rising

### 3.4.3.2 *Escape Velocity Variation with Number of Total Particles*

Here, the variation is calculated with respect to number of total particles. The numbers of total particle vary from 1000 to 10000 with the intervals of 1000. The first five graphs are for water level falling and next five are for water level rising. For showing the results in a tabular form, the corresponding table (Table 3.16) is also added.

**Table 3.16: Escape velocity variation with number of total particles for different sizes particle**

Radius of Particle (mm)	Number of Total Particles	Escape Velocity for Rising Water Level (m/s)	Escape Velocity for Falling Water Level (m/s)
0.390	1000	0.129314349	0.116784553
	2000	0.13045417	0.118069915
	3000	0.130968434	0.118648496
	4000	0.13127771	0.118996057
	5000	0.131489932	0.119234381
	6000	0.131647192	0.119410895
	7000	0.131769769	0.119548428
	8000	0.131868801	0.119659509
	9000	0.131950983	0.119751668
	10000	0.132020614	0.119829737
0.395	1000	0.129839151	0.117523879
	2000	0.130983121	0.118810253
	3000	0.131499267	0.119389338

Radius of Particle (mm)	Number of Total Particles	Escape Velocity for Rising Water Level (m/s)	Escape Velocity for Falling Water Level (m/s)
0.395	4000	0.131809677	0.119737216
	5000	0.132022679	0.119975763
	6000	0.132180517	0.120152445
	7000	0.132303545	0.12029011
	8000	0.132402942	0.1204013
	9000	0.132485427	0.12049355
	10000	0.132555315	0.120571697
0.400	1000	0.130364	0.118257173
	2000	0.131512095	0.119544643
	3000	0.132030111	0.120124268
	4000	0.132341649	0.120472484
	5000	0.132555426	0.120711268
	6000	0.13271384	0.120888129
	7000	0.132837317	0.121025936
	8000	0.132937076	0.121137241
	9000	0.133019862	0.121229587
	10000	0.133090005	0.121307816
0.405	1000	0.130888819	0.118984596
	2000	0.132041014	0.120273241

<b>Radius of Particle (mm)</b>	<b>Number of Total Particles</b>	<b>Escape Velocity for Rising Water Level (m/s)</b>	<b>Escape Velocity for Falling Water Level (m/s)</b>
0.405	3000	0.13256089	0.12085344
	4000	0.13287355	0.121202013
	5000	0.133088098	0.121441049
	6000	0.133247083	0.121618099
	7000	0.133371006	0.121756055
	8000	0.133471126	0.121867481
	9000	0.133554211	0.121959929
	10000	0.133624609	0.122038244
0.410	1000	0.131413532	0.1197063
	2000	0.132569805	0.120996195
	3000	0.133091531	0.121577
	4000	0.133405306	0.121925951
	5000	0.13362062	0.122165251
	6000	0.133780174	0.122342499
	7000	0.133904541	0.122480611
	8000	0.134005019	0.122592166
	9000	0.134088403	0.12268472
	10000	0.134159052	0.122763125



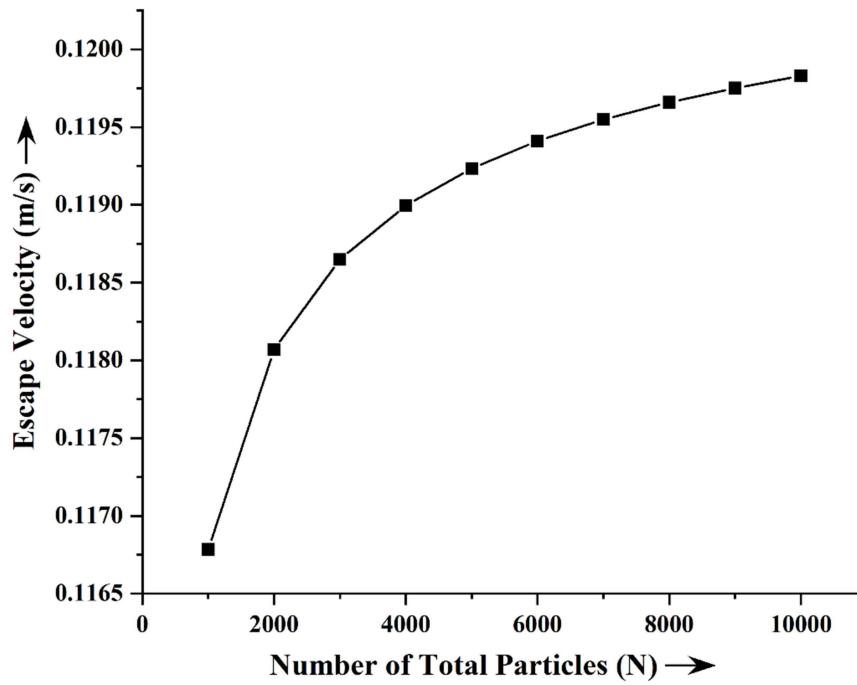


**Fig. 3.57** Escape velocity variation with number of total particles for radius of particle of 0.390 mm for water level falling

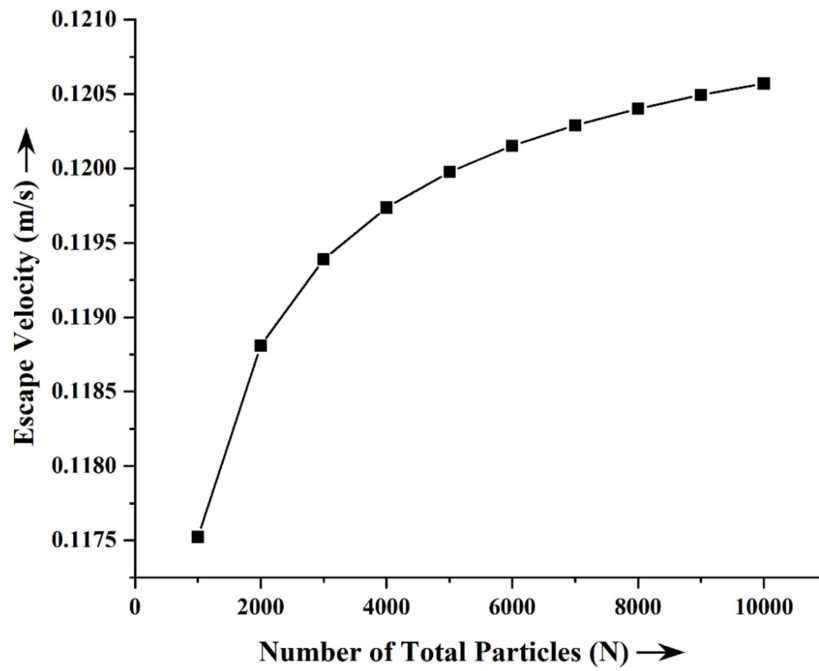


**Fig. 3.58** Escape velocity variation with number of total particles for radius of particle of 0.395 mm for water level falling

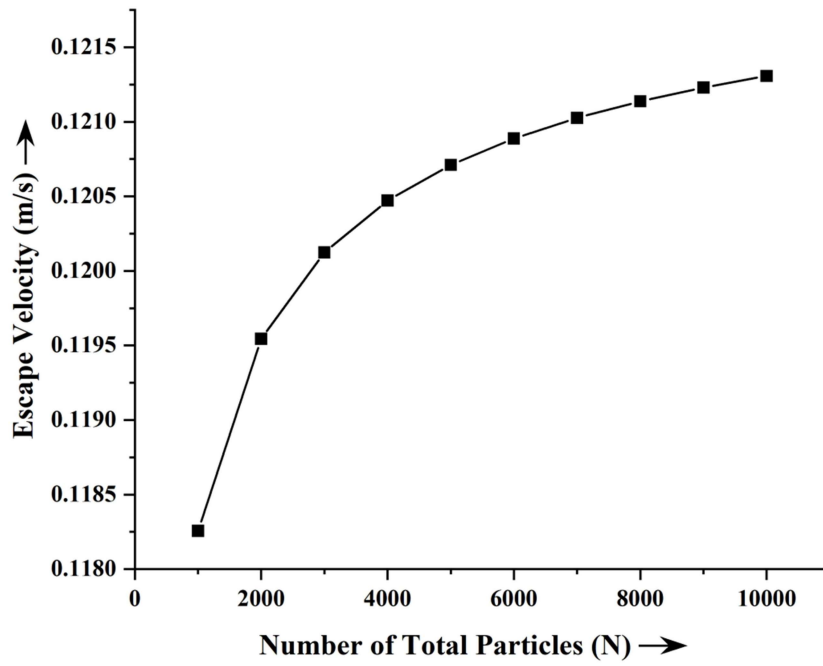


**Fig. 3.59** Escape velocity variation with number of total particles for radius of particle of 0.400 mm for water level falling

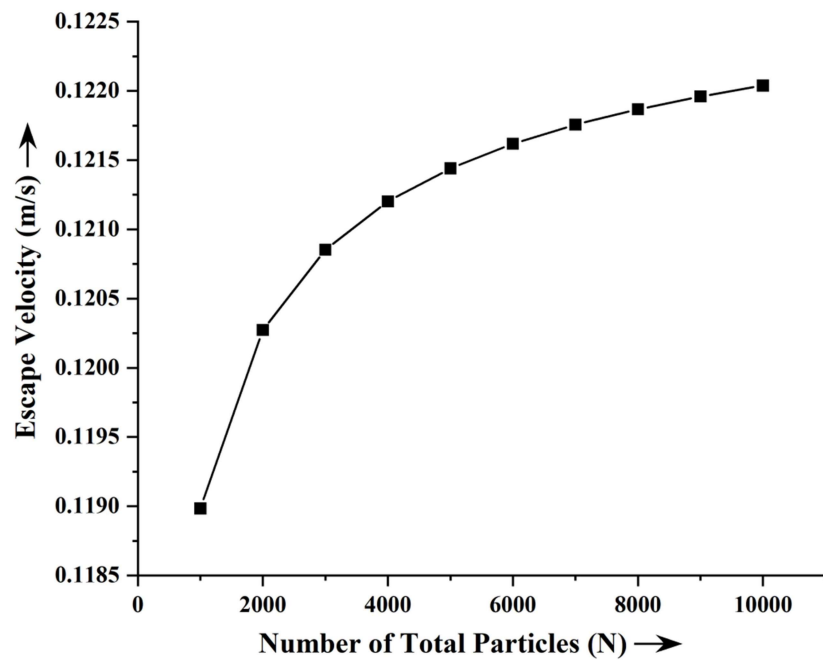


**Fig. 3.60** Escape velocity variation with number of total particles for radius of particle of 0.405 mm for water level falling

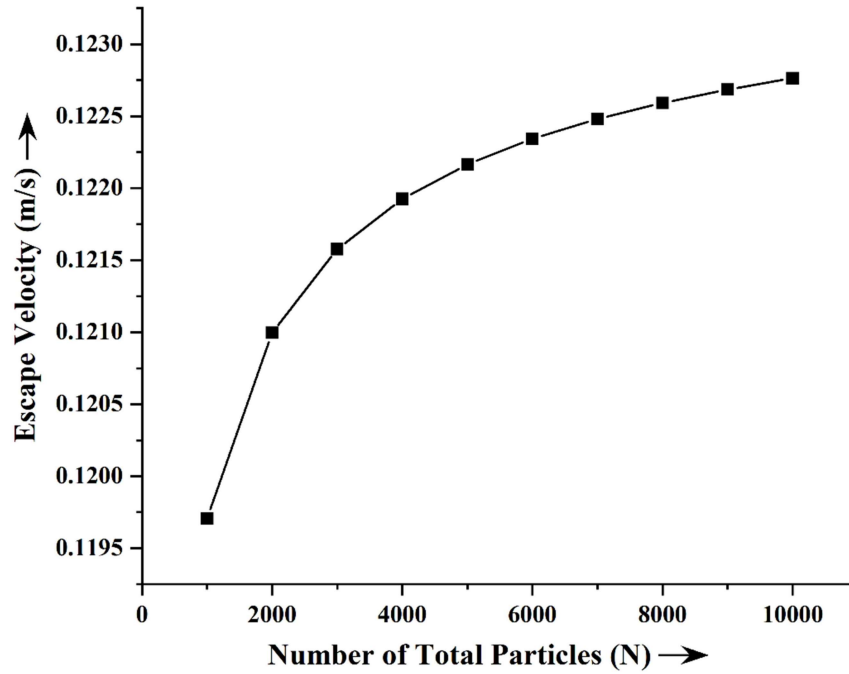


**Fig. 3.61** Escape velocity variation with number of total particles for radius of particle of 0.410 mm for water level falling

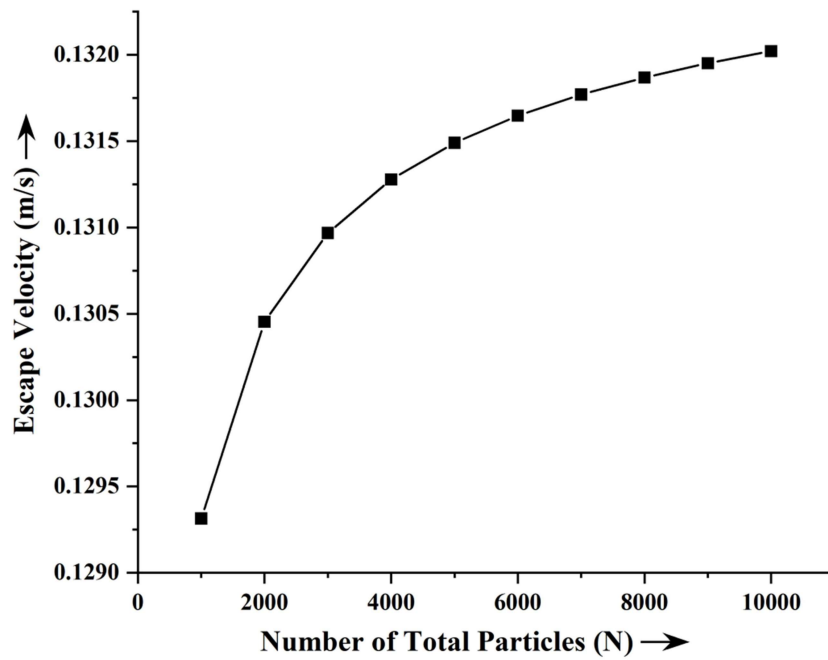


**Fig. 3.62** Escape velocity variation with number of total particles for radius of particle of 0.390 mm for water level rising

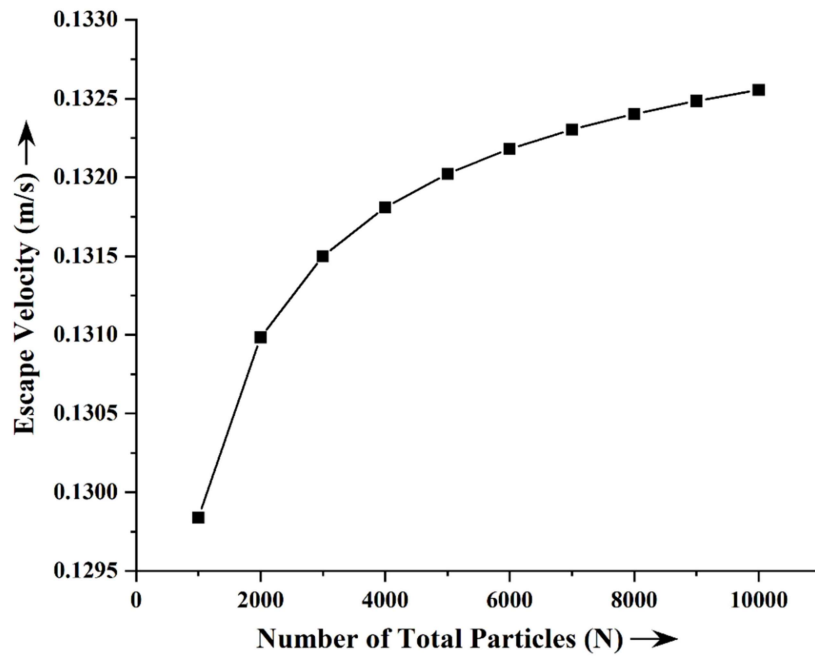


**Fig. 3.63** Escape velocity variation with number of total particles for radius of particle of 0.395 mm for water level rising

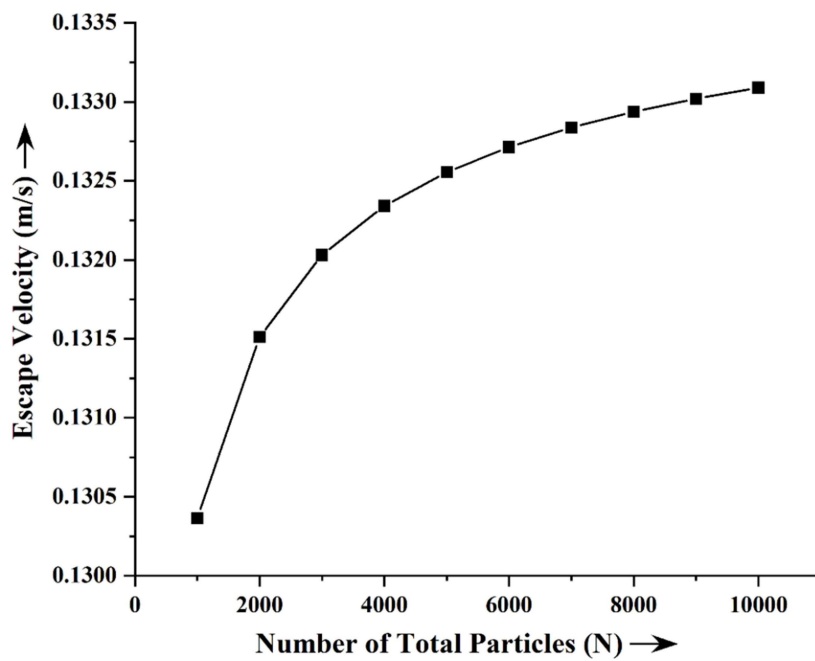


**Fig. 3.64** Escape velocity variation with number of total particles for radius of particle of 0.400 mm for water level rising

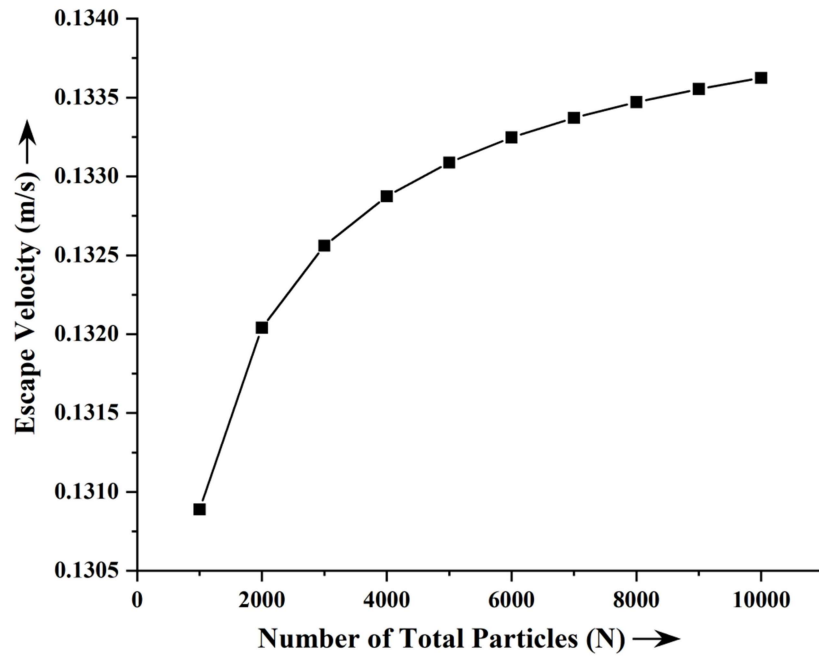


**Fig. 3.65** Escape velocity variation with number of total particles for radius of particle of 0.405 mm for water level rising

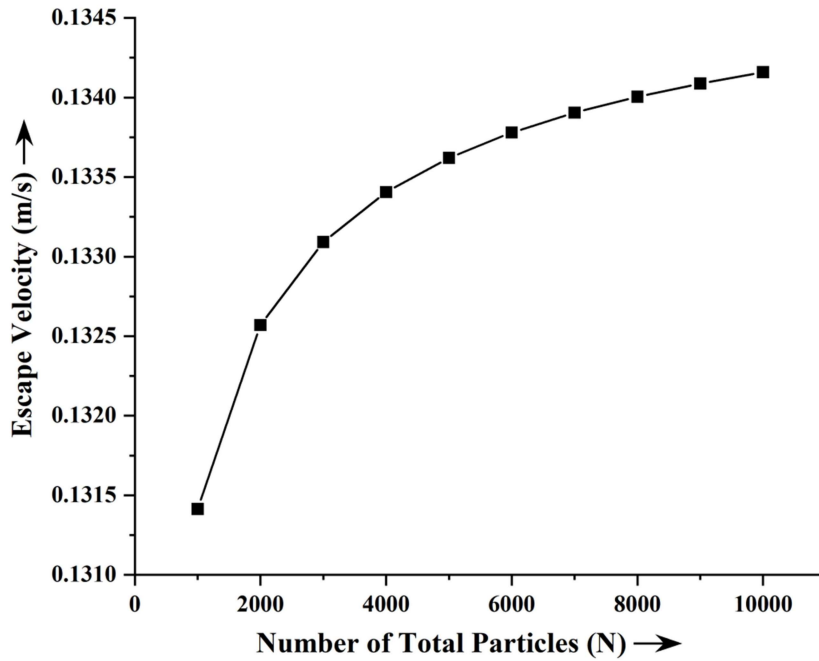


**Fig. 3.66** Escape velocity variation with number of total particles for radius of particle of 0.410 mm for water level rising

### 3.4.4 Escape Velocity Variation with Free Surface Height

Here, the variation is found out with respect to free surface height of the water level.

The free surface height has been varied from zero to toroidal block ( $H$ ) with four different intermediate points ( $\frac{1}{5}H$ ,  $\frac{2}{5}H$ ,  $\frac{3}{5}H$  and  $\frac{4}{5}H$ ) for both water level rising

and falling situation to study the dynamic behaviour of the riverbank. Five different graphs have been plotted for five different total numbers of particles (20000, 40000, 60000, 80000 and 100000). For showing the results in a tabular form, the corresponding table (Table 3.17) has also been added.

**Table 3.17: Escape velocity variation with free surface height**

Number of Total Particles	Free Surface Water Level Height ( $H_w$ )	Escape Velocity for Rising Water Level (m/s)	Escape Velocity for Falling Water Level (m/s)
20000	0	0.095504044	0.081763839
	(1/5)H	0.097040604	0.083410891
	(2/5)H	0.100956713	0.087152717
	(3/5)H	0.106991744	0.092715483
	(4/5)H	0.116830955	0.102935924
	H	0.133471538	0.121733088
40000	0	0.095507529	0.081760097
	(1/5)H	0.097053177	0.083416875
	(2/5)H	0.100991148	0.08717953
	(3/5)H	0.107062953	0.092780544

Number of Total Particles	Free Surface Water Level Height ( $H_w$ )	Escape Velocity for Rising Water Level (m/s)	Escape Velocity for Falling Water Level (m/s)
40000	(4/5)H	0.116975429	0.103089984
	H	0.133743083	0.122035519
60000	0	0.09550911	0.081758383
	(1/5)H	0.097058798	0.083419487
	(2/5)H	0.10100649	0.087191413
	(3/5)H	0.107094658	0.092809474
	(4/5)H	0.117039739	0.103158544
	H	0.133863848	0.122169956
80000	0	0.095510062	0.081757344
	(1/5)H	0.097062165	0.083421033
	(2/5)H	0.101015661	0.087198497
	(3/5)H	0.107113605	0.09282675
	(4/5)H	0.117078164	0.103199505
	H	0.133935975	0.122250228
100000	0	0.095510717	0.081756629
	(1/5)H	0.097064468	0.083422083
	(2/5)H	0.10102193	0.087203332
	(3/5)H	0.107126555	0.092838553
	(4/5)H	0.117104426	0.103227496
	H	0.133985255	0.122305066

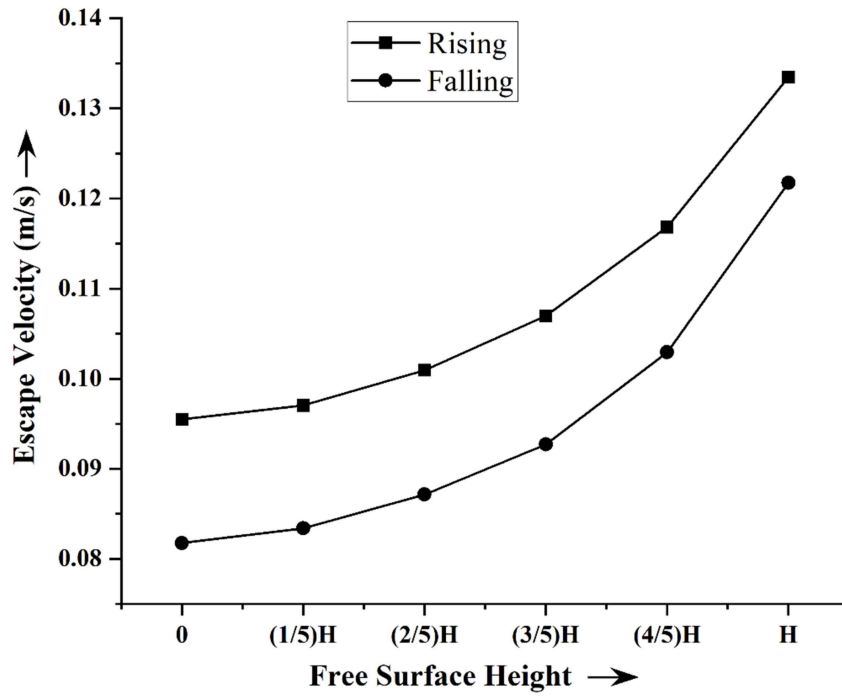


**Fig. 3.67** Escape velocity variation with free surface height for number of total particles of 20000

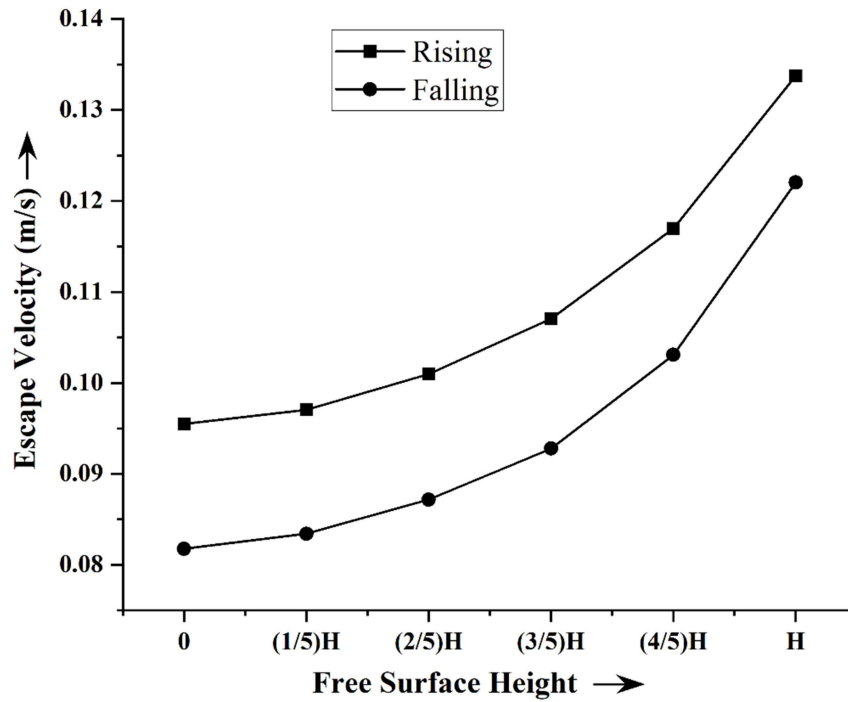


**Fig. 3.68** Escape velocity variation with free surface height for number of total particles of 40000



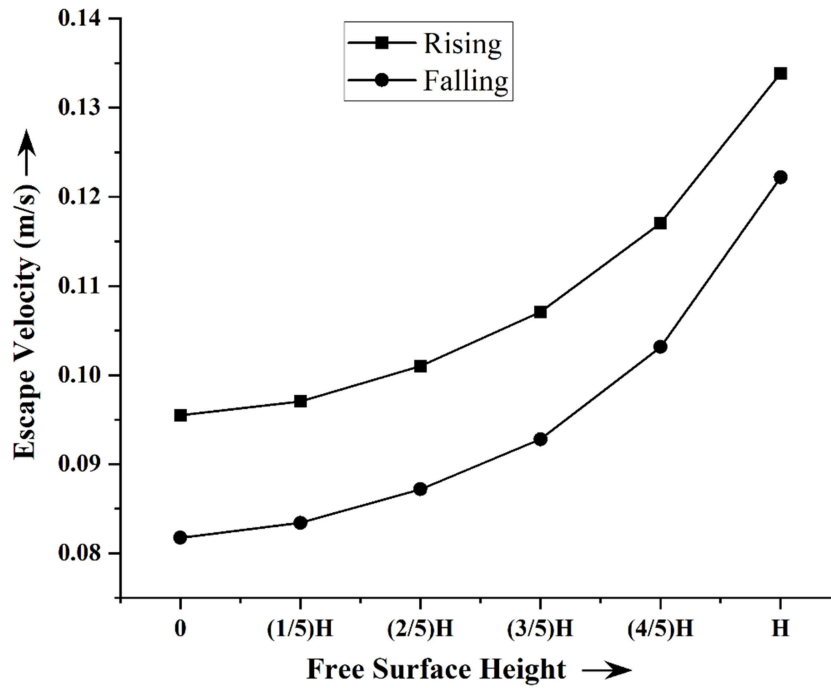


**Fig. 3.69** Escape velocity variation with free surface height for number of total particles of 60000

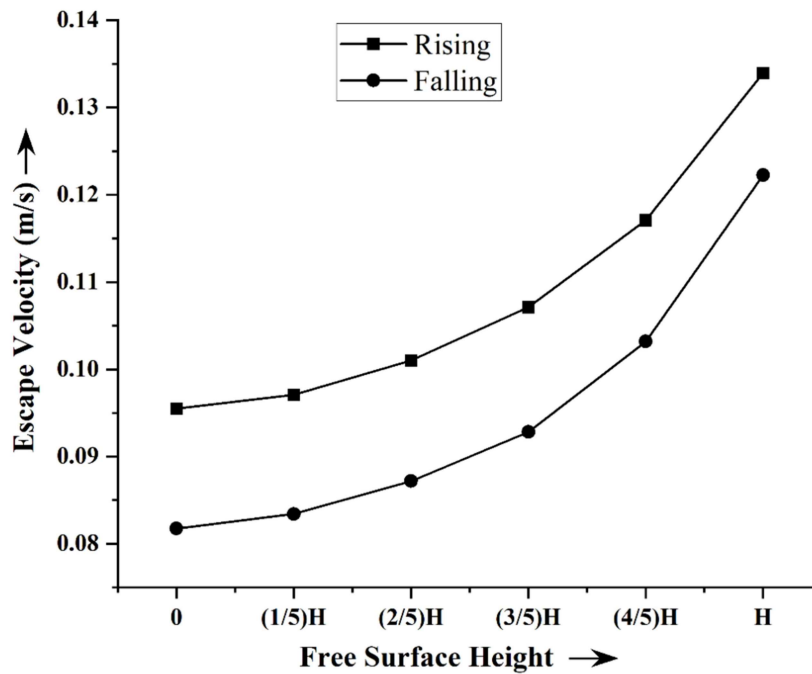


**Fig. 3.70** Escape velocity variation with free surface height for number of total particles of 80000

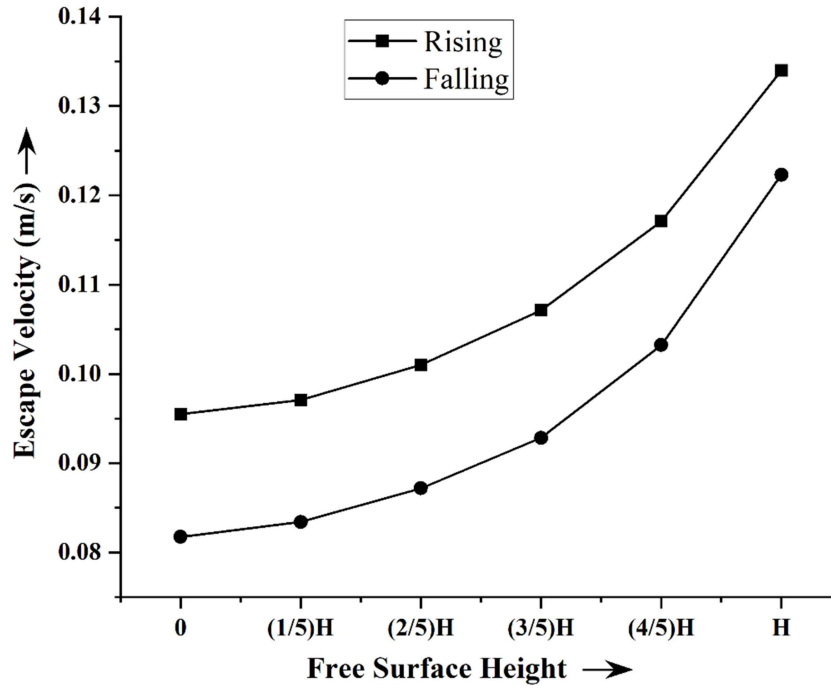


**Fig. 3.71** Escape velocity variation with free surface height for number of total particles of 100000

### 3.5 Discussions

Several analyses are made, varying different parameters for both water level rising and falling conditions.

Firstly, the analysis is made for different inter-particle distances keeping particle size and liquid-bridge volume at fixed value and the escape velocity graphs are plotted for both water level falling and rising conditions with respect to number of base particles (Fig. 3.7 to Fig. 3.16) and number of total particles (Fig. 3.17 to Fig. 3.26). As the number of base particles increases escape velocity increases for both water levels falling and rising. The initial rise is steadier and, then, it becomes flattened as the number of base particles goes on increasing. Again as the inter-particle distance increases escape velocity increases, hence, the stability also

increases. It has been observed from the graph that the escape velocity is more for water level rising as compared to water level falling. This indicates riverbank is more vulnerable in terms of stability in case of water level falling as compared to water level rising.

Secondly, analysis is done for different liquid-bridge volumes keeping inter-particle distance and particle size at fixed value and the escape velocity graphs are plotted for both water level falling and rising conditions with respect to number of base particles (Fig. 3.27 to Fig. 3.36) and number of total particles (Fig. 3.37 to Fig. 3.46). As the liquid-bridge volume increases, the escape velocity increases for both the situation of water level falling and rising. This is due the fact that the increased liquid-bridge volume enhances the force of cohesion, hence the stability. Again it is evident from the graph that the escape velocity is more for water level rising as compared to water level falling for same liquid-bridge volume. So, for same liquid-bridge volume stability is more in case of water level rising as compared to water level falling.

Thirdly, analysis is made for different particle sizes keeping inter-particle distance and liquid-bridge volume at fixed value and the escape velocity graphs are plotted for both water level falling and rising conditions with respect to number of base particles (Fig. 3.47 to Fig. 3.56) and number of total particles (Fig. 3.57 to Fig. 3.66). As the radius of the particle increases, the escape velocity increases for both the situation of water level falling and rising. This is due the fact that the increased sizes entrap more liquid which enhances the force of cohesion and net hydrostatic forces, which are resistive in nature, hence is the stability.

Lastly, the graphs of escape velocity are plotted for different free surface heights for different number of total particles in the block (Fig. 3.67 to Fig. 3.71) to

study the dynamic behaviour and its effect on the stability of the riverbank. With the increasing free surface height from 0 to riverbank height ( $H$ ) the escape velocity and so the stability increases steadily. Again, between rising and falling situation for same free surface height, it can be observed from the all figures, escape velocity is more in case of water level rising as compared to water level falling. It can also be observed from the figures that the increasing number of total particles in the block increases the escape velocity steadily. This proves that the bigger size chunk requires more force to dislodge from the riverbank surface. Therefore, the escape velocity is more.

## **CHAPTER 4**

## **CONCLUSION**

## Chapter 4

### Conclusion

#### 4.1 Concluding Remarks

Rivers and streams are often found to change their courses influencing the livelihood of people depending on them. This is why they are usually referred to as dynamic systems. Complex and interconnected variables govern the creation of rivers and streams. The geology of the catchment, the kind and quantity of vegetation present, and the rate at which water and sediment are supplied to stream systems are some of these variables. River systems adapt over time by changing their position, shape, or combination of these characteristics. The rate of these changes is usually gradual and undetectable in stable streams. Because of their dynamicity rivers throw challenges to people who deal with their variability.

In the present work two different approaches, namely micro-analysis and macro-analysis have been investigated to evaluate the generalised expression for escape velocity of the particle, i.e., the velocity that the particle needs to detach itself from the riverbank, resulting in riverbank erosion. In microscopic approach well established “Truncated Pyramid Model” for microscopic particle arrangement have been implemented and conservation of angular momentum principle have been used to determine the escape velocity of the most vulnerable particle in the arrangement. In the latter part of the analysis, in macroscopic approach, right-angled trapezoidal failure block resulting out of a tension crack with infinite numbers of particles have been investigated using a newly proposed method for transformation of micro-level forces to macro-level forces leading to generalised expressions for the bulk escape velocity. Thus, the problem of riverbank erosion develops into riverbank failure. Different conditions of varying water level have been studied for both micro-analysis

and macro-analysis applicable to both the situations on the rise of water level and fall of water level to study the dynamic behaviour of the riverbank system. It has been demonstrated that a variety of factors, including the inter-particle distance, the particle radii, the water density, the surface tension, the contact angle, and the volume of water trapped between a congregations of particles, taking its toll on the escape velocity. The escape velocity can be used to determine other parameters that are directly or indirectly connected to it, such as the volumetric rate of bank erosion caused by hydraulic forces, the entrainment rate, and so forth.

In the microscopic analysis, two different studies have been made. Firstly, varying particle sizes with a fixed value of liquid-bridge volume and secondly, varying liquid-bridge volume with a fixed value of particle size. The escape velocity variations have been plotted against the inter-particle distance for both conditions pertaining to water level rising and falling, for three different degrees of exposure ( $e$ ) of the particle, Fully exposed [ $e = 1.0$ ], Half exposed [ $e = 0.5$ ] and Fully submerged [ $e = 0.0$ ]. The results of adverse effect of inter-particle distances, particle size and the positive influence of liquid-bridge volume on escape velocity have been observed and discussed. These facts prove the bondings between the particles become weaken as the distance between the particles, the particle size increases and the water-bridge volume decreases, lowering the stability as a consequence. From the analyses, it can also be concluded that increasing degrees of exposure reduce the particle escape velocity. Again, this velocity is less in case of water level falling compared to that of water level rising when the other parameters remain constant. It proves the fact that rising water level creates positive moments that help the particles to stay together, resulting in greater stability.

In the macroscopic analysis, a right-angled trapezoidal failure block with infinite number of particles has been investigated while it is subjected to different varying conditions.

Three different analyses have been made by varying one parameter, keeping other two parameters fixed. These are liquid-bridge volume, inter-particle distance and number of particle. The results have been plotted with both number of base particles and number of total particles in the failure block, for rise and fall of water level. All three cases show a positive influence on the escape velocity of the block. This is because though the microscopic forces reduce the effect of macroscopic forces (hydrostatic force and pore water pressure force), the macroscopic forces increase at a higher rate. So, by and large, the system escape velocity rises giving the bank greater stability. It can also be observed that the increasing number of particles increases the escape velocity. This is a testimony of the fact that a bigger size chunk requires more forces to dislodge from the bank surface. Again, if a comparison is made between the rising and falling water level conditions keeping other parameters constant, it can be observed that the escape velocity is more in case of water level rising as compared to water level falling. This is because the rising water level creates a positive moment to bind the particles together. Lastly, the graphs of escape velocity are plotted for different free surface heights for different number of total particles in the block to study the dynamic behaviour and its effect on the stability of the riverbank. With an increase in the free surface height from 0 to riverbank height ( $H$ ), the escape velocity and, hence the stability increases steadily. Therefore, the newly devised macroscopic analysis has enough potential to play a significant role in the present scenario in terms of suggesting more generalised expressions for escape velocity to predict the stability of the riverbanks. This approach has the capability to incorporate variabilities associated with different riverbank systems of different nature. It can successfully complement the field studies and experimental investigations, being a reasonably robust theoretical approach. In a nut-shell, the present work analyzes the behaviour of a particle or a block subjected to changing circumstances. This may estimate the future scenario based on the present.



## **4.2 Future Scope**

A theoretical approach can always give better results when sufficient input data are collected through field studies and experimental investigations. The mechanism of riverbank failure due to undercutting may be explored in future with this model. The influence of lateral forces imposed by the waves may also be explored in detail to have a more holistic view on the mechanism of riverbank failure.

## References

1. Odgaard, A. J., and Mosconi, C. E., (1987). "Streambank Protection by Submerged Vanes." *Journal of Hydraulic Engineering*, ASCE, 113(4), 520-536.
2. Odgaard, A. J., (1987). "Streambank Erosion along Two Rivers In Iowa." *Water Resources Research*, 23 (7), 1125-1236.
3. Osman, A. M. and Thorne C. R., (1988). "Riverbank Stability Analysis. I: Theory." *Journal Modeling Erosion and Overbank Deposition of Hydraulic Engineering*, ASCE, 114(2), 134 –150.
4. Beeson, C. E., and Doyle, P. F., (1995). "Comparison of Bank Erosion at Vegetated and Nonvegetated Channel Bends." *Water Resources Bulletin*, 31: 983-990.
5. Darby, S. E. and Thorne, C. R. (1996). "Development and Testing of Riverbank Stability Analysis." *Journal of Hydraulic Engineering*, ASCE. 122 (8), 443–454.
6. Darby, S. E. and Thorne, C. R. (1996). "Numerical Simulation of Widening and Bed Deformation of Straight Sand-Bed Rivers I: Model Development." *Journal of Hydraulic Engineering*, ASCE. 122 (4), 164–193.
7. Darby, S. E., and Thorne, C. R., (1996), "Stability Analysis for Steep, Eroding, Cohesive Riverbanks." *Journal of Hydraulic Engineering*, ASCE, 122, 443-454.
8. Coufal, R., (1997). "Bed changes and sediment transport at river mouth." *Polish Academy of Sciences*, Gdansk, Poland, 55–72.
9. Abernethy, B., and Rutherford I. D., (1998). "Where along a River's Length Will Vegetation Most Effectively Stabilise Stream Banks?" *Geomorphology*, 23, 55-75.
10. Fripp, J., Burns, M., and, Caverly, J., (1998). "Stream Stability Assessment Techniques." Conference Proceedings - *Wetlands Engineering and River Restoration Conference* 1998, 19 – 21.

11. Rinaldi M. & Casagli N., (1999). "Stability of Streambanks Formed in Partially Saturated Soils and Effects of Negative Pore Water Pressures: The Sieve River (Italy)." *Geomorphology*, 26 (4), 253-277.
12. Green T. R., Beavis S.G., Dietrich C. R., Jakeman A. J. (1999). "Relating Stream-Bank Erosion To In-Stream Transport Of Suspended Sediment." *Hydrological Processes*, 13, 777-787.
13. Darby S. E., Gessler D. & Thorne C. R., (2000). "Computer Program for Stability Analysis of Steep, Cohesive Riverbanks." *Earth Surface Processes and Landforms*, 25, 175-190.
14. Pitois, O., Moucheron, P. and Chateau, X., (2001). "Rupture Energy of a Pendular Liquid Bridge." *Eur. Phys. J.*, B 23, 79-86.
15. Likos, W. J., and Lu, N. (2002). "Hysteresis of Capillary in Unsaturated Soils." *15th ASCE Engineering Mechanics Conference*, June 2-5, 2002, Columbia University, New York, NY, 1-8.
16. Rim, C. S., and Gay L. W., (2002). "Estimating Soil Moisture in Small Watersheds, Using a Water Balance Approach." *Nordic Hydrology*, 33(5), 373-390.
17. Darby, S. E., and Delbono I., (2002). "A Model of Equilibrium Bed Topography for Meander Bends with Erodible Banks." *Earth Surface Processes and Landforms*, 27(10), 1057-1085.
18. Zeng, W., and Beck, M. B., (2003). "STAND, A Dynamic Model for Sediment Transport and Water Quality." *Journal of Hydrology*, 277(1-2), 125-133.
19. Pyle, C. J., Richards, K. S., and Chandler J. H. (2003). "Digital Photogrammetric Monitoring of River Bank Erosion." *The Photogrammetric Record*, 15(89), 753-764.

20. Johanson, K., Yakov, R., Brij, M., Kristen, B. and Havala, T., (2003). "Relationship between Particle Scale Capillary Forces and Bulk Unconfined Yield Strength." *Powder technology*, 138(1), 13-17.
21. Carroll, R. W. H., Warwick, J. J., James, A. I., Miller, J. R., 2004, "Modeling Erosion and Overbank Deposition During Extreme Flood Conditions on the Carson River, Nevada." *Journal of Hydrology*, 297 (1-4), 1-21.
22. Jang, C. L, and Shimizu, Y. (2005). "Numerical Simulation of Relatively Wide, Shallow Channels with Erodible Banks." *J. Hydraul. Eng.*, 131(7), 565 – 575.
23. Duan, J. G. (2005). "Analytical Approach to Calculate Rate of Bank Erosion." *J. Hydraul. Eng.*, 131(11), 980 – 989.
24. Kotoky, P., Bezbaruah, D., Baruah, J. and Sarma, J. N., (2005). "Nature of Bank Erosion along the Brahmaputra River Channel, Assam, India." *Current Science*, 88 (4), 634-640.
25. Soulie, F., El Youssoufi, M. S., Cherblanc, F. and Saix, C, (2006). "Capillary Cohesion and Mechanical Strength of Polydisperse Granular Materials." *Eur. Phys. J. E.*, 21, 349 – 357.
26. Larsen, E. W., Fremier, A. K., and Greco, S. E. (2006). "Cumulative Effective Stream Power and Bank Erosion on the Sacramento River, California, USA." *Journal of American Water Resources Association*, 42(4), 1077-1097.
27. Lenzi, M. A., Mao, L., and Comiti, F., (2006). "Effective Discharge for Sediment Transport in A Mountain River: Computational Approaches and Geomorphic Effectiveness." *Journal of Hydrology*, 326(1-4), 257-276.
28. Meunier, P., Métivier, F., Lajeunesse, E., Mériaux, A. S. and Faurec J., (2006). "Flow Pattern and Sediment Transport in a Braided River: the "Torrent de St Pierre" (French Alps)." *Journal of Hydrology*, 330(3-4), 496-505.

29. Julian, J. P., and Torres, R., (2006). "Hydraulic Erosion of Cohesive Riverbanks." *Geomorphology*, 76(1-2), 193-206.
30. Darby, S. E. and Thorne, C. R., (2006). "Prediction of Tension Crack Location and Riverbank Erosion Hazards along Destabilized Channels." *Earth Surface Processes and Landforms*, 19(3), 233-245.
31. Amiri-Tokaldany, E. and Darby, S. E. (2006). "A Model for Stability Analysis of a Multi-Layered River Bank (SAMLRL)." *Journal of Agriculture, Science and Technology*, 8 (1), 61–76.
32. Richefeu, V., El Youssoufi, M. S., Peyroux, R. and Radiai, F, (2007). "A Model of Capillary Cohesion for Numerical Simulations of 3D Polydisperse Granular Media." *International Journal for Numerical and Analytical Methods in Geomechanics*, 32 (11), 1365-1383.
33. Achite, M., and Ouillon, S., (2007). "Suspended Sediment Transport in a Semiarid Watershed, Wadi Abd, Algeria (1973 –1995)." *Journal of Hydrology*, 343(3-4), 187-202.
34. Khosronejad A., Rennie, C. D., Salehi Neyshabouri, S. A. A. and Townsend, R. D. (2007). "3D Numerical Modeling of Flow and Sediment Transport in Laboratory Channel Bends." *J. Hydraul. Eng.*, 134(8), 1142-1146.
35. Amiri-Tokaldany, E., Darby, S. E. and Tosswell, P. (2007). "Coupling Bank Stability and Bed Deformation Models to Predict Equilibrium Bed Topography in River Beds." *J. Hydraul. Eng.*, 133(10), 1167 – 1170.
36. Papanicolaou, A. N., Elhakeem, M., and Hilldale, R. (2007). "Secondary Current Effects on Cohesive River Bank Erosion." *Water Resources Research*, 43.

37. Mu, F. and Su, X., (2007). "Analysis of Liquid Bridge between Spherical Particles." *China Particuology*, 5, 420-424.
38. Chen, D. and Duan, J. G. (2008). "Case Study: Two-Dimensional Model Simulation of Channel Migration Processes in West Jordan River, Utah." *Journal of Hydraulic Engineering, ASC*, 134 (3), 315–327.
39. Singh, R., and Kundu, D. K. (2008). "Erodibility of Major Soil Sub-groups of Eastern Region of India." *Indian J. Soil Cons.*, 36(3), 172-178.
40. Cheneler, D., Ward, M. C. L., Adams, M. J. and Zhang, Z. (2008). "Measurement of dynamic properties of small volumes of fluid using MEMS." *Sensors and Actuators B: Chemical*, 130 (2), 701–706.
41. Velmurugan, A., Swarnam, T. P., Kumar P., and Ravisankar, N. (2008). "Soil Erosion Assessment Using Revised Morgan, Morgan Finney Model for Prioritization of Dhanikhari Watershed in South Andaman." 36(3), *Indian J. Soil Cons.*, 36(3), 179-187.
42. Greimann, B., Lai, Y. and Huang, J. (2008). "Two-Dimensional Total Sediment Load Model Equations." *J. Hydraul. Eng.*, 134(8), 1142-1146.
43. Mukherjee, S. and Mazumdar, A., (2010). "Study of Effect of the Variation of Inter-Particle Distance on the Erodibility of a Riverbank under Cohesion with a New Model." *Journal of Hydro-Environment Research*, 1-8.
44. Mukherjee, S., (2011). "Application of Truncated Pyramid Model in determination of escape velocity of particles of different diameters in varying conditions." *International Journal of Soft Computing and Engineering (IJSCE)*, 1(5), 75-79.
45. Abderrezzak, K. El. K., Moran, A. D., Mosselman, E., Bouchard, J. P., Habersack, H. and Aelbrecht, H., (2014). "A Physical, Movable-bed Model for Non-uniform

- Sediment Transport, Fluvial Erosion and Bank Failure in Rivers.” *Journal of Hydro-environment Research*, 8 (2014) 95-114.
46. Bravo, R., Ortiz, P. and Pérez-Aparicio, J. L. (2014). “Incipient sediment transport for non-cohesive landforms by the discrete element method (DEM).” *Applied Mathematical Modelling*, 38 (4), 1326–1337.
  47. Zhang, M. and Yu, G. (2017). “Critical conditions of incipient motion of cohesive sediments.” *Water Resources Research*, 53 (9), 7798–7815.
  48. Thi, T. D. and Minh, D. D. (2019). “Riverbank Stability Assessment under River Water Level Changes and Hydraulic Erosion.” *Water*, 11, 2598, 1–20.
  49. Moody, J. A. (2022). “The effects of discharge and bank orientation on the annual riverbank erosion along Powder River in Montana, USA.” *Geomorphology*, 403, 108–134.
  50. Bowles, J. E. (1979). “Physical and Geotechnical Properties of Soils.” *McGraw-Hill, Inc., England*, 478.
  51. Douglas, J. F., Gasiorek, J. M. and Swaffield, J. A. (1995). “Fluid Mechanics.” *Longman Singapore Publishers (Pte) Ltd., Singapore*, 911.





# THESIS

## ORIGINALITY REPORT

8%

SIMILARITY INDEX

5%

INTERNET SOURCES

7%

PUBLICATIONS

0%

STUDENT PAPERS

## PRIMARY SOURCES

1	"Intelligent Techniques and Applications in Science and Technology", Springer Science and Business Media LLC, 2020 Publication	1%
2	Debasish Biswas, Arijit Dutta, Sanchayan Mukherjee, Asis Mazumdar. "Chapter 2 Effect of Liquid Bridge Volume on Cohesive Sediment Motion", Springer Science and Business Media LLC, 2021 Publication	<1%
3	ebin.pub Internet Source	<1%
4	patents.google.com Internet Source	<1%
5	www.scipedia.com Internet Source	<1%
6	hdl.handle.net Internet Source	<1%
7	Sanchayan Mukherjee, Asis Mazumdar. "Study of effect of the variation of inter-particle	<1%

distance on the erodibility of a riverbank under cohesion with a new model", Journal of Hydro-environment Research, 2010

Publication

8

[www.researchgate.net](http://www.researchgate.net)

Internet Source

<1 %

9

"Advanced Modelling and Innovations in Water Resources Engineering", Springer Science and Business Media LLC, 2022

Publication

<1 %

10

Applied Mechanics, 1972.

Publication

<1 %

11

[file.scirp.org](http://file.scirp.org)

Internet Source

<1 %

12

Frederick A. Leckie. "Energy Methods", Mechanical Engineering Series, 2009

Publication

<1 %

13

[accessories.part-kom.ru](http://accessories.part-kom.ru)

Internet Source

<1 %

14

[etheses.whiterose.ac.uk](http://etheses.whiterose.ac.uk)

Internet Source

<1 %

15

[www.dora.lib4ri.ch](http://www.dora.lib4ri.ch)

Internet Source

<1 %

16

Advances in Water Resources and Hydraulic Engineering, 2009.

Publication

<1 %

17

eprints.soton.ac.uk

Internet Source

<1 %

18

Ebrahim Amiri-Tokaldany. "BANK STABILITY ANALYSIS FOR PREDICTING REACH SCALE LAND LOSS AND SEDIMENT YIELD", Journal of the American Water Resources Association, 8/2003

Publication

<1 %

19

Dong Chen, Jennifer G. Duan. "Case Study: Two-Dimensional Model Simulation of Channel Migration Processes in West Jordan River, Utah", Journal of Hydraulic Engineering, 2008

Publication

<1 %

20

Sanchayan Mukherjee, Asis MazumdarP. "Influence of Inter-Particle Distance, Entrapped Water Volume and Salinity of Water on the Escape Velocity of Particles on a Riverbank", Engineering, 2011

Publication

<1 %

21

"Advances in Water Resources Management for Sustainable Use", Springer Science and Business Media LLC, 2021

Publication

<1 %

22

Arijit Dutta, Sanchayan Mukherjee, Asis Mazumdar. "Effect of the Variation of Inter-Particle Separation Distance and Separation

<1 %

# Time on Escape Velocity of Sediment Particles of a River Bank under the Action of Cohesive and Viscous Forces", Indian Science Cruiser, 2017

Publication

23

[riunet.upv.es](http://riunet.upv.es)

Internet Source

<1 %

24

[www.arlis.org](http://www.arlis.org)

Internet Source

<1 %

25

[www.ijsce.org](http://www.ijsce.org)

Internet Source

<1 %

26

Aznarul Islam, Sanat Kumar Guchhait.  
"Riverbank Erosion in the Bengal Delta",  
Springer Science and Business Media LLC,  
2024

Publication

<1 %

27

Debasish Biswas, Arijit Dutta, Sanchayan  
Mukherjee, Asis Mazumdar. "Micro analysis of  
riverbank sediment stability under different  
wetted surface conditions", IOP Conference  
Series: Materials Science and Engineering,  
2021

Publication

<1 %

28

[publications.polymtl.ca](http://publications.polymtl.ca)

Internet Source

<1 %

29

[typefaster.sourceforge.net](http://typefaster.sourceforge.net)

Internet Source

<1 %

30

Songge Zhang, Xikui Li, Youyao Du. "A numerical model of discrete element – Liquid bridge – Liquid thin film system for wet deforming granular medium at low saturation", Powder Technology, 2022

Publication

<1 %

31

Kamal El Kadi Abderrezzak, Andres Die Moran, Erik Mosselman, Jean-Pierre Bouchard, Helmut Habersack, Denis Aelbrecht. "A physical, movable-bed model for non-uniform sediment transport, fluvial erosion and bank failure in rivers", Journal of Hydro-environment Research, 2014

Publication

<1 %

32

R. Bravo, P. Ortiz, J.L. Pérez-Aparicio. "Incipient sediment transport for non-cohesive landforms by the discrete element method (DEM)", Applied Mathematical Modelling, 2014

Publication

<1 %

33

Springer Earth System Sciences, 2015.

Publication

<1 %

34

Xiangqi Li, Dengfei Wang, Fenglei Huang, Ziqi Cai, Zhengming Gao. "Stretching and rupture of a viscous liquid bridge between two spherical particles", Asia-Pacific Journal of Chemical Engineering, 2020

Publication

<1 %

35	euro-lepnina.com Internet Source	<1 %
36	doshisha.repo.nii.ac.jp Internet Source	<1 %
37	lrcdrs.bennett.edu.in Internet Source	<1 %
38	Fabio Gabrieli, Riccardo Artoni, Andrea Santomaso, Simonetta Cola. "Discrete particle simulations and experiments on the collapse of wet granular columns", Physics of Fluids, 2013 Publication	<1 %
39	Mohamed Achite, Sylvain Ouillon. "Suspended sediment transport in a semiarid watershed, Wadi Abd, Algeria (1973–1995)", Journal of Hydrology, 2007 Publication	<1 %
40	www.netl.doe.gov Internet Source	<1 %
41	"Free Surface Flows and Transport Processes", Springer Science and Business Media LLC, 2018 Publication	<1 %
42	Darby, Stephen E., and Jeff Peakall. "Modelling the equilibrium bed topography of	<1 %

submarine meanders that exhibit reversed secondary flows", Geomorphology, 2012.

Publication

43

Weiming Wu, Dalmo A. Vieira, Sam S. Y. Wang. "One-Dimensional Numerical Model for Nonuniform Sediment Transport under Unsteady Flows in Channel Networks", Journal of Hydraulic Engineering, 2004

Publication

<1 %

44

Zheyuan Liu, Bingbing Chen, Chen Lang, Lunxiang Zhang, Lei Yang, Xianwei Guo. "An improved model for predicting the critical velocity in the removal of hydrate particles from solid surfaces", Chemical Physics Letters, 2021

Publication

<1 %

45

[researchrepository.wvu.edu](https://researchrepository.wvu.edu)

Internet Source

<1 %

46

Chang-Lae Jang. "Numerical simulations of the behavior of alternate bars with different bank strengths", Journal of Hydraulic Research, 11/2005

Publication

<1 %

47

Combescot, M.. "The many-body physics of composite bosons", Physics Reports, 200807

Publication

<1 %

48

Li, W.-L.. "Dynamics of liquid meniscus bridge of a vibrating disk: consideration of flow rheology", Micro & Nano Letters, 2009.

Publication

&lt;1 %

49

Stephen E. Darby. "Prediction of tension crack location and riverbank erosion hazards along destabilized channels", Earth Surface Processes and Landforms, 05/1994

Publication

&lt;1 %

50

Stênio de Sousa Venâncio, Swami Marcondes Villela, José Luís da Silva Pinho, José Manuel Pereira Vieira. "Numerical model for hydrodynamics simulations of Trabalhador channel", Management of Environmental Quality: An International Journal, 2017

Publication

&lt;1 %

51

[bib.gfz-potsdam.de](http://bib.gfz-potsdam.de)

Internet Source

&lt;1 %

52

[core.ac.uk](http://core.ac.uk)

Internet Source

&lt;1 %

53

[eprints.gla.ac.uk](http://eprints.gla.ac.uk)

Internet Source

&lt;1 %

54

[geografiafisica.org](http://geografiafisica.org)

Internet Source

&lt;1 %

55

[iris.unitn.it](http://iris.unitn.it)

Internet Source

&lt;1 %



56

[jast.modares.ac.ir](http://jast.modares.ac.ir)

Internet Source

&lt;1 %

57

[repository.tudelft.nl](http://repository.tudelft.nl)

Internet Source

&lt;1 %

58

Azlinda Saadon, Jazuri Abdullah, Ihsan Mohd Yassin, Nur Shazwani Muhammad, Junaidah Ariffin. "Nonlinear multi independent variables in quantifying river bank erosion using Neural Network AutoRegressive eXogenous (NNARX) model", Heliyon, 2024

Publication

&lt;1 %

59

Chien-Hua Chen, Te-Yung Hsieh, Jinn-Chuang Yang. "Investigating effect of water level variation and surface tension crack on riverbank stability", Journal of Hydro-environment Research, 2017

Publication

&lt;1 %

60

Coons, J.E.. "A review of drainage and spontaneous rupture in free standing thin films with tangentially immobile interfaces", Advances in Colloid and Interface Science, 20030918

Publication

&lt;1 %

61

F. Soulié, M. S. El Youssoufi, F. Cherblanc, C. Saix. "Capillary cohesion and mechanical strength of polydisperse granular materials", The European Physical Journal E, 2007

Publication

&lt;1 %

---

62 Jang, Chang-Lae, and Yasuyuki Shimizu. "Numerical Analysis Of Braided Rivers and Alluvial Fan Deltas", Engineering Applications of Computational Fluid Mechanics, 2007. <1 %

Publication

---

63 Jennifer G. Duan. "Analytical Approach to Calculate Rate of Bank Erosion", Journal of Hydraulic Engineering, 2005 <1 %

Publication

---

64 M. Alam. "Observations on transition in plane bubble plumes", Journal of Fluid Mechanics, 09/1993 <1 %

Publication

---

65 R. Bagheri, R.A. Pearson. "Role of particle cavitation in rubber-toughened epoxies: II. Inter-particle distance", Polymer, 2000 <1 %

Publication

---

66 apps.dtic.mil <1 %

Internet Source

---

67 d-nb.info <1 %

Internet Source

---

68 export.arxiv.org <1 %

Internet Source

---

69 fdocuments.us <1 %

Internet Source

---

i-scholar.in

70

Internet Source

&lt;1 %

71

[iaswc.com](http://iaswc.com)

Internet Source

&lt;1 %

72

[iwaponline.com](http://iwaponline.com)

Internet Source

&lt;1 %

73

[researchonline.jcu.edu.au](http://researchonline.jcu.edu.au)

Internet Source

&lt;1 %

74

[theses.gla.ac.uk](http://theses.gla.ac.uk)

Internet Source

&lt;1 %

75

[vdoc.pub](http://vdoc.pub)

Internet Source

&lt;1 %

76

[wsdot.wa.gov](http://wsdot.wa.gov)

Internet Source

&lt;1 %

77

[www.coursehero.com](http://www.coursehero.com)

Internet Source

&lt;1 %

78

[www.mdpi.com](http://www.mdpi.com)

Internet Source

&lt;1 %

79

[www.studymode.com](http://www.studymode.com)

Internet Source

&lt;1 %

80

[www.usbr.gov](http://www.usbr.gov)

Internet Source

&lt;1 %

81

A. Ponce-Torres, E. J. Vega, J. M. Montanero.  
"Effects of surface-active impurities on the

&lt;1 %

82

Abernethy, B.. "Where along a river's length  
will vegetation most effectively stabilise  
stream banks?", Geomorphology, 199805

Publication

<1 %

83

Husam A. Elghannay, Danesh K. Tafti.  
"Sensitivity of numerical parameters on DEM  
predictions of sediment transport",  
Particulate Science and Technology, 2017

Publication

<1 %

84

Boris V. Balakin, Sergey Alyaev, Alex C.  
Hoffmann, Pawel Kosinski. "Micromechanics  
of agglomeration forced by the capillary  
bridge: The restitution of momentum", AIChE  
Journal, 2013

Publication

<1 %

85

Jaber Shabanian, Marc A. Duchesne, Allan  
Runstedtler, Madhava Syamlal, Robin W.  
Hughes. "Improved analytical energy balance  
model for evaluating agglomeration from a  
binary collision of identical wet particles",  
Chemical Engineering Science, 2020

Publication

<1 %

86

M. Taghavi, M.H. Dovoudi, E. Amiri-Tokaldany,  
S.E. Darby. "An analytical method to estimate  
failure plane angle and tension crack depth

<1 %

for use in riverbank stability analyses",  
Geomorphology, 2010

Publication

87

Samadi, A.. "Identifying the effects of  
parameter uncertainty on the reliability of  
riverbank stability modelling",  
Geomorphology, 20090515

Publication

<1 %

88

Wei-Song Lin, Chen-Hong Zheng. "Energy  
management of a fuel cell/ultracapacitor  
hybrid power system using an adaptive  
optimal-control method", Journal of Power  
Sources, 2011

Publication

<1 %

89

Yifei Ma, T. Matthew Evans, Noah Philips,  
Nicholas Cunningham. "Modeling the effect of  
moisture on the flowability of a granular  
material", Meccanica, 2018

Publication

<1 %

Exclude quotes

Off

Exclude matches

Off

Exclude bibliography

On